CYCLODEXTRINS IN CHROMATOGRAPHY. PART 2. MISCELLANEOUS CHROMATOGRAPHIC METHODS.

Gyula Oros[a], Tibor Cserháti[a] and Mária Szőgyi[a]

Keywords: cyclodextrins, gas chromatography/mass spectrometry, supercritical fluid chromatography, micellar electrokinetic chromatography, capillary electrokinetic chromatography, countercurrent chromatography

The objectives of the reviews are the collection, concise description, comparison and evaluation of the various chromatographic technologies except liquid chromatography using natural and modified cyclodextrins for the increase the seperation capacity of various chromatographic separation systems.

*Corresponding author
E-Mail: szogyim@t-online.hu
[a] Research Center for Natural Sciences, Hungarian Academy of Sciences, Budapest, Hungary

Introduction

Chromatographic procedures were developed and successfully employed for the separation of a high number of organic and inorganic compounds present at trace level in complicated accompanying matrices. The capacity of chromatographic separation technologies can be increased by the modification of both the stationary and the mobile phase of the system. Because of their specific adsorption character cyclodextrins (CD) and cyclodextrin derivatives (CDs) have been frequently applied for the improvement of the separation parameters (mainly chiral separation capacity) of various chromatographic methods. The chiral separation capacity of cyclodextrins has been frequently exploited for the separation of enantiomers with markedly different biological activity employing CDs. CDs and CD derivatives can be equally used as additives of stationary phase or modifier of the mobile phase. The number of studies dealing with the application of CDs and CD derivatives for the increase of the separation capacity of chromatographic systems increased considerably. Because of their versatility CDs have found application in many special branch of chromatography such as liquid chromatography (LC), gas chromatography (GC), size exclusion chromatography (SEC), gel permeation chromatography (GPC), and electrically driven separation methods (CE, CZE), and ultra performance liquid chromatography (UPLC).

Application of cyclodextrins in gas chromatography/mass spectrometry

The newest results in the application of chiral capillary gas chromatography (GC) have been recently reviewed, the various phase development methodologies were shortly discussed and the efficacy of chiral GC and chiral HPLC were compared. Samples for the application of chiral GC are provided[1].

A rapid total analytical system (TAS) was developed for the detection of the autheticity of fruit-flavoured foods and beverages. The method combined headspace solid phase microextraction (HS-SPME) with enantioselective GC-MS (Es-GC-MS). The results were evaluated by multivariate mathemathical statistical methods such as principal component analysis (PCA) and hierarchical cluster analysis (HCA). Peach, coconut, apricot, raspberry, strawberry and melon were included in the experiments. Cyclodextrin derivatives served as chiral selectors, GC analyses were carried out on both normal and narrow bore columns. It was established that the analysis time of TAS method in markedly lower than that of the conventional analytical procedure.[2]

The concentration and enantiomeric distribution of linalool (3,7-dimethyl-1,6-octadien-3-ol) was determined in the raw and roasted cocoa beans (seeds of *Theobroma cacao*). Samples of cocoa beans, commercial products, cocoa powders and chocolates were included in the investigations. Enantioselective separations were achieved by using multidimensional gas chromatography, heptakis(2,3-di-O-methyl-6-O-tert-butyldimethylsilyl)-β-CD was the chiral stationary phase. Pre-concentration of the analyte was carried out by simultaneous steam distillation-extraction at pH 7.

The results indicated that the technological processes exert a negligible effect on the original enantiomeric distribution of linalool.[3]

Various GC techniques were developed and applied for the enantiomeric separation of DDT (1,1,1-trichloro-2,2-bis(p-chlorophenyl)ethane and its derivatives. The methods included heart-cut multidimensional GC (MDGC), and comprehensive two dimensional gas chromatography (GC x GC).

Chiral separations were carried out on a β-CD-based column. The measurements indicated that both method can be successfully employed for the enantiomeric separation of DDT and metabolites.[4]

HS-SPME followed with enantioselective GC/MS was applied for the analysis of enantiomeric and non-enantiomeric distribution of monoterpenes in the headspace of *Juniperus communis L*. and *Juniperus oxycedrus* needles and berries. The measurements indicated that the results obtained with the traditional hydrodistillation and HS-SPME techniques are commensurable. It was established that the

concentration of the monoterpenes in needles and berries of *J. Communis* were sabinene (19–30 %), α-pinene (12–24 %), β-myrcene (9–20 %). *J. oxycedrus* contained mainly α-pinene (85–92 %). The investigations revealed that the distribution of monoterpenes depended consideraly on both the type of analyte (needles or berries) and on its origine.[5]

In the last years a considerable number of studies were published dealing with the recent achievements in the synthesis of new mobile and stationary phases suitable for the enantiomeric separation of a wide variety of racemic compounds using electrophoretic techniques. An excellent review has been recently published enumerating and critically evaluating chiral selectors such as cyclic and linear oligo- and polysaccharides, branched polysaccharides, polymeric and monomeric surfactants, macrocyclic and other antibiotics, crown ethers etc. The advantages and disadvantages of the application of single chiral selector and dual-selector systems are also discussed in detail. The pharmaceutical and biomedical applications of the new methods have also been discussed in detail.[6]

The separation of enantiomers of norephedrine (NEP) by CE has been investigated in detail. The enantiomer migration order (EMO) was determined in the presence of various CD derivatives such as α-, β-CD, heptakis(2,3-di-O-acetyl-6-O-sulfo)-β-CD (HDAS-β-CD) and heptakis(2,3-di-O-methyl-6-O-sulfo-β-CD (HDMS-β-CD). It was concluded from the results of CE and MNR measurements that the complex formation of NEP different with different CDs and CDs derivatives.[7]

The extractability and possible toxicity of polycyclic aromatic hydrocarbons (PAHs) in river sediments was investigated in detail, the correlation between the extractabiliy of sediment contaminants, the chemodynamic properties of each extraction method and the resulting toxicity. Sediment samples were treated with various extraction procedures such as Soxhlet extraction with acetone (SOX), membrane dialysis extraction (MDE) with n-hexane. Ultrasonic extraction with acetone (USE), and extraction with (2-hydroxypropyl)-β-cyclodextrin, (HBCD). The PAH concentration of extract was determined with gas-chromatography/mass spectrometry. It was established that the extracting efficacy of SOX and MDE methods were comparable. HBCD technique extracted only 3.4 % of the total PAH content. It was further found that the efficacy of SOX and MDE were similar. USE showed activity between SOX and MDE. It was concluded from the results that these measurements may promote the better understanding of extraction procedures.[8]

Nanogels were preparated from cyclodextrins (γ-CD) or hydroxypropyl-β-cyclodextrin) (HP-β-CD) at a constant ratio of 20 %, w/w and their capacity as nanogels for drug delivery was investigated. The measurements indicated that the addition of ethyleneglycol diglicydil ether (EDGE) was important for the formation of nanogel. Infrared analysis (IR), transmission electron microscopy (TEM), dynamic light scattering (DLS) may help the exact determination of the cross-linking degree, size and size distribution of nanogels. Addition of hydroxypropyl methylcellulose (HPMC) influenced also the formation of nanogels.[9]

Heart-cut multidimensional GC (heart-cut MDGC) carried out on three capilllary columns based on β-cyclodextrin were employed for the simultaneous enantiomeric separation of polychlorinated biphenyls (PCBs).and metylsulfonyl metabolites of PCBs ($MeSO_2$-PCBs). The measurements established that the enantiomer separation capacity of columns shows considerable differences. The method has been successfully employed for the analysis of two fish oil and one cow liver samples.[10]

A new β-CD modified hyperbranched carbosilane GC stationary phase was developed by substituting the –OH group of β-CD by hyperbranched carbosilane. The preliminary investigations indicated that the new stationary phase can be successfully applied for the separation benzenes, acrylates, ketones and alkylchlorides.[11]

Mixed GC selectors were prepared by binding a single L-valine diamide moiety to permethylated β-CD. It was established that the enantiomer separation capacity of the new stationary phases is commensurable with those of commercial preparations. The enhanced enantioselectivity of the mixed electrodes was explained by the better chiral correspondance of the analytes.[12]

Chiral gas chromatography and HPLC were employed for the study the distribution and organoleptic impact of ethyl 2-hydroxy-4-methylpentanoate (ethyl DL-leucate) enantiomers in wine. GC measuremements were carried out using γ-CD in the stationary phase. It was established that white wines contained only the R form, whereas red wines contained both enantiomers. The ratio of R/S markedly depended on the aging. The R/S ratio was about 95:5, the average total concentration was 400 μg L^{-1}. The olfactory treshold for R and S enantiomer was different.[13]

New controlled release systems were developed for the delivery of essential oils. The interaction of CDs and β-cyclodextrin polymers with linalool and camphor in the essential oil of Lavandula angustifolia was investigated in detail. GC measurements were carried out by static headspace GC (SH-GC). Multiple headspace extraction method (MHE) was employed for the study of the application possibility of a new preparation controlled release system.[14]

The role of CDs and CD derivatives in the resolution of chiral natural compounds was reviewed. Besides CDs other chiral selectors such as crown ether, macrocyclic antibiotics, cellulose, have found application in the enantiomeric separation of various bioactive compounds. Thus, the optical isomers of ephedrine show different amphetamine-like stimulus effects, while (S)(α-ionone (woody-like taste) and (R)(-)-α-ionone (violet taste) show different olfactory characteristics. CDs and various CD derivatives have been successfully employed for the chiral separation of a considerable number of chiral natural compounds such as flavanones, alkaloids, lignans, coumarins, terpenoids, amino acids, peptides, etc. CDs have also been applied to enhance the separation efficacy of miscellaneous chromatographic technologies (GC, HPLC, CE, CZE).[15]

Volatile organic compounds (VOCs) were investigated in air samples using cyclodextrin-silica hybrid solid phase. The new samplers have been successfully employed for the

determination of benzene, toluene, ethylbenzene, o-xylene, m-xylene, and p-xylene (BTEX) in air. The recoveries were 89±4 %; 90±6 %; 91±2 %; 87.0±0.9 %; 88±4 %; and 88±4 %, respectively. The investigations indicated that the results obtained with the new method comparable with those obtained by the reference method.[16]

A new procedure was developed for the preconcentration and analysis of eight phenolic compounds in environmental water samples. SPE hyphenated with liquid-phase microextraction (LPME) based on solid organic drop combined with GC-MS was employed for the separation and quantitative determination of analytes. The purification of the samples was obtained by using a column containing 60 mg of β-CD-bonded silica particles as stationary phase. The optimal conditions of the procedure were: LOD = 0.002 – 0.04 μg L^{-1} (S/N=3); LOQ = 0.007 – 0.15 μg L^{-1} (S/N = 10); RSD = ≤ 9.5 %. The recoveries were over 79 %.[17]

Enantioselective GC-MS was employed for the investigation of volatiles and aroma-active compounds in honey bush (Cyclopia subternata). Samples were obtained by high-capacity headspace sample enrichment probe (SEP). GC-MS found total 183 compounds (103 terpenoids, 56 %). Samples were also analysed by gas chromatography olfactometry (GC-O). According to the GC-O assessors some compounds sowed typical honey bush like aroma: (6E,8Z)-megastigma-4,6,8-trien-3-one; 6E,8E-megastigma-4,6,8-triene-3-one; 10-epi-γ-eudesmol; epi-α-murolol; and epi-α-cadinol.[18]

A new CE technique was developed for the analysis of pantoprazole enantiomers employing sulfobutyl-β-cyclodextrin (SBA-β-CD) as chiral additive. The parameters of the method were optimized: the best separation was obtained by using a buffer of 50 mM borax – 150 mM phosphate, pH 6.5, 20 mg mL^{-1} SE-β-CD, and 10 kV voltage. The limit of detection (LOD) and limit of quantitation (LOQ) for R-(+)-pantoprazole were 0.9 and 2.5 μg mL^{-1}, respectively. It was established that the method is suitable for the analysis of a minimum limit of 0.1 % (w/w) of R-enantiomer in pantoprazole samples.[19]

Chiral separation of cathinone derivatives was obtained by applying various CD derivatives as chiral additives. A new and easy to carry out capillary zone electrophoresis (CZE) method was developed for the enantioseparation of 19 cathinone derivatives.CDs included in the investigations were: β- and γ-cyclodextrin, carboxymethyl-β-CD, 2-hydroxypropyl-β-CD, and sulfated-β-CD. Background electrolyte (BGE) using for the optimal separation of analytes consisted of 20 mg mL^{-1} sulfated-β-CD in 50 mM ammonium acetate buffer pH 4.5 containing 10 % v/v acetonitrile. Separations were carried out at 40 ^{0}C with a separation voltage of 20 kV.[20]

A novel CZE technology was developed for the separation and quantitative determination of flavonoids in traditional Chinese medicines. The optimal condition were: background electrolyte of 20 mM borax (pH 7.5), 6 mM β-CD and 20 % (v/v) acetonitrile. Injection time was 65 s. Detection limits for five flavonoids were between 15 – 30 ng/mL. The method was successfully applied for the analysis of traditional Chinese medicine real samples[21].

It was found that neutral and acidic monosaccharide components in *Ganoderma lucidum* polysaccharide can be easily labeled with 2,3-naphtalenediamine and the saccharide-naphimidazole (NAIM) derivatives can be analysed by CE using borate buffer. Sulfated-α-CD can be used as chiral selector. The method was proposed for the analysis of natural carbohydrates by CE.[22]

HPLC and electronic microscopy was employed for the study of the influence of HP-β-CD-PLGA nanoparticles on the bioavailability and the penetration of puerarin. The measurements indicated that the complex formation of puerarin with HP-β-CD-PLGA enhance the therapeutic effect on brain ischemia-reperfusion injury in rats. The drug release kinetics and nanoparticle degradation in phosphate buffered saline (PBS) was investigated in detail. It was concluded from the data that complex formation decreased the infraction volume, therefore, the complex formation is potentially applicable for the brain injura induced by ischemic-reperfusion.[23]

Stir bar sorptive extraction (SBSE) followed by HPLC-UV detection was used for the analysis of estrogens in pork and chicken samples. Poly(dimethylsiloxane)(PDMS)/β-cyclodextrin(β-CD)/divinylbenzene-coated stir bar was prepared by the sol gel technique and used for the SBSE followed with HPLC-UV. The enrichment factor was 19 – 51-fold. The relative standard deviations ranged from 6.0 % to 9.7 %. It was stated that the method is simple, sensitive, and selective and can be successfully applied for the determination of estrogens in pork and chicken samples.[24]

The interaction of the phosphatidyl ethanolamine (PE) of *Heliobacter pilori* with free cholesterol (FC), cholesterol ester (CE), 2,6-di-O-methyl-β-cyclodextrin (dM-β-CD) was established. GC/MS and LC/MS analyses established that the composition of PEs produced by *Heliobacter pilori* and *Escherichia coli* shows marked differences. It was concluded from the results that PE is a key kandidate of nonesterified steroid-binding lipids in *H. pilori*.[25]

Methyl-β-cyclodextrin (MCD) was employed for the extraction and purification of prenylated proteins. It was established that MCD can be successfully employed as a selective for such exptraction procedures. The enzyme was further purified by one-step anion-exchange column chromatography and affinity column chromatography. The measurements suggested that MCD can be easily applied as a useful compound for selective extraction and purification of prenylated periferial membrane proteins from the cytoplasmic surface of biological membranes.[26]

Supercritical fluid chromatography (SFC) has also found application in the chromatographic analysis of various organic and inorganic compounds. Cationic β-cyclodextrin perphenylcarbamoylated derivatives were chemically bonded into vinylized silica. The product was applied as chiral stationary phase in SFC. The enantiomeric separation capacity of the new stationary phase was demonstrated on 14 racemates including flavanones, thiazides, and amino acid derivatives. It was concluded from the data that aromatic cationic moiety on β-CD enhanced the enantiomeric separation capacity compared with aliphatic cationic moiety. It was further established that the presence of acid additives results in lower retention time but can improve chiral resolution.[27]

The application of SFC for the enantiomeric separation, for the simultaneous chiral and achiral separation, impurity control and direct scaling has been recently reviewed. The advantages of SFC technique (fast analysis speed, wide polarity compatibility, lower cost of the mobile phase and high column efficiency) make SFC a method of choice for the analysis of chiral and achiral analytes.[28]

A sliding graft copolymer with grafted (polyethylene glycol) side chains by the „grafting onto" strategy was prepared. The end product contained PEG and CDs, and was characterized by ^{1}H NMR, Fourier-transformed infrared and gel permeation chromatography.[29]

High molecular weight polyrotaxanes (PRs) were prepared from poly(ethylene glycol) and α-CD. The end product was investigated by ^{1}H NMR spectroscopy, wide angle X-ray diffraction and gel-permeation chromatography.[30]

Size-exclusion chromatography was employed for the study of the size stabilization of Au nanoparticles in the presence of salt and organic solvents. The results indicated that 3α-amino-3α-deoxy-(2αS,3αS)-β-cyclodextrin is a good stabilizer for the Au nanoparticles.[31]

The antimicrobial effect of isothiocyanate (AIT) complexed with α- and β-cyclodextrins was investigated. Solid phase microextraction followed by gas chromatography was employed for the determination of the concentration of AIT in samples. The measurements indicated that the inclusion complexes showed more pronounced antimicrobial effect than the uncomplexed compounds. The method was proposed for the antimicrobial treatment of fresh-cut vegetable products.[32]

The enantiomeric separation capacity of some β-dextrin-based chiral stationary phases was compared using structurally different analytes as model compounds (coumarins, dansyl amino acids and propionic acid derivatives). The separation capacity of β-cyclodextrin, (R,S)-2-hydroxypropyl-β-cyclodextrin, and permethyl-β-cyclodextrin-based CPs were compared. Measurements were carried out in reversed phase separation mode, the mobile phase consisted of 0.1 % triethylammonium phosphate (pH 3.5)/MeOH. It was found that the best enantiomeric separations can be achieved on permethyl-β-cyclodextrin stationary phase.[33]

The inclusion complexes of warfarin enantiomers with permethylated monoamino-β-cyclodextrin (PMMABCD) was investigated with CE and ^{1}H NMR spectroscopy. It was established that the pH of the mobile phase exert a marked impact of the mobility of the complex[34].

The inclusion complex formation of isomeric monoterpenes, camphene and fenchene with β-cyclodextrin was employed for facilitate their separation. It was established that the analytes can be easily separated using re-crystallization. The structure of the inclusion complexes was investigated by ^{1}H NMR and X-ray diffraction.[35]

The application of fully or partially sub-2 μm porous silica material as column packing has been recently discussed. Its application in liquid chromatography, ultra high speed chromatography and capillary electrochromatography (CEC) is discussed in detail.[36]

CE and proton nuclear magnetic resonance spectroscopy (^{1}H-NMR) were employed for the separation of the enantiomers of sibutramine applying cyclodextrin (CD) derivatives as chiral selectors. The method of separation included 50 mM of phosphate buffer of pH 3.0 with 10 mM of methyl-β-cyclodextrin (M-β-CD);0.05 % of LOD and 0.2 % of LOQ. The method was validated and applied successfully for the separation of sibutramine enantiomers in commercial preparations.[37]

Bodypy-F1-labeled glycophosphingolipids were separated using capillary elctrophoresis and laser- induced fluorescence detection. Analytes were prepared by acylation using the N-hydroxysuccinimide ester of Bodypy-F1. Micellar electrokinetik capillary chromatography was employed for the separation of analytes. The measurements indicated that the separation capacity of TRIS/CHES/SDS/α-cyclodextrin buffer was better than that of the traditional borate/deoxycholate/methyl-β-cyclodextrin buffer. The theoretical plate number ranged from 640.000 to 741.000. The LOD was approximately 3 pM, the analysis time was lower than 5 min.[38]

A new validated capillary electrophoresis method was developed and successfully applied for the separation of dapoxetine enantiomers. Dapoxetine, a serotonin transporter inhibitor is employed for the treatment of premature ejaculation. CZE measurements were carried out in uncoated fused-silica capillary. Preliminary investigations indicated that randomly methylated γ-cyclodextrin was the best chiral selector. The optimal parameters of the enantioseparation were: 15 ^{0}C; +15 kV; 70 mM acetate; 20 v/v MetOH; pH, 4.5; and 3 mM methylated γ-CD. The optimal resolution was 7.01.

The validation parameters of the method such as repeatability, linearity range, LOD, LOQ, accuracy and robusness were also determined[39].

The enantiomeric impurities of armodafinil was investigated with a new CE method using sulfobutyl –ether-β-cyclodextrin as chiral selector. The best separation 3.3 was obtained by employing 20 mM phoshate buffer (pH 7.5). The concentration of the chiral selector was 20 mM. The LOD and LOQ of (S)-modafinil were 1.25 μg mL^{-1} and 2.50 μg mL^{-1}, respectively. It was established that the method display good selectivity, repeatabiliy, linearity and accuracy, and can be applied for the investigation of the enantiomeric impurity of armodafinil in bulk samples[40].

A CE method was developed using electrokinetic injection to simplify the dissolution testing of amoxicillin capsules. The electroforetic parameters were: 2-[4-(2-hydroxyethyl)piperazin-1-yl]ethanesulfonic acid (HEPES) buffer (pH 7.1; 200 mM containing 30 % acetonitrile and 10 % β-CD. Samples were injected employing electrokinetic injection (5 kV, for 100·s). Separations were achieved at positive polarity mode of 25 kV at 30 ^{0}C. The validation parameters such as linearity, precision, accuracy, selectivity, and sensitivity of the method were also determined.[41]

CE was employed for the enantiomeric separation of five β-antagonists using carboxymethyl-β-cyclodextrins as chiral-selector. The impact of various chromatographic parameters on the efficacy of the chiral separation was investigated in detail (the type and concentration of chiral selector, pH, composition of the background electrolyte, capillary temperature, applied voltage, and the length of capillary). The results indicated that the type and concentration of chiral selector as well as the pH exert the highest impact on the enantioselectivity. The optimal separation parameters were: 50 mM phosphoric acid containing 10 mM CM-β-CD at pH 3.5 in a capillary of 48.5 cm x 75 pM (40 cm effective length). The temperature of the uncoated capillary was 15 ^{0}C, the applied voltage was 20 kV.[42]

Micellar electrokinetic chromatography was employed for the separation of the immunosupressive drug cyclosporin A (CyA) from its impurities (cyclosporin H) and isocyclosporin). The best separation was obtained by 50 mM sodium dodecyl sulfate (SDS) in 51 mM tetraborate buffer (pH 9.2) suplemented with 15 mM TM-β-cyclodextrin (heptakis(2,3,6-tri-O-methyl)-β-cyclodextrin TM-β-CD. The temperature of the capillary was 30 ^{0}C, the running voltage 22 kV. Analyses were carried out in a fused silica capillary 50 μm i.d. x 64.5 cm total length, 56 cm to the detector. The method was validated for linearity, sensitivity, accuracy and precision. It was stated that the method can be used for the analysis of commercial available pharmaceuticals (gelatin capsules).[43]

New CD derivatives were synhesized and their enantiomeric separation capacity was assessed and compared. CD derivatives were prepared by anchoring various alkyl chain spaced imidazolium and ammonium sidearm onto the CD primary ring. The measurements indicated that these derivatives can be applied as selectors in the enantiomeric separation of amino acids and acidic racemated in aqueous capillary electrophoresis.[44]

Enantioselective capillary electrophoresis-laser-induced fluorescence (CE-LIF) technology was developed and successfully applied for the determination of D-ser in cellulose matrices. The method included derivatization with FITC followed with CE-LIF. Separations were carried out in borate buffer (80 mM, pH 9.3). The enantioselectivity (D-Serine, L-Serine) was 1.03, the resolution (R-s), 1.37. Linearity ranged from 0.025 to 100.00 mM. The method was employed for the separation of D-and L serine in various cell lines.[45]

The charge state distribution of randomly sulfated cyclodextrins (CDs) and single isomer cyclodetrins was investigated employing hydrophilic intercation liquid chromatography (HILIC). Analyses were carried out on cross-linked diol phase and on unbonded silica stationary phase. Sulfated cyclodextrins with different charge states were separated from each other. Randomly sulfated CDs showed wide charge and regioisomer distribution while HILIC investigations indicated the presence of a single species.[46]

A field-amplified sample stacking (FASS) method combined with capillary zone electrophoresis (CZE) was employed for the separation and quantitative determination of ambroxol hydrochloride in human plasma. Preconcentration was carried out with liquid-liquid extraction. Analytes were separated in a fused-silica capillary (31.2 cm x 75 μm), applied voltage was 15 kV. BGE consisted of 6.25 mM borate – 25 mM phosphate (pH 3.0) containing 1 mM β-cyclodextrin. Analytes were detected at 210 nm. The following validation parameters of the method were determined: stability, specificity, linearity, lower limit of quantitation, accuracy, precision, extraction recovery, and robustness. The caibration was linear between 2 – 500 ng mL^{-1}. The intra- and interday precisions of the lower limit of quantitation (LLOQ) were 9.61 and 11.80 %, respectively. The technique was used for the pharmacological study of ambroxol hydrochloride tables in 12 healthy volunteers.[47]

A capillary zone electrophoresis method was developed for the analysis of lavonoids in traditional Chinese medicines. The separation capacity of the technique was markedly enhanced by adding β-cyclodextrin to the background electrolyte. The optimal conditions for the separation were: 20 mM borax, (pH 7.5), 6 mM β-cyclodextrin and 20 % v/v acetonitrile, injection time 65 s. Detection limits for the analytes ranged 15-30 ng mL^{-1}. It was established that the technique can be applied for the investigation of traditional Chinese medicin real samples.[48]

It was found that the separation on microchip shod marked advantageous characters such as high efficacy, increased throughput, reduced quantitites of hazardous materials, cost saving, relatively easy instrumentation, improved portability, etc. Micellar electrokinetic chromatography (MEKC) carried out on polydimethylsiloxane microchip was employed for the separation and quantitative determination of three phenolic xenoestrogens such as octylphenol (OP), 4-nonylphenol (4-NP), bisphenol A BPA). Xenoestrogens were detected with amperometric method and were baseline separated in 55 s. Borate running buffer (8.0) contained sodium dodecyl sulfate and β-cyclodextrin. The linear range for OP, 4-NP, and BPA are 20-1.000, 15-1.000 and 20-1.000 μg L^{-1}. The detection limits were 5.0, 4.0, and 3.0 μg L^{-1}, respectively. The recoveries were between 90.2 and 109.4 %.[49]

The capacity of three methods, affinity capillary electrophoresis mass spectrometry (ACE-MS), affinity capillary electrophoresis UV detection (ACE-UV) and direct infusion mass spectrometry (DIMS) were compared for the determination of the affinity of some bioactive compounds with β-cyclodextrin. Compounds included in the investigations were: ibuprofen, s-flurbiprofen, diclofenac, phenylbutazone, naproxen, folic acid, resveratrol, and 4,4'-propane-1,3-diyl)dibenzoic acid. It was stated that the ACE-MS method is suitable to interact, separate, and rapidly scan for the simultaneous affinity of multiple interacting pairs.[50]

A chiral capillary electrophoretic method was developed for the analysis of dl-penicillamine. The cost effective neutral β-cyclodextrin was employed as chiral selector. The baseline separation of dl-penicillamine was achieved in the pH range of 2.0 – pH 10. The range or linear calibration curves were: 8.568.56 x 102 μg mL^{-1} (pH 4.5), and 8.561 x 103 μg mL^{-1} (pH 4.5; pH 7.4 and pH 9.7). The correlation coefficients were in each case 0.999. The limit of detections

were 2.58 μg mL^{-1} in acidic and neutral conditions and 1.40 μg mL^{-1} in alkaline conditions. Recoveries varied from 93.1 to 105 %.

It was suggested that the method can be employed for the investigation of other chiral amines or amino acids.[51]

A new cationic cyclodextrin, mono-6(A)-(3-methoxypropan-1-ammonium)-6(A)-β-cyclodextrin was synthesized and applied as chiral selector in CE. The new cyclodextrin derivative has three recognition sites such as β-CD, ammonium cation and methoxy group on the sidearm to contribute three corresponding driving forces (inclusion complexation, electrostatic interaction and hydrogen bonding). It was established that the new CD derivative shows excellent enantioseparation capacity for a wide range of acidic and ampholytic racemates. It was assumed that the method can be applied for the synthesis of new host-guest complexes for practical application.[52]

A new method was developed to enhance the sensitivity of enantiomeric capillary electrophoresis. The method applied large-volume stacking with electroosmotic flow pump. It was established that the sensitivity of the method can be enhanced by adding cyclodextrin to the mobile phase. It was found that the addition of CD to the system increased considerably the enantiomeric separation capacity of the CE method employed. It was further found that the procedure can be used for the investigation of real samples containing a large amount of unnecessary background salt.[53]

The application of 1-adamantanecarboxylate for the desorption of elutes retained on a CD bonded silica was investigated in detail. Solid phase extraction followed with micellar electrokinetic chromatography was employed for the analysis of 4-tert-butylphenol and 2,2-di(4-hydroxyphenyl)propane. It was found that the desorption capacity of 1-adamantanecorboxylate was higher than that of traditional desorption agents.[54]

A new positively charged monolithic stationary phase was developed and applied for the chiral separation of acidic compounds. The new monolithic stationary phase was prepared by incorporating vinylbenzyl trimethylammonium (VBTA) as a positively charged achiral co-monomer to glycydyl methacrylate-β-cyclodextrin (GMA/β-CD). The characteristics of the monomer were investigated by scanning electron microscopy, optical microscopy, pressure drop/flow-rate curves and nitrogen adsorption analysis. The system was optimized, and the separation of 41 pairs of structurally different anionic chiral analytes was obtained. It was established that the separation capacity of the new monolithic was superior to that of similar traditional monolithic stationary phases. It was further established that the combination of the new monolitic column with capillary electrochromatography-mass spectrometry enhanced considerably the enantiomeric separation efficacy of the system. It was further found that the application of triple quadrupole MS system further increased the performance of the CEC-MS method.[55]

Chemometric techniques were employed for the optimization of the efficacy of cyclodextrin-modified micellar electrokinetic chromatography using head column field amplified sample stacking for the analysis of the acid metabolites of the lipoxygenase pathways in human polymorphonuclear leukocytes. The following compounds were included in the investigation: leukotriene B-4, 6-trans-12-epi-leukotriene B-4, 5(S)-hydroxy-6-trans-8,11,14-cis-eicosatetraenoic acid, 12(S)-hydroxy-6-trans-8,11,14-cis-eicosatetraenoic acid, and 15(S)-hydroxy-6-trans-8,11,14-cis-eicosatetraenoic acid. The optimum MEC conditions were: 80 mM sodium borate buffer, pH 10.7, containing 16.6 mM sodium dodecil sulfate and 15 mM α-cyclodextrin. The separation voltage was 12.5 kV, the column temperature 23^0C. The limits of quantification ranged from 30 to 50 ng mL^{-1}, and the limits of detections were between 10 and 17 ng mL^{-1}. It was stated that the method is suitable for the determination of various arachidonic acid metabolites produced by cells and can be applied for the investigation of lipoxygenase inhibitors.[56]

High performance capillary electrophoresis HPCE) was employed for the separation and quantitative determination of free amino acids during fermentation of Bacillus subtilis. Before measurements amino acidc were derivatized with phenylisothiocianate. The optimal analytical system consisted of 30 mM phosphate and 3 mM β-cyclodextrin at pH 7.0. The separation voltage was 20 kV, the detection wavelength 254 nm. It was established that the separation capacity of the method was comensurable with those obtained with the traditional methods using ninhydrin.[57]

The including complex formation between cyclodextrins and polyphenols was investigated by capillary electrokinetic chromatography. Polyphenols included in the experiments were trans-resveratrol, astilbin, taxifolin, ferulic acid and syringic acid. The binding constants were calculated based on the effective electrophoretic mobility of guest molecules. The results indicated that the complex formation depends considerably on the sterical correspondence between the host and guest molecules. It was further established that the complexation procedure is enthalpy-controlled and Van der Waals force and release of high-enthalpy water molecules play a marked role in the formation of inclusion complexes.[58]

Chiral separation and determination of excitory amino acids was carried out using CE followed laser induced fluorescence detection. Analytes were derivatized with 4-fluoro-7-nitro-2,1,3-benzoxadiazol and the enantiomers were separated by CE. The enantiomeric separation capacity was enhanced by adding two CD derivatives to the background electrolite. It was found that the system separated both Asp and glutamated enantiomers. The LOD was 17 and 9 nM, respectively, the LOQ was 50 nM for both analites. It was concluded from the data that the method is suitable for the analysis of excitatory amino acids in brain samples.[59]

The analysis of antimalaries has also been reviewed. The review discuss the capillary electrophoresis methods with special emphasis on chiral separation methods. A considerable number of chiral selectors were employed for the enantiomeric separation of antimalarials such as oligosaccharides (cyclodextrins, oligomaltoclextrins), neutral (amylose, dextrin and dextran) and charged (chondroitin sulfate, heparin, dextransulfate), polysaccharides, and proteins. However, in some cases micellar electrokinetic capillary chromatography or non aqueous CE can be applied for the enantiomeric separation

of antimalarials without using chiral selector in the mobile phase. Moreover, the review discuss the quantitative application of CE in the analysis of antimalarias in biological and food matrices.[60]

Cyclodextrin modified CE was employed for the separation and quantitative determination of hydroxy acids in cosmetics. The method was developed by chemometric techniques using phosphate concentration, surfactant concentration and methanol percentages as variables. The optimal analytical conditions were: running buffer of 150 mM phosphate solution (pH 7) containing 0.5 mM CTAB, 3 mM γ-CD, 25 % methanol, 20 s sample injection, and UV detection at 200 nm at 0.5 psi, separation voltage was -0.1V kV. The temperature was 25^{0}C. The LOD (S/N = 3) was 625 nM both salicylic acid and mandelic acid. The correlation coefficient was over 0.998, the RSD and relative error were lower than 9.21 %. The method was successfully applied to several commercial cosmetic products.[61]

Microwave-assisted extraction followed with capillary electrophoresis was employed for the determination of eight isoquinoline alkaloids in Chelidonium majus L. Both the parameters of MAE and CE were optimized: optimal MAE extraction was carried out at 60^{0}C, 5 min, extracting agent being methanol:water:HCL in ratios of 90:10:0.5 v/v/v. Optimal composition of BGE consisted of 500 mM Tris-H3PO4 bufffer (pH 2.5) containing 50 % methanol and 2 mM HP-β-cyclodextrin. It was stated that the solvent consumption and analysis time of the new method is superior comparing with the traditional methods.[62]

Capillary electrophoresis was employed for the separation of repaglinide enantiomers in pharmaceutical formulations using 2,6-di-O-methyl-β-cyclodextrin (DM-β-CD) as chiral selector. The optimal conditions of the analysis were: UV detection at 243 nm, separation voltage 20 kV, BGE 1.25 % (w/v) in 20 mM sodium phosphate (pH 2.5). The linear caibration curve was 12.5 – 400 μg mL^{-1}. LOD was 100 ng mL^{-1}, the intra-day and inter-day precisions were 2.8 ad 3.2 %, respectively. Recoveries ranged from 97.7 to 100.9 %. It was established that the method is fast and convenient and can be used for the determination of repaglinide enantiomers in quality control of pharmaceutical product.[63]

The enantioseparation of lipoic acid an antioxidant in dietary supplements was obtained by using CE and trimethyl-β-cyclodextrin as chiral selector. Analyses were carried out in sulfonated capillary with the effective voltage of +18 kV and at the detection wavelegth at 200 nm. The best separation was achieved with BGE 100 mM phosphate buffer (pH 7.0) containing 8 mM trimethyl-β-cyclodextrin. Analyses were carried out at 20^{0}C. It was established that the method is suitable for the determination of lipoic acid in dietary supplements.[64]

A RP-HPLC procedure was developed for the separation and quantitative determination of resibufogenin and cinofufagin. The infuence of the nature of organic solvent and cyclodextrins, the concentration of γ-CD, the temperature of the separation on the separation efficacy of the system was investigated in detail. It was assumed that the influence of CD on the retention may be due to the formation of inclusion complexes between the analytes and the cyclodextrin. It was found that CD forms 1:1 inclusion complexes with the analytes resulting in modified retention behaviour. The investigations indicated that the complex formation is spontaneous, exotherm, and enthalpy driven. It was further found that the method can be applied for the analysis of resibufogenin and cinobufagin in different Chansu (Bufonis venenum) samples.[65]

It was found that neutral and acidic monosaccharides are readiliy labeled with 2,3-naphtalenediamine and the resulting saccharide-naphthimidazole derivatives (NAIM) can be separated by CE in borate buffer. Enantiomeric separations were obtained by using sulfated-α-cyclodextrin as chiral selector in phosphate buffer. The method allowed the simultaneous determination of absolut configuration and sugar composition in the mucilage polysaccharide of the medicinal herb Dendrobium huoshanense. It was also established that heparin disaccharides can be successfully derived with the method, however, heparin derivatives with the same degree of sulfation cannot be separated by CE.[66]

A capillary electrophoretic techniqe was developed and applied for the separation of flavonoids by β-cyclodextrin modified CE. The optimal separation conditions were: background electrolite 20 mM borax (pH 7.5) containing 6 mM β-cyclodextrin and 20 % acetonitrile. Injection time was 65 s. Detection limit for five flavonoids ranged 15-30 ng mL^{-1}. It was found that the procedure can be successfully employed for the determination of flavonoids in traditional Chinese medicine real samples.[67]

The chiral selectors applied recently in HPLC and CE have been reiewed and the importance of chiral separations in human healthy care, biophysics, biochemistry and other up to date field of scientific research is emphasized. The review lists the most important chiral selectors and chiral stationary phases reported in the last years.[68]

Rotational electromagnetic stirring, rotating evaporation, differential scanning calorimetry, fourier-transform infrared spectroscopy, X-ray powder diffractometry, scanning electron microscopy and HPLC methods were employed for the preparation and investigation of the quercetin/hydroxypropyl-β-cyclodextrin 1:1 inclusion complex. The objectives of the investigations were the increase of the water solubility of quercetin. The investigations revealed that the complex formation improved six times the water solubility of quercetin.[69]

A cyclodextrin-modified capillary electrophoretic method was developed for the enantiomeric separation of cathinone derivatives. The influence of various components of the CE separation system was investigated in detail. Native-β-CD, carboxymethyl-β-CD, hydroxypropyl-β-CD, sulfated-β-CD were included in the investigation. The results indicated that the best enantioselectivity can be obtained by using negatively charged sulfated-β-CD as chiral selector. The optimal CE conditions were: 20 mg mL^{-1} sulfated-β-CD in 50 mM ammonium acetate buffer (pH 4.5) containing 10 % ACN at a cassette temperature of 40 ^{0}C, and at 20 kV. It was established that a set of 19 cathinone derivatives (except methedrone) were enantioseparated by the CE method.[70]

Pantoprazole enantiomers were separated using CE and sulfobutylether-β-cyclodextrin (SBE-β-CD) chiral additive. The procedure was optimized and the best separation system

was applied for the analyses. BGE consisted of 50 mM borax-150 mM phosphate (pH 6.5), 20 mg mL^{-1} SBE-β-CD, and 10 kV applied voltage. The LOD and LOQ were for R-(+)-pantoprazole 0.9 and 2.9 μg mL^{-1}, respectively. It was stated that the method can be applied for the determination a minimum limit of 0.1 % (w/w) of R-enantiomer in-S-pantoprazole bulk samples.[71]

Countercurrent chromatography has been employed for the separation of the three main α-acids present in the extract of commercially available hops (*Humulus lupulus L.*). The extract contain individual isomerized α-acid (co-, n-, and ad-) in addition to cis/trans diastereomers for each congener. The first step of separation was carried out using hexane and aqueous buffer. The second step was suitable for the separation of cis/trans diastereomers and applied quaternary solvent system. It was established that the presence of β-cyclodextrin enhanced the separation capacity of the system. It was further established that the purity of the end products (individual α-acids, iso α-acids, individual tetrahydro isomerized α-acids) was in each case over 95 %). It was found that the composition of the mobil phases, pH and buffer-to-sample ratio influence considerably the efficacy of the separation.[72]

The influence of α-, β-, and γ-cyclodextrins on the CE migration time of 11 guanidine/imidazoline derivatives, and imidazoline receptor ligands was investigated in detail. The data were evaluated by performed quantitative structure-mobility relationship (QSMR) method. The calculations indicated that the QSMR calculation method can be successfully employed as an initial screening predictive tool for CE migration behaviour of other related guanidine/imidazoline derivatives in the presence of native cyclodextrins.[73]

The recent developments in the synthesis and application of new cyclodextrin derivatives has also been reviewed, and their application in chromatographic separation processes has been discussed. The new results obtained in liquid chromatography (LC), capillary electrochromatography (CEC), gas chromatography and supercritical fluid chromatography (SFC). The use of open tubular CEC (OT-CEC), paked bed-CEC (P-CEC), pseudostationary phase CEC (PSP-CEC) has been discussed in detail.[74]

Electromembrane extraction followed by cyclodextrin-modified capillary electrophoresis was employed for the preconcentration and quantitative analysis of trimipramine (TPM) enantiomers in biological matrices. TPM enantiomers migrated through a thin layer of 2-nitrophenyl octyl ether (NPOE). Response surface technology (RSM) was applied for the optimization of different variables. The optimal conditions were NPOE as supported liquid membrane, inter-electrode distance of 5 mm, stirring rate 1000 rpm, 51 V, potential difference, 34 min extraction time, acceptor phase pH 1.0 and donor phase pH 4.5. BGE consisted of 100 mM phosphate buffer (pH 2.0) containing 10 mM α-CD as chiral selector. The applied voltage was 18 kV, the temperature 20 ^{0}C. The range of quantitation was 20 - 500 ng mL^{-1}. The intra- and interday RSDs (n=6) were <6 % for both enantiomers. LOQ and LOD were 20 and 7 ng mL^{-1}, respectively. It was stated that the procedure can be applied for the determination of the concentration of TPM enantiomers in plasma and urine samples without any pre-treatment.[75]

Achiral ionic liquid, DM-β-CD and TM-β-CD were employed for the enantioseparation of three β-blockers such as PIN, OX and PRO. Good separation was achieved by using dual CDs containing DM-b-CD and TM-β-CD. The investigations indicated that under optimal conditions the detection limit of the enantiomer pairs ranged from 0.10 to 0.65 nM. It was further established that the procedure can be successfully applied for the determination of this class of β-blockers in spiked usine samples with acceptable recoveries.[76]

A novel stacking method of repetitive large volume sample injection followed with sweeping micellar electrokinetic chromatography (MEKC) was employed for the determination of androgenic steroids in urine. Testosterone (T), epitestosterone (E), and epitestosterone glucuronide (EG) were included in the experiments. A phosphate buffer was filled into an uncoated fused silica capillary, the samples were injected into the capillary at 10 psi for 20 s then stacked at -10 kV for 1 min using phosphate buffer containing SDS. Injecting and stacking steps were repeated five times. Separation was carried out at -20 kV, the buffer contained methanol, SDS and (2-hydroxypropyl)-β-cyclodextrin. Analytes were detected at 254 nm. The linearity range was 5 – 200 ng mL^{-1} for T; 20 – 200 ng mL^{-1} for E; 0.5 – 500 ng mL^{-1} for EG. LODs were 1.0 ng mL^{-1} for T; 5.0 ng mL^{-1} for E; and 200.0 pg mL^{-1} for EG. RSD values in intra-day (n=3) and inter-day measurements (n=5) were below 10.0 %. It was stated that the method can be applied for monitoring of doping by sportsmen.[77]

Cyclodextrin-modified micellar electrokinetic chromatography was employed for the chiral separation of the four stereoisomers of vinpocetine in separation time of 9.5 min and resolution of 1.043.87, 2-hydroxy-β-cyclodextrin was applied as chiral selector. Enantiomer separation was carried out in buffer of 40 mM HP-β-CD in 50 mM phosphate buffer containing 40 mM SDS. The separation temperature was 25 ^{0}C, the separation voltage 25 kV.[78]

Fat soluble isoquinoline enantiomers were separated by employing β-cyclodextrin-modified micellar capillary electrokinetic chromatography. The enantioselective separation of 1-phenyl-R,S-tetrahydroisoquinoline (ER,ES). Electrochemical detection (EC) was applied for the determination of analytes. An effectual micellar suspension of 35 ml L^{-1} phosphate buffer saline (pH 7.85) containing 30 mM sodium desoxycholate, 20 mM β-CD and 20 % (v/v) acetonitrile formed the running buffer. Analytes were baseline separated in 12 min, separation voltage was 20 kV. The RSD (=5) of migration time and peak areas are 2.3 % (ER), 2.7 % (ES), 2.0 % (ER) %, 3.5 % (ES). LODs were 0.5 μmol L^{-1} for ER and 0.2 μg L^{-1} for ES. The method has been successfully applied for the determination of ER from ES in synthetic drug intermediate.[79]

A double junction interface was employed for the reservation of separation efficacy and for the alleviation of ion suppression from sulfated β-cyclodextrin (S-β-CD) in electrokinetic chromatography-electrospray ionization-mass spectrometry. The good separation capacity of the novel system was verified in the analysis of dihydroxyphenylalanin and methyldihydroxyphenylalanine. Enantiomers were separated either (counter-migration mode;

0.1 % S-β-CD) or carrier mode (2 % S-β-CD). It was found that no ion suppression was observed during the analysis, and the sensitivity of the method was improved considerably.[80]

Chemically bonded cationic β-cyclodextrin derivatives were employed as chiral stationary phase for the enantioseparation of aromatic compounds and pharmaceuticals. Vinylene-functionalyzed cationic β-cyclodextrins were co-polymerized with vinylzed silica in the presence of conjugated monomers. The chemically immobilized cationic β-cyclodextrins were employed as chiral stationary phases in packed column supercritical fluid chromatography. The good separation characteristics of the new chiral stationary phases was verified.[81]

Abbreviations

ACE-MS = affinity capillary electrophoresis mass spectrometry
ACN = acetonitrile
AIT = isothiocyanate
BGE = bacground electrolyte
BPA = bisphenol A
CD-CSPs = cyclodextrin chiral stationary phases
CEC = capillary electrochromatography
CE-LIF = capillary electrophoresis-laser induced fluorescence
CZE = capillary zone electrophoresis
DIMS = direct infusion mass spectrometry
EDGE = ethylenegycol diglicidyl ether
DLS = dynamic light scattering
EKC = electrokinetic chromatography
EMO = enantiomeric migration order
E = epitestosterone
EG = epitestosterone glucuronide
Es-GC-MS = enantioselective GC-MS
FASS = field-amplified sample stacking
FC = free cholesterol
GCxGC=comprehensive two dimensional gas chromatography
GC/MS = gas chromatography/mass spectrometry
GMA = glycidyl methacrylate
HCA = hierarchical cluster analysis
H-DAS-β-CD= heptakis(2,3-di-O-acetyl-6-O-sulfo)-β-CD
H-DMS-β-CD = heptakis(2,3-di-O-methyl-6-sulfo)-β-CD
HEPES=hydroxypropyl-β-2-[4-(2-hydroxyethyl)pipera-zin-1-yl]ethanesulfonic acid
HRE = heat reflux extraction
HILIC = hydrophic interaction liquid chromatography
HPCE = high performance capillary electrophoresis
HPMC = hydroxypropyl methylcellulose
HRE = heat reflux extraction
HSA = human serum albumin
HS-SPME = headspace solid phase microextraction
LD = liquid desorption
LLE = liquid-liquid extraction
LOD = limit of detection
LLOQ = lowest limit of quantitation
LOQ = limit of quantitation
LVSEP = large volume sample stacking
MAE = microwave-assisted extraction
MD = in vivo microdialysis sampling
MDGC = heart-cut multidimensional gas cromatography
MDE = membrane dialysis extraction
MDMA = 3,4-methylenedioxymethamphetamine
MHE = multiple headspace extraction
MEKC = micellar electrokinetic chromatography
MAE = microwave-assisted extraction
NAIM = saccharide-naphthimidazole derivatives
NEP = norephedrine
4-NP = 4-nonylphenol
NPOE = 2-nitrophenyl octyl ether
OP = octylphenol
OT-CEC = open tubular CEC
PCA = principal component analysis
p-CEC = packed-bed CEC
PE = phosphatidylethanolamine
PEG = polyethylene glycol
PMMABCD = permethylated momoamino-β-cyclodextrin
psp-CEC = pseudostationary CEC
QSMR = quantitative structure-mobility relationship
RSM = response surface methodology
SBE-β-CD = sulfobutylether-β-cyclodextrin
SBSE = stir bar sorptive extraction
SDS = sodium dodecyl sulfate
SEP = high capacity headspace sample enrichment probe
SFC = supercritical fluid chromatography
SOX = Soxhlet extraction with acetone
SH-GC = static headspace gas chromatography
SBE-β-CD = sulfobutylether-β-cyclodextrin
TAS = total analysis system
TEM = transmission electron microscopy
T = testosterone
TFC = turbulent-flow chromatography
TPM = trimipramine
U-PLS = unfolded-partial least squares regression
USE = ultrasonic extraction
VOCs = volatile organic compounds
VBTA = vinylbenzyl trimethylammonium

References

[1]Beesley, T., Majors, R. E., *LC-GC Europe* **2012**, *25*, 232-237.

[2]Cagliero, C., Bicchi, C., Cordero, C., Rubiolo, P., Scorbini, B., Liberto, E., *Food Chem.* **2012**, *132*, 1071-1079.

[3]Schmarr, H., Engel, K, H., *Eur. Food Res. Technol*., **2012,** *235*, 827-834.

[4]Naude, Y., Rohwer, E. R., *Anal. Chim. Acta*, **2012**, *730*, 120-126.

[5]Foudil-Cherif, Y., Yassaa, N., *Food Chem*, **2012**, *351*, 1796-1800.

[6]Tsioupi, D. A., Stefan-van Staden, R. I., Kapnissin-Christodulou, C. P., *Electrophoresis*, **2012,** *34***,** 178-204.

[7]Lomsadze, K., Vega, E. D., Salgado, A., Crego, A. L., Scriba, G. K. E., Marina, M. L., Chankvetadze, B., *Electrophoresis*, **2012**, *33*, 1637-1647.

[8]Schulze, T., Seiler, T. B., Streck, G. Braunbeck, T. Hollert, H., *J. Soils. Sed.*, **2012**, *12*, 1419-1434.

[9]Moya-Ortega, M. D., Alvarez-Lorenzo, C., Sigurdson, H. H. Concheiro, A., Loftsson, T., *Carbohydr. Polym*. **2012**, *87* 2344-2351.

[10]Perez-Fernandez, V., Castro-Puyana, M., Gonzalez, M. J., Garcia, M. A., Gomara, B., *Chirality*, **2012**, *24*, 577-583.

[11]Chen, G. W., Zh*ang, C., Li, W. J., Zhou, C. J., Feng, S. Y.*, Chin. Chem. Lett., **2012**, *23*, 1259-1262.

[12]Stephany, O., Tisse, S., Coadou, G., Boullon, J. P., Peulon-Agasse, V., Cardinael, P., *J. Chromy. A*, **2012**, *1270*, 254-261.

[13]Lystra, G., Tempere, S., de Revel, G., Barbe, J. C., *J. Agr. Food Chem.*, **2012**, *60*, 1503-1509.

[14]Ciobanu, A., Mallard, I. Landy, D., Brabie, G., Nistor D., Fourmentin, S., *Carbohydr. Polym*., **2012**, *87*, 1963-1970.

[15]Zhang, X. P., Zhang, C. Y., Sun, G. L., Xu, X. D., Tan, Y. F., Wu, H. F., Cao, R. N., Liu, J., Wu, J. W., *Instr. Sci.Technol.*, **2012**, *40*, 194-215.

[16]Mauri-Aucejo, A. R., Llobat-Estelles, M., Egea, M. G., Guillem, C., Amoros, P., *Analyst*, **2012**, *137*, 1275-1283.

[17]Faraji, H., Husain, S. W., Helalizadeh, M., *J. Sep. Sci.*, **2012**, *35*, 107-113.

[18]Le Roux, M., Cronje, J. C., Burger, B. V., Joubert, E., *J. Agr. Food Chem.*, **2012**, *60*, 2657-2664.

[19]Guan, J., Yan, F., Shi, S., Wang, S. L., *Electrophoresis*, **2012**, *33*, 1631-1636.

[20]Mohr, S., Pilaj, S., Schmid, M. G., *Electrophoresis*, **2012,** *33*, 1624-1630.

[21]Ning, Z., Zhong, H., Kong, C., Lu, Y., *Asian J. Chem*. **2012,** *24* 2965 – 2968.

[22]Kuo, C. Y., Wang, S. H., Lin, C. C., Liao, S. K. S., Hung, W. T.Fang, J. M., Yang, W. B., *Molecules*, **2012,** *17*, 7387-7400.

[23]Tao, H. Q., Meng, Q. F., Li, M. H., Yu, H., Liu, M. F., Du, D., Sun, S. L., Yang, H. C., Wang, Y. M. Ye, W., Yang, L. Z., Zhu, D. L., Jiang, C. L., Peng, H. S., *Naunyn-Schmiedeberg Arch. Pharmacol.*, **2013**, *386*, 61-70.

[24]Hu, C.. He, M., Chen, B. B., Hu, B., *J. Agr. Food Chem*., **2012**, *60*, 1049-1005.

[25]Shimomura, H., Hosoda, K., Hayashi, S., *J. Bacter.*, **2012**, *194*, 2658-2667.

[26]Saito, N., Ishida, Y., Seno, K., Hayashi, F., *Prot. Exp. Purif.*, **2012**, *82*, 168-173.

[27]Wang, R. Q., Ong, T. T., Ng, S. C., *J. Chromy. A*., **2012**, *1224*, 97-103.

[28]Wang, R. Q., Ong, T. T., Tang, W. H., Siu-Choon, N., *Trac-Trends Anal. Chem.*, **2012**, *37*, 83-100.

[29]Araki, J., Ohkawa, K., Uchida, K., Murakami, Y., *J. Polymer Sci. Part A-Polym. Chem.*, **2012**, *50*, 488-494.

[30]Sun, H. Y., Han, J., Gao, C., *Polymer*, **2012**, *53*, 2884-2889.

[31]Liu, F. K., *Chromatographia*, **2012**, *75*, 19-20.

[32]Piercey, M. J., Mazzanti, G., Budge, S. M., Delaquis, P. J.. Paulson, A. T., Hansen, L. T., *Food Microbiol*., **2012**, *30*, 213-218.

[33]Varga, G., Fodor, G., Ilisz, I., Szeman, J., Visy, J., Szente, L., Peter, A., *J. Pharm. Biomed. Anal*., **2012**, *70*, 71-76.

[34]Tarkanyi, G., Nemeth, K., Mizsei, R., Toke, O., Visy, J., Simonyi, M., Jicsinszky, L., Szeman, J., Szente, L., *J. Pharm. Biomed. Anal.*, **2013**, *72*, 292-298.

[35]Ceborska, M., Asztemborska,M., Luboradzki, R., Liptowski, J., *Carbohydr. Polym*., **2013**, *91*, 110-114.

[36]Wang, Y., Ai, F., Ng, S,C., Tan, T. T. T., *J. Chromy. A.*, **2012**, *1228*, 99-109.

[37]Lee, Y. J., Choi, S., Lee, J., Nguyen, N., Lee, K., Kang, J. S., Mar, W., Kim, K. H., *Arch. Pharm. Res*., **2012**, *35*, 671-681.

[38]Sarver, S. A., Keithley, R. B., Essaka, D. C., Tanaka, H., Yoshimura, Y., Palcic, M. M., Hindsgaul, O. Dovichi, N. J., *J. Chromy. A*, **2012**, *1229*, 268-274.

[39]Neumajer, G., Sohajda, T., Darcsi, A., Toth, G., Szente, L., Noszal, B., Beni, S., *J. Pharm. Biomed. Anal.*, **2012**, *62*, 42-47.

[40]Wang, W., Xiang, S. Y., Zhou, X. J., Ji, Y. B., Xiang, B. R., *Molecules*, **2012**, *17*, 313-314.

[41]El-Sabawi, D., Hamdan I. I., Haj, Ali, D., *J. Liquid Chrom. Rel. Technol.*, **2012**, *35*, 573-589.

[42]Zhou, J., Yao, H. C., Shao, H., Li, Y. H.,Zhang, Z. Z., *J. Liquid Chrom. Rel. Technol.*, **2012**, *35*, 50-58.

[43]Gotti, R., Furlanetto, S., Santagati, R. N., *Anal. Lett*., **2012**, *45*, 665-676.

[44]Zhou, J., Dai, I., Wang, S. Y., Zhu, E. W., Hai, J. F., Liu, Y.S. Tang, J., Tang, W. H., *RSC Advances*, **2012**, *2*, 5088-9093.

[45]Singh, N. S., Paul, R. H., Sichler, M., Moaddel, R., Bernier, M., Wainer, I. W., *Anal. Biochem*., **2012**, *421*, 460-466.

[46]Estrada, R., Vigh, G., *J. Chromy. A*.. **2012**, *1226*, 24-30.

[47]Li, J., Bi, Y. W., Wang, L., Sun, F. L., Chen, Z., Xu, G. L., Fan, G. R., *J. Pharm. Biomed. Anal.*, **2012**, *66*, 218-224.

[48]Ning, Z., Zhong, H., Kong, C., Lu, Y., *Asian J. Chem*., **2012**, *24*, 2965-2968.

[49]Yang, H. J., Zhang, Q. L., Zhao, J. J., *Water, Air, Soil Pollut.* **2012**, *223*, 3461-3469.

[50]Mironov, G. G., Logie, J., Okhonin, V., Renaud, J. B., Mayer, P. M., Berezovski, M. V., *J. Am. Soc. Mass. Spectr*., **2012**, *23*, 1232-1240.

[51]Song, L. J., Guo, Z. P., Chen, Y., *Electrophoresis*, **2012**, *33*, 2056-2063.

[52]Dai, Y., Wang, S. Y., Zhou, J., Liu, Y.,Sun, D. P., Tang, J., Tang, W. H., *J. Chromy. A*, **2012**, *1246*, 98-102.

[53]Kawai, T., Koino, H., Sueyoshi, K., Kitigawa, F., Otsuka, , K., *J. Chromy. A*, **2012**, *1246*, 28-34.

[54]Wang, G., Wang, T. L. He, H. B., *Asian J. Chem*., **2012**, *24*, 3566-3570.

[55]Bragg, W., Shamsi, S. A., *J. Chromy. A.*, **2012**, *1267*, 144-155.

[56]Abromeit, H., Schaible, A. M., Werz, O., Scriba, G. K. E., *J. Chromy. A.*, **2012,** *1267*, 217-223.

[57]Ren, Y. L., Zhou, J. Y., Zhang, X. Y., Li, Z. D., Zhong, J., Yang, J., Xu, T., Tan, H., *Biotechnol. Bioprocess Eng*., **2012**, *17*, 1244-1251.

[58]Zhang, Q. F., Cheung, H. Y., Shangguan, X. C., *J. Sep. Sci*., *2012*, *35*, 3347-3353.

[59]Wagner, Z., Tabi, T., Jako, T., Zachar, G., Csillag, A., Szoko, E., *Anal. Bioanal. Chem*., **2012**, *404*, 2363-2368.

[60]Amin, N.C., Blanchin, M. D., Ake, M., Fabre, H., *J. Chromy. A*., **2012**, *1264*, 1-12.

[61]Liu, P. Y., in, Y. H., Feng, C. H., Chen, Y. L., *Electrophoresis*, **2012**, *33*, 3079-3086.

[62]Zhou, Q. H., Liu, Y. P., Wang, X., Di, X., *Talanta*, **2012**, *99*, 932-938.

[63]Li, C., Jiang, Y., *J. Chrom. Sci.*, **2012**, *50*, 739-743.

[64]Kodama, S., Taga, A., Aizawa, S., Kemmei, T., Honda, Y., Suzuki, K., Yamamoto, A., *Electrophoresis*, **2012**, *33*, 2441-2445.

[65]Xing, J. F., Chen, L. N., Song, J., Guo, C. N., Jang, G. D., Zeng, A. G., *J. Sep. Sci*., **2012**, *35*, 1884-1892.

[66]Kuo, C. Y., Wang, S. H., Lin, C. C., Liao, S. K- S.Hung, W, T., Fang, J. M., Yang, W. B., *Molecules*, **2012**, *17*, 7387-7400.

[67]Ning, Z., Zhong, H., Kong, C., Lu, Y., *Asian J. Chem*., **2012**, *24*, 2965-2968.

[68]Kalikova, K., Riesova, M., Tesarova, E., *Centr. Eur. J. Chem*., **2012**, *10*, 450-471.

[69]Yang, L., Yan, Q. H., Liu, B. G., Zhang, Y., Zhang, Y., Zhang, J. W., *Asian J. Chem*., **2012**, *24*, 3141-3144.

[70]Mohr, S., Pilaj, S., Schmid, M. G., *Electrophoresis*, **2012**, *33*, 1624-1630.

[71]Guan, J., Yan, F., Shi, S., Wang, S. L., *Electrophoresis*, **2012**, *33*, 1631-1636.

[72]Dahlberg, C. J., Harris, G., Urban, J., Tripp, M. L., Bland, J. S., Carrol, B. J., *J. Sep. Sci.*, **2012**, *35*, 1183-1189.

[73]Filipic, S., Nikolic, K., Vovk., I., Krizman, M., *Electrophoresis*, **2013**, *34*, 471-482.

[74]Xiao, Y., Ng, S.C., Tan, T. T. T., Wang, Y., *J. Chromy. A.*, **2012**, *1269*, 52-68.

[75]Fakhari, A. R., Tabani, H., Nojavan, S., Abedi, H., *Electrophoresis*, **2012**, *33*, 506-515.

[76]Jin, Y., Chen, C., Meng, L. C., Chen, J. T., Li, M. X., Zhu., Z. W., *Talanta*, *2012*, *89*, 149-154.

[77]Wang, C. C., Chen, J. L., Chen, Y. L., Chen, H. L., Wu, S. M., *Anal. Chim. Acta*, **2012**, *744*, 99-104.

[78]Ibrahim, W, A. W.Abd, Wahib, S. M. Hermawan, D., Sanagi, M. M., Abdoul-Eniein, H. Y., *Chirality*, **2012**, *24*, 252-254.

[79]Cheng, H. Y., Zhang, Q. L., Tu, Y. F., *Curr. Pharm. Anal*., **2012**, *8*, 37-43.

[80]Hung, S. H., Cheng, W. S., Huang, J. L., Wang, C. W. Her, G. R., *Electrophoresis*, **2012**, *33*, 546-551.

[81]Wang, R. Q., Ong, T. T., Ng, S. C., *Tetrahedron Lett.*, **2012**, *53*, 2312-2315.

Received: 27.09.2013.

Accepted: 09.10.2013.

PREPARATION AND STRUCTURE OF *C,C,N*-TRIARYL SUBSTITUTED IMINE: $TiCl_4$–1,4-DIAZABICYCLO[2.2.2]OCTANE-MEDIATED IMINATION OF 1-AROYL-2,7-DIMETHOXYNAPHTHALENE AND SPATIAL ORGANIZATION OF THE PRODUCED IMINE MOLECULE IN CRYSTAL

Akiko Okamoto[a], Atsushi Nagasawa[a], and Noriyuki Yonezawa[a]

Keywords: Triarylimine, $TiCl_4$–DABCO mediator, Non-coplanarly organized aromatic-rings accumulating molecules

$TiCl_4$–DABCO-mediated reaction of 1-monoaroylated 2,7-dimethoxynaphthalene compound and aromatic amine afforded triaryl-substituted imine compounds with/without cleavage of a methoxy group on the starting naphthalene compound. Three aromatic rings of methyl ether-cleaved imine molecule in crystal are accumulated perpendicularly to each other in crystal.

Corresponding Authors
Fax:+81-42-388-7601
E-Mail:aokamoto@cc.tuat.ac.jp
[a] Department of Organic and Polymer Materials Chemistry, Tokyo University of Agriculture and Technology 2-24-16 Naka-machi, Koganei, Tokyo 184–8588, Japan

Introduction

Non-coplanarly organized aromatic-rings accumulating compounds, e.g., biphenyls and binaphthyls, have been demonstrated as unique building blocks in construction for many functional materials.[1-8] Thus, organic reaction affording novel molecular motifs of non-coplanarly organized aromatic-rings accumulating compounds with minute spatial structural characterization have attracted attention of the chemists in the wide-range of organic molecular science and polymer materials fields. Recently, the authors have reported specific and characteristic electrophilic aromatic aroylation of naphthalene derivatives. In this reaction, two aroyl groups are regioselectively and effectively introduced at the 1,8-positions of the naphthalene ring accompanying with acid-mediated retroaroylation.[9] The 1-monoaroylated naphthalenes, which correspond to the intermediates in the diaroylation, are also obtained by choice of acidic mediator.[10] According to X-ray crystal structure analyses, the aroyl groups in these *peri*-aroylated naphthalene compounds are attached in a non-coplanar fashion to the naphthalene rings.[11-15] In a natural consequence, the authors have planned introduction of additional aromatic ring planes to the core of the aroylnaphthalene molecules to realize more crowded inner spatial situation in aromatic-rings accumulating molecule. As one of the molecular transformation approaches to obtain such spatial organization, the authors designed conversion of ketonic carbonyl group in 1-monoaroylnaphthalene to imino moiety by the reaction with aromatic amines. This attempt has led the authors to reveal novel reaction behaviour of *peri*-aroylated 2,7-dimethoxynaphthalene derivatives and the unique spatial organization of the resulting imine compounds in crystal. Herein, the authors report imination reaction of 1-monoaroylnaphthalene with aromatic amine, i.e., introduction reaction of the third aromatic ring to a naphthalene molecule of non-coplanarly organized two-aromatic-rings accumulating structure and discuss the reaction mechanism. In addition, the authors introduce the spatial organization features of the resulting triarylimine molecule.

Results and discussion

Table 1 shows the results of reaction of 1-(4-chlorobenzoyl)-2,7-dimethoxynaphthalene (**1**) with *p*-anisidine (**2**). When molecular sieves 4A[14] was added, no reaction proceeded (entry 2) as well as the reaction without additive compounds (entry 1). In *p*-toluenesulfonic acid (TsOH)-mediated reaction,[15] imine **3** was slightly obtained with recovery of starting material **1** (entry 3). $TiCl_4$–1,4-diazabicyclo[2.2.2]octane (DABCO)-mediated reaction[16] moderately afforded imine **3** (14 %) in a similar manner of TsOH-mediated one, whereas the reaction also gave the methyl–oxygen bond cleaved species, i.e., imine **4** (22 %) and 1-monoaroylnaphtahlene **5** (14 %) (entry 4).

Table 1. Imination of 1-(4-chlorobenzoyl)-2,7-dimethoxy-naphthalene[a] (**1**)

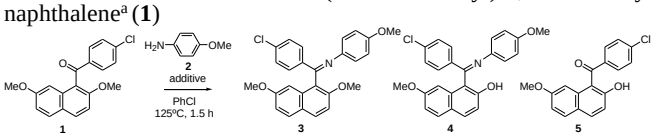

Entry	Additive	Product distribution (%)[b]			
		1	**3**	**4**	**5**
1	None	100	0	0	0
2	MS4A[c]	100	0	0	0
3	TsOH[d]	90	10(6)	0	0
4	$TiCl_4$,DABCO[e]	50(44)	14(10)	22(10)	14(8)

[a]Reaction conditions: 1-(4-chlorobenzoyl)naphthalene (**1**, 1.0 mmol), *p*-anisidine (**2**, 1.1 mmol), chlorobenzene (5 mL). [b]Calculated on the basis of ^{1}H NMR spectra. Isolated yields are given in parentheses. [c]MS4A (100

 DOI: 10.17628/ecb.2014.3.13-17

mg). [d]TsOH (*p*-toluenesulfonic acid; 0.1 mmol). [e]$TiCl_4$ (1.7 mmol), 1,4-diazabicyclo[2.2.2]octane (DABCO; 3.3 mmol).

There are two possible reaction routes for imine **4,** i.e., methyl–oxygen bond cleavage reaction of imine **3** and imination of 2-hydroxy-7-methoxy-1-monoaroylnaphthalene **5** (Scheme 1)**.** Imine **3** formed no ether-cleaved products by treatment with $TiCl_4$–DABCO mixture (Scheme 2).

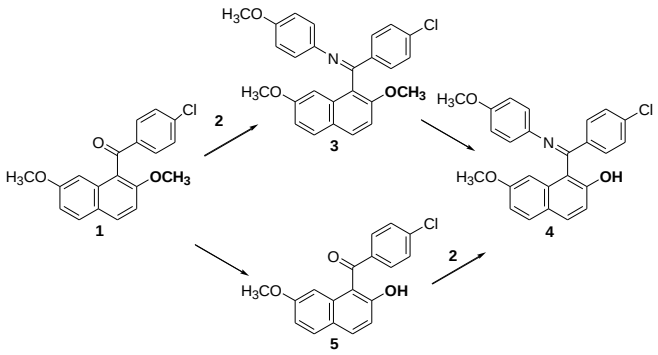

Scheme 1

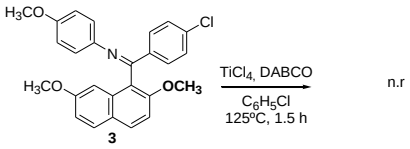

Scheme 2

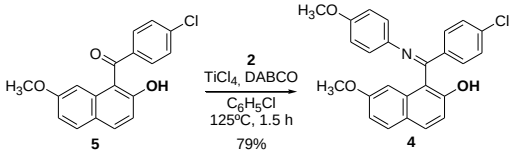

Scheme 3

On the other hand, the methyl ether-cleaved 1-monoaroylnaphthalene **5** was transformed into imine **4** in a high yield (79 %) when $TiCl_4$, DABCO, and amine **2** were treated as entry 4 in Table 1 (Scheme 3). These results strongly indicate that imine **4** was formed via the latter reaction route. In other words, imination of 1-monoaroylated 2-hydroxy-7-methoxynaphthalene **5** readily proceeds than that of the parent compound, 1-monoaroylated 2,7-dimethoxynaphthalene **1**. 1-Monoaroylnaphthalene **1** was converted quantitatively to the methyl ether-cleaved 1-monoaroylnaphthalene **5** by the aid of $TiCl_4$–DABCO mixture in the absence of amines (Scheme 4). On the contrary, no reaction occurred by the same treatment of 2,7-dimethoxynaphthalene (Scheme 5). Furthermore, reaction of 1-monoaroylnaphthalene **1** in monochlorobenzene at 125°C for 1.5 h with $TiCl_4$ yielded 1-monoaroylnaphthalene **5** (75 %) and 2,7-dimethoxynaphthalene **6** (25 %), whereas that with DABCO formed no products (Scheme 6).

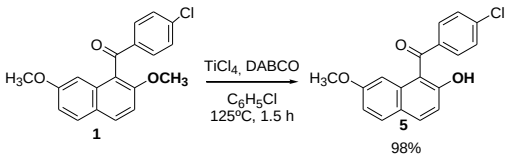

Scheme 4

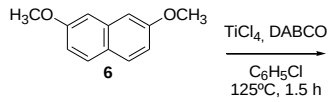

Scheme 5

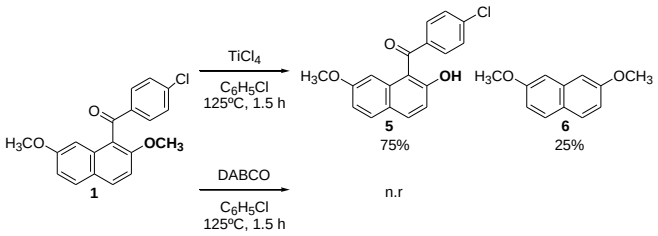

Scheme 6

Based on these results, this methyl ether cleavage reaction is obviously promoted by $TiCl_4$. It is widely recognized that $TiCl_4$ rarely catalyzes scission of aryl methyl bonds except for that some special assistance. So, it's strongly suggested that this $TiCl_4$ promoted cleavage of aryl methyl ether should be assisted by neighboring group effect of the adjacent aroyl substituent, probably by coordination of the

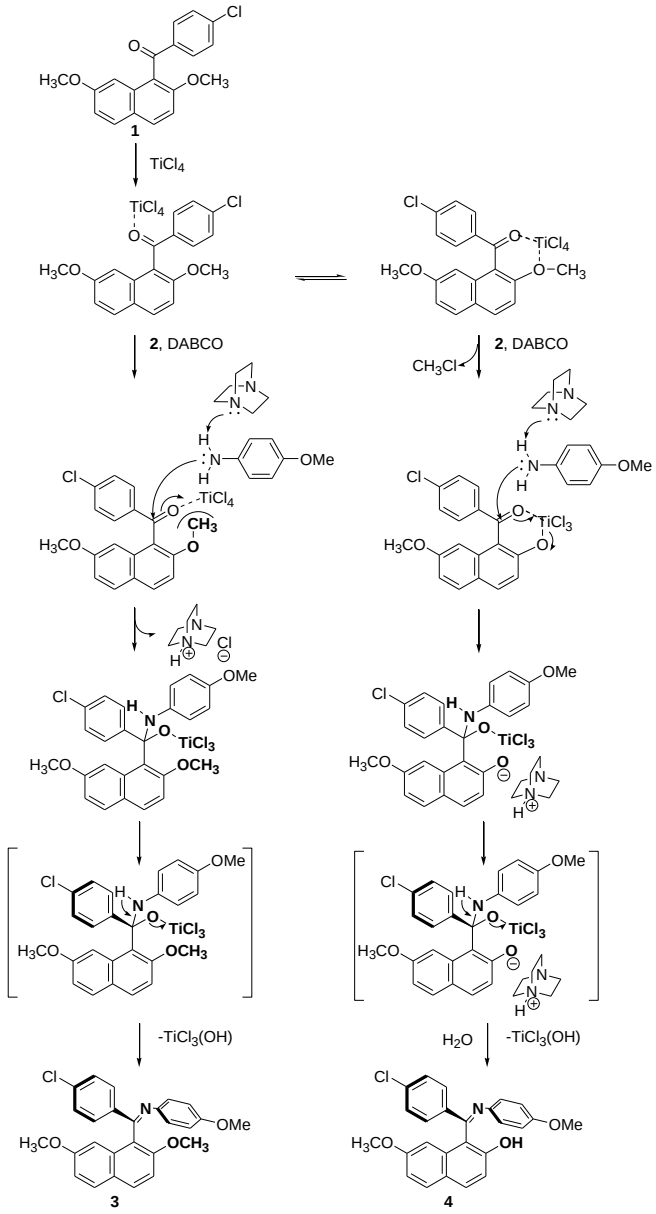

 DOI: 10.17628/ecb.2014.3.13-17

heteroatoms of the substituents to titanium atom.[17]

Scheme 7

Scheme 7 well-explains the plausible reaction mechanism. The $TiCl_4$–DABCO-mediated imination of 1-monoaroylnaphthalene **1** to imine **3** presumably proceeds via three steps: 1) the carbonyl oxygen coordinates to titanium atom of $TiCl_4$, 2) nucleophilic attack of the nitrogen atom of aniline to $TiCl_4$-activated ketonic carbonyl group of 1-monoaroylnaphthalene **1** proceeds with simultaneous abstraction of proton from the adduct by DABCO, and 3) deprotonation from nitrogen atom of hemiaminal forms imino moiety.

As the carbonyl carbon atom of 1-monoaroylnaphthalene **1** is sterically hindered, the second step of nucleophilic attack of amine is considered essentially rate-determining step for total imination reaction. So, the aroyl group-assisted methyl ether-cleavage reaction of 1-monoaroylnaphthalene **1** presumably undergo with comparable susceptibility as well as the nucleophilic attack of the amine **2** to the ketonic carbonyl carbon. As the attack of amine **2** to the carbonyl carbon of methyl ether-cleaved-1-monoaroylnaphthalene **5** thus obtained should be less affected by steric hindrance than the parent compound **1**, it smoothly affords imine **4**.

Figure 1 displays the crystal structure of analogous imine **7**, which has no methoxy group on the *N*-linked benzene. In the crystal of analogous imine **7**, two molecules of imine **7** form a 2:1 set with a DABCO molecule. Each of the aromatic rings is connected almost perpendicularly against two other aromatic rings. The dihedral angles of the *C*-linked 4-chlorophenyl ring and the *N*-linked phenyl ring with the naphthalene ring are 80.39(6)° and 82.35(6)°, respectively. The dihedral angle between *C*- and *N*-linked benzene rings is 87.09(7)°.

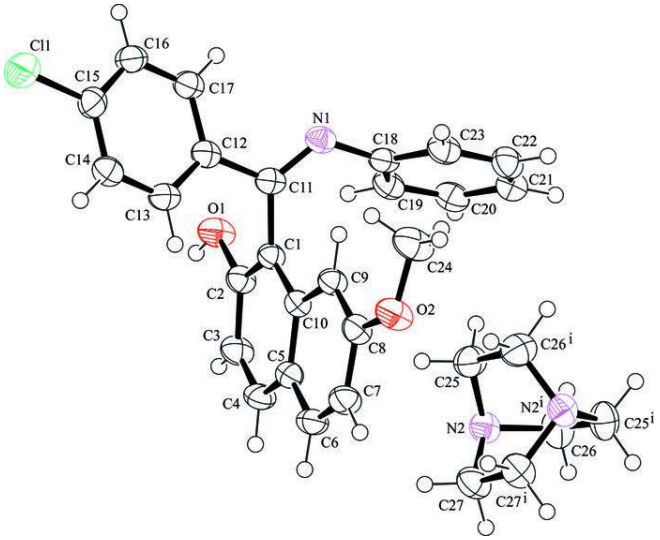

Figure 1. Molecular structure of analogous imine **7**, with the atom-labeling scheme and displacement ellipsoids drawn at the 50% probability level [Symmetry code (i)1-x, y, 3/2-z].

Conclusively, $TiCl_4$–DABCO-mediated imination of 1-monoaroylated 2,7-dimethoxynaphthalene successfully yield *C,C,N*-triaryl substituted imine compounds with/without cleavage of 2-positioned methoxy group. In crystal of an imine compound, the three aromatic rings are situated perpendicularly to each other realizing stable spatial organization.

Experimental

All reagents were of commercial quality and were used as received. Solvents were dried and purified using standard techniques.

Measurements

^{1}H NMR spectra were recorded on a JEOL JNM-AL300 spectrometer (300 MHz) and a JEOL ECX400 spectrometer (400 MHz). Chemical shifts are expressed in ppm relative to internal standard of Me_4Si (δ 0.00). ^{13}C NMR spectra were recorded on a JEOL JNM-AL300 spectrometer (75 MHz). Chemical shifts are expressed in ppm relative to internal standard of $CDCl_3$ (δ 77.0). IR spectra were recorded on a JASCO FT/IR-4100 spectrometer. Elemental analyses were performed on a Yanaco CHN CORDER MT-5 analyzer. High-resolution FAB mass spectra were recorded on a JEOL MStation (MS700) ion trap mass spectrometer in positive ion mode.

X-ray Crystallography

For the crystal structure determination, the single-crystal of the compound $C_{24}H_{18}ClNO_2 \cdot 0.5C_6H_{12}N_2$ was used for data collection on a four-circle Rigaku RAXIS RAPID diffractometer (equipped with a two-dimensional area IP detector). The graphite-mono-chromated Cu Kα radiation (λ = 1.54187 Å) was used for data collection. The lattice parameters were determined by the least-squares methods on the basis of all reflections with $F^2 > 2\sigma(F^2)$. The data collection and cell refinement were performed using *PROCESS-AUTO* software. The data reduction was performed using *CrystalStructure*. The structures were solved by direct methods using *SIR2004* and refined by a full-matrix least-squares procedure using the program *SHELXL97*. All H atoms were found in a difference map and were subsequently refined as riding atoms, with the aromatic C–H = 0.95 Å and methyl C–H = 0.98 Å, and with $U_{iso}(H) = 1.2U_{eq}(C)$.

Synthetic procedures of 1-(4-chlorobenzoyl)-2,7-dimethoxy-naphthalene (1)

To a solution of 2,7-dimethoxynaphthalene (**6**, 0.200 mmol, 68.2 mg) and 4-chlorobenzoyl chloride (0.22 mmol, 38.5 mg) in dichloromethane (0.5 mL), $AlCl_3$ (0.22 mmol, 29.3 mg) was added by portions at 0°C under nitrogen atmosphere. After the reaction mixture was stirred at r.t. for

3 h, it was poured into iced water (20 mL) and the mixture was extracted with $CHCl_3$ (15 mL×3). The combined extracts were washed with 2 M aq. NaOH, saturated aq. NaCl and dried over anhydrous magnesium sulfate. The solvent was removed under reduced pressure to give powdery product. The crude product was purified by recrystallization (hexane, isolated yield 78 %).

1-(4-Chlorobenzoyl)-2,7-dimethoxynaphthalene (1)

Colourless needles (hexane), Mp 121.5–122 °C; IR (KBr): 1667, 1628, 1586, 1512 cm^{-1}; ^1H NMR δ (300 MHz, $CDCl_3$): 7.87 (1H, d, *J* =9.0 Hz), 7.78 (2H, d, *J* = 8.4 Hz), 7.72 (1H, d, *J* = 9.0 Hz), 7.39 (2H, d, *J* = 8.4 Hz), 7.16 (1H, d, *J* = 9.0 Hz), 7.02 (1H, dd, *J* = 2.4, 9.0 Hz), 6.78 (1H, d, *J* = 2.4 Hz), 3.79 (3H, s), 3.73 (3H, s) ppm; ^{13}C NMR δ (75 MHz, $CDCl_3$): 196.81, 158.96, 155.02, 139.71, 136.45, 132.94, 131.28, 130.87, 129.72, 128.86, 124.34, 121.06, 117.15, 110.05, 101.88, 56.239, 55.168 ppm; Calcd for $C_{19}H_{15}O_3Cl$: C, 69.83%; H, 4.63%; Found: C, 69.61%; H, 4.74%.

Imination of 1-(4-chlorobenzoyl)-2,7-dimethoxynaphthalene (1)

To a solution of 1-(4-chlorobenzoyl)-2,7-dimethoxynaphthalene (**1**, 0.2 mmol, 65.4 mg) in monochlorobenzene (1 mL), mixtures of aniline (0.22 mmol, 20.5 mg), $TiCl_4$ (0.33 mmol, 62.4 mg), DABCO (1.32 mmol, 148.0 mg) and monochlorobenzene (1 mL) were added by portions at 90°C under nitrogen atmosphere. After the reaction mixture was stirred at 125 °C for 1.5 h, the resulting solution was filtrated to remove the precipitate. The solvent was removed under reduced pressure to give crude material. The crude product was purified by silicagel column chromatography (chloroform; isolated yield: imine **3**, 10 %; imine **4**, 10 %, 2-hydroxy compound **5**, 8 %).

Spectral data and elemental analyses

Imine 3

Colourless blocks ($CHCl_3$/hexane) Mp. 174–175 °C, IR (KBr) 1625, 1502, 1238, 1029, 830 cm^{-1}; ^1H NMR δ (300 MHz, $CDCl_3$): 7.72 (1H, d, *J* = 9.0 Hz), 7.66 (2H, d, *J* = 8.4 Hz), 7.60 (1H, d, *J* = 9.0 Hz), 7.29 (2H, d, *J* = 8.4 Hz), 7.25 (1H, d, *J* = 9.0 Hz), 7.02 (1H, d, *J* = 9.0 Hz), 6.92 (1H, dd, *J* = 9.0, 2.4 Hz), 6.74 (2H, d, *J* = 8.8 Hz), 6.68 (1H, d, *J* = 2.4 Hz), 6.53 (2H, d, *J* = 8.8 Hz), 3.72 (3H, s), 3.70 (3H, s), 3.60 (3H, s) ppm; ^{13}C NMR δ (75 MHz, $CDCl_3$): 163.86, 158.73, 156.27, 154.96, 144.33, 138.11, 136.46, 132.80, 130.46, 129.80, 129.51, 128.64, 124.06, 121.15, 118.58, 116.85, 113.40, 109.87, 102.72, 56.11, 55.32, 55.23 ppm; HRMS (FAB; *m*-nitrobenzyl alcohol [*m*-NBA]) m/z: $[M+H]^+$; Calcd for $C_{26}H_{23}O_3NCl$, 432.1371; Found 432.1366; Anal. Calcd for $C_{26}H_{23}O_3NCl$: C 72.15%, H 5.11%. Found: C 72.30%, H 5.13%.

Imine 4

Colourless blocks ($CHCl_3$/hexane), Mp. 184–185 °C; IR (KBr) 3407, 1626, 1502, 1225, 1207, 826 cm^{-1}; ^1H NMR δ (300 MHz, $CDCl_3$): 7.71 (d, *J* = 8.8 Hz, 1H), 7.69 (d, *J* = 8.8 Hz, 2H), 7.64 (d, *J* = 8.8 Hz, 1H), 7.62 (d, *J* = 9.2 Hz, 1H), 7.53 (d, *J* = 9.2 Hz, 1H), 7.31 (d, *J* = 8.8 Hz, 2H), 7.27 (d, *J* = 8.8 Hz, 2H), 7.09 (d, *J* = 8.4 Hz, 2H), 7.03 (d, *J* = 8.8 Hz, 1H), 6.94 (dd, *J* = 2.4, 9.2 Hz, 1H), 6.87 (d, *J* = 7.6 Hz, 1H), 6.84 (d, *J* = 10.0 Hz, 2H), 6.77 (dd, *J* = 2.4, 8.6 Hz, 1H), 6.72 (m, 4H), 6.66 (d, *J* = 2.4 Hz, 1H), 6.57 (d, *J* = 9.2 Hz, 2H), 6.21 (d, *J* = 2.4 Hz, 1H), 3.76 (s, 3H), 3.69 (s, 3H), 3.64 (s, 3H), 3.20 (s, 3H) ppm; ^1H NMR δ (300 MHz, DMSO-d_6): 10.01 (s, 1H), 7.67–7.56 (m, 5H), 7.41 (d, *J* = 8.4 Hz, 2H), 6.97 (d, *J* = 8.7 Hz, 1H), 6.84–6.75 (m, 3H), 6.57 (d, *J* = 8.7 Hz, 2H), 6.46 (d, J = 2.1 Hz, 1H), 3.59 (s, 3H), 3.52 (s, 3H) ppm; ^{13}C NMR δ (75 MHz, $CDCl_3$): 169.19, 166.95, 162.91, 158.94, 157.82, 157.11, 157.01, 150.87, 143.50, 137.98, 137.64, 137.03, 135.45, 135.35, 135.20, 134.36, 133.38, 131.05, 130.68, 130.33, 129.88, 129.69, 129.24, 128.85, 124.55, 124.14, 123.72, 121.73, 118.59, 116.33, 116.15, 114.96, 114.52, 114.14, 113.84, 111.37, 106.53, 103.58, 55.45, 55.26, 55.24, 54.44 ppm; HRMS (FAB; *m*-NBA) m/z: $[M+H]^+$; Calcd for $C_{25}H_{21}O_3NCl$, 418.1162; Found 418.2110; Anal. Calcd for $C_{26}H_{23}O_3NCl$: C 71.97 %, H 4.87 %. Found: C 71.85 %, H 4.82 %

1-(4-Chlorobenzoyl)-2-hydroxy-7-methoxynaphthalene (5)

Yellow platelets (hexane), Mp. 118–118.5 °C; IR (KBr): 3434, 1623, 1583, 1513, 1214, 843 cm^{-1}; ^1H NMR δ (300 MHz, $CDCl_3$): 11.35 (s, 1H), 7.85 (d, 1H, *J* = 9.0 Hz), 7.63 (d, 1H, *J* = 9.0 Hz), 7.58 (d, 2H, *J* = 8.7 Hz), 7.40 (d, 2H, *J* = 8.7 Hz), 7.07 (d, 1H, *J* = 9.0 Hz), 6.91 (dd, 1H, *J* = 2.4, 9.0 Hz), 6.58 (d, 1H, *J* = 2.4 Hz), 3.37 (s, 3H) ppm; ^{13}C NMR δ (75 MHz, $CDCl_3$): 199.1, 162.6, 158.2, 138.8, 138.7, 136.5, 133.8, 130.7, 130.2, 128.9, 123.7, 116.4, 115.8, 113.4, 106.5, 54.5 ppm; Anal. Calcd for $C_{18}H_{13}ClO_3$: C 69.13, H 4.19. Found: C 69.11, H 4.09.

Imine 7

Colourless blocks ($CHCl_3$/hexane), Mp. 172–173 °C; IR (KBr): 3407, 2937, 2592, 1625, 1585, 1509, 1227 cm^{-1}; ^1H NMR δ (300 MHz, DMSO-d_6): 10.13, (s, 1H), 7.66–7.60 (m, 4H), 7.44 (d, 2H), 7.00 (t, 2H), 6.95 (d, H), 6.86–6.76 (m, 4H), 6.52 (d, 1H), 3.64 (s, 3H), 3.29 (s, 6H) ppm; ^{13}C NMR δ (75 MHz, DMSO-d_6): 164.4, 158.2, 153.7, 151.0, 137.6, 135.7, 132.2, 130.3, 130.0, 129.7, 128.7, 128.2, 123.8, 122.9, 119.2, 115.1, 115.0, 114.9, 102.6, 55.1, 47.3 ppm; HRMS (FAB; *m*-NBA) m/z: $[M+H]^+$; Calcd for $C_{24}H_{19}ClNO_2$, 388.1110; Found, 388.1104.

Acknowledgement

This work was partially supported by the Iron and Steel Institute of Japan (ISIJ) Research Promotion Grant, Tokyo, Japan.

References

[1]Gasparrini, F.; Pierini, M.; Villani, C.; Filippi, A.; Speranza, M.; *J. Am. Chem. Soc.*, **2008**, *130*, 522.

[2]Shah, N. H.; Butterfoss, G. L.; Nguyen, K.; Yoo, B.; Bonneau, R.; Rabenstein, D. L.; Kirshebaum, K.; *J. Am. Chem. Soc.*, **2008**, *130*, 16622.

[3]Alfonso, I.; Burguete, M. I.; Galindo, F.; Luis, S. V.; Vigara, L.; *J. Org. Chem.*, **2007**, *72*, 7947.

[4]Zhang, F. R.; Song, H. B.; Zi, G. F.; *Dalton Trans.*, **2011**, *40*, 1547.

[5]Genet, J.-P.; *Acc. Chem. Res.*, **2003**, *36*, 908.

[6]Lucchi, O.; *Pure Appl. Chem.*, **1996**, *68*, 945.

[7]Maruoka, K.; "Asymmetric Phase Transfer Catalysis", Wiley-VCH, Weinheim, **2008**.

[8]Scerba, M. T.; Leavitt, C. M.; Diener, M. E.; DeBlase, A. F.; Lectka, T.; *J. Org. Chem.*, **2011**, *76*, 7975.

[9]Okamoto, A.; Yonezawa, N.; *Chem. Lett.*, **2009**, *38*, 914.

[10]Okamoto, A; Mitsui, R.; Yonezawa, N.; *Chem. Lett.*, **2011**, *40*, 1283.

[11]Nakaema, K.; Noguchi, K.; Okamoto, A.; Yonezawa, N.; *Acta Cryst.*, **2008**, *E64*, o2497.

[12]Mitsui, R.; Okamoto, A.; Noguchi, K.; Yonezawa, N.; *Acta Cryst.*, **2007**, *E63*, o4120.

[13]Sasagawa, K.; Sakamoto, R.; Hijikata, D.; Yonezawa, N.; Okamoto, A.; *Acta Cryst.*, **2013**, E69, o651.

[14]Taguchi, K.; Westheimer, F. H.; *J. Org. Chem.*, **1971**, *36*, 1570.

[15]Luo, F-T.; Ravi, V. K.; Xue, C.; *Tetrahedron*, **2006**, *62*, 9365.

[16]Higuchi, M.; Yamamoto, K.; *Polym. Adv. Technol.*, **2002**, *13*, 765.

[17]Tsurutani, T.; Shinokubo, H.; Oshima, K.; *Tetrahedron Lett.*, 1**999**, *40*, 8121.

[18]Nagasawa, A.; Mitsui, R.; Kato, Y.; Okamoto, A.; Yonezawa, N.; *Acta Cryst.*, **2010**, *E66*, o2498.

Received: 19.09.2013.
Accepted: 06.10.2013.

PYRIDAZINE AND ITS RELATED COMPOUNDS. 25[1] SYNTHESIS OF NEW ARYLAZOPYRAZOLTHIENO[2,3-*c*]-PYRIDAZINE TYPE DISPERSION DYES

A. Deeb,[a]* N. Aouf,[a] F. Yassine[a] and W. Shehta[a]

Keywords: arylazopyrazolthieno[2,3-c]pyridazines, 5-amino-3,4-diphenylthieno[2,3-*c*]pyridazine-6-carbohydrazide, colour fastness, dispersion dyes

Acetylacetone was coupled with diazotized aryl amines to give arylazoacetylacetones; these when refluxed with 5-amino-3,4-diphenylthieno[2,3-*c*]pyridazine-6-carbohydrazide in glacial acetic acid yielded the corresponding 5-amino-6-[[4-arylazo-3,5-dimethylpyrazol-1-yl]-carbonyl]-3,4-diphenylthieno[2,3-*c*]pyridazine dyes. The dyes were applied to polyester fabric, and their spectral and fastness properties measured.

Corresponding Authors
E-Mail: dralideeb@hotmail.com
[a] Department of Chemistry, Faculty of Science, Zagazig University, Zagazig, Egypt

INTRODUCTION

Interest in the design of azo dyes containing heterocyclic moieties stems from their high degree of brightness compared to azo dyes derived from anilines.[2] The thiophene derivatives based azo dyes are known as disperse dyes with excellent brightness of shade. This class of dyes was established as an alternative to more expensive anthraquinone dyes.[3] The heterocyclic nature of the thiophene ring has also allowed for excellent sublimation fastness on the dyed fibers.[4] Additionally, the sulfur atom plays a decisive role by acting as an efficient electron sink as explained by valence bond theory.[5] On the other hand heterocyclic annulated pyridazines continue to attract considerable attention which mainly arises from the large variety of interesting pharmacological activities observed with pyridazine derivatives.[6] Recently, our researches have been devoted to the synthesis of condensed tricyclic systems of potential biological activity with a thiophene ring as the central nucleus.[7-9] As a continuation of these studies we report here the synthesis of some 6-[[4-(arylazo)-3,5-dimethylpyrazol-1-yl]carbonyl]thieno[2,3-*c*]pyridazine dyes from 5-amino-3,4-diphenyl-6-ethoxycarbonylthieno[2,3-*c*]-pyridazine and an evolution of their properties on polyester fibers.

Our synthesis began with the preparation of ethyl 5-amino-3,4-diphenylthieno[2,3-*c*]pyridazine-6-carboxylate **3**, which was obtained from the reaction of 3-chloro-4-cyanopyridazine **1** or 4-cyanopyridazine-3-thione **2** with ethyl mercaptoacetate or ethyl chloro(bromo)acetate, respectively.[10] Compound **3** reacted with 85% excess of hydrazine hydrate in refluxing ethanol to give 5-amino-3,4-diphenylthieno[2,3-*c*]pyridazine-6-carbohydrazide **4,** (Scheme 1).[9]

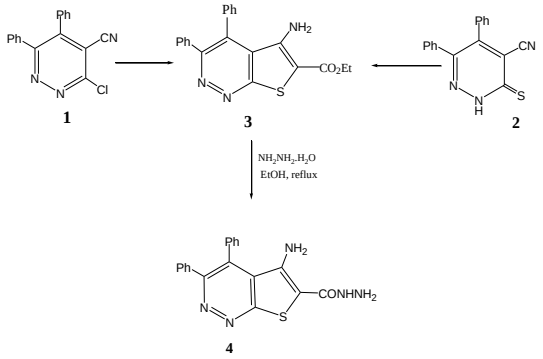

Scheme 1.

Arylamine derivatives **5** were diazotized using sodium nitrite in hydroch-loric acid; the temperature was maintained below 5 °C in an ice bath. The diazotized products **6** were then coupled with active methylene compounds such as acetylacetone in sodium acetate buffered solution to give the azobenzeneacetylacetone derivatives **7** in good yields, respectively (Scheme 2). Spectral data[11,12] for such compounds indicate them to have a hydrazone configuration , characterization data for compounds **7a-l** were described in the previous part.[13]

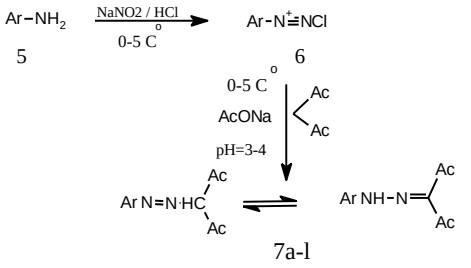

Scheme 2.

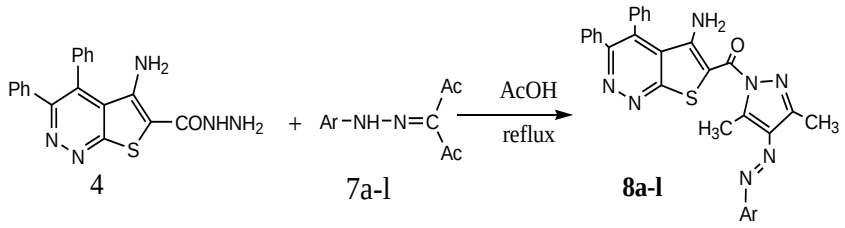

Scheme 3. Compounds **7** and **8**: a (Ar=Ph); **b** (Ar=2-MeC$_6$H$_4$); **c** (Ar=3-MeC$_6$H$_4$); **d** (Ar=4-MeC$_6$H$_4$); **e** (Ar=2-MeOC$_6$H$_4$); **f** (Ar=4-MeOC$_6$H$_4$); **g** (Ar=2-ClC$_6$H$_4$); **h** (Ar=3-ClC$_6$H$_4$); **i** (Ar=3-NO$_2$C$_6$H$_4$); **j** (Ar=4-NO$_2$C$_6$H$_4$); **k** (Ar=2-naphthyl); **l** (Ar=3-pyridyl)

Compound **4**, when reacted with the azobenzeneacetylacetone derivatives **7a-l** in glacial acetic acid at refluxing temperature yielded the 5-amino-6-[[4-arylazo-3,5-dimethylpyrazol-1-yl]carbonyl]-3,4-diphenylthieno[2,3-*c*]pyridazine **8a-l** (Scheme 3). The reaction proceeds in two stages, viz., the initially formed hydroxypyrazoline subsequently loses water by an acid-catalysed reaction.[14,15]

Dyeing of polyester fabrics and dyeing properties

Color measurement

The effect of the nature of different substituents on dyeing behavior, color hue, and depth was investigated. This investigation depends on some spectral data of the dyed materials. The most commonly used function *f(R)* is that developed theoretically by Kubelka and Munk. In their theory, the optical properties of a sample are described by two values: *K* is the measure of the light absorption, and *S* is a measure of the light scattering. On textiles, *K* is determined primarily by the dyestuffs and *S* only by the substrate. From the wavelength, Kubelka and Munk calculate Eq. (1) for the reflectance *R* of thick, opaque samples with the constants of *K* and *S*:

$$\frac{K}{S} = \frac{(1-R)^2}{2R} \qquad (1)$$

In this equation *R* is used as a ratio, e.g., 32 % reflectance as 0.32. The *K/S* value at ë max was taken as a measure of color depth.

On the other hand, the psychometric coordinates (*L**, *a**, *b**) for each dyed sample were obtained to illustrate the color hues, where *L** is the lightness, ranging from 0 to 100 (0 for black and 100 for white); *a** is the red-green axis, (+) for red, zero for grey, and (-) for green; and *b** is the yellow-blue axis, (+) for yellow, zero for gray, and (-) for blue.

The parent dyestuff in each group is taken as the standard in color difference calculation (ΔL^*, ΔC^*, ΔH^* and ΔE^*). The results are measured using CIE-LAB techniques and given in Table 1, Where ΔL^* is the lightness difference, ΔC^* the chroma difference, ΔH^* the hue difference and ΔE^* the total color difference. A negative sign of ΔL^* indicates that the dyed fiber becomes darker than the standard , but a positive sign indicates that the dyed fiber becomes lighter than the standard. A negative sign of ΔC^* indicates that the dyed fiber becomes duller than the standard, but a positive sign indicates that the dyed fiber becomes brighter than the standard. A negative sign of ΔH^* indicates that the color directed to red color, while a positive sign indicates that the color directed to yellowish.

The values of *K/S* of **8a-l** vary from 3.0 to 13.7. The introduction of different groups in dyes **8a-l** increases the strength of *K/S* values and deepens the color compared with the parent dye **8a** (Table 1).

The replacement of the phenyl by tolyl, anisyl, chlorophenyl, nitrophenyl, naphthyl and pyridyl groups in the pyrazolazo moiety decreases the value of *K/S*. indicating that the dye **8k** show higher affinity towards dyeing of polyester fabrics than the other dyes. Dyes **8b-f** and **8h-l** with positive ΔC^* values are brighter than the parent dye **8a** while the other dyes are duller than the parent dye. Dyes **8b-l** with negative ΔL^* values are darker than the parent dye **8a**. The positive value of *a** and *b** indicates that all groups shift the color hues of the dye to reddish direction on the red-green axis and to the yellowish direction in the yellow-blue axis, respectively.

Assessment of color fastness

Most influences that can affect fastness are light, washing, heat, perspiration, and atmospheric pollution. Conditions of such tests are chosen to correspond closely to treatments employed in manufacture and ordinary use conditions.[16] Results are given after usual matching of tested samples against standard reference (the grey scale).[16] The results revealed that these dyes have good fastness properties (Table 2).

Experimental

All melting points were determined on a Gallenkamp electric melting point apparatus. Thin-layer chromatography (TLC) analysis was carried out on silica gel 60 F_{254} precoated aluminum sheets. Infrared spectra were recorded on FTIR 5300 Spectrometer and Perking Elmer Spectrum RXIFT-IR System, using the potassium bromide wafer technique. ^{1}H-NMR spectra were recorded on Varian Gemini 200 MHz spectrometer using the indicated solvents and tetramethylsilane (TMS) as an internal reference. Electron impact mass spectra were obtained at 70 eV using a GCMS–qp1000 EX Shimadzo spectrometer. Elemental analysis (C,H,N) were carried out at the micro-analytical Center of Cairo University, Giza, Egypt.

 DOI: 10.17628/ecb.2014.3.18-23

Table 1 Optical measurements of compounds **8a-l**

Dye	*R, %*	*a**	*b**	*L**	*C**	*H**	ΔL^*	ΔC^*	ΔH^*	ΔE^*	*K/S*
8a	5.63	6.35	28.3	53.73	28.84	1.25	-	-	-	-	10.5
8b	7.33	5.17	22.17	49.52	22.76	1.12	-8.22	7.64	-1.5	11.32	8.5
8c	8.00	4.08	27.98	51.47	28.28	1.22	-4.45	6.92	0.13	8.23	3.0
8d	5.28	4.68	27.04	50.37	27.44	1.19	-7.45	11.86	-0.85	14.04	11.8
8e	2.85	5.12	32.68	53.92	33.09	1.43	-4.26	24.32	-0.26	24.70	12.0
8f	3.88	2.14	33.75	54.40	33.82	0.88	-11.3	17.82	-1.90	21.18	7.20
8g	5.30	7.76	25.34	44.53	26.48	1.14	-14.0	-0.59	-2.78	14.29	13.7
8h	6.10	6.38	21.10	40.81	22.04	.095	-10.2	3.18	-2.83	11.06	6.2
8i	2.60	7.10	20.19	42.90	25.22	1.09	-12.9	3.58	-5.98	8.06	13.5
8j	4.77	8.42	33.46	45.98	34.50	1.49	-18.7	9.66	-6.98	22.17	13.2
8k	2.08	1.36	37.67	60.54	37.70	1.63	-10.7	19.34	-2.84	22.31	8.5
8l	2.95	7.01	31.00	51.01	29.81	1.29	-12.1	12.44	-3.8	10.91	12.5

Table 2. Fastness properties of compounds **8a-l**

Dye	Washing,75 °C	Rubbing		Sublimation		Acid perspiration	Light, 40 h
		Dry	Wet	180 °C	210°C		
8a	4	3-4	3	3-4	3	4	4
8b	4	4	4	3-4	3	4	5
8c	4	4	4	4	3-4	4	4
8d	4	3	3	3-4	3	4	4-5
8e	4	3-4	3-4	4	3-4	4	5
8f	3-4	3	4	4	3-4	4	5
8g	4	4	3-4	3-4	3	3-4	4
8h	4	3-4	3	3-4	3	4	4
8i	4	4	3-4	4	3-4	4	4-5
8j	4	4	4	3-4	3	4	6-7
8k	4-5	4	4	3-4	3-4	4	6
8l	4	4	3	4	3	4	5

The elemental analyses were found to agree favorably with the calculated values. The dyeing assessment fastness tests, and color measurements were carried out at Misr Company for Spinning and Weaving, El-Mahala El-Kobra, Egypt. The syntheses of carbohydrazide **4**,[9] and arylazoacetylacetone **7**[12] were conduted according to known procedures.

Synthesis of 5-amino-6-[[4-arylazo-3,5-dimethylpyrazol-1-yl]-carbonyl]-3,4-diphenylthieno[2,3-c]pyridazine, 8a-l: General procedure

A mixture of 5-amino-3,4-diphenylthieno[2,3-*c*]pyridazine-6-carbohydrazide **4** (1.1 g, 3 mmoles) and the arylazoacetylacetone derivatives **7a-l** (3 mmoles) was refluxed in glacial acetic acid (25 cm^3) with stirring for 10 h. The reaction mixture was cooled to room temperature and poured into water (100 cm^3). The separated solid was filtered off, washed with water, dried and recrystallized from dimethylformamide.

5-Amino-6-[[4-phenylazo-3,5-dimethylpyrazol-1-yl]carbonyl]-3,4-diphenylthieno[2,3-c]pyridazine (8a, $C_{30}H_{23}N_7OS$)

Yellow crystals in 69.4% yield. M.p.: 140-142 °C; IR: ý = 3,400, 3,316 (NH_2), 3,060 (CH_{arom}), 2,925 CH_{aliph}), 1,676 (CO), 1,512 (N=N) cm^{-1}; MS: *m/z* = 529 [M^+, 5.35%], 424 [M - Ph-N=N, 5.3%], [M - substituted pyrazole, 50%].

5-Amino-6-[[4-(2-methylphenylazo)-3,5-dimethylpyrazol-1-yl]carbonyl]-3,4-diphenylthieno[2,3-c]pyridazine (8b, $C_{31}H_{25}N_7OS$)

Deep yellow crystals in 88.2% yield. M.p. 131-133 °C; IR: ý = 3,450, 3,370(NH_2), 3,056 (CH_{arom}), 2,924 CH_{aliph}), 1,678 (CO), 1,623 (C=N) 1,502 (N=N) cm^{-1}. MS: *m/z* = 544 [M^+ +1, 12.8%], 424 [M – $N=NC_6H_5Me$, 9.2%], 330 [M – substituted pyrazole, 5.7%].

 DOI: 10.17628/ecb.2014.3.18-23

5-Amino-6-[[4-(3-methylphenylazo)-3,5-dimethylpyrazol-1-yl]carbonyl]-3,4-diphenylthieno[2,3-c]pyridazine (8c, $C_{31}H_{25}N_7OS$)

Yellow crystals in 59.6% yield. M.p.: 132-134 °C; IR: ý = 3,360(NH_2), 3,059 (CH_{arom}), 2,924 CH_{aliph}), 1,678 (CO), 1,620 (C=N), 1,590 (C=C), 1,502 (N=N), cm .

5-Amino-6-[[4-(4-methylphenylazo)-3,5-dimethylpyrazol-1-yl]carbonyl]-3,4-diphenylthieno[2,3-c]pyridazine (8d, $C_{31}H_{25}N_7OS$)

Yellow crystals in 66.2% yield. M.p.: 150-152 °C; IR: ν = 3,400, 3,320(NH_2), 3,060 (CH_{arom}), 2,925 CH_{aliph}), 1,671 (CO), 1,623 (C=N), 1,590 (C=C), 1,502 (N=N), cm^{-1}; ^1H NMR (200 MHz, DMSO-d_6): δ = 2.33 (s, 3H, *p*-CH_3), 2.36 (s, 3H, 3-CH_3), 2.77 (s, 3H, 7-CH_3), 6.28 (s, 2H, NH_2), 6.89-7.25 (m, 4H, Phenylazo), 7.46-7.78 (m, 10H, 2Ph).

5-Amino-6-[[4-(2-methoxyphenylazo)-3,5-dimethylpyrazol-1-yl]carbonyl]-3,4-diphenylthieno[2,3-c]pyridazine (8e, $C_{31}H_{25}N_7O_2S$)

Yellow crystals in 71% yield. M.p.: 165-167 °C; IR: ν = 3,450, 3,400(NH_2), 3,057 (CH_{arom}), 2,923 CH_{aliph}), 2,852 (OCH_3), 1,668 (CO), 1,628 (C=N), 1,598 (C=C), 1,500 (N=N), cm^{-1}; ^1H NMR (200 MHz, DMSO-d_6): δ = 2.23 (s, 3H, 3-CH_3), 2.33 (s, 3H, *p*-CH_3), 2.77 (s, 3H, 7-CH_3), 3.83 (s, 3H, *o*-OCH_3), 6.27(s, 2H, NH_2), 6.88-7.24 (m, 4H, Phenylazo), 7.45-7.79 (m, 10H, 2Ph).

5-Amino-6-[[4-(4-methoxyphenylazo)-3,5-dimethylpyrazol-1-yl]carbonyl]-3,4-diphenylthieno[2,3-c]pyridazine (8f, $C_{31}H_{25}N_7O_2S$)

Yellow crystals in 71.5% yield. M.p.: 150-152 °C; IR: ν = 3,372, 3,337(NH_2), 3,060 (CH_{arom}), 2,924CH_{aliph}), 2,854 (OCH_3), 1,670 (CO), 1,630 (C=N), 1,597 (C=C), 1,505 (N=N) cm^{-1}; ^1H NMR (200 MHz, DMSO-d_6): δ = 2.22 (s, 3H, 3-CH_3), 2.32 (s, 3H, *p*-CH_3), 2.78 (s, 3H, 7-CH_3), 3.84 (s, 3H, *p*-OCH_3), 6.26(s, 2H, NH_2), 6.89-7.23 (m, 4H, Phenylazo), 7.44-7.78 (m, 10H, 2Ph).

5-Amino-6-[[4-(2-chlorophenylazo)-3,5-dimethylpyrazol-1-yl]carbonyl]-3,4-diphenylthieno[2,3-c]pyridazine (8g, $C_{30}H_{22}ClN_7OS$)

Red crystals in 89.7% yield. M.p.: 130-132 °C; IR: ν = 3,420, 3,350 (NH_2), 3,090 (CH_{arom}), 2,925CH_{aliph}), 1,685 (CO), 1,637 (C=N), 1,600 (C=C), 1,506 (N=N) cm^{-1}; ^1H NMR (200 MHz, DMSO-d_6): δ = 2.34 (s, 3H, 3-CH_3), 2.77 (s, 3H, 7-CH_3), 6.27(s, 2H, NH_2), 7.27-7.49 (m, 4H, Phenylazo), 7.41-7.79 (m, 10H, 2Ph).

5-Amino-6-[[4-(3-chlorophenylazo)-3,5-dimethylpyrazol-1-yl]carbonyl]-3,4-diphenylthieno[2,3-c]pyridazine (8h, $C_{30}H_{22}ClN_7OS$)

Red crystals in 76.9% yield. M.p.: 150-152 °C; IR: ν = 3,385, 3,305(NH_2), 3,059(CH_{arom}), 2,921CH_{aliph}), 1,670 (CO), 1,634 (C=N), 1,591 (C=C), 1,507 (N=N), cm^{-1}; ^1H NMR (200 MHz, DMSO-d_6): δ = 2.35 (s, 3H, 3-CH_3), 2.76 (s, 3H, 7-CH_3), 6.26(s, 2H, NH_2), 7.28-7.48 (m, 4H, Phenylazo), 7.42-7.78 (m, 10H, 2Ph). MS: *m/z* = 564 [M^+, 4.2%], 463 [M – 1, 6.3%],424 [M - N=NC_6H_5Cl, 2.2%], 330 [M – substituted pyrazole, 9%].

5-Amino-6-[[4-(3-nitrophenylazo)-3,5-dimethylpyrazol-1-yl]carbonyl]-3,4-diphenylthieno[2,3-c]pyridazine (8i, $C_{30}H_{22}N_8O_3S$)

Redich-brown crystals in 59.3% yield. M.p.: 159-161 °C; IR: ν = 3,439, 3,360(NH_2), 3,052(CH_{arom}), 2,922CH_{aliph}), 1,673(CO), 1,639 (C=N), 1,590 (C=C), 1,515, 1,333 (NO_2), 1,500 (N=N), cm^{-1}; ^1H NMR (200 MHz, DMSO-d_6): δ = 2.34 (s, 3H, 3-CH_3), 2.77 (s, 3H, 7-CH_3), 6.27(s, 2H, NH_2), 7.17-7.99 (m, 4H, Phenylazo), 7.41-7.79 (m, 10H, 2Ph). MS: *m/z* = 575 [M + 1, 0.09%], 424 [M - N=$NC_6H_5NO_2$, 30.2%].

5-Amino-6-[[4-(4-nitrophenylazo)-3,5-dimethylpyrazol-1-yl]carbonyl]-3,4-diphenylthieno[2,3-c]pyridazine (8j, $C_{30}H_{22}N_8O_3S$)

Redich-brown crystals in 50.3% yield. M.p.: 156-157 °C; IR: ν = 3,430, 3,364(NH_2), 3,050(CH_{arom}), 2,925CH_{aliph}), 1,670 (CO), 1,634 (C=N), 1,591 (C=C), 1,516, 1,335 (NO_2), 1,507 (N=N), cm^{-1}; ^1H NMR (200 MHz, DMSO-d_6): δ = 2.34 (s, 3H, 3-CH_3), 2.77 (s, 3H, 7-CH_3), 6.27(s, 2H, NH_2), 7.18, 8.10 (d,2H; d,2H Phenylazo), 7.41-7.79 (m, 10H, 2Ph). MS: *m/z* = 575 [M + 1, 0.02%], 424 [M - N=$NC_6H_5NO_2$, 33.2%].

5-Amino-6-[[4-(2-naphthylazo)-3,5-dimethylpyrazol-1-yl]carbonyl]-3,4-diphenylthieno[2,3-c]pyridazine (8k, $C_{34}H_{25}N_7OS$)

Brown crystals in 81.2% yield. M.p.: 118-120 °C; IR: ν = 3,425, 3,364(NH_2), 3,058(CH_{arom}), 2,924CH_{aliph}), 1,673 (CO), 1,624 (C=N), 1,592 (C=C), 1,506(N=N), cm^{-1}; ^1H NMR (200 MHz, DMSO-d_6): δ = 2.35 (s, 3H, 3-CH_3), 2.76 (s, 3H, 7-CH_3), 6.26(s, 2H, NH_2), 7.41-8.01 (m, 17H, naphthyl and 2Ph); MS: *m/z* = 580 [M + 1, 1%], 424 [M - N=$NC_{10}H_7$, 1%] and 330[M – substituted pyrazole, 10%].

5-Amino-6-[[4-(3-pyridylazo)-3,5-dimethylpyrazol-1-yl]carbonyl]-3,4-diphenylthieno[2,3-c]pyridazine (8l, $C_{29}H_{22}N_8OS$)

Brown crystals in 47.6% yield. M.p.: 237-239°C; IR: ν = 3,390, 3,3308(NH_2), 3,058(CH_{arom}), 2,921CH_{aliph}), 1,677 (CO), 1,600 (C=N), 1,562 (C=C), 1,504 (N=N) cm^{-1}; ^1H NMR (200 MHz, DMSO-d_6): δ = 2.33 (s, 3H, 3-CH_3), 2.77 (s, 3H, 7-CH_3), 6.27(s, 2H, NH_2), 7.34-8.45 (m, 14H, pyridyl and 2Ph); MS: *m/z* = 532 [M + 3.04, 1%], 424 [M - N=NC_5H_4N, 4.03%] and 330[M – substituted pyrazole, 10.8%].

 DOI: 10.17628/ecb.2014.3.18-23

Dyeing procedures

Preparation of dye dispersion

The required amount of dye (2% shade) was dissolved in DMF and added dropwise with stirring to a solution of Dekol-N (2 g/dm^3), an anionic dispersing agent of BASF, then the dye was precipitated in a fine dispersion ready for use in dyeing.

Dyeing of polyester at 130°C under pressure using Levegal PT (*carrier of Buyer*)

The dye bath (1:20 liquor ratio), containing 5 g/dm^3 Levegal PT (Bayer) as carrier, 4% ammonium sulfate, and acetic acid at pH 5.5, was brought to 60°C, the polyester fabric was entered and run for 15 min. The fine dispersion of the dye (2%) was added, and the temperature was raised to boiling within 45 min, dyeing was continued at boiling temperature for about 1 h, then the dyed material was rinsed and soaped with 2% nonionic detergent to improve rubbing and wet fastness.

Assessment of color fastness (Table 2)

Fastness to washing, perspiration, light, and sublimation was tested according to the reported methods.

Fastness to washing

A specimen of dyed polyester fabric was stitched between two pieces of undyed cotton fabric, all of equal diameter, and then washed at 50°C for 30 min. The staining on the undyed adjacent fabric was assessed according to the following grey scale: 1-poor, 2-fair, 3-moderate, 4-good, and 5-excellent.

Fastness to perspiration

The samples were prepared by stitching pieces of dyed polyester fabric between two pieces of undyed cotton fabric, all of equal diameter, and then immersing in the acid medium for 30 min. The staining on the undyed adjacent fabric was assessed according to the following grey scale: 1-poor, 2-fair, 3-moderate, 4-good, and 5-excellent. The acid solution (pH 3.5) contained sodium chloride 10 g/dm^3, lactic acid I g/dm^3, disodium ortho-phosphate 1 g/dm^3, and histidine monohydrochloride 0.25 g/dm^3.

Fastness to rubbing

The dyed polyester fabric was placed on the base of crockmeter (Atlas electronic type), so that it rested flat on the abrasive cloth with its long dimension in the direction of rubbing. A square of white testing cloth was allowed to slide on the tested fabric back and forth 20 times by making ten complete turns of the crank. For wet rubbing lest, the testing square was thoroughly wet in distilled water. The rest of the procedure was the same as the dry test. The staining on the white testing cloth was assessed according to grey scale: 1-poor, 2-fair, 3-moderate, 4-good, and 5-excellent.

Fastness to sublimation

Sublimation fastness was measured with an iron tester (Yasuda no. 138). The samples were prepared by stitching pieces of dyed polyester fabric between two pieces of undyed polyester, all of equal diameter, and then treated at 180 and 210°C for 1 min. Any staining on the undyed adjacent fabric or change in tone was assessed according to the following grey scale: 1-poor, 2-fair, 3-moderate, 4-good, and 5-excellent.

Fastness to light

Light fastness was determined by exposing the dyed polyester on a Xenotest 150 [Original Hanau, chamber temperature 25-30°C, black panel temperature 60 °C, relative humidity 50-60%, and dark glass (UV) filter system] for 40 h. The changes in color were assessed according to the following blue scale. I-poor, 3-moderate, 5-good. and 8-very good.

Color assessment

Table 1 reports the color parameters of the dyed fabrics assessed by tristimulus colorimetry. The color parameters of the dyed fabrics were determined using a SPECTRO multichannel photodetector (model MCPD1110A), equipped with a D65 source and barium sulfate as a standard blank. The values of (he chromaticity coordinates, luminance factor, and the position of the color in the CIE-LAB color solid are reported.

Conclusions

A set of 12 disperse dyes **8a-l** were synthesized by reaction of 5-amino-3,4-diphenylthieno[2,3-*c*]pyridazine-6-carbohydrazide **4** with arylazoacetylacetone derivatives. Most of them were investigated for their dyeing characteristics on polyester. They give bright intense hues from yellow to orange-yellow on polyester fabrics, due to the variations in polarity. The dyed fabrics exhibit good (4) washing, perspiration, rubbing and good to excellent (4-5) sublimation fastness properties (Table 2). The remarkable degree of levelness and brightness after washings is indicative of good penetration and the excellent affinity of these dyes for the fabric due to the accumulation of polar groups. This in combination with the ease of preparation makes them particularly valuable.

REFERENCES

[1]For part 24, see reference [13].

[2]Weaver MA, Shutteworth L. *Dyes and Pigments*, **1982**, *3*, 81-121.

[3]Towns AD, *Dyes and Pigments*, **1999**, *42*, 3-28.

[4]Hallas G and Towns D, *Dyes and Pigments*, **1997**, *35*, 45-55.

[5]Gordon P. E. and Gregory P., In: *Organic chemistry in colour* Berlin: Springer, **1983**,p. 139.

[6]Heinish G., Kopelent H., *Progress in Medicinal Chemistry: Pharmacologically Active Pyridazine Derivatives*, **1992**, Part 2, Vol. *29*, 141. Ed. By G P Ellis and G B West (Amsterdam: Elsevier Science Puplishers,

[7]Deeb, A., Kotb, M., El-Abassy, M., *Phosphorus, Sulfur and Silicon*,**2004**, *179*, 2245.

[8]Deeb A, El-Abassy M, *Phosphorus, Sulfur and Silicon*, **2006**, *181*, 397-404.

[9]Deeb A, El-Abassy M, *Phosphorus, Sulfur, and Silicon*, **2006**, 181:879-890.

[10]Deeb A., Said, S. A., Hamed, M. M., Yasin, F., *J. Chin. Chem. Soc*. **1990**, *37*, 287.

[11]Shawali, A. S., Abdel Galil, F. M., *Tetrahedron*, **1971**, *27*,:4305-4316.

[12]Ho, Y. W., Wang, I. J., *Dyes and Pigments*, **1995**, *29*, 117-129.

[13]Deeb A., Yassin, F., Ouf, N., Shehta, W., *Chem. Heterocycl. Compd*. **2010**, *262*, 512.

[14]Maradiya, H. R., Patel, V. S., *Chem. Heterocycl. Compds*, **2002**, *38*, 1324-1330.

[15]Sing, S. P., Kumar, D., *Heterocycles*, **1990**, *31*, 855-860.

[16]Society of *Dyes and Colorists Standard methods for the determination of color fastness of textiles and leather*, 5th edn. Society of Dyes and Colorists, Bradford **1990**.

Received: 18.08.2013.
Accepted: 07.10.2013.

PREPARATION, CHARACTERIZATION AND ELECTROCHEMICAL PROPERTIES OF CATION SELECTIVE MEMBRANES

Urfi Ishrat[a] and Rafiuddin[a]*

Keywords: Polystyrene-based strontium phosphate membrane; membrane potential; charge density

Polystyrene based strontium phosphate membranes (SPM) prepared by applying different pressures. The membrane potential was measured with uni-univalent electrolytes (KCl, NaCl, and LiCl) solutions using saturated calomel electrode (SCEs). The effective fixed charge density of these membranes was determined by TMS method and it showed dependence of membrane potential on the porosity, charge on the membrane matrix, charge and size of permeating ions. The membranes were characterized by X-ray diffraction, scanning electron microscopy, and IR spectroscopy. The order of surface charge density for electrolytes is found to be KCl > NaCl > LiCl. Other important parameters such as transport number, distribution coefficient, charge effectiveness and related parameters were calculated. The membrane was found to be mechanically stable, and can be operated over a wide pH range. Moreover, the experimental results were found to be quite satisfactorily with theoretical values.

Corresponding Authors
Tel/Fax: +91-571-2703515
E-Mail: rafi_amu@rediffmail.com
[a] Membrane Research Laboratory, Department of Chemistry, Aligarh Muslim University, Aligarh 202002

Introduction

Membrane can be employed in several applications, including drinking water treatment, waste water treatment and reclamation, and industrial water treatment, to produce high water quality. The membrane has also been applied to water softening due to rejection efficiency for monovalent and multivalent ions in hard water. It was found that an increase of NaCl concentration or a presence of divalent cations increased membrane fouling.[1] The behavior of membrane systems has extensively been investigated by studying the transport properties of artificial membrane used by some of the recent analytical and electronic, techniques have added impetus to such investigations.[2,3] The inorganic precipitated membranes have acquired particular significance in the last two decades. These membranes have several advantages over organic ion-exchangers e.g. their ability to withstand ionizing radiations and very high temperatures without undergoing degradation and their remarkably high selectivity for heavy toxic metals. [4,5]

Variety of transport phenomena arise across a membrane when subjected to different driving forces.[6,7] Some of these phenomenons such as ion migration, electro osmosis, self diffusion, salt migration and membrane potential etc. occurring across the ionic membrane have been described by spiegler[8] applying the principles of non-equilibrium of thermodynamics.

A precipitated membrane is a system consisting of a thin inorganic precipitate such that when in contact with salt solutions containing some of the precipitated generating ions, two oppositely charged layer at each membrane solutions interface are formed. These layers are due to the absorbed ions on the precipitated membrane which can easily be joined or removed from membrane. The electrical properties of these membranes can dramatically change due to the absorption, deposition or diffusion of ions into these structures.

In this paper, we describe the preparation of strontium phosphate membranes using an appropriate concentration of polystyrene (25%) as a binder were found to be quite stable by applying different pressures.[9] An attempt has been made to examine the validity of the recently developed method used for one determination of charge densities are based on the equations for membrane potential using different electrolyte concentration by Torell, Meyer, and Siever (TMS).[10,11] The evaluation of charge density of membrane which is an important parameter controlling the membrane phenomenon have been used to calculate the membrane potential at different electrolyte concentration using the extended TMS theory to test the applicability of these recently developed equation for membrane potential for system under investigation.

TMS developed a theory of membranes with charges fixed within the lattice. This theory has been described in detail by Lakshminarayanaiah and has been applied by Siddiqi et al for the determination of thermodynamic fixed charge density of precipitated membranes.

Experimental

Preparation of membrane

Strontium phosphate membranes were prepared by method suggested be Beg and coworkers.[12,13] The main reagents used for the synthesis are 0.2 mol trisodium phosphate solution (E. Merch. India with purity of 99.90%)

with 0.2 mol strontium chloride solution. The precipitate obtained was well washed with deionized water to remove free electrolyte and dried at 50 °C. The dried precipitate was ground into fine powder by pestle mortar and then sieved through 200 mesh (granule size ≤0.075 mm) pure amorphous polystyrene (Otto Kemi, India , Analytical reagent) used as a binder were also ground and sieved through 200 mesh. For membrane of adequate mechanical strength optimum quantity of binder to be embedded by using ratio of precipitate and binder. The membranes prepared by embedding 25 % of polystyrene were most suitable for our experiment. Those containing large amount of binder (>25 %) did not give reproducible results while those containing lesser amount (< 25%) were quite unstable. The temperature at which the membrane were mould was kept at 90 °C and then mixture was kept into cast die having diameter 2.45 cm and placed in an oven maintain at 200 °C for about half an hour to equilibrate the reaction mixture, then die was transferred to a pressure device (SL-89,UK) and different pressures like 50, 70, 90 and 110 MPa were applied.

For the evaluation of membrane fixed charge density, measurements of membrane potential were carried out by constructing a concentration cell.

Measurement of membrane potential

The prepared membranes were placed between two collared glass tubes each having a hole for introducing the electrolyte solution and saturated calomel electrodes (SCEs). The solutions were stirred by means of magnetic stirrers. The cell potential was taken as a measure of membrane potential. The measurements were carried out at 25 °C (±0.1 °C). The Electrochemical cell of the type

SCE	solution	Membrane	solution	SCE
	C_2	Diffusion potential	C_1	
	Donnan potential		Donnan potential	

was used to measure electrical potentials arising across the membrane by maintaining a tenfold difference in concentration (C_2/C_1 = 10) and using. The various salt solutions (chloride of Li^+, Na^+ and K^+) were prepared from analytical-grade reagents (BDH) with deionizer water. The experiment and the potentials were measured at 25 ºC.

Characterization of Membrane

Water Content (% Total Wet Weight).

First, the membranes were soaked into water to elute diffusible salt, blotted quickly with Whatsman filter paper to remove surface moisture and immediately weighed. These were further dried to a constant weight in a vacuum over P_2O_5 for 24 hours. The water content (total wet weight) was calculated as,

$$\text{Total wet weight (in \%)} = \frac{W^{w} - W^{d}}{W^{w}} \times 100$$

where

W^w is the weight of the soaked/wet membrane, and

W^d is the weight of the dry membrane.

Scanning electron microscopy (SEM)

The characterization, composite pore structure, micro/macro porosity, homogeneity, thickness, cracks and surface morphology of membranes have been well studied by scanning electron microscope (SEM) micrographs[14,15] **Fig. 1**. In the SEM, different interactions give images based on topography, elemental composition or density of the sample. A SEM can magnify up to about 100,000 xs.

FTIR Studies

The FTIR spectrum of polystyrene (*A*), Composite of strontium phosphate and polystyrene (*B*), and pure strontium phosphate(*C*), dried at 40 ºC, were taken by KBr disc method at room temperature (**Fig. 2).**

XRD Analysis

Powder X-ray diffraction (XRD) pattern was obtained in an aluminum sample holder for composite of strontium phosphate and polystyrene in the original form using a PW, 1148/89-based diffractometer with Cu Kα radiations shown in **Fig. 3**.

Effect of pH.

A series of solutions of varying pH in the range of 2 –11 were prepared, keeping the concentration of the relevant ion constant (1×10^{-2} mol L^{-1}). The value of electrode potential at each pH was recorded, and plot of electrode potential versus pH was plotted **Fig. 6**.

Result and discussion

A number of investigators using Scanning electron microscopy (SEM) have studied the characterization of membrane morphology.[16] From SEM images (**Fig 1)** well-ordered precipitates, composite pore structure, micro/macro porosity, surface texture homogeneity, thickness and crack free membranes has been widely studied,[17,18] SEM images of the strontium phosphate membranes were taken at 50-110 MPa pressures (**Fig 1)**.

The SEM images are composed of dense and loose aggregation of small particles and formed pores probably with non-linear channels. Particles are irregularly condensed and adopt a heterogeneous structure composed of masses of various sizes. The surface openings also seem to decrease with increasing applied pressure from 50-110 MPa.

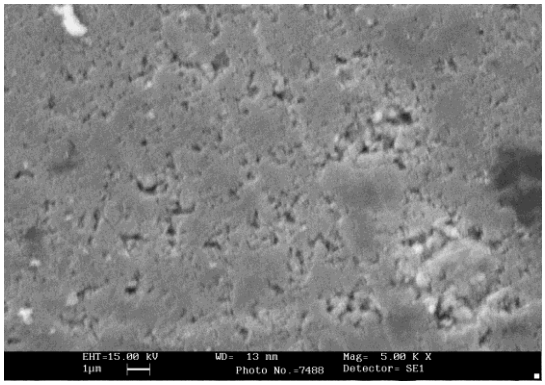

a)

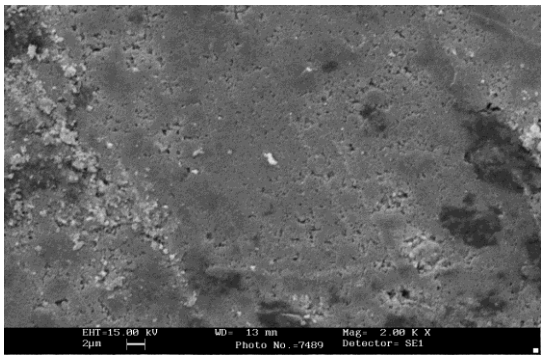

b)

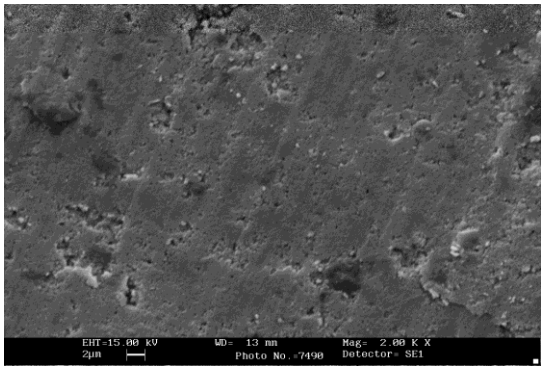

c)

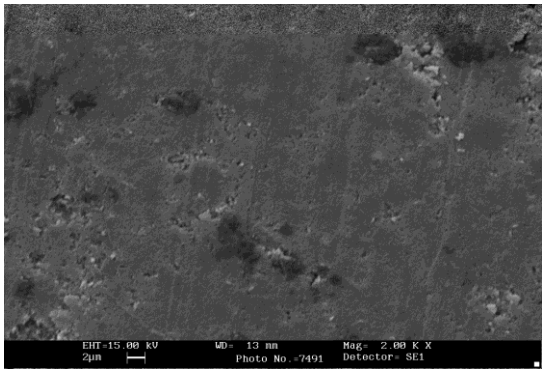

d)

Figure 1. SEM images of polystyrene-based SPMs (a), (b), (c) and (d) prepared at different applied pressures (50, 70, 90 and 110 MPa), respectively.

The FTIR spectra were performed to a certain composition and the possible addition sites of the strontium phosphate membrane and pure polystyrene. The spectra contained weak to strong intensity peaks assigned to various functional groups in the material synthesized (**Fig 2**). The peaks in the range 696 to 874 cm^{-1} show the presence of aromatic ring in the polystyrene based strontium phosphate membrane [19]. The peaks 2852 and 2927 cm^{-1} support the C-H bond frequency due to stirring moiety in the material. The characterization peaks of phosphate groups are present in the spectra exhibiting the presence of phosphate group attached to the metal in the composite. The IR result, generally showing the negative shift in the spectra for most of the functions in the synthesized material is shown in **Fig 2**.

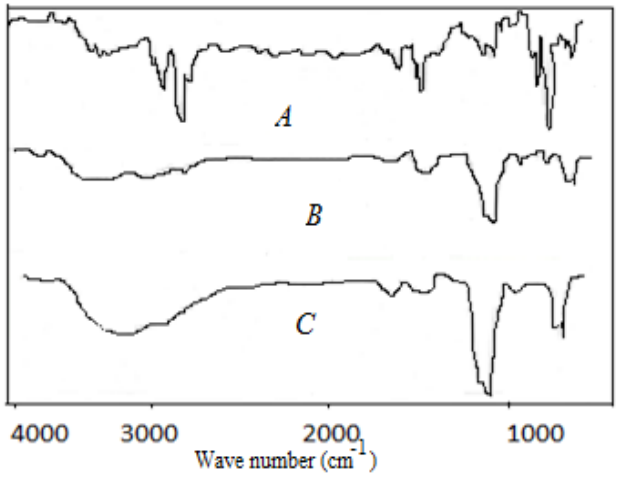

Figure 2. IR spectra of polystyrene *(A)*, composite (*B*), strontium phosphate (*C*).

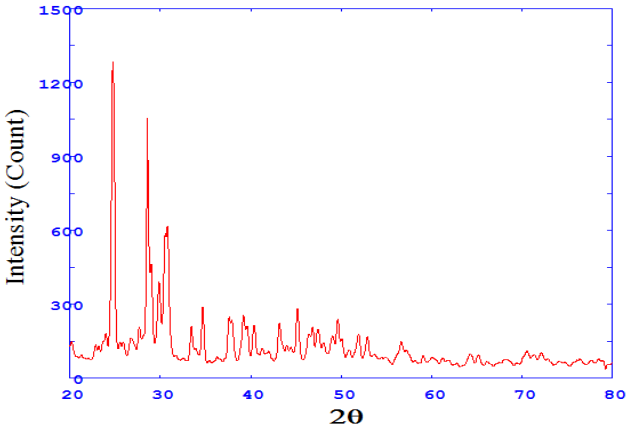

Figure 3. XRD pattern of polystyrene based strontium phosphate composite material.

The polymeric nature of the composite has also been supported from the other studies (Vide Supra). And the X-ray diffraction pattern of strontium phosphate cation exchange material recorded in powdered sample exhibited some sharp peaks in the spectrum in **Fig 3**. It is clear from the figure that the nature of composite cation exchange material is semi-crystalline.

The characterization parameters of the polystyrene-supported strontium phosphate membrane are given in **Table 1**.

Table 1. Characterization parameters of SPMs at different pressure

P, MPa	Membrane thickness, (cm)	H_2O content (wt. %, wet membrane	Porosity, (unit less)	Swelling (wt.%, wet membrane
50	0.090	0.0476	0.0201	no swelling
70	0.080	0.0361	0.0150	no swelling
90	0.070	0.0240	0.0115	no swelling
110	0.060	0.0123	0.0067	no swelling

This membrane shows a negligibly small swelling when immersed in sodium chloride solution. Porosity is determined by relationship:

$$\varepsilon = \frac{W^{w} - W^{d}}{AL\rho}$$

where W^d is the weight of the dry membrane and W^w is the weight of the wet membrane, ρ the density of water and L and A the thickness and area of the membrane respectively(g\(cm^3.g\cm^3))Like the swelling, the membrane has low porosity. The electrical potential increases with increasing pressure. The thickness of the membrane was measured by taking the average thickness of the membrane by using screw gauze and the swelling is measured as the difference between the average thickness of the membrane equilibrated with 1 M NaCl for 24 h and the dry membrane. Membrane was tested for chemical resistance in strongly oxidant, acidic and alkaline media. In acidic (1 M HCl) and in alkaline media (1 M NaOH) few significant modifications were observed after 24, 48 and 168 h, demonstrating that the membrane was quite effective in such media. However, in strong oxidant media the synthesized membrane became fragile in 48 h and broken after 168 h, losing mechanical strength. In general membranes having the same chemical composition were found to absorb same amount of water, where density of the ionisable groups are same throughout the membrane.[20]

When two-electrolyte solutions of different concentrations are separated by a membrane, the mobile species penetrate the membrane and various transport phenomenons like diffusion potential, electro osmosis, are induced in the system. This field maintains on macroscopic scale electro neutrality by increasing the speed of slow moving ion and decreasing that of the faster ion. The magnitude and sign of the potential depend on the characteristics of the membrane and the permeating species .If the membrane carries no fixed charges or sites the electric potential across the membrane would be the same as the liquid junction potential .On the other hand, if the membrane carries some charges the magnitude of the potential is usually determined by the concentration of the electrolyte solution surrounding the membrane and its sign by the nature of the fixed charge.

The charges fixed in the lattice are determined by the theory developed by Teorell, Meyer and Sievers.[21] In the TMS method there is an equilibrium process at each solution membrane interface which has a formal analogy with the Donnan equilibrium. With this, there is an internal salt diffusion potential, which was first represented by the Henderson equation and later by the more nearly correct Planck expression.

According to TMS theory, the membrane potential in $\delta\Psi_m$, mV (applicable to a highly idealized system) is given by the equation (1) at 25 °C.

$$\Delta\Psi_m = 59.2\left(\log\frac{C_2\sqrt{4C_1^2 + D^2} + D}{C_1\sqrt{4C_2^2 + D^2} + D} + U\log\frac{\sqrt{4C_2^2 + D^2} + UD}{\sqrt{4C_1^2 + D^2} + UD}\right) \quad (1)$$

where

$U=(u-v)/(u+v)$

u and v are the mobilities of the cation and anion

(m^2 V^{-1} s^{-1}), respectively, in the membrane phase.

C_1 and C_2 are concentrations of the electrolyte solution on either side of the membrane and

D is the charge on the membrane expressed in equivalent per liter.

To evaluate this parameter for the simple case of a 1:1 electrolyte and a membrane carrying a net negative charge of D = 1 as well as $D \leq 1$, theoretical concentration potentials across the membrane were calculated as a function of –log C_2, the ratio C_2/C_1 being kept at a constant value of 10 for different mobility ratios u/v and potted as in graph by smooth curves in **Fig. 4**. The experimental $\delta\Psi_m$ values for strontium phosphate with KCl electrolyte were

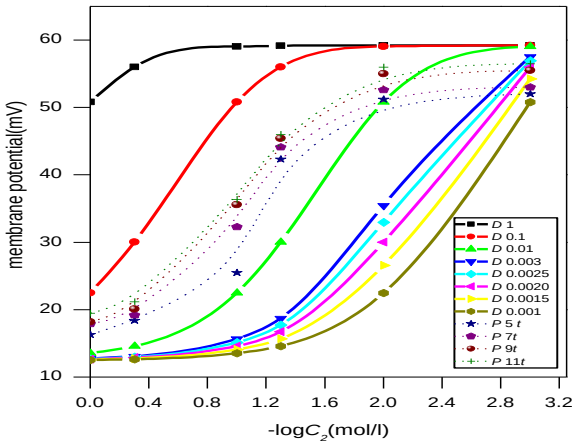

plotted in the same graph as function of -log C_2.

Figure 4. Plots of membrane potential vs –log C_2 for SPMs prepared at different pressures 50-110 MPa. Smooth curves are the theoretical concentration potentials for D =1 at different mobility ratio. Broken lines are the experimental values $\Delta\Psi_m$ for different concentration of KCl solution.

For various electrolyte solutions the observed membrane potential of SPM at 25 ± 1 ºC are given in Table 2.

The magnitude of the membrane potential depends on several factors, like the ratio of counter ion to co-ion mobility, concentration of salt solution and the exchange characteristics of the membrane material for various cations.

Table 2. $\delta\Psi^m \pm 0.5$ mV across the strontium phosphate membranes in contact with 1:1 electrolyte solutions at different concentrations.

Concentration C_2, **mol L^{-1}**	**Applied pressure(** ***MPa*****)**											
	50			**70**			**90**			**110**		
	KCl	NaCl	LiCl	KCl	NaCl	LiCl	KCl	NaCl	LiCl	KCl	NaCl	LiCl
1.0	16.3	19.0	20.0	17.9	20.0	20.5	18.2	21.0	22.2	19.5	22.9	23.8
0.50	18.4	25.9	26.6	19.2	25.6	27.0	20.1	36.5	37.4	21.2	37.2	39.1
0.10	25.5	26.4	28.0	32.3	35.2	36.6	35.6	37.0	38.0	36.4	38.8	39.9
0.05	42.3	45.3	46.2	49.1	48.5	49.0	51.5	52.6	53.3	52.0	53.0	53.5
0.01	51.2	52.0	52.5	52.6	53.2	54.0	55.0	55.5	56.0	57.0	56.5	57.0
0.001	52.0	52.5	53.0	53.0	54.5	54.8	55.5	56.0	56.3	58.5	57.0	57.5

The values of membrane potential (Table 2) reveal the following order $Li^+ > Na^+ > K^+$. The higher membrane potential observed with Li^+ is due to the fact that Li^+ is not thermodynamically favoured in the membrane phase.

The coinciding curve for all membrane gave the values for the charge density *D* within the membrane phase. The values of the *D* obtained in this for various membrane electrolyte systems are given in **table 3**. The surface charge density *D* of strontium phosphate membrane is found to depend on applied pressure. The increase in the values of *D* with higher applied pressure may be due to increase of charge per unit volume of the membrane and the order for electrolytes used is KCl > NaCl > LiCl.

Table 3. Calculated values of membrane charge density ($D\pm0.1\text{x}10^{-3}$ eqv. L^{-1}) for various SPMs electrolyte systems using TMS equation.

Applied pressure, MPa	Electrolyte, *D*x10-3		
	KCl	NaCl	LiCl
50	1.20	1.10	0.90
70	1.40	1.20	1.00
90	2.50	2.00	1.80
110	3.60	2.40	2.10

The values for the membrane potential are of the order of positive mV and decrease with an increase of external electrolytes concentration. This shows membrane is negatively charge (cation selective)[22,23] and selectivity of the cation increases with dilution. The selectivity character of ion exchange membrane with (1:1), (1:2), (1:3) has been reported.[24,25]

This TMS method gave satisfactory result for fixed charge density evaluation. This technique has been used to estimate the capacity of thin polymer membranes of polyvinyl chloride and poly vinyl acetate. It has also been used to determine the charge of Keratin, to evaluate the fixed charge on thin parlodian and parchment supported membranes. In addition to the Eqn. (1), Teorell, Meyer and Sievers further extended their theory and derived another equation for membrane potential considering the total potential, as the Donnan potential $\delta\Psi_{donnan}$, between the membrane surfaces and the external solutions, and the diffusion potential $\delta\Psi_{diff}$,within the membrane.[26,27]

$$\delta\Psi_{m,e}=\delta\Psi_{don}+\delta\Psi_{diff} \qquad (2)$$

where

$$\delta\Psi_{don} = -\frac{RT}{V_k T}\ln\left(\frac{\gamma''_{\pm}C_2C_{1+}}{\gamma'_{\pm}C_1C_{2+}}\right) \qquad (3)$$

R, *F* and *T* have their usual significance, $\gamma'_{\pm}$ and $\gamma''_{\pm}$ are the mean ionic activity coefficient C_{1+} and C_{2+} are the cation concentration on the two sides of the charged

$$C_+ = \sqrt{\left(\frac{V_x D}{2V_k}\right)^2 + \left(\frac{\gamma_{\pm}C}{q}\right)^2} - \frac{V_x D}{2V_k} \qquad (4)$$

where V_k and V_x refer the valency of cation and fixed charge group on the membrane matrix, q is the charge effectiveness of the membrane and is defined by the equation (5).

$$q = \sqrt{\frac{\gamma_{\pm}}{K_{\pm}}} \qquad (5)$$

where $K_{\pm}$ is the distribution coefficient expressed as

$$K_{\pm} = \frac{\overline{C_i}}{C_i}; \qquad \overline{C_i} = C_i - D \qquad (6)$$

where C_i is the i^{th} ion concentration in the membrane phase and C_i is the ith ion concentration of the external solution. The diffusion potential, $\delta\Psi_{diff}$ was expressed in the form

$$\delta\Psi_{diff} = -\frac{RT\varpi - 1}{V_k F\varpi + 1}\times\ln\left(\frac{(\varpi+1)C_{2+} + (V_x/V_K)D}{(\varpi+1)C_{1+} + (V_x/V_k)D}\right) \qquad (7)$$

Here $\varpi = u/v$ is the mobility ratio of the cation to anion in the membrane phase. The total membrane $\delta\Psi_{m,e}$ potential was, thus, obtained by simple addition of Eqns. (3) and (7).

 DOI: 10.17628/ecb.2014.3.24-31

$$8\Psi_{m,e} = -\frac{RT\varpi - 1}{V_k F\varpi + 1} \times \ln\left(\frac{(\varpi+1)C_{2+} + (V_x/V_K)D}{(\varpi+1)C_{1+} + (V_x/V_k)D}\right) \quad (8)$$

$$\Delta\psi^m = \frac{RT}{F}(t_+ + t_-)\ln\frac{C_2}{C_1} \quad (9)$$

$$\frac{t_+}{t_-} = \frac{u}{v} \quad (10)$$

In order to test the applicability of these theoretical equations for the system under investigation, the Donnan potential and diffusion potential were separately calculated from membrane potential measurement using a typical membrane prepared at 70 MPa pressure. Eqs.(9) and (10) were first used to get the values of transport numbers t_+ and t_- from experimental membrane potential data and consequently, the mobility ratio $\varpi = u/v$ within the membrane phase. The values of mobility ratio (ϖ) of the electrolytes in the membrane phase were found to be high at lower concentration of all electrolytes (KCl, NaCl, LiCl). Further increase in concentration of electrolytes led to a sharp drop in the values of ϖ as given in **Fig 5.**

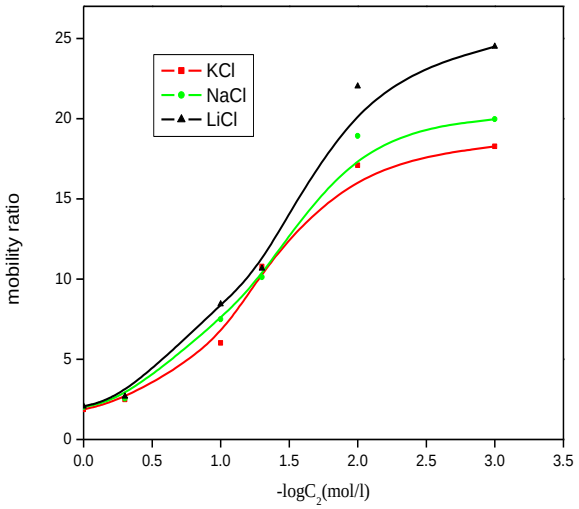

Figure 5. Plots of mobility ratio against –log C_2 for SPM using 1:1 electrolytes.

The higher mobility is attributed to higher transport number of comparatively free cations of electrolytes and also be similar trend as the mobility in least concentrated solution. The values of t_+ calculated from observed membrane potential are given in **Table 4**.

Here, t_+ is not a true transport number since water permeation has not been taken into account, however , in dilute solutions the values of t_+ approach closer to the true values. **Fig. 6** shows that the transport number decreases with increase in concentration of the salt solution.

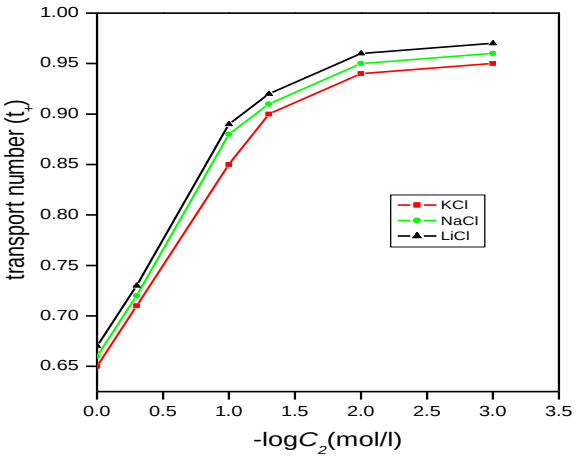

Fig. 6. Plots of t_+ (transprot number) of various electrolytes

As the concentration of the electrolytes increased, the values of distribution coefficient decreased, thereafter, a stable trend was observed as shown in **Fig. 7**. The large deviation in the value at lower concentration of electrolytes was attributed to the high mobility of comparatively free charges of the strong electrolyte.

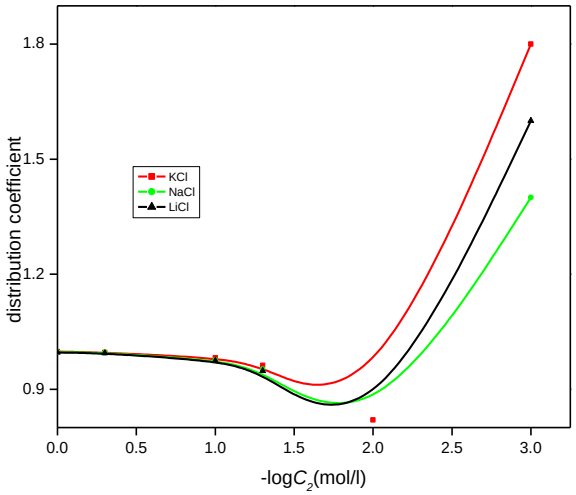

Figure 7. Plots of the distribution coefficient against –log C_2 for SPM using various 1:1 electrolytes.

Donnan potential at various electrolyte concentration were then calculated from the parameters, C_{2+}, ϖ , q'' and $K_\pm$ by using Eqs. 3-7 and values of the parameters derived for the systems have been given in **Table 5**. The values of γ_+ were the usual values for electrolytes. For comparison, the experimentally obtained values of membrane potentials for the system have also been drawn in the same figure. It may be noted that the experimental data follow the theoretical curve quite well. Whereas some deviations may be due to various non-ideal effects, such as swelling and osmotic effects, membrane inhomogeneity and hydrophobic/hydrophilic effects which were prominent and simultaneously present in the membrane.[27] These effects are often simultaneously present in charged membranes.

Table 4. The calculated values of the parameters (t_+, $K_\pm$, q'', C_{2+}, and ϖ) of SPM prepared at a pressure of 70 *MPa* with different concentration of electrolytes using Eqs. (4)- (6), (9) and (10).

KCl(electrolyte)C_2	t_+	$K_\pm$	q''	C_{2+}	ϖ
1.00	0.65	0.99	1.00	0.9937	1.760
0.50	0.66	0.996	1.001	0.4937	2.220
0.10	0.77	0.98	1.009	0.0938	4.00
0.05	0.89	0.962	1.018	0.0439	6.020
0.01	0.94	0.820	1.104	0.0051	13.89
0.001	0.95	0.80	1.118	0.0007	15.56
NaCl(electrolyte)C_2	t_+	$K_\pm$	q''	C_{2+}	ϖ
1.00	0.66	0.997	1.001	0.9916	1.94
0.50	0.70	0.995	1.002	0.4916	2.53
0.10	0.79	0.976	1.012	0.0918	4.20
0.05	0.91	0.952	1.024	0.0421	7.55
0.01	0.95	0.76	1.147	0.0041	15.56
0.001	0.96	1.40	1.245	0.0009	16.81
LiCl(electrolyte)C_2	t_+	$K_\pm$	q''	C_{2+}	ϖ
1.00	0.67	0.996	1.002	0.990	2.02
0.50	0.73	0.994	1.003	0.490	2.63
0.10	0.89	0.974	1.013	0.091	4.70
0.05	0.92	0.948	1.027	0.415	8.14
0.01	0.96	0.740	1.162	0.004	16.81
0.001	0.97	1.600	1.390	0.0001	18.26

The pH response profile for the membrane was tested by use of (1×10^{-2} mol L^{-1}) electrolytes solution over the pH range 2.0 – 11.0. The pH was adjusted by introducing small drops of hydrochloric acid (0.1 M) or sodium hydroxide (0.1 M) into the solutions. The influence of the pH response on the composite membrane electrode is shown in **Fig 8**.

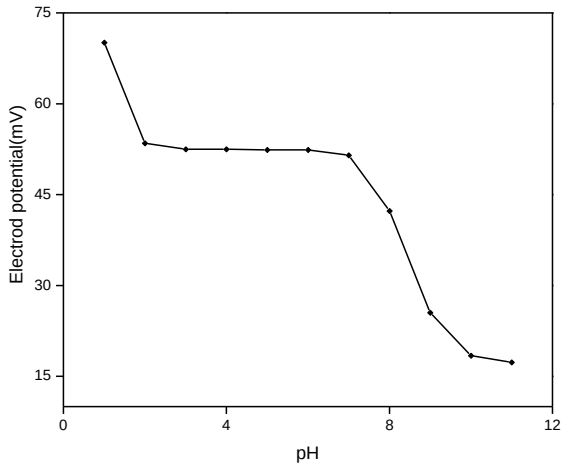

Figure 8. The effect of pH of the KCl solutions (1×10^{-2} mol L^{-1}) on the potential response of membrane.

As seen in figure, the potential remained constant from pH 2.0 to 7.0, beyond which some drifts in the potentials were observed. The observed drift at higher pH values could be due to the formation of some Hydroxyl complexes of cations (K^+, Cl^+, Li^+) the solution. At the lower pH values, the potentials increased, indicating that the membrane responded to protonium ions, as a result of the some extent protonation of phosphorus atoms of the phosphate. In the other hand, at lower pH values H_3O^+ ions start to contribute to the charge transport process by the membrane, thereby causing interference.

Conclusions

With uni-univalent electrolyte (KCl, NaCl, and LiCl) solution membrane potential were measured for inorganic membranes using saturated calomel electrodes. The membrane potential offered by electrolytes is in the order LiCl > NaCl > KCl and the obtained data indicates that the behavior investigated membrane is cation selective and the order of selectivity of cation transporting through the membrane has been found as $K^+ > Na^+ > Li^+$. The effective fixed charge densities and transport number of strontium phosphate membrane were evaluated by a TMS method. Charge density values obtained, by the frequently used TMS procedure, has been used to test the recently extended TMS equation by computing membrane potentials at different concentrations. Membranes prepared at high pressure (110 MPa) carry higher charge density and have narrow surface openings and low porosity. And the strontium phosphate membranes work well in the pH range 2.0–7.0. The theoretical predictions for membrane potential are borne out quite satisfactorily by our experimental results for all membranes.

Nomenclature

$C_{1,,}C_2$ Concentration of electrolyte solution either side of the membrane (mol L^{-1})

 DOI: 10.17628/ecb.2014.3.24-31

$\bar{C}_{1+}$	Cation concentration in membrane phase 1 (mol L^{-1})
C_{2+}	Cation concentration in membrane phase 2 (mol L^{-1})
C_i	i^{th} ion concentration of external solution (mol L^{-1})
D	Charge density in membrane (eq L^{-1})
F	Faraday constant (C mol^{-1})
$K_{\pm}$	Distribution coefficient of ions
$K_{2\pm}$	Distribution coefficient of ions (electrolyte solution C_2)
P	Pressure (5-11 MPa)
q_1	Charge effectiveness of membrane phase 1
q_2	Charge effectiveness of membrane phase 2
R	Gas constant (J K^{-1} mol^{-1})
SCE	Saturated calomel electrode
SEM	Scanning electron microscopy
TMS	Teorell, Meyer and Sievers
XRD	Powder X-Ray diffraction
FTIR	Fourier Transform Infrared Studies
t_+	Transport number of cation
t_-	Transport number of anion
u	Mobility of cations in the membrane phase (m^2 V^{-1} s^{-1})
U	$(u\text{-}v/(u+v)$
V	Mobility of anions in the membrane phase
V_k	Valency of cation
V_x	Valency of fixed charge group
$\gamma'_{\pm'}, \gamma''_{\pm}$	Mean ionic activity coefficient for electrolytes solution C_1 and C_2
ϖ	Mobility ratio (TMS extension theory)
$\Delta\Psi_m$	Membrane potential (mV)
$8\Psi_{m,e}$	Membrane potential (mV) (TMS extension theory)
$8\Psi_{don}$	Donnan potential (mV)
$8\Psi_{diff}$	Diffusion potential (mV)

Acknowledgement

The authors are thankful to the Chairman, Department of Chemistry for providing research facilities, All India Institute of Medical Sciences (AIIMS),New Delhi for providing SEM micrograph, Zakir Hussain College of Engineering and Technology AMU for X-Ray Analysis and financial assistance provided by the University Grant Commission (UGC). India is also acknowledged**.**

References

[1]Hong, S., *J. Membr. Sci*., **1997,** *132*, 159–181

[2]Lakshminarayanaih, N. and Siddiqui. F. A., *Biophys. J*, **1971**, *11*, 603.

[3]Kobatake, Y. and Kamo, N., *J. Polym. Sci*., **1972**, *5*, 257.

[4]Nabi S.A., Shallo, A. H., Khan, Ganie Sajad. A., Synthesis, characterization and analytical applications of titanium(IV) molybdosilicate: A cation ion-exchanger *Colloid Surf A: Phsicochem Aspect*., **2007**, *302*, 241-250.

[5]Zhang. H., Pang, J. H., Wang, D., Li, A., Li, X., Jiang, Z., *J. Membr. Sci.*, **2005**, *26*, 56–64.

[6]Lakshminarayanah, N., *Chem. Rev*. **1965**, *65*, 493.

[7]Lakshminarayananaiah.N.,"Membrane Electrodes", Academic Press, New York, **1976**.

[8]Spiegler, K. S., *Trans, Faraday Soc.*, **1958**, *54*, 1408.

[9]Ishrat, U., Rafiuddin, *Desalination*, **2012**, *8-12*, 286.

[10]Torell, T., *Proc Natl. Acad. Sci. (USA*), **1935**, *21*, 152.

[11]Meyer, K., Sievers, H. J. F., *Helv. Chim. Acta*, **1936**, *19*, 649, 665, 987

[12]Jabeen, F., Rafiuddin, *J. Sol-Gel Sci. Technol.*, **2007**, *44*, 195-202

[13]Beg, M. N., Siddiqi, F. A., Singh, S. P., Prakash, P., Gupta, V., *Electrochim. Acta*., **1979**, *24*, 85-88.

[14]Huang, L., Wang. Z., Sun, J., Zhili, L.M.Q, Yan, Y., Zhao, D. U., *J. Am. Chem. Soc*., **2000**, *122*, 3530.

[15]Izutsu, H., Mizukami. F., Nair, P. K., Kiyozumi, Y., Maeda K., *J. Mater.Chem.*, **1997**, *7(5)*, 767-771.

[16]Santos, L. R. B., Pulcinelli, S. H., Santilli, C. V., *J. Sol-Gel. Sci. Technol*., **1997**, *8*, 477.

[17]Resina, M., Macanas, J., de Gyves, J., Munoz, M., *J. Membr. Sci.*, **2001,** *289*, 150-158.

[18] Arfin, T., Rafiuddin, *J. Electroanal. Chem*., **2009**, *636*, 113-122.

[19]Nakamoto, K., *Infrared and Raman Spectra of Inorganic and Coordinate Compounds*, Wiley-Interscience, New York, **1986.**

[20]Koter, S., Piotrowski, P., Kerrs, J., *J. Membr. Sci*., **1999**, *153*, 83.

[18](a)Teorell, T., *Proc. Soc. Expt. Biol. Med*. **1935**, *33*, 282; (b) *Proc. Natl. Acad. Sci., USA*. **1953**, *21*, 152; (c) *Z Elektrochem*. **1951**, *55*, 460; (d) *Proc. Biophys. Biophys. Chem*., **1953,** *3*, 305.

[22]Jabeen. F., Rafiuddin, *J. Porous Matter*., **2009**, *16*, 257-265.

[23]Arfin, T., Rafiuddin, *Electrochim. Acta.*, **2009,** *54*, 6928-6934.

[24]Singh, K., Tiwari, A. K, Rai, J. P., *Ind. J. Chem.*, **1985**, *24*, 825.

[25]Singh, K., Tiwari, A. K., *Proc. Indian Natl. Sci. Acad. A.*, **2004**, *70*, 477.

[26]Matsumoto, H., Tanioka, A., Murata, T. Higa, M., Horiuchi, K., *J. Phys. Chem. B*, **1998**, *102*, 5011-5016.

[27]Chou, T. J., Tanioka, A., J. Coll. Interface Sci., **1999**, *212*, 293-300.

Received: 19.06.2013.
Accepted: 25.10.2013.

SORPTION STUDIES OF SOME BIOLOGICALLY IMPORTANT UNIVALENT SALTS USING POLYANILINE PICRATE AS SORBENT

C. Dhivya,[a] S. Anbu Anjugam Vandarkuzhali,[a] P. Saroja,[a] R. Santhi,[a] and N. Radha[a]*

Keywords: polyaniline picrate, sorption isotherms, Ion Exchange Capacity, antimicrobial studies.

Polyaniline picrate (PANIPI) was synthesized via facile chemical polymerisation route. The as synthesized PANIPI was characterized using UV-Visible, FT-IR and PXRD spectroscopic techniques. Adsorption capacity of the as prepared resin was evaluated from the sorption process. Sorption isotherms were constructed using Langmuir, Freundlich, Redlich-Peterson and Temkin models. The spectral changes after the sorption process were studied using UV-Visible and FT-IR techniques. Facile pH for the adsorption is found to be 5-7. A comparison of ion exchange capacities of PANIPI revealed selectivity of 3:2 for sodium and potassium chlorides. The nanosized PANIPI is a potent antimicrobial agent and can be utilized as a biocompatible material.

Corresponding Author
Tel: +91 9943842908
E-Mail: radha.chem1955src@gmail.com
[a] PG and Research Department of Chemistry, Seethalakshmi Ramaswami College, Tiruchirappalli- 620 001, Tamil Nadu, India.

Introduction

Univalent ions like Li^+, Na^+, K^+, NH_4^+ and Cl^- are biologically important as they are involved in osmoregulation occuring in all living cells. The mobility of these ions across the cell membrane is facilitated through ion channels.[1] The specific role of these channels is to provide proper Na^+/K^+ ionic balance in living species. Many macrocyclic ligands and polymer analogues have been utilized to understand various ion recognition and transport in biological tissues.[2]

Sorption processes[3] are used widely to understand the ion transport mechanism across polymeric materials. Mechanism of sorption depends on the chemical nature of the metal ion, adsorbent and environmental conditions such as ionic strength, pH and temperature.

Among various conducting polymers[4,5] which possess unique features for incorporating and adsorbing ions in the polymer matrix, polyaniline (PANI)[6-8] has attracted researchers due to its ease of preparation and high environmental stability. PANI hybrid materials are shown to possess excellent applications in tissue engineering,[9,10] antimicrobial wound dressings[11-13] and as coatings for cotton fabrics,[14] making it a highly biocompatible material. Of all polyanilines, PANIPI possess a unique feature of having a chromogenic dopant picric acid, making it an excellent material to visualize the exchange of ions. The paucity of data in PANIPI prompted us to use it as a probe to evaluate the sorption process and exchange mechanism.

In this article we have synthesized PANIPI via a facile one pot procedure and analyzed its antimicrobial activities. The as synthesized polymer is characterized by UV-Vis, FT-IR and PXRD techniques. The morphology of the sample is analyzed using SEM. Herein univalent chloride salts (LiCl, NaCl, KCl and NH_4Cl) are utilized to explore the sorption characteristics on the polymer PANIPI, which is very simple and "green". Moreover, the exchange of ion is detected by visible spectroscopy proving it as an efficient adsorbent for probing ion selectivities. In addition, the antimicrobial activities of the PANIPI renders it as a biocompatible material.

Experimental

Materials and Methods

All the chemicals and reagents used were of analytical grade. Double distilled water was employed for all the experiments.

Synthesis of PANIPI

The PANIPI was synthesized by chemical oxidative polymerisation.[15] Aqueous solution of aniline (0.1 M) and picric acid (0.05 M) was magnetically stirred and ammonium peroxydisulphate (0.1 M) was added dropwise over an interval of one hour until a dark green precipitate was obtained. At the end of the stipulated time the solution was filtered on a Whatmann No.1 filter paper and washed with distilled water and alcohol. The resulting dry powder was further stirred ultrasonically (ultrasonic cleaning bath 50 kHz, Ultrasonic Ney) with alcohol, acetone and ether filtered and dried. The as prepared precipitate was stored in a vaccum desiccator and used directly for the sorption experiments and antimicrobial studies.

Spectral analysis

PANIPI (1 mg) was dissolved in 25 ml of DMF and the UV-Visible spectra of the solution obtained were recorded

in the region 300-1000 nm using Perkin–Elmer Lambda 25 spectrophotometer. FT-IR spectra were recorded as KBr pellets on a Perkin Elmer RXI FT-IR spectrophotometer. X-ray diffraction measurements were made with a Rigaku Ultima III X-ray diffractometer using CuK$_\alpha$ target (λ = 1.5418 Å).

Sorption Experiments

Sorption capacity of the adsorbent was evaluated by the batch process. PANIPI (1 mg) and salts of varying concentrations (25 ml, 10^{-6}-10^{-1} M) were ultrasonically stirred for 30 mins. After 30 mins, solutions were withdrawn, filtered and the concentration of the picrate ion released (C_e) was ascertained from the calibration curves at absorption maxima (λ_{max}=360 nm). Release of picrate ion (C_0) in the absence of salts was considered as the standard. pH measurements (Digital pH meter EQ 160, Equiptronics) were used to study the dosage effect of sorbent (10 mg) and adsorbate (2 M). The midpoints of the pH curves were taken for determining the $K_{PI^-}^{Cl^-}$ values.

Effect of pH was calculated by varying pH from 1 to 14. Alkali metal ion concentrations were estimated using flame photometer (Elico 360 A) and ammonium ions by Nessler's method. The separation factors α, were determined from these values.

Sorption isotherms such as Langmuir, Freundlich, Redlich-Peterson and Temkin isotherms were applied for this study. For accuracy, all the experiments were performed thrice and the mean of the three values were taken with an error of 2 %. Graphs were constructed with Origin 8.6 software and the slopes and intercepts were calculated using linear regression analysis.

Antimicrobial studies

Antibacterial and antifungal activities of PANIPI were tested against various gram positive and gram negative bacteria and fungus (*Candida albicans*) obtained from microbial type culture collection and gene bank (MTCC), Institute for Microbial Technology, Chandigarh, India employing agar well diffusion method.[16]

For antibacterial studies, nutrient agar medium and for antifungal studies potato dextrose agar were used. The agar media were sterilized in aliquots of 15 ml at a pressure of 6.804 kg for 15 minutes. The nutrient agar media were transferred into sterilized petri dishes in a laminar air flow unit. Petriplates were prepared by transferring the nutrient agar and kept in laminar air flow unit. After solidification of the media, the strains were swabbed on the petri plates and a sterile cork borer was used to puncture the solidified agar mass. Four wells of uniform dimension were prepared and a drop of PANIPI in DMSO (25, 50 75, 100 μg ml^{-1}) was added using micropipette and incubated for 48 hours at 37 °C in the incubation chamber. Zone of inhibitions were measured using Intech antibiotic zone reader (model IN-1215, India). Triplicates were used to ensure the activity of the synthesized material.

Results and Discussion

Structural characterization of sorbent

In the UV-Visible spectra (Fig. 1a) of PANIPI (1 mg) in DMF (25 ml), the signature peaks of the PANI matrix are observed at 360 nm and 621 nm.[17,18] The characteristic picrate ion peak (360 nm) seems to be merged with the intense Π–Π^* band of PANI matrix.

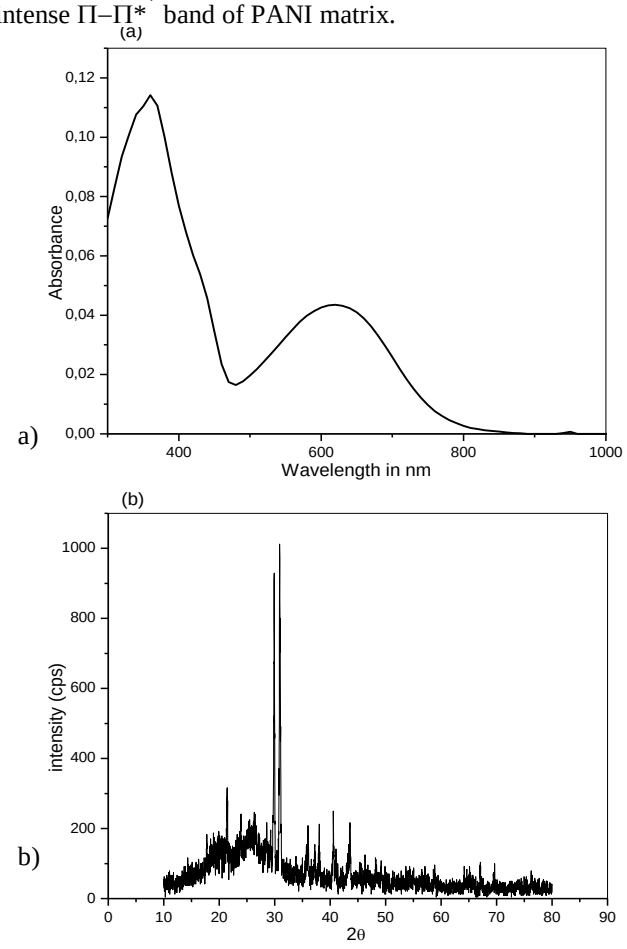

Figure 1. UV-Visible spectrum (a) and PXRD pattern (b) of PANIPI

In the FT-IR spectrum (Table 4) of PANIPI, bands at 3425, 3246 cm^{-1} correspond to N-H stretching vibrations, while the C-H stretching vibrations are observed at 3080, 2984, 2847 and 2827 cm^{-1}. Peaks around the region 3400-2800 cm^{-1} which are partly masked by the extended absorption tail of the protonated PANI[19] correspond to emeraldine salt (ES) structure. The stretching vibrations at 1588 and 1491 cm^{-1} are assigned to quinoid (N=Q=N) and benzenoid (N=B=N) moieties.[20] At 1300 cm^{-1} the stretching vibrations of C-N and NO_2 have overlapped. The absorption at 1137 cm^{-1} is due to charge delocalistion on the polymer backbone.[21] The bending vibrations in the PANI matrix appear as three distinct bands at 797, 699 and 504 cm^{-1}.

PXRD pattern (Fig. 1b) of PANIPI exhibits crystalline morphology with well defined sharpening of peaks at 2θ values of 30° (d~ 2.90 Å). The domain size was calculated using Scherrer's formula[22] and is found to be 2-9 nm. This small size provides large surface area for the sorption of ions. The SEM micrograph of PANIPI[15] shows granular morphology.

 DOI: 10.17628/ecb.2014.3.32-39

Sorption Isotherms

PANIPI was equilibrated with salt solutions of varying concentrations, ultrasonically at ambient conditions. Ion exchange occurs readily with the picrate ion present on the resin. Ultrasonic stirring ensured the elimination of concentration gradients that arise during the sorption process.

Langmuir Isotherm

The linearised Langmuir isotherm[23] (1) is used to find the maximum amount of salts adsorbed (q_m) by PANIPI. From the slope and intercept (Fig 2a), K_L (Table 1) the coefficient related to affinity is determined.

$$\frac{1}{q_e} = \frac{1}{K_L q_m C_e} + \frac{1}{q_m} \quad (1)$$

Further analysis of Langmuir equation is made on the basis of separation factor (R_L)[24] calculated using equation (2).

$$R_L = \frac{1}{1 + K_L C_0} \quad (2)$$

As R_L is less than one, the sorption process is favoured, which implies the presence of homogenous active binding sites on the PANIPI surface, resulting in monolayer chemisorption.

Thermodynamic Studies

Gibbs free energy change (Table 1) calculated using equation (3) is found to be negative indicating the feasibility and spontaneity of the sorption process.

$$\Delta G^\circ = -RT \ln K \quad (3)$$

Freundlich Isotherm

The sorption data are further fitted to Freundlich adsorption isotherm[25] (Fig 2b), describing the sorption equilibrium for both monolayer and multilayer adsorption. Freundlich isotherm constants K_F (sorption capacity) and n (intensity of sorption) are calculated (Table 1) from the expression (4),

$$\log q_e = \log K_F + \frac{1}{n} \log C_e \quad (4)$$

The n values obtained for the sorption process fulfills Freundlich isotherm condition[26] ($0 < n < 1$). Though Langmuir and Freundlich isotherm conditions are obeyed, both monolayer and multilayer adsorption of ions occur on PANIPI. In order to improve the R^2 values Redlich Peterson and Temkin models are employed.

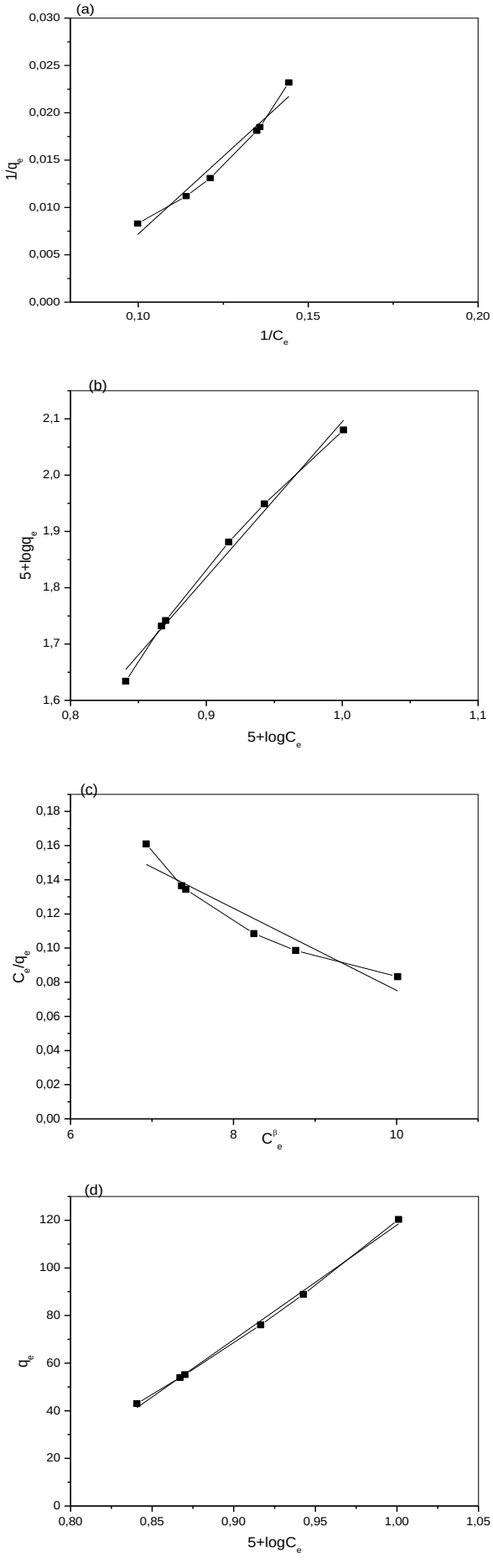

Figure 2. Sorption isotherm of NH_4Cl (a) Langmuir (b) Freundlich (c) Redlich-Peterson (d) Temkin

 DOI: 10.17628/ecb.2014.3.32-39

Table 1. Isothermal Parameters of Langmuir and Freundlich sorption Isotherms for PANIPI as adsorbent

Salts	Langmuir constants				Freundlich constants				-Δ*G*°, kJ mol^{-1}
	q_m, mg g^{-1}	K_L, L mg^{-1}	R^2	[a]*S.D*	K_F, L mg^{-1}	*n*	R^2	*S.D*	
NH_4Cl	39.11	0.078	0.954	0.004	0.215	0.362	0.988	0.013	6.426
LiCl	5.36	0.013	0.763	0.014	0.001	0.188	0.935	0.014	5.224
NaCl	26.74	0.080	0.904	0.026	0.124	0.335	0.983	0.011	6.239
KCl	7.15	0.013	0.965	0.019	0.013	0.242	0.988	0.010	5.279

[a]standard deviation

Table 2. Isothermal Parameters of Temkin and Redlich-Peterson sorption Isotherms for PANIPI as adsorbent

Salts	Redlich Peterson constants				Temkin constants				Cationic radius *r*, Å
	K_{RP}, Lmg^{-1}	α_{RP}	R^2	*S.D*	K_T, L mg^{-1}	b_T, kJ mol^{-1}	R^2	*S.D*	
NH_4Cl	3.169	0.076	0.896	0.017	5.687	0.012	0.996	0.015	1.48
LiCl	0.756	0.123	0.648	0.069	5.328	0.015	0.994	0.032	[a]3.40
NaCl	2.386	0.080	0.826	0.057	5.502	0.012	0.995	0.083	0.95
KCl	1.653	0.103	0.923	0.023	5.429	0.014	0.998	0.089	1.33

[a]hydrated radius

Redlich- Peterson Isotherm

Redlich-Peterson isotherm[27] (Fig. 2c) is used as a compromise between Langmuir and Freundlich models. The linear form of this equation (5) contains three unknown parameters

$$\frac{C_e}{q_e} = \frac{1}{K_{RP}} + \frac{\alpha_{RP}}{K_{RP}} C_e^{\beta} \qquad (5)$$

K_{RP}, α_{RP} and β. A minimization procedure is adopted to maximize the coefficient of determination R^2. However, the low value of R^2 (Table 2) indicate that this model is not suitable for the sorption process.

Temkin Isotherm

The Temkin[28] isotherm equation (6) relates,

$$q_e = \frac{RT}{b_T} \ln K_T + \frac{RT}{b_T} \ln C_e \qquad (6)$$

K_T the equilibrium binding constant (mg L^{-1}) and b_T the Temkin constant related to energy of adsorption (kJ mol^{-1}). These values are determined from the slope and intercept (Table 2) of the plot q_e vs log C_e (Fig. 2d). The Temkin isotherm model exhibit a high R^2 (0.99) value compared to other models applied.

Based on all these results and from the plot of K_T vs cationic radii (Fig. 3), the relative order of sorption of univalent chlorides on PANIPI resin is given below

$$NH_4^+ > Na^+ > K^+ > Li^+$$

It can be seen that ammonium ion exhibits the maximum sorption potential (K_T). This may be due to the presence of hydrogen bonding on the amine sites of PANI matrix. Among the alkali metal chlorides, NaCl has the highest sorption potential (K_T). This may be due to the ionic nature and size of NaCl. When KCl is used as the adsorbate, the sorption potential is lower than NaCl probably due to the bigger size of K^+ compared to Na^+. Li^+ being the smallest among the alkali metal chlorides prefer to exist as a hydrated species and therefore possess low sorption potential.

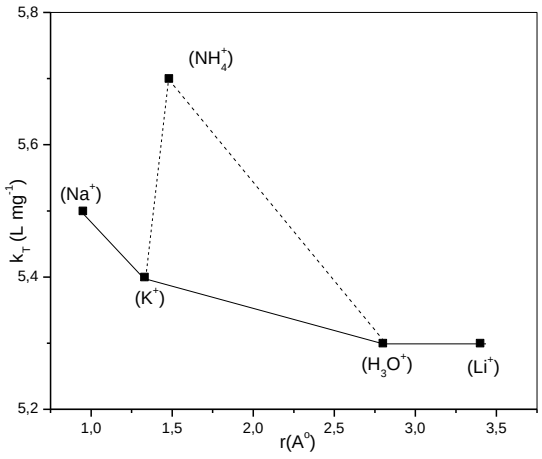

Figure 3. Temkin constant K_T (L mg^{-1}) vs ionic radii *r* (Å)

Sorption at high concentration

As sorption process will be complete at higher ionic strengths, the experiments were conducted at higher concentration (2 M) with 10 mg of PANIPI resin. The observed decrease in pH with time (Fig. 4) indicates the sorption of ions on PANIPI resin with subsequent release of picric acid in aqueous solution. At high concentration also, NH_4^+ is found to possess high exchange capacity as inferred from $K_{PI^-}^{Cl^-}$ and α values (Table 3).

 DOI: 10.17628/ecb.2014.3.32-39

Table 3. UV-Visible spectral results and ion exchange characteristics of PANIPI resin

Salts	λ_{max}, nm		*y*	[a]1-*y*	[b]$K_{PI^-}^{Cl^-}$	[c]IEC, meq g^{-1}	[b]α
	Benzenoid (B)	Quinoid (Q)					
PANIPI	360	621	0.70	0.30	-	-	-
NH_4Cl	361	620	0.57	0.42	4.89×10^{-7}	1.99	27.69
LiCl	361	617	0.62	0.37	6.30×10^{-7}	1.96	12.96
NaCl	378	577	0.91	0.09	5.62×10^{-8}	2.71	0.74
KCl	365	619	0.63	0.36	4.89×10^{-7}	1.99	0.70

[a]1-$y=OD_Q/OD_B$ [chlorides]; [b]2 M; [c]10^{-1}-10^{-6} M

Table 4. FT-IR Spectral data of PANIPI before and after sorption

Vibrational assignment	N-H str	Ar C-H str /NH_2^+	$C=N^+$	N=Q=N	N=B=N	CN str	Ar C-N-C bending	C-H bending	C-C ring deformation	Cl stretching	C-N-C torsion
PANIPI	3425 3246	3080, 2984, 2847 2827	2800- 2400	1588	1491	1300	1137	797	699	-	504
NH_4Cl	3407 3219	3081, 2925	2471, 2343	1574	1490	1282	1133	798	702	610	504
LiCl	3440	2830	2358	1596	1491	1300	1139	790	697	609	504
NaCl	3409 3225	3010- 2951, 2900	2400- 2000	1585	1495	1303	1141	804	703	590	505
KCl	3430	2808	2483 2361	1588	1491	1300	1135	795	699	612	503

The varying trends of these parameters for the alkali metal ions may be due to competition between sorption and desorption process.

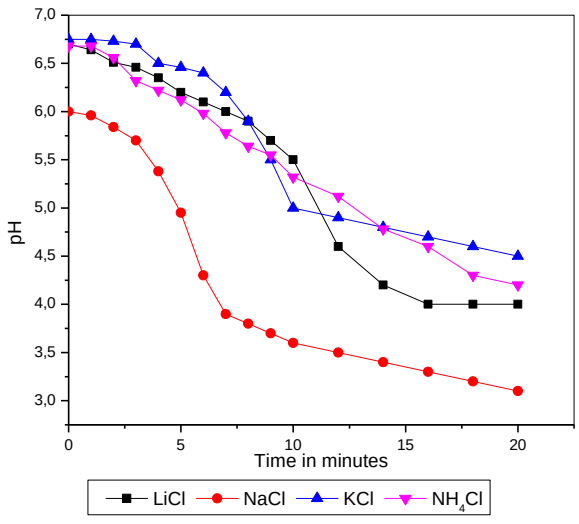

Figure 4. Variation of pH with time [2 M salts]

Sorption Mechanism

A tentative mechanism is proposed for the sorption process. The easily polarisable picrate ion renders hydrophilicity and the chloride ions are attracted towards the PANI surface (Scheme I). Anion selectivity is influenced by the counterions, since Cl^- ion is small and highly electronegative compared to the picrate ion. Hence the movement of anions occur as ion pairs. The anions bind to the imine sites on the quinoid rings and the NH groups on the benzenoid rings. This phenomenon causes changes in the stretching frequencies of the NH group at 3200 cm^{-1} and also affects the C-N-C bending vibrations. The sorption of ions initially occurs as a monolayer. Multilayer formation on PANI surface, may take place subsequently due to ion pairing.

Effect of pH

The sorption process of PANIPI is found to be highly pH dependent. In acidic medium, protonic acid doping of PANIPI readily occurs releasing the picric acid. However, in this pH range sorption is not a favoured process. This may be due to the doping of the vacant imine sites on the PANIPI resin.

 DOI: 10.17628/ecb.2014.3.32-39

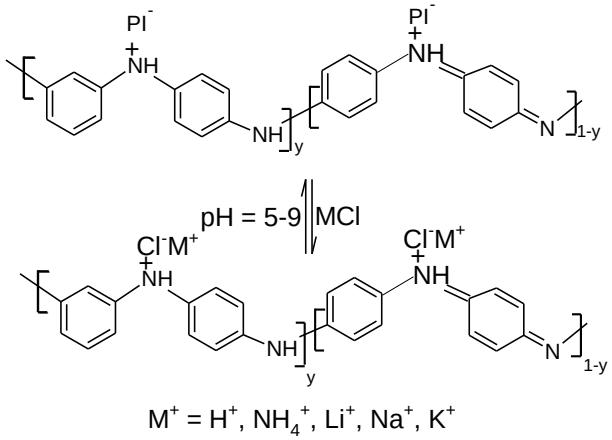

Scheme I. Sorption process on PANIPI

The favourable pH range for sorption process is 5-9 as can be inferred from the adherence to the isotherm models (Fig. 5). Above pH 9, the solutions tend to be alkaline and dedoping of PANIPI to emeraldine base (EB) may result. As the pH increases further, OH^- ions bind to the imine sites on the PANI matrix producing a hydroxylated emeraldine base[29] (Scheme II).

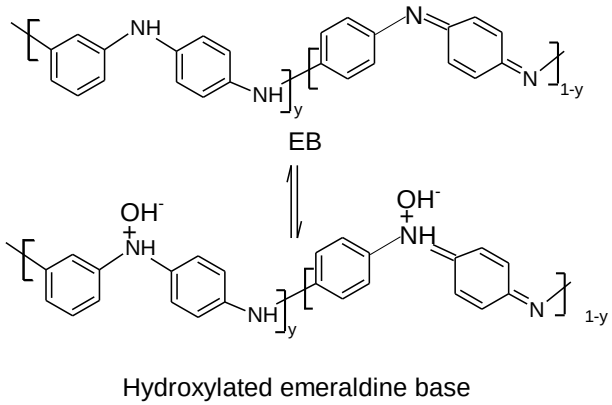

Scheme II. Emeraldine base structures in alkaline medium

Structural characterization after sorption

UV-visible spectra

PANIPI is found to contain ~70% benzenoid and ~30% quinoid forms as inferred from benzenoid and quinoid absorption intensities in the UV-Visible spectra (Table 3). Sorption process may lead to the changes in these percentages depending on the electrolytes used (Table 3). Sorption of electrolytes such as NaCl produce 90 % of benzenoid forms compared to PANIPI, while NH_4Cl produce only 60 % benzenoid forms. LiCl and KCl does not alter the composition of these forms originally present in PANIPI.

FT-IR spectra

The changes in the IR spectral bands of PANIPI after sorption, confirm the presence of ion pairs of the electrolytes on PANI matrix. The peaks at 3425 and 3246 cm^{-1}, due to amine and imine stretching of N-H in PANIPI are sensitive to ions. These vibrations are either blue or red shifted after the sorption process depending upon the electrolytes used. (Table 4). NaCl shows a blue shift (15 and 24 cm^{-1}), whereas LiCl and KCl show red shifts. The band features around 2800-2400 cm^{-1} confirms the presence of ES structure in PANI. Quinoid and benzenoid ring vibrations at 1588, 1491 cm^{-1} are not much affected. The stretching vibrations around 1300 cm^{-1}, characteristic of ES structure are blue shifted for NaCl, KCl and NH_4Cl whereas red shifted for pseudo protonic acid dopant LiCl.[30] In NH_4Cl, a twin band found at 1284 cm^{-1} indicates electronic transitions within the ring, besides confirming the binding of ammonium ion to NH of benzenoid rings. The chloride ions existing as ion-pairs on the PANI matrix are inferred from vibrations in the region 590-612 cm.$^{-1}$

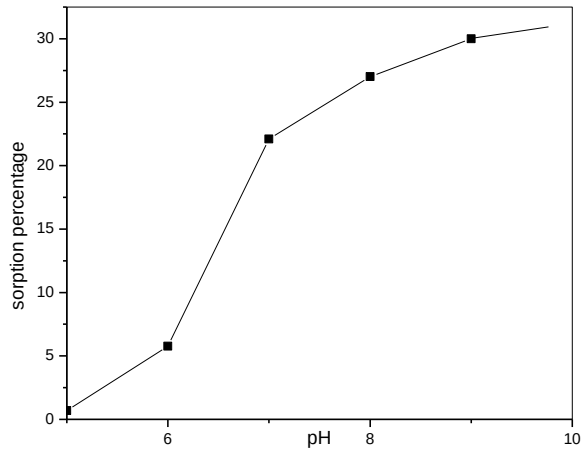

Figure 5. Sorption percentage as a function of $[H^+]$

Ion exchange capacity

The ion exchange capacity (IEC)[31] of PANIPI towards these ions vary between 1.95-2.71 meq g^{-1} (Table 3). These values indicate the suitability of PANIPI as a good polymeric material suitable for ion transport. The IEC ratio of Na^+-K^+ (3:2) agrees well with the distribution of ions in sodium-potassium pumps (3:2) present in living cells. It is quite intriguing to find that PANIPI acts similar to Na^+/K^+ ATPase pumps in cells.[32] The other ion selectivities of PANIPI is similar to potassium (Table 3). Hence it could be inferred that PANIPI is highly selective and is able to discriminate between the various ions, similar to the cell membranes present in the living organisms. The added advantage of PANIPI is that it also possesses antimicrobial activities making it a highly suitable material for tissue implants.

Antimicrobial Activity of PANIPI

PANIPI exhibits considerable antibacterial activity for the bacterial strains tested. The zone of inhibitions obtained for PANIPI in DMSO (25-100 μg mL^{-1}) against gram positive (*Staphylococcus aureus*) and gram negative (*Shigella dysenteriae*, *Salmonella enterica*, *Klebsiella pneumonia*) bacteria are shown in Fig 6a. The minimum inhibitory concentration (MIC) of 50 μg mL^{-1} of PANIPI is required

 DOI: 10.17628/ecb.2014.3.32-39

for *Streptococcus pyogenes, Bacillus subtilis, Enterococcus faecalis* (gram positive) and *Escherichia coli, Pseudomonas aeruginosa* (gram negative) bacteria (Fig 6b).

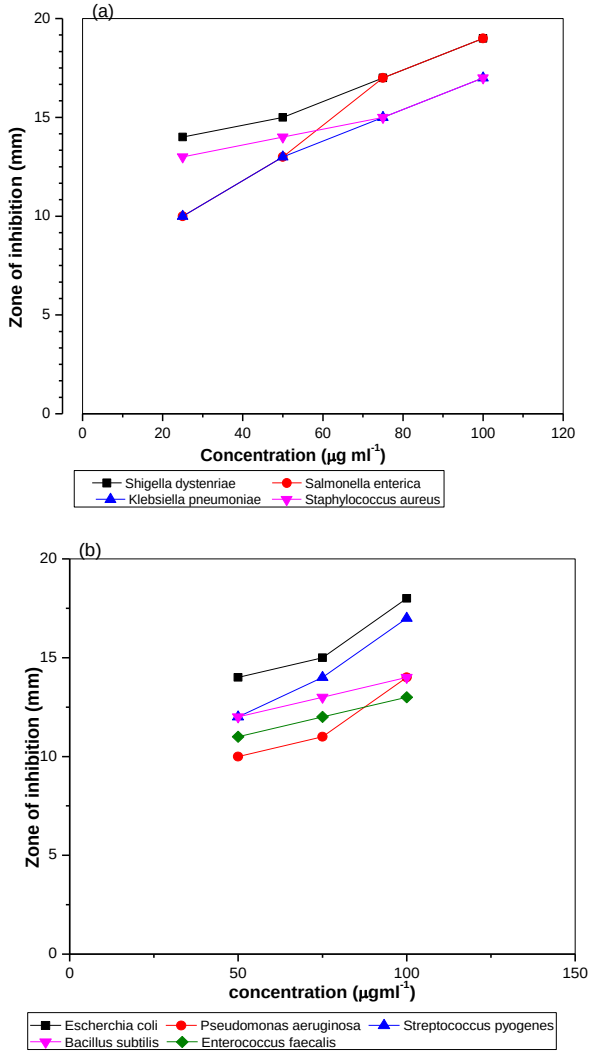

Figure 6. Antibacterial effect of PANIPI against bacteria

As the concentration of PANIPI is increased, the zone of inhibition also increased. PANIPI is also found to be an effective antifungal agent when tested against *Candida albicans*. The zone of inhibition produced is comparable with that obtained against *Shigella dysenteriae* (Fig. 7) (MIC 25 µg ml^{-1}).

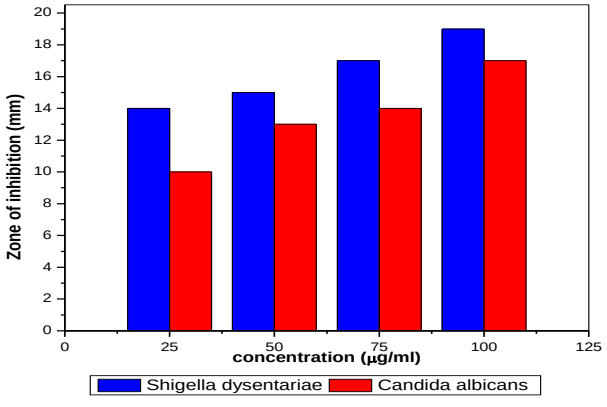

Figure 7. Comparison of antibacterial and antifungal effect of PANIPI

The X-ray diffraction studies (Fig. 2) reveal that the size of PANIPI fall in nanometer regime. Nanomaterials[33] are known to disturb the balance between oxidant and anti-oxidant processes occurring in the living cells. Hence it could be envisaged that the nanosized PANIPI[34] binds electrostatically to cell membranes creating an imbalance in oxidative reductive mechanism leading to cell lysis and death.

Conclusions

In summary, we have synthesized PANIPI via facile chemical polymerisation route. The as synthesized PANIPI is characterized using UV-Visible, FT-IR and PXRD spectroscopic techniques. The morphology of the samples are analysed using PXRD and SEM. The Π- Π* transitions of quinone-imino groups were confirmed from the UV-Visible spectral data. The ES structure of PANIPI is also confirmed by FT-IR analysis. Sorption capacity of the as prepared PANIPI is evaluated from the sorption process. Among the sorption isotherms such as Langmuir, Freundlich, Redlich-Peterson and Temkin isotherms, Temkin isotherm is found to be satisfactory as evidenced from the R^2 values. The relative order of sorption is found to be $NH_4^+ > Na^+ > K^+ > Li^+$. The UV-Visible absorption and FT-IR spectra of PANIPI after the sorption process confirm the presence of ion pairs in the PANI matrix . From the IEC results it is found that Na^+/K^+ ratio is similar to that of Na^+/K^+ ATPase pump in living cells. PANIPI shows excellent antimicrobial activities against various bacterial and fungal strains. From these results it is concluded that, the nanosized PANIPI can be utilized as a biocompatible material for fabrication of biological membranes.

Acknowledgement

The authors thank UGC-SERO Hyderabad for the minor project, ACIC, St.Joseph's college, Trichy for FT-IR spectra, Dept. of Physics, NIT- Trichy for PXRD, CISL of Annamalai University for the SEM image and Eumic Analytical Lab, Trichy for the antimicrobial studies. The authors are grateful to the Management, Seethalakshmi Ramaswami College, Trichy for the infrastructure.

References

[1]Hille, B., *Ion Channels of Excitable Membranes*, 3rd Edition, Sunderland, Mass: Sinauer Associates Inc., **2001**, 5.

[2]Huheey, J. E., Keiter, E.A., Keiter, R.L., *Inorganic Chemistry-Priniciples of structure and Reactivity*, 4th Edition, Pearson Education, **2005**, 529.

[3]Ingelzakis, V.J., Poulopoulos, S.G., *Adsorption, Ion exchange and catalysis-Design of operations and Environmental Applications*, 1st Edition, Elsevier Science, **2006**, 264.

[4]Mac Diarmid, A.G., *Angew. Chem. Int. Ed.*, **2001**, *40*, 2581.

[5]Li, D., Huang, J., Kaner, R.B., *Acc. Chem. Res.*, **2009**, *42*(1), 135.

[6]Ansari, R., *Acta Chim. Slov.*, **2006**, 53, 88.

[7]Ghorbani, M., Eisazadeh, H., Ghoreyshi, A.A., *Iranica. J. Energy and Environ.*,**2012**, 3(1), 66.

[8]Kanwal, F., Rehman, R., Anwar, J., Saeed, M., *Asian J. Chem.*, **2013**, 25(5), 2399.

[9]Li, M., Guo, Y., Wei, Y., Mac Diarmid, A.G., Lelkes, P. L., *Biomaterials*, **2006**, 27, 2705.

[10]Nikolaidis, M. R. G., Ray, S., Bennet, J., Easteal, A. J., Cooney, R.P., *Macromolecular Bioscience*, **2010**, 10, 1424.

[11]Prasad, R. G. S. V., Chaitanya, K. S. V., Tejoram, M., Basavaraju, D., Rao, K. N., Kumar, R. R., Sreenivasan, S., Phani, A. R., *J. Pharm. Res.*, **2012**, 5, 370.

[12]Shi, N., Guo, X., Jing, H., Gong, J., Sun, C.,Yang, K., *J. Mater. Sci. Technol.*, **2006**, 22, 289.

[13]Nikolaidis, M. R. G., Easteal, A. J., Stepanovic, S., US *20100196306A1*.

[14]Seshadri, D.T., Bhat, N.V., *Indian J. Fibre Textile* Res., **2005**, 30, 204.

[15]Dhivya, C., Vandarkuzhali, S. A. A., Santhi, R., Radha, N., *Indian J. App. Res*., **2013**, 6(3), 62.

[16]Jotiram K. P., Prasad, R. G. S. V., Jakka, V. S., Aparna, R. S. L., Phani, A. R., *Nano Biomed. Eng.*, **2012**, 4(3), 144.

[17]Sindhimeshram, D. C., Gupta. M. C., *Indian J. Chem.*, **1995**, 34A, 260.

[18]Samui, A. B., Patanakar, A. S., Satpute, R. S., Deb, P. C., *Synth. Meth.*, **2002,** 125, 423.

[19]Roy, B. C., Gupta, M. D., Bhoumik, L., Ray, J. K., *Synth. Meth.*, **2002**,130, 27.

[20]MacDiarmid, A. G., Epstein, A. J., Prasad, P. N., *Frontiers Polym. Res.*, Plenum Press, **1991**, 259 .

[21]Wan, M., Yang, J., J. *Appl. Polym. Sci*., **1995**, 55, 399.

[22]Guinior, *X-Ray diffraction in crystals, imperfect crystals and amorphous bodies*, W H Freeman, **1963.**

[23]Langmuir, I., J. *Am. Chem. Soc.*,**1918**, 40, 1361.

[24]Ansari, R., Dezhampanah, H., *Eur. Chem. Bull.*, **2013**, 2(4), 220,

[25]Freundlich, H.Z., *J. Phys. Chem.*,**1906**, 57A, 385.

[26]Nagashanmugam, K.B., Srinivasan, K., *Indian J. Chem. Technol.*, **2011**, 18, 391.

[27]Redlich, O., Peterson, D.L., *J. Phys. Chem.*, **1959**, 63, 1024.

[28]Temkin, M.J., Pyzhev, V., *Acta Physiochim. USSR.*, **1940**, 12, 217.

[29]Wang. J., *Synth. Meht.*, **2002**, 132, 49.

[30]Min,G., *Synth. Meth.*, **2001**, 119, 273.

[31]Khopkar, S.M., "*Basic concepts of Analytical chemistry*", New Age International Pvt. Ltd., **2008**.

[32]Hall, John E., Guyton, Arthur, C., "*Textbook of medical physiology"*, Elsevier Saunders, **2006**.

[33]Karunakaran, C., Gomathishankar, P., Manikandan, G., *Indian J. Chem. Technol*., **2011**, 18, 169.

[34]Nikolaidis, M.R.G., Benett, J., Swift, R. S., Easteal, A.J., Ambrose, M., *Acta Biomater.*, **2011**, 7, 4204.

Received: 17.09.2013.
Accepted: 25.10.2013.

INHIBITION OF MILD STEEL CORROSION BY 1-(8-HYDROXYQUINOLIN-2-YLMETHYL)UREA

S. S. Syed Abuthahir,[a,b] A. Jamal Abdul Nasser[a] and S. Rajendran[b]*

Keywords: Corrosion inhibitors, EIS, mild steel, organic inhibitors, 1-(8-hydroxyquinolin-2-ylmethyl)urea**,** SEM, EDAX and biocidal activities.

The corrosion behavior of mild steel in the presence of organic inhibitor namely 1-(8-hydroxyquinolin-2-ylmethyl)urea (HUF) has been investigated in aqueous solution containing 60 ppm of Cl^-. Weight loss measurements and electrochemical impedance spectroscopy (EIS) were applied to analyze the effect of the organic compound on the corrosion inhibition of mild steel. The organic inhibitor that totally covered the mild steel surface was identified, exhibiting strong corrosion inhibition. Fluorescence spectral analysis was used to detect the presence of iron-inhibitor complex. The surface morphology has been analyzed by FTIR, UV-Visible spectroscopy, Scanning Electron Microscope (SEM) and EDAX. The inhibitor 1-(8-hydroxyquinolin-2-ylmethyl)urea has the ability to prevent the growth of certain microorganisms.

* Corresponding Authors
E-Mail: srmjoany@sify.com
[1] PG & Research Department of Chemistry, Jamal Mohamed College, Tiruchirappalli 620 020, India. Email: syedchem05@gmail.com, ajanasser@yahoo.com
[2] Department of Chemistry, RVS School of Engineering and Technology, Dindigul-624 005, India.

Introduction

Corrosion is the gradual destruction of material, usually metal by chemical reaction with its environment. Mild steel under water containing chloride is eroded gradually by means of chemical reactions.[1-3] The corrosion is severe due to the presence of chloride ions and dissolved oxygen. Mild steel is widely used in infrastructure in marine environments.[4]mild steel is widely used in industries. It comes in contact with chloride ions very frequently under numerous conditions and circumstances in industries. Various organic compounds have been reported as inhibitors for controlling corrosion of mild steel in water containing chloride ions. But the inhibitive efficiencies of organic compounds when used alone were found to be very less.[5]In various industries water being in great demand and the largest source of water is sea water which is at a peak in corrosively due to the presence of sodium chloride. Moreover mild steel the cheapest as well as highly applicable material in industries gets attacked by chloride ions. So it becomes a basic need to investigate various corrosion inhibitors for mild steel in sodium chloride solution. Most inhibitors are organic compounds containing polar groups strongly adsorbed on the metal surface.[6,7]

The aim of the present study is to evaluate corrosion inhibitive performance of *1-(8-hydroxy quinolin-2yl-methyl) urea* to mild steel immersed in aqueous solution containing 60 ppm Cl^-. The corrosion inhibition efficiency was evaluated using weight loss method and electrochemical impedance spectroscopy. The protective film formed on the metal surface characterized with the help of surface analytical techniques such as fluorescence, FTIR and UV-Visible spectroscopy. The surface morphology has been analyzed by SEM and EDAX. The biocidal activity was measured against certain organisms.

Experimental Techniques

Mild steel specimen; (0.0267% S, 0.061% P, 0.5 % Mn, 0.1 % C and the rest iron) of dimensions 1.0 cm ×4.0×0.2 cm were polished to mirrors finish and degreased with acetone.

Weight loss method

Mild steel specimens triplicate were immersed in 100 ml of the solution containing 60ppm of Cl^-in the presence and absence of *1-(8-hydroxy quinolin-2yl-methyl) urea* for one day. The weight of the specimens before and after immersion was determined using a shimadzu, model AY62. The corrosion products were cleaned with Clark's solution.[8] The inhibition efficiency (*IE)* was then calculated using the equation:

$$IE = 100[1-(w_2-w_1)]\% \quad (1)$$

where w_1 is the weight loss value in the absence of inhibitor and w_2 is the weight loss value in the presence of inhibitor.

AC impedance spectra

Impedance studies were carried out in a CHI electrochemical workstation with impedance model 643, Austin, USA. A three electrode cell assembly was used. The working electrode was mild steel. The exposed surface area was 1 cm^2. A saturated calomel electrode (SCE) was used as the reference electrode and a rectangular platinum foil was used as the counter electrode. The real part (*Z'*) and the imaginary part (*Z'*) of the cell impedance were measured in ohms at various frequencies. AC impedance spectra were recorded with initials $E_{(v)}$ =0 V, high frequency limit was 1×10^5 Hz, low frequency limit was 1 Hz, amplitude =0.005 V and quiet time t_q=2 s. The values of charge transfer resistance R_t and the double layer capacitance C_{dl} were calculated.

$$C_{dl} = \tfrac{1}{2}\,\pi R_t f_{max}$$

where $f_{max}$is maximum frequency.

Surface Characterization studies

The mild steel specimens were immersed in various test solution for a period of one day. After one day the specimens were taken out and dried. The nature of the film formed on the surface of the metal specimen was analyzed by various surface analysis techniques.

Surface analysis by UV-Visible spectroscopy

UV-Visible spectra were recorded in a Cary Eclipse Varian (Model U.3400) spectrophotometer.

Surface analysis by fluorescence spectroscopy

Fluorescence spectra of solutions and also the films formed on the metal surface were recorded using Jasco-F-6300 spectra fluorometer.

Surface analysis by FTIR spectroscopy

The spectra were recorded in a bruker (Model Tensor 27) spectrophotometer. The film was carefully removed, mixed thoroughly with KBr and made into pellets and the FTIR spectra were recorded.

SEM Analysis

SEM (Tescan, Vega 3, USA) provides a pictorial representation in the surface to understand the nature of the surface film in the absence and presence of inhibitors and extent of corrosion of mild steel. The SEM micrographs of the surface are examined.

Energy Dispersive Analysis of X-rays (EDAXs)

The mild steel specimen immersed in blank and in the inhibitor solution for a period of one day was removed, dried and observed in an Energy Dispersive Analysis of X-rays (EDAXs) to examine the elements presents on the metal surface. The elements present on the metal surface were examined using Bruker computer controlled Energy Dispersive Analysis of X-rays (Brucker, Nano, GMBH, Germany).

Bacterial Enumeration

Bacterial cell are count based on their colony forming unit (CFU) by standard plate count. The protocols are as follows. Label the plate 10^{-2}, 10^{-4}, 10^{-6} and 10^{-8} at the bottom of plate and one plate as a blank or control. Using aseptic technique transfer 1 ml of four different cultures to 99 ml of sterile saline blank. A test tube labelled 10^{-2} and the dilution is proceeded by taking 1 ml from 10^{-2} test tube to the next 99 ml sterile saline blank labeled as to the next 99 ml sterile saline blank labeled as 10^{-4} and proceed until 10^{-8}. Shake all the test tubes for equal distribution of bacteria. Transfer 1ml of the sample into each of the labelled plates 10^{-2} to 10^{-8} correspondingly. Containing agar medium all the plates are immersed and incubate at 37 ^{0}C for 24 hours. After the incubation, select the plate containing 30 to 300 colonies and count the colonies. The number of CFU are calculated as CFUs/dilution × amount plated = No.of bacterial cell/ml.

Results and Discussion

Weight loss method

The corrosion rates (*CR)* of mild steel immersed in aqueous solution containing 60 ppm Cl^- and also inhibition efficiencies (*IE*) in the absence and presence of inhibitor HUF obtained by weight loss method are given in table-1. It is observed that 250 ppm of HUF offer 75% of inhibition efficiencies.

Table 1. Corrosion rates (*CR*) of mild steel immersed in an aqueous solution containing 60 ppm Cl^- in the presence and absence of inhibitor systems at various concentration and the inhibition efficiency (*IE* %) obtained by weight loss method.

Cl^-, ppm	HUF, ppm	*CR*, mdd	*IE*, %
60	0	34.55	-
60	50	14.51	58
60	100	12.43	64
60	150	10.36	70
60	200	9.67	72
60	250	8.63	75

AC impedance spectra

AC impedance spectra [electrochemical impedance spectra] have been used to confirm the formation of protective film on the metal surface.[9-12] The AC impedance spectra of mild steel immersed in aqueous solution containing 60 ppm of Cl^-in the absence and presence of inhibitors are shown in Fig. 1(Nyquist plots) and Fig.2 (Bode plots). The impedance parameters namely charge transfer resistance (R_t) double layer capacitance (C_{dl}) and impedance lg(z/ohm) are given in Table 2. If a protective film is formed on the metal surface,R_t value increases and the C_{dl} value decreases.

Table 2. The AC impedance spectra of mild steel immersed in aqueous solution containing 60 ppm of Cl^- in the absence and presence of inhibitor system

Systems	R_t, Ωcm^2	C_{dl}, F cm^{-2}	log(Z ohm^{-1})
60ppm Cl^-	20.19	5.235×10^{-5}	0.973
60ppm Cl^- + 250ppm HUF	27.00	3.901×10^{-5}	1.170

When mild steel is immersed in aqueous solution containing 60ppm of Cl^-, R_t value is 20.19 Ω cm^2 and C_{dl} value is 5.235×10^{-5} F cm^{-2}. When HUF is added to the aqueous solution containing 60ppm of Cl^- R_t value increases from 20.19 Ω cm^2 to 27.00 Ω cm^{2}and the C_{dl} value decreases from 5.235×10^{-5} F cm^{-2} to 3.901×10^{-5} F cm^{-2} . The impedance value increases from 0.973 to 1.170. This account for the high inhibition efficiency of HUF system and a protective film is formed on the metal surface. This is also supported by the fact that for the inhibitor system the phase angle increases from 47 to 50.60º (Fig. 2).

 DOI: 10.17628/ecb.2014.3.40-45

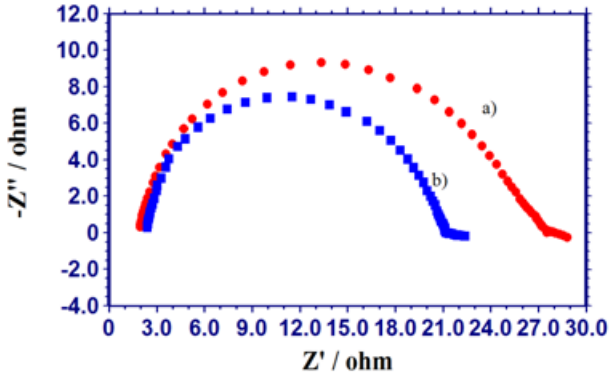

Figure 1. AC impedance spectra (Nyquist plots) of mild steel immersed in various test solutions: a) aqueous solution containing 60 ppm of Cl^-; b) aqueous solution containing 60 ppm Cl^- + 250 ppm HUF.

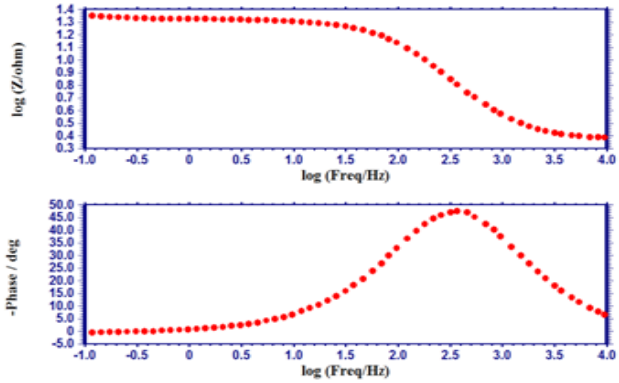

Figure 2a. AC impedance spectra (Bode Plot) of mild steel immersed in aqueous solution containing 60 ppm of Cl^-

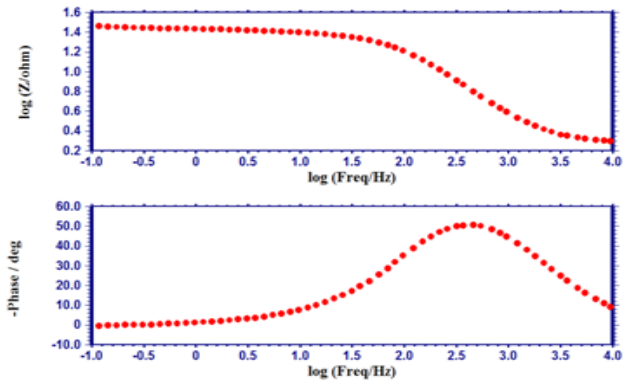

Figure 2b. AC impedance spectra (Bode Plot) of mild steel immersed in solution containing 60 ppm of Cl^-+ 250 ppm of HUF

Analysis of the UV-Visible spectra

The UV-Visible absorption spectrum of an aqueous solution containing HUF is shown in Figure 3a. Peaks appear at 380 nm and 440 nm. When Fe^{2+} solution is added to the solution new peaks appear at 580 nm. There is increase intensity of peaks also. This confirm the formation of Fe^{2+}-HUF complex in solution.[13, 14]

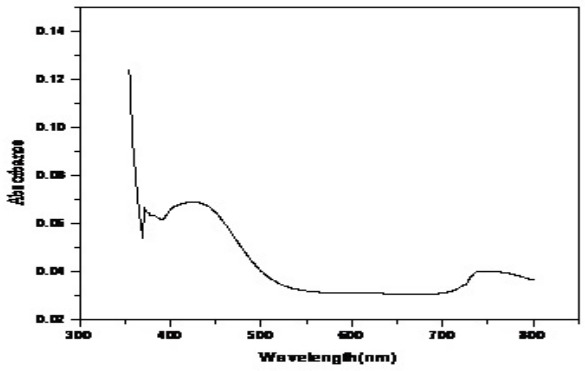

Figure 3a. UV-absorption spectrum of solution containing HUF

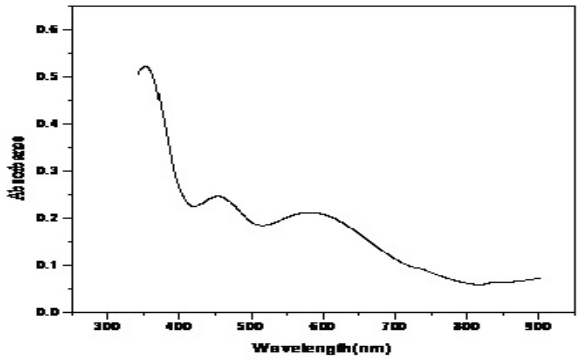

Figure 3b. UV- absorption spectra of solution containing HUF-Fe^{2+}

Fluorescence spectra

The emission spectrum (λ_{ex}:480 nm) of solution containing HTF-Fe^{2+} solution is shown in Figure 4a. The emission spectrum of the film formed on the metal surface after immersion in solution containing 250 ppm of HUF is shown in Figure 4b. Peaks appear at 490 nm. Hence it is concluded that the protective film consists of HUF-Fe^{2+} complex. The number peak obtained is only one. Hence it is confirmed that the complex of somewhat highly symmetric in solution.[15]

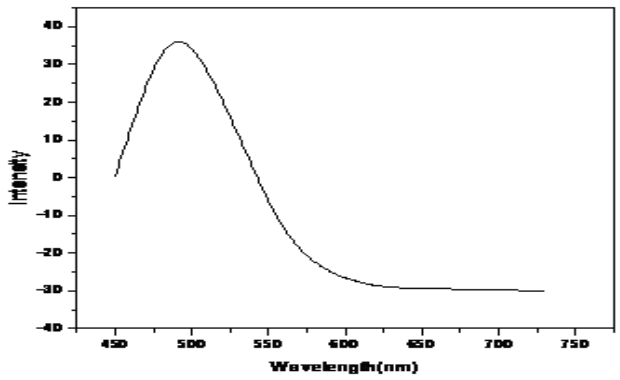

Figure 4. a) Fluorescence spectrum of HUF solution

 DOI: 10.17628/ecb.2014.3.40-45

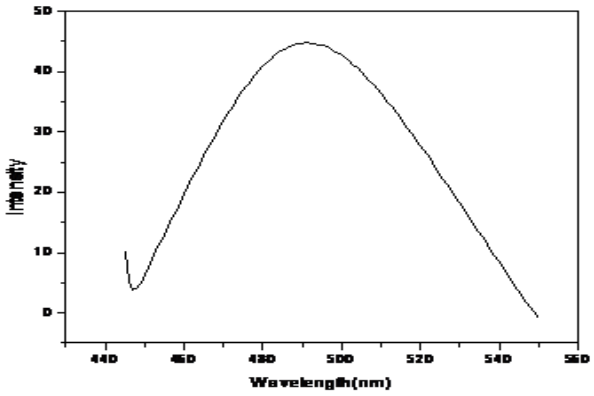

Figure 4. b) Fluorescence spectra of film formed on metal surface after immersion in solution containing 60 ppm Cl^-+ 250ppm of HUF

FTIR Spectra tests

The FTIR spectra have been used to analyze the film formed on the metal surface.[16] The FTIR spectrum (KBr) of pure 1-(8-hydroxyquinolin-2ylmethyl)urea (HUF) is shown in Figure 5a. The OH stretching frequency appears at 3490.94 cm^{-1}. The C=O stretching frequency appears at 1610.59 cm^{-1}. The aliphatic CH stretching frequency appears at 2986.03 cm^{-1}. The peak due to secondary nitrogen (NH) appears at 3150 cm^{-1}. The peak due to pyridine nitrogen (C=N) appears at 1512.33 cm^{-1}. The peak due to aromatic C=C appears at 1540.98 cm^{-1}. The peak due to primary nitrogen is absent in the region 3400 cm^{-1}, this is due to the tautomeric nature of urea moiety.

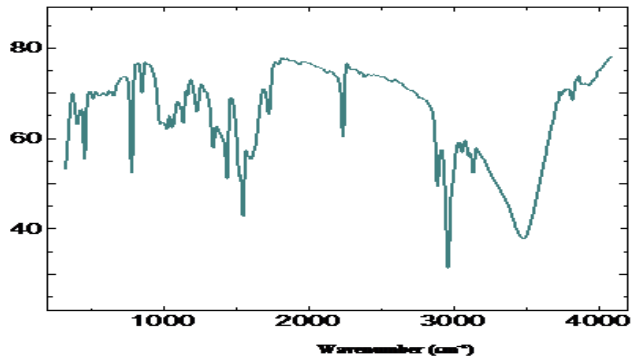

Figure 5a. FTIR spectra of pure HUF

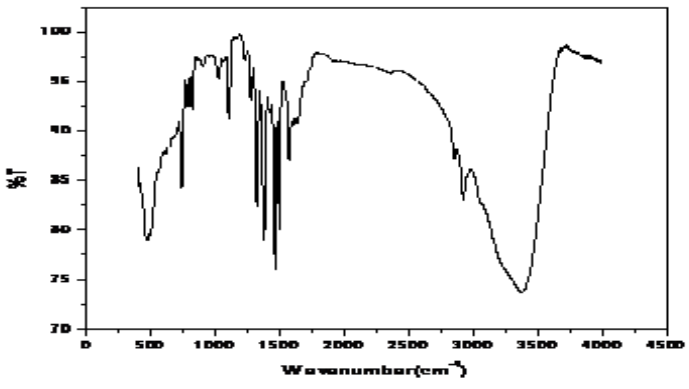

Figure 5b. FTIR spectra of film formed on metal surface after i HUF

The FTIR spectrum (KBr) of the film formed on the metal surface after immersion in the aqueous solution containing 60 ppm of Cl^- + 250 ppm of HUF for a period of one day is shown in Figure 5b. The phenolic OH stretching frequency has shifted from 3490.94 cm^{-1} to 3400 cm^{-1}. The pyridine nitrogen (C=N) stretching has shifted from 1512.33 cm^{-1} to 1570 cm^{-1}. The C=O stretching frequency has shifted from 1610.59 cm^{-1} to 1690 cm^{-1}. The aliphatic CH stretching frequency appears at 2926.03 cm^{-1}. That it is concluded that oxygen atom of phenolic group and nitrogen atom of pyridine ring have coordinated with Fe^{2+} formed on the metal surface.

The structure of the resulting HUF-Fe^{2+} complex is shown in Figure 6.

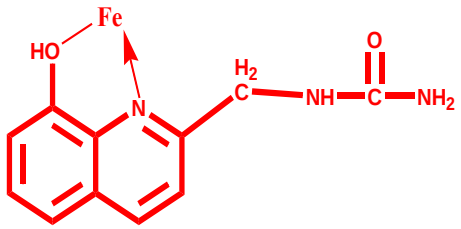

Figure 6. Structure of Fe^{2+} complex

This view is in agreement with the structure proposed by M.Albrecht *et al*. for zinc complex.[17]

SEM Analysis of Metal Surface

SEM provides a pictorial representation of the surface. To understand the nature of the surface film in the absence and presence of inhibitors and the extent of corrosion of mild steel, the SEM micrographs of the surface are examined.[18-20] The SEM images of different magnification (×20) of mild steel specimen immersed in aqueous containing 60 ppm Cl^- for one day in the absence and presence of inhibitor system are shown in Figures 7a, 7b and 7c respectively. The SEM micrographs of polished mild steel surface (control) in Figure 7a show the smooth surface of the metal. This shows the absence of any corrosion products (or) inhibitor complex formed on the metal surface.

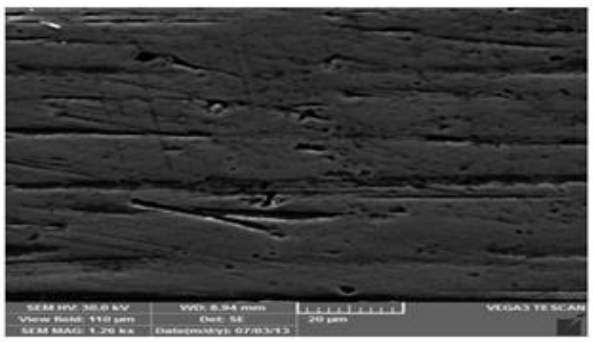

(a)

 DOI: 10.17628/ecb.2014.3.40-45

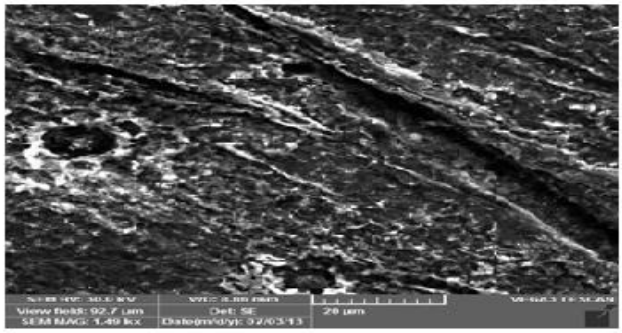

(b)

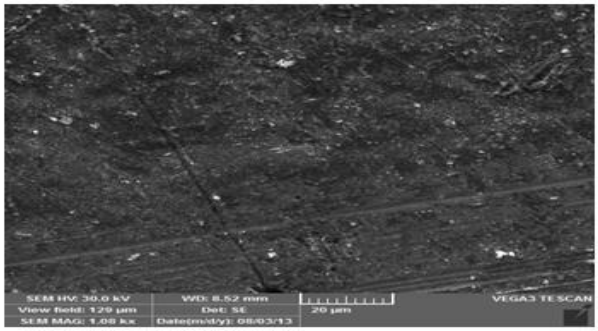

(c)

Figure 7. SEM analysis of mild steel; magnification × 20 (control). (b) Mild steel immersed in aqueous solution containing 60 ppm of Cl^-, magnification × 20 (blank). (c) Mild steel immersed in aqueous solution containing 60 ppm of Cl^- + 250ppm of HUF magnification × 20

The SEM micrographs of mild steel immersed in aqueous containing 60 ppm Cl^- (Figure 7b) show the roughness of the metal surface which indicates the highly corroded area of mild steel. However, Figure 7c indicates that in the presence of inhibitor (60 ppm Cl^- + 250 ppm HUF) the rate of corrosion is suppressed, as can be seen from the decrease of corroded areas. The metal surface is almost free from corrosion due to the formation of insoluble complex on the surface of the metal.

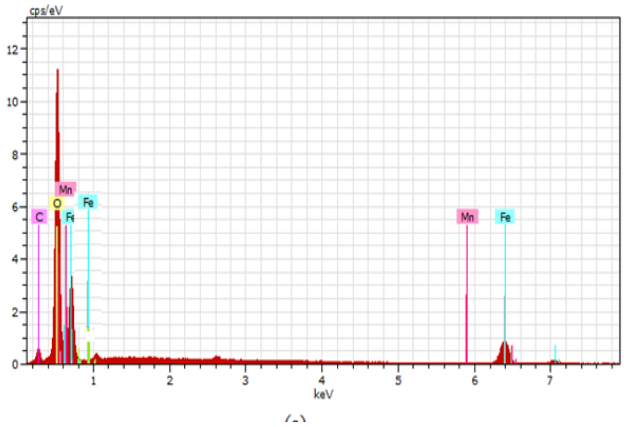

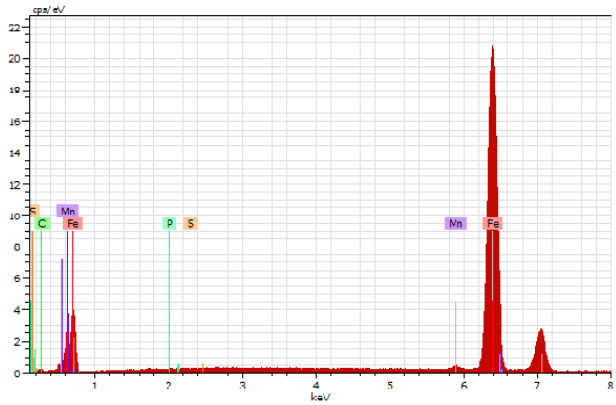

(b)

in aqueous solution containing 60 ppm of Cl^-. (b) Mild steel sample after immersion in aqueous solution containing 60 ppm of Cl^- + 250 ppm of HUF.

Energy Dispersive Analysis of X-Rays (EDAXs)

The EDAXs survey spectra were used to determine the elements present on the metal surface before and after exposure to the inhibitor solution. The objective of this section was to confirm the results obtained from chemical and electrochemical measurements that a protective surface film of inhibitor is formed on the metal surface. To achieve this, EDAX examinations of the metal surface were performed in the absence and presence of inhibitors system.[19-22]

EDAX spectrum of mild steel immersed in aqueous solution containing 60 ppm Cl^- is shown in Figure 8 (a). They show the characteristics peaks of some of the elements constituting the mild steel sample. The EDAX spectrum of mild steel immersed in aqueous solution containing 60ppm Cl^- + 250 ppm HUF is shown in Figure 8 (b). In addition, the intensity of O signals is reduced and the intensity of Fe signal is increased. The appearance of Fe signal and this enhancement of O signal are due to the presence of inhibitor. These data show that metal surface covered the Fe, S, C, P and Mn atoms.

Bacterial Enumeration count

The results of bacterial enumeration count[23-25]of the aqueous solution containing 60 ppm of Cl^- and 60 ppm of Cl- with HUF inhibitor are presented in Table 3. The aqueous solution containing 60 ppm of Cl^- without inhibitor shows more bacterial count against the growth of pathogenic bacteria strains such as E. Coli, Streptococcus, Pseudomonas and Entrobacter. The aqueous solution containing 60 ppm of Cl^- with inhibitor HUF shows less bacterial count against the growth of pathogenic bacteria strains such as E. Coli, Streptococcus, Pseudomonas and Entrobacter. A good result was obtained when addition of HUF inhibitor to the corrosive media.

Table 3. Colonies forming unit (CFU) of mild steel in aqueous solution containing 60 ppm of Cl^- in the absence and presence of HUF inhibitor obtained by bacterial enumeration count method.

Systems	Colonies Forming Unit (per ml)			
	E.Coli	Strepto-coccus	Pseudo-monas	Entero-bacter
60ppm Cl^-	$140x10^6$	146×10^6	130×10^6	127×10^6
60 ppm Cl^- + 250 ppm HUF	84×10^6	75×10^6	78×10^6	76×10^6

Conclusion

The present study leads to the following conclusions. The formulation consisting of 60 ppm of $Cl^-$and 250 ppm of HUF offers 75 % inhibition efficiency in controlling corrosion of mild steel. AC impedance spectra reveal that a protective film is formed on the metal surface. FTIR, fluorescence and UV-Visible spectra reveals that the protective film consists of HUF-Fe^{2+} complex formed on metal surface. SEM and EDAX confirm the presence of a protective film on the metal surface. The bacterial enumeration has been reduced by the addition of HUF inhibitor to the corrosive media.

Acknowledgement

The authors are thankful to their management of Jamal Mohamed College, Tiruchirappalli,Tamilnadu, India. S. S. Syed Abuthahir and Dr. S. Rajendran are thankful to Dr. N. Kaliammal, Director, B. Kothandaraman, CEO and Dr. K. V. Kupusamy, Chairman of RVS Educational Trust's Group of Institutions, Dindigul-05, Tamilnadu, India.

References

[1]Satyanarayana, M. G. V., Kalpana, Y., Himabindu, V and Kumar, K., *Corros. Eng. Sci. Technol*., **2012**, *47(1)*, 38-44.

[2]Al-Baker, N., Shawabkeh, R and Rihan, R., *Corros. Eng. Sci. Technol*., **2011**, *46(7)*, 767-776.

[3]Durodola, B. M., Olugbuyiro, J. A. O., Moshood, S. A., Fayomi, O. S. and Popoola, A. P. I., *Int. J .Electrochem. Sci.*, **2011**, *6*, 5605-5616.

[4]Zou, Y., Wang, J., and Zheng, Y. Y., *Corros. Sci*.**,** **2011**, *53(1)*, 208-216.

[5]Brasher, D., *Nature*, **1962**, *193*, 868; Brasher, D. and Mercer, A., *Brit. Corros. J.*, **1968,** *3(3)*, 136; Mercer, A. and Jenkins, I., *Brit. Corros. J.*, **1968,** *3*, 144.

[6]Damaskin, B. B., Pietrij, O. A., and Batrokov, W. W., *Adsorpcija Organiczeskich Sojedinienjina Electrodach, Moskva*, **1968.**

[7]Okamoto, G., Nagayama, M., Kato, J. and Baba, T., *Corros. Sci.*, **1962**, *2*, 21-27.

[8]Wranglen, G., *London, Chapman and Hall*, **1985**, 236.

[9]Sathiyabama, J., Rajendran, S., Arockia Selvi, J., Jeyasundari, J., *Open Corros. J.*, **2009,** *2*, 84.

[10]Shyamala Devi, B., Rajendran, S., *Eur. Chem.Bull*., **2012,** *1*, 150.

[11]Rajendran, S., Paulraj, J., Rengan, P., Jeyasundari,J., Manivannan, M., *J. Dent. Oral. Hyg.*, **2009,** *1*, 1.

[12]Rajendran, S., Anuradha, K., Kavipriya, K., Krishnaveni, A., AndelinThangakani, J., *Eur. Chem. Bull*., **2012,** *1*, 503.

[13]Rajendran, S., Maria Joany, R., Apparao, B. V. and Palaniswamy, N., *Indian J. Chem. Technol*., **2002**, *9*, 197-200.

[14]Rajendran, S., Earnest John Peter, B. R., Peter Pascal Reces, A., John Amalraj, A. and Sundaravadivelu, M., *Trans. SABST*., **2003**, *38(1)*, 11-15.

[15]Jayasundari, J., Rajendran, S., SayeeKannan, R., Brightson Arul Jacob, Y., *Eur. Chem. Bull*., **2013**, *2(9)*, 585-591.

[16]Rajendran, S. and John Amalraj, A., *Bull. Electrochem.*, **2005,** *21*, 185-191.

[17]Albrecht, M. Witt, K., Weis, P., Wegelius, E., Frohlich, R. *Inorg. Chim. Acta*, **2002,** *341*, 25-32.

[18]Gopi, D., Manomozhi, S., Govindaraju, K. M., Manisankar, P., Rajeswari, S., *J. App.Electrochem.*, **2007,** *37(4)*, 439-449.

[19]Amin, M. A., Abd El-Rehim, S. S., El-Sherbini, E. F. F., Bayoumi, R. S., *Electrochimica Acta*, **2007,** *52(11)*, 3588-3600.

[20]Amin, M. A., Abd El-Rehim, S. S., Abdel-Fatah, *Corros. Sci.*, **2009**, *51(4)*, 882-894.

[21]Rahim, S. S. A., Hazzazi, O. A., Amin, M. A., Khelad, K. F., *Corros. Sci.*, **2008**, *50(8)*, 2258-2271.

[22]Migahed, M. A., Azzam, E. M. S., Morsy, S. M. J., *Corros. Sci.*, **2009,** *51(8)*, 1636-1644.

[23]Reynolds, K., Farinha, J., *Richland College*, **2005**.

[24]Maruthamuthu, S., Ponmariappan, S., Indira, K. R., Rengaswamy, N. S and Subramanian, A., *Bull. Electrochem.*, **2000**, *166*, 209.

[25]Atia, A. A and Saleh, M. M., *J. Appl. Electrochem.*, **2003**, *33*, 171.

Received: 07.10.2013.
Accepted: 26.10.2013.

PREPARATION OF EFFICIENT CATALYSTS – ADSORBENTS FOR CLEANING OF GASES FROM SULFUR COMPOUNDS

V. Bakhtadze,[a] V. Mosidze,[a] R. Janjgava,[a] N. Chochishvili,[a] D. Dzanashvili,[a] N. Kharabadze,[a] M. Pajishvili[a]

Keywords: catalyst-adsorbent, manganese oxides, sulfur compounds

The process of cleaning of hydrocarbon gases by the concentrates of manganese natural ores (Chiatura deposit, Georgia) from sulfur compounds has been investigated. It was shown that critical sulfur content of the adsorbent mass in temperature range of 350-400 ^{0}C comprises 15-17 wt. %. The technology of preparation of pelletized oxide-manganese catalyst-adsorbent is proposed. The effect of the parameters of pelletizing process: compacting pressure, composition, type and properties of stabilizing components on formation of secondary structure was established. The data of activity and some physical-chemical characteristics of pelletized oxide-manganese catalyst-adsorbent are presented.

Corresponding Authors*
Tel: +995 93 963070
Fax: +995 032301430
E-Mail: vbakhtkat@yahoo.com
[a] Iv. Javakhishvili Tbilisi State University, R. Agladze Institute of Inorganic Chemistry and Electrochemistry, Mindeli str. 11

Introduction

According to the data of publications of Energetic Informational Agency of USA Energetic Ministry: "Natural Gas Annual" and "International Energy Annual", all over the World nearly to 100 billion m^3 of gases are used annually, for chemical purposes, which consists 2,5-3 % of produced gas. This gas is mainly formed at oil deposits and is a valued raw material for gas refining factories. Along with it, it is well known that a major part of the reserves of natural gases is due to those deposits which involve sulfur compounds (preferentially in the form of hydrogen sulfide - H_2S) to a variable extent. There are a number of small and large oil deposits, in the oil-gas composition of which a concentration of H_2S is high and varies from 3.6 wt. % to 20-30 wt. %.[1-3] Respectively, a low rate of refining of such oil, condensate and gases may be explained by high content of sulfur compounds in them, which causes a damage of buildings and communications and serious environmental problems. Moreover, sulfur compounds are strong catalytic toxic substances in account of which the use of hydrocarbon gases for energetic and technological purposes is limited. From above mentioned, a complete separation of hydrogen sulfide from oil gases and its refining is of great importance for attaining of environmental safety.

In industry one or another method is used for oxidation of hydrogen sulfide in gases depending on the concentration. If the concentration of H_2S > 10 wt. %, an oxidation in gaseous phase (method of Claus) is used; at hydrogen sulfide concentration up to 10 wt. %, an oxidation in liquid phase is more rational and at hydrogen sulfide content: 0.2-0.3 wt. %, solid adsorbents are used. Within recent years an alternative methods of hydrogen sulfide utilization are considered more commonly which provide a production of hydrogen, available for energetic purposes together with sulfur. One of the promising methods involves the thermal catalytic decay of hydrogen sulfide at the temperatures higher than 370-380 ^{o}C. Oxides of vanadium, nickel, cobalt and manganese are recommended as catalysts for this process.[4-5]

In chemical industry an absorbers, prepared from zinc oxide, are mainly used for cleaning of synthesis-gas from sulfur compounds. Results of executed thermodynamic and experimental investigations confirm that, except from zinc oxide, active catalysts-adsorbents for H_2S utilization may be produced from manganese oxides, too. It is important also, that zinc and manganese sulfides are characterized by high stability even at small partial pressures of hydrogen.

Existing methods for gas cleaning from hydrogen sulfide are rated to large volumes. By opinion of specialists, for small and medium deposits of oil gases so-called block-modulus plants are considerably more efficient which are successfully promoted in various countries: Germany, China, Brazil, Russia and etc. At such plants a solid adsorbents are used. Iron-manganese concentrates of Baltic Sea, recommended for gas cleaning, contain 10-23 wt. % of manganese, nearly 25-27 % of iron and other compounds. Adsorbents of such type are the particles of irregular spheric shape of 5.0-50.0 mm size and have various fractional compositions. Use of solid adsorbents, instead of liquid ones, excludes an existence of harmful wastes of the production. Cleaned gas is a raw material for gas generator plants and is an ecologically pure natural gas for various technological purposes.[1] Previously the systematic investigations were carried out on the use of manganese catalysts in chemical industry[6] and for solving of ecological problems.[7] In the papers[8] the adsorbents of sulfur, based on low-grade manganese ores, were investigated and proposed for practical use. The concentrate of manganese natural ore (CMNO) was tested on critical and total sulfur content (Fig.1).

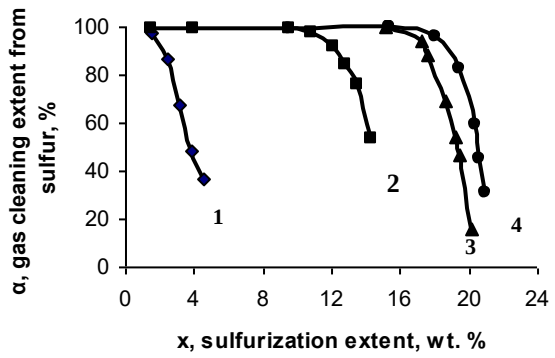

Figure 1. Dependence of the extent of gas cleaning from sulfur (α) on the extent of sulfurization of CMNO (X) at various temperatures: 1-200 °C; 2-300 °C; 3-370 °C; 4-415 °C. (Gas volume rate – 1000 h^{-1}; CS_2 concentration- 40 g m^{-3} by sulfur).

The logarithmic dependence of the fraction of residual sulfur in a gas on an extent of mass sulfurization can be described by equation:

$$\lg a = \lg a_0 + BX \qquad (1)$$

where a - is a fraction of residual sulfur in a gas at the degree of mass sulfurization, X;

a_0– is a fraction of residual sulfur in a gas in the presence of fresh adsorbent;

B- is a constant.

The plot of the dependence of lg a on X is linear, the slope of which is equal to B and the portion, cutted from an ordinate by straight line, gives lg α_o , that is to say, a fraction of residual sulfur in a gas, in the presence of fresh adsorbent (Fig.2). Calculated value of activation energy of the process of gas cleaning from CS_2 in the range of temperature from 200 °C to 400 °C comprises 5 kcal mol^{-1}, indicative of diffusion character of the process.

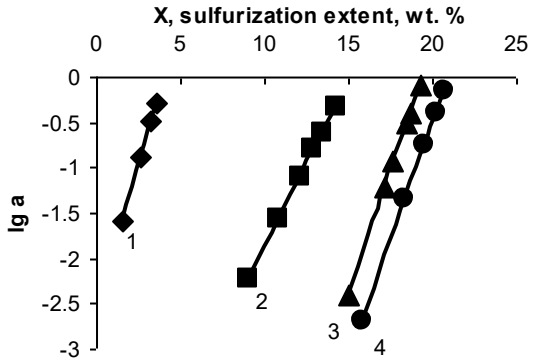

Figure 2. The logarithmic dependence of the fraction of residual sulfur in a gas (lg a) on an extent of mass sulfurization (X) for the process of gas cleaning from CS_2 at various temperatures, °C: 1 – 200; 2 – 300; 3 – 370; 4 – 415.

The dependence of critical sulfur content of CMNO on temperature at cleaning of nitrogen-hydrogen mixture from carbon disulfide and hydrogen sulfide has shown (Fig. 3) that with increasing of temperature the critical sulfur content of the mass by sulfur is enhanced. At temperature of 200 °C an overshoot of carbon disulfide is observed. At temperature of 290-300 °C an overshoot of CS_2, as well as of H_2S takes place nearly simultaneously. At temperature of 350 °C an overshoot of H_2S is proceeded at early stage, but degree of gas cleaning from CS_2 is maintained up to 95-96 %, for a long time.[9]

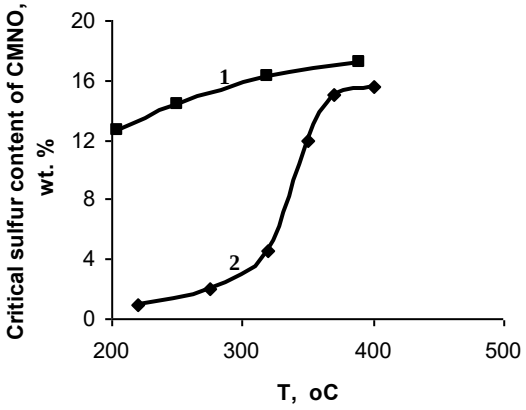

Figure 3. Dependence of critical sulfur content of CMNO on temperature at cleaning of nitrogen- hydrogen mixture (H_2:N_2=3:1) from H_2S (1) and CS_2 (2).

An analysis of scientific publications permits to note positive sides of the use of solid adsorbents, obtained from manganese natural ores in sulfur cleaning processes: sufficiently large sulfur capacity – up to 15.0 wt. %, cheapness and ecologically pure industrial wastes.

The following moments may be listed as negative ones:

Inspite of the efficiency, a wide practical use of such catalysts in modern high-technology processes is limited by their insufficient operating characteristics: small specific surface, low mechanical and thermal stability, single use of a mass.

The aim of presented work involves: the study of the process of cleaning of hydrocarbon gases by the concentrates of manganese natural ores (Chiatura deposit, Georgia) from sulfur compounds, an analysis of the reasons of limited utility of massive (carrier- less) oxide-manganese catalysts-adsorbents in industry and an advisability of elaboration of pilled compositions on their basis with optimal physical-chemical characteristics. The technology for preparation of pilled catalysts from the powders, containing manganese oxides, is proposed. An activation of prepared tablets was studied in the process of cleaning of natural gas from hydrogen sulfide. An effect of the parameters of pilling process: compacting pressure, composition, type and properties of stabilizing components on the formation of secondary structure was determined. Some physical-chemical characteristics of the pills are presented. A pilot lot of manganese catalyst- adsorbent was manufactured by elaborated technology at rotor pilling

machine of two-way filling. It was shown that pilled oxide-manganese catalysts-adsorbents by total and critical sulfur content, mechanical strength and thermal stability, as well as by availability of initial raw material is competitive with some well-known types of zinc-containing adsorbents used in the industry.

Experimentals

Sample preparation.

The concentrates of manganese natural ores of Chiatura deposit (Georgia) were used for preparation of the tablets. Chemical composition of initial concentrates before and after reducing by nitrogen-hydrogen mixture at 650-700 ºC for 2 h is presented in Table 1.

Table 1. Chemical composition of the concentrates of manganese oxide ores (wt. %)

№	MnO_2	MnO	SiO_2	Al_2O_3	Fe_2O_3	CaO
I	20.0-92.0	--	2.0-45.0	2.0-10.0	1.5-5.0	2.5-20.0
II	1.0-3.0	30.0-90.0	2.0-25.0	2.0-13.0	1.5-5.0	2.5-25.0

I-Initial sample; **II-** Reduced by nitrogen-hydrogen mixture at 650-700 °C, 2 h.

Table 2. Effect of phase composition of manganese oxides on mechanical strength of the tablets

Sample composition, wt. %	Mechanical strength of the pills at compacting pressure, kg cm^{-2}		
	50	100	150
I - 10.0MnO, 80.0($CaO.2Al_2O_3$), 10.0H_2O	55.0	60.0	75.0
The same as I, reduced by H_2 at 400-450 °C, 2 h	50.0-60.0	55.0-60.0	70-75
II-80.0MnO_2, 10.0($CaO.2Al_2O_3$), 10.0H_2O	50.0	60.0	70.0-80.0
The same as II, reduced by H_2 at 400-450 °C, 2 h	-	-	-

Granulometric composition of initial and reduced manganese concentrates is roughly the same and comprises 0.05-0.1 mm. The mixture of the oxides of calcium and aluminum was used as a binder. Moisture content in a charge was varied from 5.0 to 15.0 wt. %. Laboratory mechanical press was used for tableting. Compacting pressure – 50, 100, 150 kg cm^{-2}. Pellets size ϕ = 8÷9 mm, height – h = 5÷6 mm.

Methods

The porosimeters of low and high pressure - MA-3M-1 were used to determine the mean radius and volume of the pores of the samples of oxide-manganese catalysts-adsorbents. Desulfurization process was studied at flouring plant. Methane was used as cleanable gas. A gas, after passing a flow meter, was entered in a saturator, where was saturated by a steam thereafter into a vessel by reaction:

$$BaS+2H_2O = Ba(OH)_2 + H_2S \quad (2)$$

A gas was enriched by hydrogen sulfide and was headed into a reactor for cleaning. Quartz tube of 20 mm diameter and of 250 mm length was used as a reactor. It was equipped by Ni-Cr alloy spiral for heating. Gas analysis before and after reactor was carried out by the method of iodometric titration.

Results and Discussion

In Table 2 the data on mechanical strength of the pellets, prepared from initial and preliminary reduced concentrates of manganese ores, are given. The pellets prepared from the powders of manganese ores without reduction, as well as of reduced by hydrogen, are characterized by high mechanical strength. The pellets, prepared from non-reduced concentrates (simple II), in contrast of simple I, are decomposed in the form of fine powder after reducing by nitrogen-hydrogen mixture at 400-450 ºC (2 hours).

With increasing of compacting pressure of the pellets, a significant variation of porous structure is observed. The pellets, prepared at low pressure (50 kg cm^{-2}), have the same volume of the pores V= 0.285 $cm^3\ g^{-1}$. This index for the pellets, prepared at compacting pressures – 100 and 150 kg cm^{-2}, comprises 0.195 and 0.142 $cm^3\ g^{-1}$, respectively (Table 3).

Table 3. Dependence of variation of some parameters of the tabletes on the value of compacting pressure at mechanical hand-operated pump

Samples	Compacting pressure, P, kg cm^{-2}	Total volume of pores, $cm^3\ g^{-1}$	Specific surface S, $m^2\ g^{-1}$	Density g cm^{-3}
I	50	0.2854	7.7	2.3
II	100	0.1958	9.1	2.5
III	150	0.1413	22.33	2.7
Pilot	70-75	0.1848	49.75	2.5-2.8

Testing of the pellets in the course of cleaning of natural gas from hydrogen sulfide has shown that with increasing of temperature a sulfur content of a catalyst-adsorbent is increasing at an instant of overshoot of hydrogen sulfide (Fig. 4). Total sulfur content of pellets after 500 hours operation attains 18-20 wt. %.

 DOI: 10.17628/ecb.2014.3.46-49

Table 4. Some physical-chemical characteristics of pilot lot of pelleted oxide-manganese catalyst-adsorbent (pellet size *D*=9 mm, height *h*=5 mm)

Radius of pores			Total volume of pores, $cm^3 g^{-1}$	Specific surface, $m^2 g^{-1}$	Mechanical strength, $kg\ cm^{-2}$	Bulk density, $kg\ dm^{-3}$
***r* < 100Å**	***r*-100-1000 Å**	***r* >1000 Å**				
80 ÷100	250 ÷750	3500÷5000	0.28-0.30	40.0– 50.0	80.0-90.0	1.6-1.8

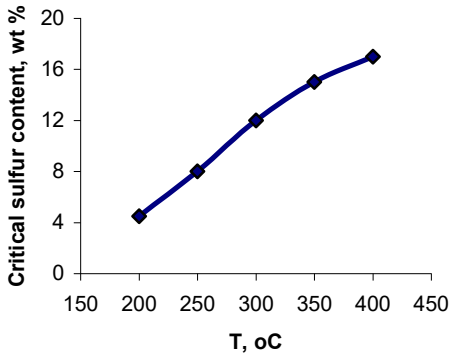

Figure 4. Dependence of critical sulfur content of pelleted manganese catalyst-adsorbent on the temperature at cleaning of methane from H_2S (V_{cat}=10 ml, G_{cat}=16g, W=1000 h^{-1}, flow rate of H_2S – 180 mg h^{-1} by sulfur, particle size comprises 1/4 part of whole granule).

High sulfur absorbance of manganese contacts in reducing medium may be explained by an ability of manganese oxides for stopping of reducing processes at the stage of sulfide formation. Because of this fact they are different from iron oxides in which the process is proceeded up to the formation of metallic iron. Cubic structures of Mn (II) oxide and of sulfide - MnS close by parameters, are favourable to total sulfurization of the oxides of Mn (II) and Mn (III):

Parameters	MnO	MnS
a, Å	4.436	5.611

Pilot lot of oxide-manganese catalyst - adsorbent in amount of 30 kg was manufactured by elaborated technology[10] at rotor pelletizing machine of two-way filling (Table 4). The prepared pellets, are characterized by a totality of the pores of various radius. Along with it, the main part involves the pores of low and medium radius.

The phase composition of pilot sample of sulfided oxide-manganese catalyst-adsorbent was studied by the thermal and X-ray diffraction methods. It was shown that in the temperature range of 300-700 °C an intensive oxidation of sulfide sulfur occurs. Manganese lower valence sulphur oxyacid salts of various compositions may be formed as the products of oxidation. End product of oxidation, manganese sulfate with an impurity of manganese sulfide begins to dissociate at the temperatures of 800-850 °C.

Conclusions

Performed investigation has shown that pelleted oxide-manganese catalyst-adsorbent absorbs efficiently a sulfur at cleaning of natural gas from H_2S in temperature range from 350 °C to 400 °C. Critical sulfur content comprises 15-17 wt. s%. Pellets of oxide-manganese catalyst-adsorbent, prepared by elaborated method, by its activity, absorbance and operating regime is in good competition with some types of zinc-containing adsorbent and by mechanical strength and thermal stability has the better indexes.

References

[1]Katkov, A., Malov, E., Koptenarmusov, V., Polonic, A., Mazgarov, A., Vildanov, A., Bazhirova, N., 4th *Int. Conf. "Cooperation for Solution of Waste Problem*", 31 January-1 February, E-Publishing, Kharkov, Ukraine. **2007**, 152 – 154.

[2]Kalanova, Sh., Zakumbaeva, G. J., *Trans.Acad. Sci. Kazakh SSR*, **1990,** *6*, 44–54.

[3]Babich, L., Moulijn, I., *Fuel* **2003,** *82*, 607–631.

[4]Startsev A., Zagoruiko A., Baljiminaev B., Sidiakin M., Kuznetsov P., Voroshina O., Zakharov I.. *RU Patent 2216506.* **2003.**

[5]Bakhtadze V., Mosidze V., .Janjgava R., Kartvelishvili D., *7th International ISTC seminar*, November 2-4 **2004**, Ekaterinburg, Russia. *Plenary Lectures and Proceedings of the Conference*. **2005**, 177 – 179.

[6]Ioseliani D., V. Bakhtadze V., *Georgian Academy of Sciences, Chemistry and Chemical Technology, Proceedings, "Metsniereba"*. **2001**, 120 – 133.

[7]Bakhtadze V., Kharabadze N., Moroz E., *J. Catalysis in the industry.* **2007**, *3*, 3 – 9.

[8]Chochishvili N., *Bulletin of the Academy of sciences of the Georgian SSR*, **1977,** *86*, 132 -136.

[9]Chochishvili N., *Bulletin of the Academy of sciences of the Georgian SSR*, **1985,** *117*, 325 – 328.

[10]Bakhtadze V., .Janjgava R., Kartvelishvili D., Kardanakhishvili T., . Mosidze V., *Georgian Patent U 1027*, **2003.**

Received: 18.10.2013.
Accepted: 07.11.2013.

AN ASSESSMENT OF BIOGEOCHEMICAL CYCLES OF NUTRIENTS IN THE INNER GULF OF THAILAND

Gullaya Wattayakorn[a]* and Pongjit Jaiboon[a]

Keywords: nutrient budgets, biogeochemical budgets, net ecosystem metabolism, Inner Gulf of Thailand

The nutrient dynamics of the Inner Gulf of Thailand were studied using a simple steady-state budget model, according to the Land–Ocean Interaction in the Coastal Zone modelling guidelines. Two sampling campaigns were carried out during the wet (October 2011) and the dry (February 2012) seasons. For each season, budgets for water and salinity, dissolved inorganic phosphate (DIP) and nitrogen (DIN) were determined. The study indicates that the Inner Gulf exports water at the rate of 133-562 MCM.day^{-1} in the form of residual flux (V_R) at the inner-outer Gulf interface. This results in supply of salt to the inner-outer Gulf interface at the rate of $4.3x10^3$–$17x10^3$ ton.d^{-1}. Exchange between the Inner Gulf water and the adjoining seawater replaces this salt loss. Mass balance calculations indicate that the Inner Gulf is a net source for DIP and DIN to the adjacent outer Gulf water at the rate of $4.0x10^4$-$3.4x10^6$ molP.d^{-1} and $4.1x10^6$- $20.5x10^6$ molN.d^{-1}, during the dry and wet season respectively. The high DIP and DIN exports during the wet season probably reflect the inputs coming from the agricultural, domestic and industrial wastes during the severe flooding over Thailand in 2011. Stoichiometric analysis yields the values of net ecosystem metabolisms (NEM; p-r) and net nitrogen production (nfix-denit) in the Inner Gulf at the rate of $4.4x10^3$ tons C.d^{-1} and $0.7x10^3$ tons N.d^{-1}, indicating that the Inner Gulf is an autotrophic (sink of nutrients) and net nitrogen fixing (nfix-denit >0) ecosystem during the wet season. However in the dry season, the Inner Gulf remains to be autotrophic (p-r = 47 tonsC.d^{-1}) but shifted to be a net denitrifying ecosystem (nfix-denit = -88 tonsN.d^{-1}). Results from the nitrogen and phosphorus biogeochemical cycling revealed the importance of river discharges in the transport and transformation of these substances within the Inner Gulf of Thailand.

* Corresponding Authors
Fax: +6622550780
E-Mail: gullaya.w@chula.ac.th; gullaya@gmail.com
[a] Department of Marine Science, Faculty of Science, Chulalongkorn University, Pathumwan, Bangkok, 10330, Thailand

Introduction

The Gulf of Thailand is a semi-enclosed shallow coastal sea located in a tropical area at latitude 13ºN and longitude 100º30'E (Fig. 1). It is situated immediately to the northwest of the South China Sea, from which it is separated by two sills. Monsoon seasons and the intrusion of seawater from the South China Sea are the major factors which have profound effects on the oceanographic conditions within the Gulf.[1] In addition, strong seasonal variations in precipitation and river discharges lead to seasonal variations in water column conditions. Geographically, the Gulf of Thailand may be divided into the Upper and Lower Gulf. The Upper Gulf is the catchment basin of four large rivers namely, the Chaophraya, the Tachin, the Bangpakong and the Maeklong River on the northern side. Among these, the Chaophraya is the largest river contributing about 49% of the Gulf's surface water, with the discharge of $22x10^3$ MCM.yr^{-1}. Primary production prevailing in the Gulf of Thailand is known to be relatively high, as the result of high nutrient input through rivers and from agricultural fertilizers, household sewage and shrimp farms along the coast, as well as urban runoff from the City of Bangkok.[1] Widespread eutrophication is a growing problem, ranking as the most severe threat to the Inner Gulf due to increasing input of nutrients from the land-based sources. Water quality is generally lower than acceptable standards in the Inner Gulf region, especially at the river entries.[2-7]

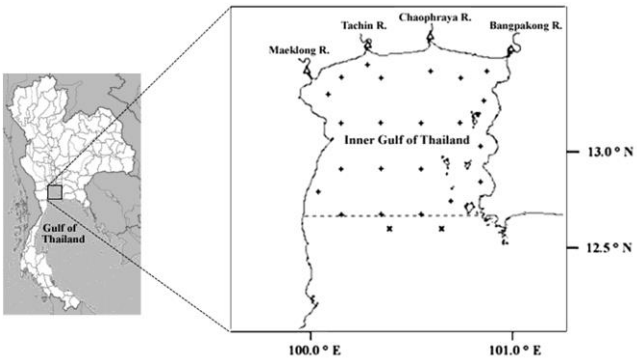

Figure 1. Map of the Inner Gulf of Thailand.

We have limited knowledge about the biogeochemistry of the Gulf of Thailand and many processes are not well known, in particular the biogeochemical budgets of carbon and nutrients. The key questions include is the Gulf a source or sink for carbon, nitrogen and phosphorus (CNP) remain unanswered. In addition there are shortcomings in our knowledge of some of the important physical, chemical and biological controls on nutrient biogeochemical cycles. A few processes are affected either by human activities directly or through climate change.

The transformations of these nutrient elements are important because the combination of net fluxes of water, dissolved nutrients and organic matter will determine the role of the system either as a heterotrophic system (source of nutrients) or autotrophic system (sink of nutrients).[8] Although exchange of materials such as water and salt, dissolved nutrients and organic matter in semi-enclosed shallow seas and estuaries has received much attention in recent years,[9-15]. The dynamics of nutrients in the Gulf of Thailand have not been well studied so far and information about the sources and processes controlling their

mobilization and fate are still lacking. The present study explores some aspects of the nutrient dynamics in the Inner Gulf of Thailand by using the modelling protocol developed by the Land-Ocean Interactions in the Coastal Zone (LOICZ).[8] The overall aim of the study is to construct biogeochemical budget model for the Inner Gulf of Thailand, in order to understand the processes controlling nutrient dynamics, their stoichiometry and metabolism over a range of temporal and spatial scales.

Experimental

Study area

The site of this study is the innermost area of the Upper Gulf of Thailand (Inner Gulf), located at 12º40′– 13º36′N and 99º57′-101º00′E (Fig. 1). The Inner Gulf is roughly rectangular in shape, about 100 km long and 100 km wide, with an average depth of 15 m and a volume of $150x10^9 m^3$. The Gulf is surrounded by highly populated area and some heavily polluting industries. Some untreated effluents have been discharged from industrial sites into the small tributaries that feed into the Inner Gulf. In addition, domestic wastewater generated by residents in and around the area is discharged into open ditches, which ultimately draining into the Gulf.[7] About 50 per cent of the land-based contaminants and nutrients are delivered into the Gulf by the four major rivers at the head of the Upper Gulf, hence frequent algal blooms have become common in the Gulf.[1,2,7]

The average freshwater discharges during 1999-2000 were estimated to be $8.2x10^3$, $8.1x10^3$, $22x10^3$ and $6.6x10^3$ $MCM.yr^{-1}$for the Maeklong, Tachin, Chaophraya and Bangpakong River, respectively.[16] Runoffs from these rivers have produced a strong salinity gradient from about 5 psu near shore to between 31 and 32 psu at the mouth of the Inner Gulf.[17] The average annual rainfall from 1979 through 2006, measured at monitoring stations around the Inner Gulf, was approximately 1,395 mm. Most precipitation occurs during May to October, the highest precipitation is usually received in the month of September, with an average rainfall of 344 mm, which amounts to 20 % of the average annual rainfall. Evaporation over the area is about 4 $mm\ d^{-1}$.[18]

Sample collection and analysis

Two cruises were carried out aboard the R/V Chulavijai of Chulalongkorn University, in October 2011 and February 2012. During each survey 15-20 stations (Fig. 1) in the Inner Gulf were occupied at both high and low tide. Coincidentally with each survey, the four major rivers were sampled on the days preceding each cruise. Rivers were sampled at low tide to minimize saltwater intrusion. Sampling was conducted from a bridge or small boat which allowed access to mid-channel. Discrete water samples were collected from the 1.0 m of the surface and 1.0 m of the bottom, stored in 1-L acid-washed polypropylene bottles and were filtered through acid-washed 47 mm diameter Whatman GF/F filters. The filtered water samples were analysed for dissolved inorganic nutrients (NH_4^+, NO_2^-+NO_3^-, PO_4^{3-}) in the laboratory. Dissolved organic nitrogen (DON) and phosphorus (DOP) concentrations were estimated as the difference between the total dissolved nutrient pools and the dissolved inorganic nutrient concentrations.[19,20]

Physical parameters were measured with a conductivity–temperature–pressure instrument (CTD) at a 0.1-m vertical interval. Other water quality parameters were obtained via the YSI 556 multi-probe system during the sampling operation. Rainfall and evaporation data were obtained from Thailand Meteorological Department while discharge data were obtained from the Royal Irrigation Department.

Results and Discussions

Data availability

Data used in this budgeting study are shown in Tables 1 and 2. Groundwater discharge and outfalls were assumed to be negligible. Fig. 2 presents a longitudinal transect of water salinity in the Inner Gulf of Thailand during the two sampling periods, revealing some vertical stratification in the region of freshwater influence. Examples of distribution patterns of DIN and DIP in the Inner Gulf are shown in Fig. 3.

Table 1. Model input parameters and assumptions

Parameter	October 2011 $10^6\ m^3\ day^{-1}$	February 2012 $10^6\ m^3\ day^{-1}$
Precipitation	113	27
Evaporation	38	40
Discharge	487	146
Groundwater, other sources	0 (assumed)	

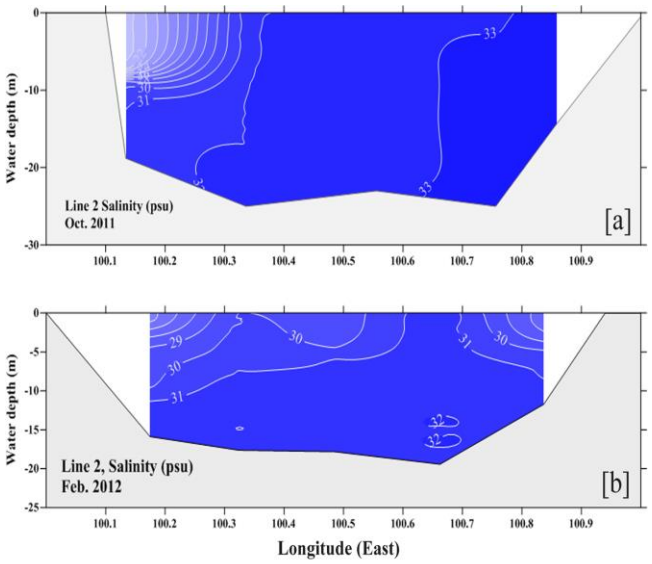

Figure 2. Longitudinal transect of water salinity in the study area during [a] October 2011 and [b] February 2012.

 DOI: 10.17628/ECB.2014.3.50-54

Table 2. Chemical composition of water samples from rivers (FW), Inner Gulf (System) and adjacent seawater (SW)

Oct-2011	Salinity, psu	NH_4^+, µM	NO_3^-	DIN	DON	PO_4^{3-}	DOP
FW	0	27.5	11.8	39.4	24.19	3.9	0.47
System	28.5	6.4	0.77	7.1	15.25	0.46	1.22
SW	32.0	8.1	0.24	8.3	9.58	0.86	1.96
Feb-2012							
FW	0	22.2	25.2	47.4	14.8	2.7	1.1
System	31.3	3.65	1.77	5.4	24.34	0.55	0.49
SW	33.8	3.26	0.97	4.2	27.19	0.38	0.39

Water and salt budgets

Since no significant vertical stratification in salinity was observed in the Inner Gulf (Fig. 2), therefore in this work the one layer single box LOICZ model[8] was applied to calculate nutrient and carbon fluxes, with the model constrained by water and salt budgets. Assuming a steady-state and conservation of mass, water and salt budgets were calculated for the Inner Gulf, for the period October 2011 and February 2012 using daily precipitation, evaporation and river discharge data. Water and salt budgets are calculated by the following equations.

$$dV_S/dt = V_O+V_P+V_E+V_G+V_R \quad (1)$$

$$d(V_S S_S)/dt = V_R S_R+V_X(S_O-S_S) \quad (2)$$

where

V_S denotes the volume of the Inner Gulf,

V_Q the dominant river discharges into the Inner Gulf,

V_P the precipitation,

V_E the evaporation,

V_G the ground water discharge,

V_R the residual volume transport from the Inner Gulf to the adjacent sea area,

S_S the average salinity of the Inner Gulf system,

Therefore, the average salinity of the adjacent sea area, $S_R=(S_S+S_O)/2$, and V_X the water exchange volume between the Inner Gulf and the adjacent sea.

dV_S/dt is estimated from the seasonal variation of mean sea surface of the Inner Gulf, V_Q is obtained from the Royal Irrigation Department, V_P and V_E are obtained from Thailand Meteorological Department; while V_O and V_G are assumed to be zero due to no data were available during the study periods.

The water and salt budgets are thus used to calculate the magnitude of all the flows across the system boundaries. Residual volume transport V_R decreased by about 1/4 as the river discharges V_Q decreased by about 1/3 from October 2011 to February 2012. The horizontal exchange volume V_X is estimated from Eq. (2) and the result is shown in Table 3. V_X in February 2012 is less than 1/4 of that in October 2011 and this is due to the decrease of the strength of estuarine circulation in the Inner Gulf.

Salt must be conserved in the system;[8] hence salt flux out of the system carried by residual flow (V_R) must be balanced via mixing (V_X). Average residence time of the Inner Gulf water (τ) can be estimated by the following equation.

$$\tau = V_S/(V_X+V_R) \quad (3)$$

The water exchange time (τ) for the Inner Gulf was 28 and 80 days in the wet and dry season respectively (Table 3). Once all the flows are known, the amounts of dissolved inorganic nutrients flowing into and out of the system can be calculated.

Nutrients budgets

The flux of a nutrient across the system boundary is equal to the average flow volume multiplied by the average concentration of the nutrient in that flow. The difference between the amount flowing in and out is the amount added or removed within the system during the budget period. Nutrient budget of the Inner Gulf is calculated by the following equation.

$$d(V_S C_S)/dt=V_Q C_Q+V_P C_P-V_R C_S+V_X(C_S-C_O)+\Delta C \quad (4)$$

where

C_S denotes the nutrient concentration of the system,

C_Q that of river water,

C_P that of rain,

C_O that of the adjacent sea area and

ΔC the nutrient flux by the biochemical processes such as photosynthesis, decomposition and release from the bottom in the box.

C_Q is estimated from the observed data and C_P is assumed to be zero because we have no data. In case of *DIP* budget, positive ΔC means that decomposition plus bottom release is larger than photosynthesis but negative ΔC means that photosynthesis is larger than decomposition plus bottom release.

Table 3. Water fluxes (precipitation V_P, evaporation V_E, runoff input V_Q, residual flow (V_R), salinity of the Inner Gulf and adjacent seawater (S_{syst}, S_{sea}), mixing water between Inner Gulf and sea (V_X) and water exchange time (τ) in the Inner Gulf in October 2011 and February 2012.

Sampling period	V_P	V_E	V_Q	V_R	S_{syst}	S_{sea}	V_X	τ
	MCM day^{-1}				psu	psu	MCM day^{-1}	days
Oct-11	113	-38	487	-562	28.5	32.9	4787	28
Feb-12	27	-40	146	-133	31.3	33.8	1752	80

Table 4 Estimated rates of non-conservative fluxes, *p-r* and (*nfix-denit*), unit: mmol m^{-2} d^{-1}

Sampling period	Δ*DIP*	Δ*DIN*	(*p-r*)	ΔN_{obs}	ΔN_{exp}	(*nfix-denit*)
Oct-2011	-0.34	-2.05	36.5	0.19	-5.51	5.70
Feb-2012	0.004	-0.42	0.39	-0.79	-0.06	-0.73

When we assume that the main primary producer in the system is phytoplankton, we may estimate nitrogen fixation (nfix) minus denitrification (denit) by the following equation.[8]

$$nfix - denit = \Delta N - 16\Delta DIP \quad (5)$$

Temporal variations of average nutrients concentrations in the system are shown in Table 2. DIN concentration in the system was higher in the wet season as compared to dry season but DIP concentration was lower. DIN/DIP ratio was 16 (Redfield ratio) in the wet season but it was lower than 16 in the dry season. This suggests that the limiting nutrient of photosynthesis in the Inner Gulf was DIP in the wet season but it changed to DIN in the dry season.

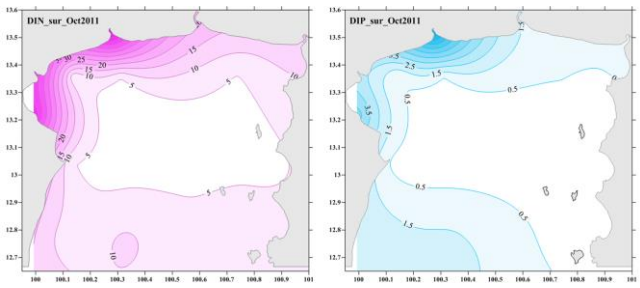

Figure 3. Spatial distribution of DIN and DIP in the study area in October 2011

For the Inner Gulf of Thailand, model output indicated that total nutrient fluxes from the Inner Gulf to the adjacent outer Gulf region in the wet season are -2.9×10^6 mol d^{-1} for NO_3^-, -17.5×10^6 mol d^{-1} for NH_4^+ and -3.4×10^6 mol d^{-1} for PO_4^{3-}, which are 1, 8, and 93 times higher than those in the dry season. The high nutrients exports during the wet season probably reflect the inputs coming from the agricultural, domestic and industrial wastes during the severe flooding over Thailand in 2011. During the present study, the system showed the removal of *DIP* at the rate of 0.34 mmol m^{-2} d^{-1} (October 2011) serving as a sink and almost in balance in February 2012. On the other hand, DIN values in the Inner Gulf are negative in both sampling periods, which showed the removal of DIN at the rate of 2.05 and 0.42 mmol m^{-2}d^{-1} in October 2011 and February 2012, respectively, serving as a sink for DIN. Table 4 summarizes the net ecosystem metabolism of the Inner Gulf of Thailand. Negative values of (nfix-denit) suggests a denitrifying system in the Inner Gulf during the low flow period.

Conclusions

The LOICZ biogeochemical modelling results of non-conservative fluxes, p-r and (nfix-denit) indicate that in the Inner Gulf of Thailand photosynthesis was larger than decomposition plus bottom release in the wet season but photosynthesis was nearly the same as decomposition plus bottom release in the dry season. Nitrogen fixation was higher than denitrification in the wet season but denitrification was larger than nitrogen fixation in the dry season. The results presented in this study may help scientists to summarise existing and new data in consistent and rigorous formats that may be more useful to coastal zone managers. It is also assumed that they may assist in the development of more applied models that could be used by managers in the decision-making process. The findings give insight into the way nutrient inputs are modified as they move from the land to coastal waters and how these, in conjunction with internal biological fluxes, affect the system metabolic processes. This may create an interest in the present system to be compared with other shallow coastal systems and to strengthen the understanding of nutrient behaviour to place further these findings in a regional and global context.

Acknowledgements

Funding for this investigation was provided by the Higher Education Research Promotion and National Research University Project of Thailand, Office of the Higher Education Commission (CC1030A) and the Integrated Innovation Academic Center: IIAC Chulalongkorn

University Centenary Academic Development Project (CU56-CC06). The authors would like to thank the Meteorological Department and Royal Irrigation Department for kindly providing valuable rainfall and discharge data. We thank Dr. Sompop Rungsupa and the crew of the R/V Chulavijai for their help in the field, and two anonymous reviewers for constructive comments that improved the manuscript.

References

[1]Piyakarnchana, T., "Changing state and health of the Gulf of Thailand Large Marine Ecosystem", In: Sherman. K. and Tang, Q. (eds), *Large Marine Ecosystems: Assessment, Sustainability and Management*, Blackwell Science, Malden, **1999,** 240.

[2]Chongprasith, P. and Srinetr, V., "Marine water quality and pollution of the Gulf of Thailand", In: Johnson, D.M. (ed), *SEAPOL Integrated Studies of the Gulf of Thailand*, Bangkok, Thailand, **1998**, *1*, 139.

[3]Wattayakorn, G., King, B., Wolanski, E. and Suthanaruk, P., *Cont. Shelf Res*., **1998**, *18*, 641.

[4]Talaue-McManus, L., *Transboundary Diagnostic Analysis for the South China Sea*, East Asian Seas Regional Coordination Unit Technical Report Series 14, United Nations Environment Programme, Bangkok, Thailand, **2000**.

[5]Wattayakorn, G., *J. Sci. Res. Chula. Univ., Special Issue I (NRC-EHWM)*, **2003**, *28(2)*, 15.

[6]Wattayakorn, G., *Coast. Marine Sci.*, **2005a**, *29 (2)*, 87.

[7]Wattayakorn, G., "Environmental Issues in the Gulf of Thailand", In: E. Wolanski (ed.), *The Environment in Asia Pacific Harbours*, Springer, Netherland, **2005b**, 497.

[8]Gordon, D. C., Boudreau, P. R., Mann, H., Ong, J.E., Sivert, W.L., Smith, S.V., Wattayakorn, G., Wulff, P. and Yanagi, T., *LOICZ Biogeochemical modeling guidelines*, LOICZ reports and studies, LOICZ, Texel, The Netherlands, **1996**, *5*, 96.

[9]Kemp, W. M., Smith, E. M., Marvin-Dipasquale, M., Boynton, W. R., *Marine Ecol. Prog. Ser*., **1997**, *150*, 229.

[10]Yanagi, T., *Japan J. Oceanogr*., **1999**, *55*, 439.

[11]Chen, C. T. A., Wang, S. L., Wang, B. J., and Pai, S.C., *Marine Chem*., **2001**, *75*, 281.

[12]Wattayakorn, G., Prapong, P. and Noichareon, D., *J. Sea Res.*, **2001**, *46*, 133.

[13]Baskin, V. N., Park, S. U., Choi, M. S., and Lee, C. B., *Biogeochemistry*, **2002**, *57/58*, 387.

[14]Camacho-Ibar, V., Carriquiry, J. D., Smith, S. V., *Estuaries* , **2003**, *26 (5)*, 1220.

[15]Liu, K. K., Atkinson, L., Quiñones, R. and Talaue-McManus, L., *Carbon and Nutrient Fluxes in Continental Margins: A Global Synthesis*, IGBP Book Series. Berlin: Springer**, 2008**.

[16]Department of Water Resources, Royal Thai Government, *National Water Development Report for Thailand*, World Water Development Programme (WWAP) Report, **2006.**

[17]Robinson, M.K., *The physical oceanography of the Gulf of Thailand, Naga Expedition.* NAGA Report, *3(1)*, 125, University of California, Scripps Institution of Oceanography, **1974**.

[18]Koontanakulvong, S. and Chaowiwat, W., *Corrected MRI GCM data for Thailand*, Technical Report, Water Resources System Research Unit, Faculty of Engineering, Chulalongkorn University, **2010**.

[19]Strickland, J. D. H. and Parsons, T. R., *A Practical Handbook of Seawater Analysis, Bulletin 167*, 2nd ed., Fisheries Research Board of Canada, Ottawa, **1972**.

[20]Grasshof K., Ehrharat M. and Kremling K., *Methods of Seawater Analysis*, 2nd ed., Verlag Chemier, Weinheim, **1983**.

Received: 31.10.2013.
Accepted: 07.11.2013.

SYNTHESIS OF TERTIARY ALIPHATIC AMINES

Wang Xiaofei[a], Liu Shu[a]*, Yu Tingyun[a] and Chai Yang[a]

Keywords: tertiary aliphatic amines, synthesis methods, review

Higher tertiary aliphatic amines are widely used in various industries, however, these are not manufactured in China. A substantial amount of C_4 fraction is available from the growing petroleum industry which provides the opportunity for the integration of refining with the petrochemicals plant. C_4 olefins can be used as starting materials for aliphatic amine production via butene oligomerization. In this paper, the industrial scale synthetic methods for production of tertiary aliphatic amines including the amination of olefins are reviewed.

*Corresponding Authors
*E-mail: liuxinlin-yj@163.com
Fax: 86-24-56860869
[a] Liaoning Shihua University, Fushun, Liaoning, P.R. China.

Introduction

The rapid growth of petroleum industry in China provides favourable conditions for C_4 utilization. C_4 olefins can be transformed into heavy olefins via oligomerization, and then be used as feedstock for the production of a variety of fine chemicals, such as tertiary amine.

Higher aliphatic amines (C_8-C_{22}) are often used as organic intermediates in the production of dye, oil, plastics, cosmetics and textile industry, mining and metal processing, etc. Primary amines are convertible into secondary and tertiary amines or diamines. The secondary and tertiary amines are raw materials to produce quaternary ammonium salts, polyoxyethylene aliphatic amines and tertiary amine oxides. About 98% of the secondary amines are used for preparing dialkylmethylated tertiary amines.[1]

Application of tertiary alkylamines

Tertiary alkylamines, based on the number of long-chain alkyl groups, involve mono-, di- and tri-tertiary alkylamines.[2] Among them, the trialkylamines are the most widely used derivatives.[3] The tertiary alkylamines can be used directly as intermediates during the production of various chemicals,[4] such as surfactants during the production of citric acid, fuel oils, cosmetics and as starting materials for the production of preservatives, fungicides and metal extracting agents.[5]

The reactions of tertiary amines with alkylating agents such as alkyl halides, alkyl sulfate or benzyl chloride result in quaternary ammonium salt, a group of widely used cationic surfactants. Long chain alkyl dimethylamines can be transformed into long chain alkyldimethylamine oxides by hydrogen peroxide. These amine oxides are often used as household cleansing products such as shampoos, shower gels, facial cleansers, foaming agents and other type of detergents.

Betaines, important amphoteric surfactants, are prepared by the reaction of dimethyl amine with chloroacetic acid and sodium hydroxide.[6] The preparation of octodecyl betaine is showed in Scheme 1.

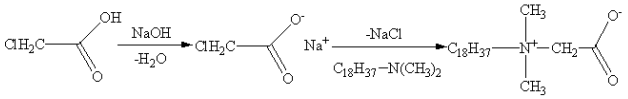

Scheme 1 Preparation process of octodecyl betaine

Betaines are often used as antistatic electric agents, softeners, detergents and wetting agents in textile industry; shampoos, classical detergents and baby cosmetics in daily chemical industry; fuel additives, metal antirusting agents, disinfectants, fungicides, etc.

Production of tertiary alkylamines

As the raw material for the production of biodegradable detergents, the preparation of tertiary alkylamines has caught much attention. Therefore, several methods have been developed, such as Liu Carter method, reductive-methylation, aliphatic alcohol amination, amination of chloroalkane, alcohol sulfation, bromination of α-olefin, amination of α-olefin epoxide, etc. Among them, the method of aliphatic alcohol amination is more popular.

In 1988, Feng[7] first reported the way to synthesize aliphatic tertiary amines from alcohol in China. This method was much attractive for its simple operation and little wastage. The key to this process was to develop catalysts with high selectivity and high activity. Li[8-13] discovered a catalyst system in which Cu and Ni were used as the main components, and adding the third one such as Zn, Co, Cr, La, Ba, Mg, Mo, Sn etc., to improve the catalytic performance. The catalyst Cu-Ni/$A1_2O_3$-SiO_2, invented by Kao (a Japanese company) in 1998, gave a conversion of 98 – 99 % for the amination of alcohol.[14] At present, the alcohol is used as the starting material for aliphatic tertiary amines by more than 95% of manufacturers including Kao, P&G and Lonza Lion. In China, more than 30 manufacturers are using this method. However, the strict requirements on the purity of raw materials, alcohol and methylamine, to be higher than 99% leads to a high cost. Therefore, the starting materials do not catch up with the standard in China.[15]

Tertiary amine synthesis routes

The route of industrial production for tertiary amine is shown in Figure 1.

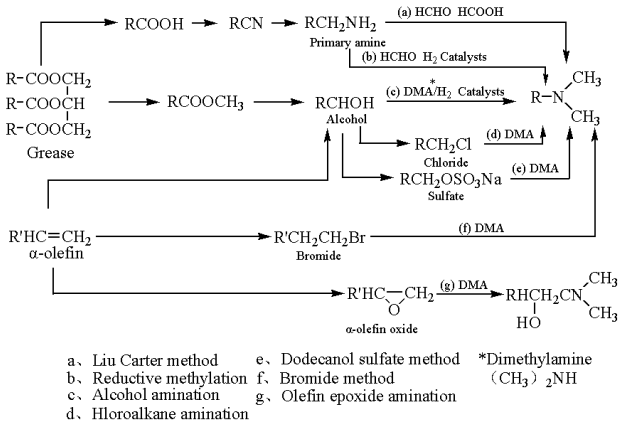

Figure 1. The manufacturing process of the aliphatic tertiary amines

(a) Liu Carter method (methylation of formic acid and formaldehyde)

At 373K, aliphatic tertiary amine can be prepared from primary amine, formaldehyde and formic acid.

$$RNH_2 + 2HCHO + 2HCOOH \xrightarrow{373K} RN(CH_3)_2 + 2H_2O + 2CO_2$$

The reaction mechanism for the above reaction is as follows: [17,18]

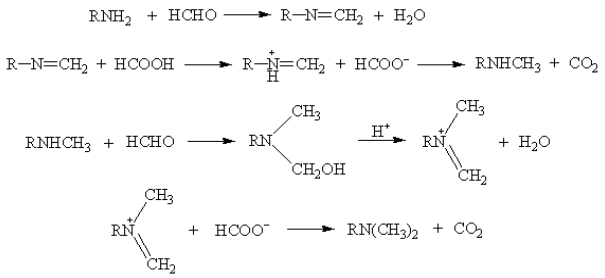

This method has disadvantages such as long process, many side reactions, high consumption of starting materials, treating of the waste gas, and bad quality of products.

(b) Reductive-methylation

The aliphatic tertiary amine can also be prepared by the reaction of primary amine with formaldehyde and hydrogen.

$$RNH_2 + 2HCHO + 2H_2 \xrightarrow[\text{Humidification, pressure}]{\text{Catalysts}} RNH(CH_3)_2 + 2H_2O$$

The reaction mechanism is as follows:[19]

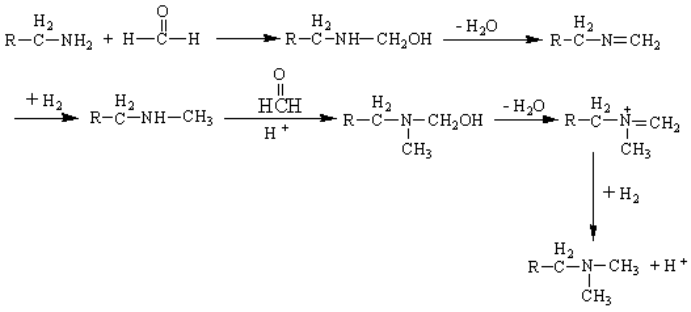

(c) Aliphatic alcohol amination

This method is important for the production of mono-long chain tertiary amine and has been used by Kao for a long time. The primary product has a purity of 95-99 %. d 99 % after distillation.

$$ROH + NH(CH_3)_2 \xrightarrow[\text{Hydrogenation Cat.(Cu Co Ni)}]{200\sim250^\circ C} RN(CH_3)_2 + H_2O$$

The reaction mechanism is as follows:[17,18]

Main reaction:

$$RCH_2OH \xrightarrow{Cu} RCHO + 2CuH$$

$$RCHO + Me_2NH \longrightarrow RCH(OH)NMe_2$$

$$RCH(OH)NMe_2 + 2CuH \xrightarrow{Ni} RCH_2NMe_2 + H_2O$$

Side reaction:

$$2Me_2NH \xrightarrow{Ni} MeNH_2 + Me_3N$$

$$RCH_2OH + MeNH_2 \longrightarrow RCH_2NHMe \longrightarrow (RCH_2)_2NMe$$

$$RCH_2OH \longrightarrow RCHO \longrightarrow RCH(OH)\text{-}CH(CHO)\text{-}R'$$

The product can then be used to prepare quaternary ammonium cation, alkyl betaines and amine oxides, sanitizers, algicides, antistatic agents, fabric softener, etc.[16]

(d) Amination of chloroalkane

The chloroalkanes can be synthesized from aliphatic alcohols, and then transformed into aliphatic tertiary amines by amination.

$$ROH + HCl \xrightarrow[ZnCl_2\ Cat.]{110\sim150^\circ C} RCl + H_2O$$

$$RCl + NH(CH_3)_2 \xrightarrow[130\sim140^\circ C,\ 0.1\sim0.2MPa]{NaOH} RN(CH_3)_2 + NaCl + H_2O$$

The reaction mechanism is as follows[18]:

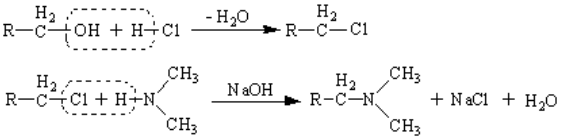

As an important way to produce alkyl dimethyl amine, this process consists of two reaction steps, giving a total yield of about 80%.

(e) Alcohol sulfation

Dodecyl dimethyl amine can be prepared by the reaction from sodium lauryl sulfate and dimethylamine.

$$C_{12}H_{25}OSO_3Na + NH(CH_3)_2 \xrightarrow[0.1\sim0.2MPa]{NaOH,\ 120\sim160^\circ C} C_{12}H_{25}N(CH_3)_2 + NaSO_4 + H_2O$$

The method is being used by Albright &Wilson in England, and by the Third Synthetic Detergent Factory of Shanghai. The purity of product is 95 %.

 DOI: 10.17628/ecb.2014.3.55-57

(f) Bromination of α-olefins

Aliphatic tertiary amines can be obtained through three successive steps: bromination of α-olefins, amination and decomposition of quaternary ammonium salts.

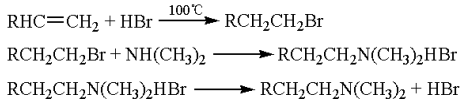

In China, the purity of the final product is *ca.* 98%, and the byproducts are mainly primary and secondary amines. The recycling of hydrogen bromide is still a problem to be solved.[20] Moreover, the shortage for α-olefin and the high level of byproducts limit its industrial use.[16]

(g) Amination of α-olefin epoxide

α-Olefins can be easily transformed into epoxide compounds by chorohydrin process. However, it is reported[23] that the chorohydrin method consumes much energy and chlorine, discharges large amount of wastewater containing calcium chloride, calcium hydroxide and organic chloride. In 1998, Drago[24] proposed the BAP (bicarbonate activated peroxide) system, in which the HCO_3^- was converted into HCO_4^- by H_2O_2. This observation led a new catalyst system for amination of olefins. The reaction mechanism：

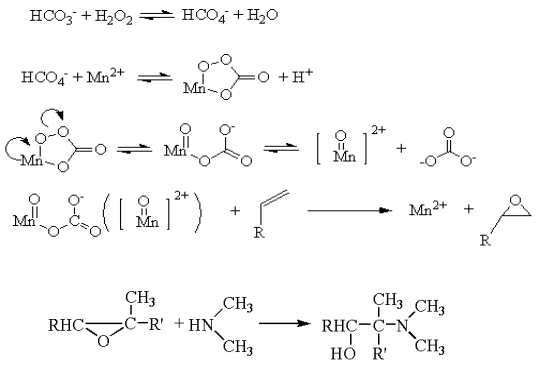

It will be a new route to prepare tertiary amine by dimethylamine and epoxide compound.

Summary

As shown in Figure 1, the primary amine and aliphatic alcohols are produced from natural grease, and the halides and epoxides are prepared by α-olefins using routes (f) and (g).

(1) The grease can been converted into primary amines through hydrolysis, cyanidation and hydrogenation process sequentially. Then the aliphatic tertiary amines can be obtained by route “a” or “b”. The whole technical process consists of too many reaction steps and the hydrolysis of grease is carried out at high temperature and high pressure (5.5MPa-6.5MPa). [21-22]

(2) The routes “c”, “d” and “e” are competitive for their mild conditions, good product quality and non-corrosive pollution. However, much higher purities are required for the raw materials (alcohol and methylamine).[15] For example, lauryl alcohol (dodecanol), used in route “c”, needs a purity of more than 99%, and is provided by Mitsubishi Corporation in China.[11]

(3) The route “f”, involving the recycling of hydrogen bromide is not practical in China. Although the productions of epoxide compounds by chorohydrination or with peroxyacid as oxidant in route (g) are not practical, yet the amination of α-olefin epoxides prepared with hydrogen peroxide is a meaningful route.

References

[1]Huang, H.Z. *Spec. Petrochem. (Tianjin, China)*, **1993**(4), 6.

[2]Zeng, G. S., Chen, G. and Chen, H. *Grease Chem.*, **2001**, *4*, 3.

[3]John Colling, D. R. *Daily Chem.l Ind. Inform.*, **2002**(11), 9.

[4]Zhang, B.H. *Deterg. Cosmet.*, **1996**(3), 2.

[5]Liu, Z. Q., Wang, Y. G. and Lian, G. B. *Fine Spec. Chem.*, **2007**, *15*(22), 4.

[6]Wang, J. H. *Hebei Chemicals*, **2006**(2), 2.

[7]Feng, Z. S. and Tang, X. F. *China Surfactant Deterg. Cosmet.*, **1988**, 1, (1), 5.

[8]Li, Q. X. *China Surfactant Deterg. Cosmet.*, **1999**, (2), 5.

[9]Li, Q. X., Xing, Y. Z., Wei, H. W., Li, M. and Hou, S. Z. *China Surfactant Deterg. Cosmet.*, **2002**, 32, (5), 3.

[10]Li, Q. X. and Zhang, G. Y. *China Surfactant Deterg. Cosmet.*, **2001**, (4), 5.

[11]Li, Q. X., Zhang, G. Y. and Peng, S. Y. Chin. J. Catal., **2001**, 22, (1), 4.

[12]Xing, Y. Z., Li, Q. X., Zhou, J. Y., Wei, H. W., Li, M. and Hou, S. Z. *Deterg. Cosmet.*, **2000**, 23, 3.

[13]Tan, P. and Li, Q. X. *Appl. Chem. Ind.*, **2003**, 32, (2), 3.

[14]Dong, G. X. *Vocational College Newspaper*, **2003**, 2, 4.

[15]Xu, B. C. *Chem. Ind. Eng.*, Beijing, **2007**, Vol, 2.

[16]Chang, Z. C. *Surfactant Industry*, **2000**, (1), 1-10.

[17]Lang, M. L. *Science Press*, Beijing, **1990**.

[18]Yao, M. Z., Cheng, L. B. and Wang, J. R. *China Petrochemical Press*, Beijing, **1994**.

[19]Jiang, Z. Y., Wang, X. E., Wang, Z. Y. and Ke, L. *Fine Chem.*, **1990**, 7, (4-5), 3.

[20]Zhang, B. H. *Shijiazhuang Chemical*, **1996**, 1, 3.

[21]Wang, H. *Food and Grease*, **2000**, (4), 2.

[22]Xin, Y. N. and Zhu, X. L. *China Oils*, **2002**, 27, (6), 3.

[23]Zhang, S. D. Xu, C. H. Feng, L. R. and Qiu, F. L. *Chin. J. Synth. Chem.*, **2003**, 11, (4), 6.

[24]Benjamin, S. L., Matthew, V., Victoria, J., DeRose, and Kevin, B. *JACS*, **2002**, (124), 9.

Received: 09.09.1013.
Accepted: 10.11.2013.

THE CORROSION INHIBITION OF ISONICOTINAMIDE (ISN) - Zn^{2+} SYSTEM CONTROLS THE CORROSION OF CARBON STEEL IN 1 M HYDROCHLORIC ACID SOLUTION

C. Rajarathinam[a], A. John Amalraj[b]*, C. Kumar[c], A. Peter Pascal Regis[a], Susai Rajendran[d,e], S. Maria Michael[f] and J. Wilson Sahayaraj[g]

Keywords: Corrosion, carbon steel, Isonicotinamide, synergistic effect.

The corrosion inhibition efficiency of Isonicotinamide (ISN) in controlling the corrosion of carbon steel in 1 M hydrochloric acid solution (HCl) in absence and presence of Zn^{2+} has been studied by weight loss method. Weight Loss study reveals that the formulation consisting of 10 ppm of ISN and 10 ppm of Zn^{2+} has 78% inhibition efficiency. The results of polarisation study shows that the formulation function controls the anodic reaction predominantly. The AC impedance spectra reveal that a protective film formed on the metal surface. FTIR spectrum reveal that the protective film consists of Fe^{2+}-ISN complex on the anodic sites of metal surface and $Zn(OH)_2$ formed on cathodic sites of metal surface.

* Corresponding Authors
Fax: 91-0431-2332010
E-Mail: amalrajevr@gmail.com
[a] PG and Research Department of Chemistry, St.Joseph's College (Autonomous), Trichy - 620002, Tamil Nadu, India.
[b] PG and Research Department of Chemistry, Periyar E.V.R college (Autonomous), Trichy - 620023, Tamil Nadu, India.
[c] Bharathiar Matric higher secondary school, Elumalai, Madurai - 625535, Tamil Nadu, India.
[d] PG and Research Department of Chemistry, GTN Arts College, Dindigul-624 005, Tamilnadu, India.
[e] Research Centre, RVS School of Engineering and Technology, Dindigul -624 005, Tamilnadu, India
[f] M/S. Light alloy products limited,Vellore distrct – 632505,Tamilnadu, India
[g] Department of Chemistry, Jeppiaar Engineering College, Chennai- 600119, Tamil Nadu, India.

INTRODUCTION

Corrosion is a natural phenomenon involving the reversion from metallic to compound state. So it becomes evident that corrosion cannot be fully prevented instead it can be controlled to a greater extent. Many researchers have used various nitrogen-containing compounds in their corrosion inhibition investigations. These compounds included quaternary ammonium salts,[1-7] polyamino-benzoquinone polymers,[8] azoles,[9-16] substituted aniline-N-salicylidenes,[17] amides,[18,19] heterocyclic compounds[20], and cationic surfactants.[21,22]

The present work is undertaken:

-To evaluate the influence of isonicotinamide (ISN) with Zn^{2+} on corrosion behavior of carbon steel immersed in 1 M HCl solution by weight-loss method.

-To evaluate the type of inhibitor by polarization study.

-To evaluate the protective film by AC impedance spectroscopic study.

-To analyze the nature of protective film formed on the carbon steel by FTIR spectra.

METHODS AND MATERIALS

Preparation of specimens

Carbon steel specimens (0.0267% sulphur, 0.06% phosphorous, 0.4% manganese, 0.1% carbon and the rest iron) of dimensions 1.0 cm x 4.0 cm x 0.2 cm were polished to a mirror finish and degreased with trichloroethylene.

Weight-loss method

Carbon steel specimens in triplicate were immersed in 100 ml of 1 M HCl solutions containing various concentrations of the inhibitor in the presence and absence of Zn^{2+} for one hour. The weight of the specimens before and after immersion was determined using Shimadzu balance, AY62 model. The corrosion products were cleansed with Clarke's solution.[23] From the change in weight of the specimens, corrosion rates were calculated with the help of the following relationship:

$$CR = \frac{\Delta m}{A * t} \quad (1)$$

where

CR - corrosion rate

Δm - loss in weight (mg)

A - surface area of the specimen (dm^2)

t - period of immersion (days)]

The inhibition efficiency (IE, %) was then calculated using the equation

$$IE = 100\left(1 - \frac{W_2}{W_1}\right) \quad (2)$$

where W_1 and W_2 are the corrosion rates in the absence and presence of the inhibitor, respectively.

Potentiodynamic polarization study

Polarization studies were carried out in an H & CH electrochemical work station impedance analyzer model CHI660A. A three electrode cell assembly was used. The working electrode was carbon steel. A saturated calomel electrode (SCE) was used as the reference electrode and a rectangular platinum foil was used as the counter electrode.

AC impedance study

The instrument used for polarization was also used for AC impedance study. The cell set up was the same as that used for polarization measurements. The real part and imaginary part of the cell impedance were measured in ohms at various frequencies. The values of charge transfer resistance(R_t) and the double layer capacitance(C_{d1}) were calculated.

Surface Examination

The carbon steel specimens were immersed in various test solutions for a period of one day, after one day the carbon steel specimen were taken out and dried.

The nature of the film formed on the surface of metal specimen was analysed by FTIR spectroscopic study.

FTIR Spectra

FTIR spectra were recorded in a Perkin-Elmer 1600 spectrophotometer. The film was carefully removed, mixed thoroughly with KBr made in to pellets and FTIR spectra were recorded.

RESULTS AND DISCUSSION

Analysis of results of weight loss method

The corrosion inhibition efficiency of carbon steel in the absence and presence of various concentrations of inhibitor obtained by the weight - loss method in one hour system are given in the Table 1 to 3.

The corrosion rates (*CR*) are also given in these tables.

The weight - loss method reveals that the isonicotinamide alone shows some inhibition efficiency at higher concentration. But Zn^{2+} alone is corrosive nature. For example 10 ppm of ISN alone is 12 inhibition effciency; 10 ppm of Zn^{2+} alone is corrosive nature. But it is interestingly noted that the formulation consisting of 10 ppm of ISN and 10 ppm of Zn^{2+} system shows 78% inhibition effciency.

This is due to the fact that there is synergistic effect exist between ISN and Zn^{2+} system. This means that the mixed inhibitors shows good inhibition efficiency than individuals.

Table 1. Corrosion rates (*CR*) of Carbon steel in 1 M HCl in the presence and absence of inhibitor and obtained by weight loss method

No	ISN, ppm	Zn^{2+}ppm	*IE*, %	*CR*, mdd
1	0	0	-	36.00
2	10	0	12	31.68
3	20	0	15	30.60
4	30	0	18	29.52
5	40	0	22	28.08
6	50	0	26	26.64
7	60	0	28	25.92

Table 2. Corrosion rates (*CR*) of Carbon steel in 1 M HCl in the presence and absence of inhibitor and obtained by weight loss method

S.No	ISN, ppm	Zn^{2+}, ppm	*IE*, %	*CR*, mdd
1	0	0	-	36.00
2	0	10	-8	38.88
3	0	20	-12	40.32
4	0	30	-14	41.04
5	0	40	-17	42.12
6	0	50	-17	42.12
7	0	60	-20	43.20

Analysis of potentiodynamic polarization study

The polarization curves of carbon steel immersed in ISN-HCl solution in the presence and absence of inhibitors are shown in Figure 1. The corrosion parameters are given in Table 4. When carbon steel immersed in isonicotinamide-1 M HCl solution, corrosion potential (E_{corr}) -664 mV vs SCE. The formulation consisting of 10 ppm of isonicotinamide and 10 ppm of Zn^{2+} shifts the corrosion potential to -565 mV vs SCE, ie corrosion potential shifts to anodic direction (from -664 mV to -565 mV). This suggest that the anodic reaction is controlled predominantly indicating the reduction resolution of metal as more isonicotinamide molecules are transported to the anodic sides in the presence Zn^{2+} ions.

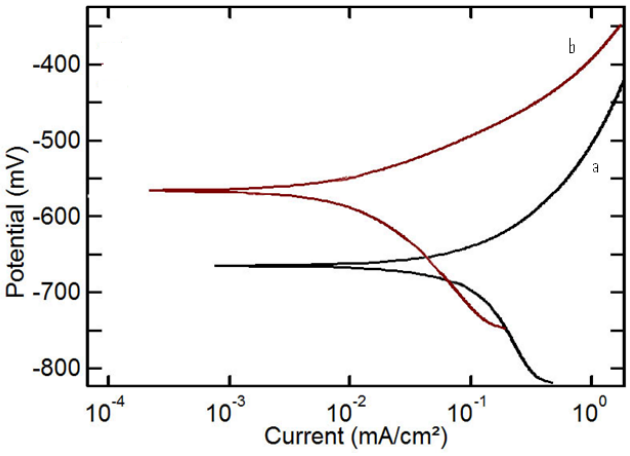

Figure 1. Polarization curves of carbon steel immersed in various test solution: a) 10 ppm of ISN + 1 M HCl; b) 10 ppm of ISN + Zn^{2+} 10 ppm +1 M HCl

Table 3. Corrosion rates (*CR*) of Carbon steel in 1 M HCl in the presence and absence of inhibitor and obtained by weight loss method

S.No	ISN, ppm	Zn^{2+}, ppm	*IE*, %	*CR*, mdd
1	0	0	-	36.00
2	10	10	78	7.92
3	10	20	64	12.96
4	10	30	35	23.40
5	10	40	24	27.36
6	10	50	20	28.80
7	10	60	12	31.68

Now the shifts in the anodic cathodic slopes can be compared. The addition of 10 ppm of Zn^{2+} shifts the anodic slope value 64 mV $decade^{-1}$ to 56 mV $decade^{-1}$, will the corresponding shift cathodic slope is from 91 mV $decade^{-1}$ to 106 mV $decade^{-1}$. Thus formulation of 10 ppm of isonicotinamide and 10 ppm of Zn^{2+} controls the anodic predominately and to some extent controls the cathodic reaction by the formation $Zn(OH)_2$ and cathodic sides of the metal surface.

The corrosion current (I_{corr}) for isonicotinamide is 0.04343 A cm^{-2}. It is defused to 0.007224 A cm^{-2} by the addition 10 ppm of Zn^{2+}. The current of the iron dissolution is decreased significantly indicating that the metal surface was passive by the formed inhibitor layer. The passivity ion is probably due to the formation of isonicotinamide – Fe^{2+} surface layer. The significant reduction in corrosion current for inhibitor formulation may indicate more adsorption of the inhibitors and better inhibitions performance. This result suggests that a protective film (isonicotinamide – Fe^{2+}-complex) is formed on the metal surface. This protects the metal from corrosion.

Table 4 : Corrosion parameters of carbon steel immersed in various test solution obtained by polarization method.

System	E_{corr}, mV vs SCE	b_c,	b_a,	I_{corr},
		mV $decade^{-1}$		A cm^{-2}
10 ppm of ISN + 1 M HCl	-664	64	91	0.04343
10 ppm of ISN + 10 ppm of Zn^{2+} + 1 M HCl	-565	56	106	0.007224

Analysis of AC impedance spectra

The AC Impedance spectra of carbon steel immersed in various test solution are shown in Figure 2. The AC impedance parameters, namely the charge transfer resistance (R_t) and the double layer capacitance (C_{dl}) are given in Table 5.

Impedance parameters for corrosion of carbon steel immersed in 1 M HCl in the presence and absence of inhibitor system obtained from AC impedance curves.

Table 5. Corrosion parameters of carbon steel immersed in various test solution obtained by AC impedance spectra.

S.No.	System	R_t, Ω cm^2	C_{dl}, F cm^{-2}
1.	ISN 10 ppm + 1 M HCl	0.675	6.980 x 10^{-4}
2.	ISN 10 ppm+ Zn^{2+} 10 ppm + 1 M HCl	1.24	2.375 x 10^{-4}

AC Impedance parameters namely a charged transfer resistance (R_t) and the double layer capacitance(C_{dl}) are given in Table 5. When carbon steel immersed in 10 ppm of isonicotinamide and 1 M HCl, the R_t value is found to be 0.675 Ω cm^2 and C_{dl} value is 6.980 x 10^{-4} F cm^{-2}. When 10 ppm of Zn^{2+} is added to the above system, the R_t value increases from 0.675 Ω cm^2 to 1.24 Ω cm^2 and C_{dl} value decreases from 6.980 x 10^{-4} F cm^{-2} to 2.375 x 10^{-4} F cm^{-2}. The increased R_t values and decreased double layer capacitance value obtained from impedance studies justify the good performance of ISN as an inhibitor in 1 M HCl. This behavior source that the protective film obtained act as a barrier to the corrosion process that clearly existence and formation of the protective film on the metallic surface.[24,25]

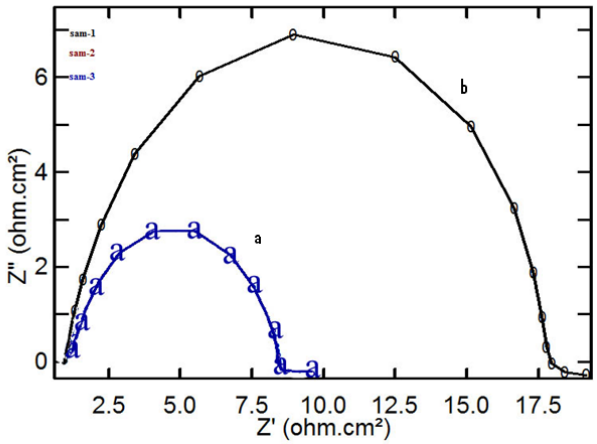

Figure 2. AC impedance spectra of carbon steel immersed in various test solution, a) 10 ppm of ISN + 1 M HCl, b) 10 ppm of ISN + Zn^{2+} 10 ppm + 1 M HCl

Surface analysis

The structure of isonicotinamide is shown in Scheme 1.

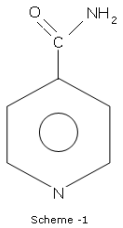

Scheme -1

It contains C=O group, C-N group and N-H Stretching vibrations group.The protective film formed on the surface of the metal in the presence of isonicotinamide system and isonicotinamide – Zn^{2+} system in 1 M HCl has been analysed by FTIR spectroscopy.

 DOI: 10.17628/ECB.2014.3.58-62

Analysis of FTIR spectra

The FTIR spectrum (KBr) of pure isonicotinamide is shown in figure 3a. C=O stretching frequency appears at 1682 cm^{-1}. The C-N stretching frequency appears at 1121 cm^{-1} The N-H stretching frequency appears at 3362 cm^{-1}. The FTIR spectrum (KBr) of the film formed on the surface of the metal after immersion, the solution containing 10 ppm of isonicotinamide and 10 ppm Zn^{2+} in 1 M HCl is shown in figure 3b. It is found that C=O stretching frequency of isonicotinamide decreased from 1682 cm^{-1} to 1617 cm^{-1}. The C-N stretching frequency of isonicotinamide has decreased from 1121 cm^{-1} to 1018 cm^{-1}. The N-H stretching frequency of isonicotinamide has decreased from 3362 cm^{-1} to 3359 cm^{-1}.

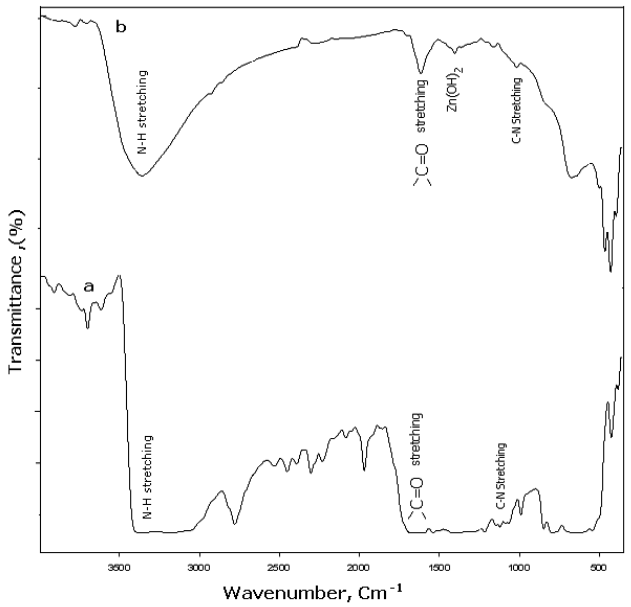

Figure 3. FTIR spectra; a) Pure solid Isonicotinamide; b) Film formed on the metal surface after the immersion of the solution of 10 ppm of Isonicotinamide and 10 ppm Zn^{2+} in 1 M HCl

It is interfered that isonicotinamide has coordinated with Fe^{2+} oxygen atom and nitrogen atom resulting in the formation of Fe^{2+}- ISN complex on the anode sites of the metal surface.[26,27] The bond at 1401 cm^{-1} is due to $Zn(OH)_2$ formed on the cathodic sites of the metal surface.

CORROSION INHIBITION MECHANISM FOR (ISN- Zn^{2+}) SYSTEM

The weight – loss study reveals that the formulation consisting of 10 ppm of Zn^{2+} and 10 ppm of isonicotinamide has 78% inhibition efficiency. The FTIR spectrum reveals that the protective film consist of Fe^{2+} - isonicotinamide complex and $Zn(OH)_2$. In order to explain the above observations, the following mechanism of corrosion inhibition is proposed.[28-34]

When the environment consisting of 10 ppm of Zn^{2+} and 10 ppm of isonicotinamide are prepared, there is a formation of Zn^{2+} - ISN complex.

When carbon steel is introduced in this solution there is diffusion of Zinc complex towards the metal surface.

On the metal surface zinc complex is converted into iron complex on the anodic site.

$$Zn^{2}\text{- ISN+ } Fe^{2+} \rightarrow Fe^{2+}\text{-ISN+ } Zn^{2+}$$

The released Zn^{2+} combined with OH^- to form $Zn(OH)_2$ on the cathodic sites.

$$Zn^{2+} + 2OH^- \rightarrow Zn(OH)_2\downarrow$$

Thus, the protective film consists of Fe^{2+}-ISN and $Zn(OH)_2$.

CONCLUSION

The weight – loss study reveals that the formulation consisting of 10 ppm of Zn^{2+} and 10 ppm of isonicotinamide has 78% inhibition efficiency. Synergistic effect exists between isonicotinamide and Zn^{2+} system.

The results of polarization study suggest that the formulation of 10 ppm of ISN and 10 ppm of Zn^{2+} system controls the anodic reaction predominantly.

The AC impedance spectral studies reveal that the protective film obtained act as a barrier to the corrosion process that clearly existence and formation of the protective film on the metallic surface.

The protective film consists of Fe^{2+} - ISN and $Zn(OH)_2$ by FTIR spectroscopy.

ACKNOWLEDGEMENT

The authors are thankful to their respective managements for their help and constant encouragement.

REFERENCE

[1]Beloglazov, S. M., Dzhafarov, Z. I., Polyakov, V. N. and Demushia, N. N., *Prot. Met,,***1991**, *27*, 810.

[2]Nahl´e, A. H, *Corros. Prevent. Control*, **1997**, *44*, 99.

[3]Nahl´e, A. H, *Corros. Prevent. Control*, **1998**, *45*, 124.

[4]Nahl´e, A. H, *Bull. Electrochem.*, **2002**, *18*, 105.

[5]Nahl'e, A. H. and Walsh, F. C., *Corros. Prevent. Control*, **1995**, *42*, 30.

[6]Savithri, B. V. and Mayanna, S. M., *Indian J. Chem. Technol.*, **1996,** *3*, 256.

[7]Vasudevan, T., Muralidharan, S., Alwarappan, S. and Iyer, S.V.K., *Corros. Sci.*, **1995**, *37*, 1235.

[8]Muralidharan, S., Phani, K. L. N., Pitchumani, S., Ravichandran, S. and Iyer, S. V. K., *J. Electrochem. Soc.*, **1995**, *142*, 1478.

[9]Benali, O., Larabi, L., Traisnel, M., Gengembre, L. and Harek, Y., *Appl. Surf. Sci.*, **2007**, *253*, 6130.

[10]Ashry, E. S. H. E., Nemr, A. E., Essawy, S. A. and Ragab, S., *Prog. Org.Coat.*, **2008**, *61*, 11.

[11]Khaled, K. F., *Electrochim. Acta*, **2003**, *48*, 2493.

[12]Popova, A., *Corros. Sci.*, **2007**, *49*, 2144.

[13]Popova, A., Christov, M., Raicheva, S. and Sokolova, E., *Corros. Sci.*, **2004**, *46*, 1333.

[14]Popova, A., Christov, M., Zwetanova, A., *Corros. Sci.*, **2007**, *49*, 2131.

[15]Sastri, V. S., Perumareddi, J. R., Lashgari, M. and Elboujdaini, M., *Corros.*, **2008**, *64*, 283.

[16]Tebbji, K., Aouniti, A. and Attayibat, A., *Indian J. Chem. Technol.*,**2011**, *18*, 244.

[17]Talati, J. D., Desai, M. N., Shah, N. K., *Mater. Chem. Phys.*, **2005**, *93*, 54.

[18]Tuken, T., Yazici, B. and Erbil, M., *Turk. J. Chem.*, **2002**, *26*, 735.

[19]Fattah, A. A., Mabrouk, E. M.and Elgalil, R. M. A., Ghoneim, M. M., *Bull. Soc .Chim. Fr.*,**1991**, *1*, 48.

[20]Granese, S. L., Rosales, B. M., Oviedo, C., Zerbino, J.O., *Corros. Sci.*, **1992**, *33*, 1439.

[21]Al-Lohedan, H. A., Khamis, E.and Issa, Z. A., *Adsorp. Sci. Technol.*, **1996**, *13*,137.

[22]Qiu, L. G., Xie, A. J.and Shen, Y. H., *Mater. Chem. Phys.*, **2005**, *91*, 269.

[23]Wranglen, G., *Introduction to Corrosion and Protection of Metals(London, U.K:Chapman and Hall)*, **1985**, 236.

[24]Kannan, P., Lavanya, K.and Natesan, M., *Res. J. Chem. Sci.*, **2012**, *2*, 50.

[25]Wilson sahayaraj, J., John Amalraj, A., Susai Rajendran and Vijaya, N., *J. Chem.*, **2012**, *9*, 1746.

[26]Nakamoto, K., *'Infrared and Raman Spectra of Inorganic and Coordination Compounds', Wiley and Sons, New York, 4th edition*, **1986**, 95.

[27]Silverstein, R. M., Bassler, G. C.and Morril, T.C., *Spectrometric Identification of Organic compounds*, John Wiley and Sons, New York , **1986**, 72.

[28]Wilson sahayaraj, J., John Amalraj, A., Susai Rajendran and Muthumegala, T.S., *Zastit. Mater.*, **2010**, *51*, 231.

[29]Kavipriya, K., Sathiyabama, J., Rajendran, S.and Nagalakshmi, R., *Eur. Chem. Bull.*, **2013,** *2(7)*, 423.

[30]Sribharathy, V., Susai Rajendran, Rengan, P.and Nagalakshmi, R *Eur. Chem. Bull.*,**2013**, *2(7)*, 471.

[31]Gowri, S., Sathiyabama, J., Rajendran, S., Angelin Thangakani, J., *Eur. Chem. Bull.*,**2013**, *2(6)*, 355.

[32]John Amalraj, A., Wilson Sahayaraj, J.,Kumar, C., Susai Rajendran, Peter Pascal Regis, A., Selvaraj, S. K. and Mohan, R., *Eur. Chem. Bull.*,**2013**, *2(6)*, 315.

[33]Angelin Thangakani, J., Rajendran, S.,Sathiyabama, J., Lydia Christy, J., Suriya Prabha, A. and Pandiarajan, M., *Eur. Chem. Bull.*,**2013**, *1(5*), 265.

[34]Gowri, S., Sathiyabama, J., Prabhakar, P. and Rajendran, S., *Int. J. Res.Chem. Environ.*, **2012**, *3(1)*, 156.

Received: 18.09.2013.
Accepted: 10.11.2013.

SYNTHESIS OF COUMARIN DERIVATIVES: A GREEN PROCESS

Reshu Chaudhary[a] and Monika Datta[a]*

Keywords: coumarin, solvent free condition; heteropoly acids, bentonite

Coumarins are an important class of organic compounds having biological activities. In the present work coumarin derivatives have been synthesized under solvent free conditions from substituted phenols and ethyl acetoacetate in the presence of catalysts. A catalyst based on clay and heteropoly acid has been synthesized and found to be a potential catalyst for synthesis of coumarin derivatives.

Corresponding Authors
Tel: +919811487825
E-Mail: monikadatta_chem@yahoo.co.in
[a] Department of Chemistry, University of Delhi, Delhi-110007

Introduction

Coumarins are an important class of compounds because a large number of natural product contains this heterocyclic nucleus. They have a wide variety of biological activities i.e. fluorescence sensors,[1] brightening agents,[2] anticoagulants,[3] insecticides[4] etc. coumarins can also be synthesized and the method should be simple, efficient and cheap because of diverse biological activities. There are many ways of synthesizing the coumarin such as knoevengel condensation [5], claisen rearrangement,[6] Perkin reaction,[7] pechmann reaction[8] etc. using a wide variety of reagents like H_2SO_4,[9] $HClO_4$,[10] P_2O_5,[11] ionic liquids[12] and solid acid[13,14] catalysts. Most of the reports are on the synthesis of coumarin derivatives having electron releasing groups and these methods also have the disadvantage of long reaction time and low yield.[15,16]

Using our methodology i.e. phosphotungstic acid (a heteropoly acid) intercalated bentonite coumarin derivatives having electron withdrawing groups can be synthesized with high efficiency and yield in a very short time.

Heteropoly acids are very well known solid acid catalysts. Heteropolyacids (HPAs), also known as polyoxometalates (POMs), are early-transition-metal oxygen anion clusters that exhibit very interesting properties depending on their molecular size, composition, and architecture.[17-19] They are stronger acids than conventional acid catalysts. Being stronger acids, heteropoly acids will have significantly higher catalytic activity than conventional catalysts such as mineral acids, mixed-oxides, zeolites, etc. Their excellent thermal stability[20] also makes HPAs good candidates for application in catalysts and sensors that may require extreme environments. In particular, in organic media, the molar catalytic activity of heteropoly acid is often 100–1000 times higher than that of H_2SO_4.[21-23]. This makes it possible to carry out the catalytic process at a lower catalyst concentration and/or at a lower temperature. Further, heteropoly acid catalysis lacks side reactions. Moreover solid acids offer many advantages by their nature, over soluble counterparts such as aluminium chloride and hydrogen fluoride. The substitution of liquid acids by solids as catalysts for organic synthesis offers a potential for superior effectiveness and environmental integrity. Although they differ in structure from liquid acids, solid acid catalysts work by the same principle. Clays have also been proposed as suitable catalysts for this purpose.[24-26] Today clays are important materials with a large variety of applications such as adsorbents, decoloration agents, ion exchangers, and catalysts.[27] The use of clays, as heterogeneous catalysts, offers many advantages over homogeneous acid catalysts such as ease of separation, mild reaction conditions, better selectivity of the desired product, and elimination of waste disposal problems. In a large number of organic reactions clays have been used as catalysts on laboratory/industrial scales. Properties of clays can be further improved by making pillared clays. Pillared clays are clays with high permanent porosity obtained by separating the clay sheets by a molecular prop or pillaring agent. These pillaring agents can be organic, organometallic, or inorganic complexes. Pillared clay (PILC) possesses several interesting properties, such as large surface area, high pore volume and tunable pore size (from micropore to mesopore), high thermal stability, strong surface acidity and catalytic active substrates/metal oxide pillars. These unique characteristics make PILC an attractive material in catalytic reactions. It can be made either as catalyst support or directly used as catalyst.[28-30]

In the present work we have synthesized the coumarin derivatives using phosphotungstic acid intercalated Bentonite via pechmann condensation of phenols with ethyl acetoacetate using microwave irradiation in excellent yield and high purity.

Experimental

Catalyst preparation

Na-Bentonite. 1.0 g of bentonite clay was added into a 250 ml conical flask containing 50 ml of 1.0 M NaCl this clay suspension was stirred for 16 hours. The residue after centrifugation was washed several times with double distilled water till complete removal of chloride ions. The residue thus obtained after above procedure was dried in an oven at 100°C to generate the Na form of the Bentonite (Na-Ben).

Table 1. Effect of the amount of catalyst on the reaction efficiency

S. No.	Catalyst, mg	Time, s.	Yield of 4-methyl-6-hydroxy coumarin with various catalysts, in %					
			Ben	Al-Ben$_2$	H^+-Ben	PAAC-Ben$_2$	PTA	PTA-Ben
1	20	60	33	46	50	55	56	72
2	30	60	40	52	57	62	64	80
3	40	60	50	62	67	72	74	90
4	50	60	58	70	74	78	80	99
5	60	60	58	70	74	78	80	99

Al-Pillared Bentonite (Al-Ben). In a 250 ml conical flask containing 1.0 g of Na-Ben, in 100 ml of double distilled water, 50 ml of the pillaring solution (keggin ion) was gradually added with vigorous stirring for 16 hours. The residue was washed several times with double distilled water till the complete removal of chloride ions was confirmed by $AgNO_3$ test. The residue, thus obtained was dried in an oven at 100°C is referred to as Al-Pillared Bentonite (Al-Ben).[31]

Acid activated Bentonite (H^+-Ben). 5.0 g of Na-Ben was added into a 100 ml beaker containing 50 ml of 3N H_2SO_4, this mixture was exposed to microwave radiation for 30 minutes. The residue was washed several times with double distilled water till the complete removal of SO_4^{2-} ions was confirmed by $BaCl_2$ test. The residue thus obtained was dried in an oven at 100°C to generate the Acid activated Bentonite (H^+-Ben).[32]

Pillared Acid activated Bentonite (PAA-Ben). 1.0 g of H^+ Ben, was added into a 250 ml conical flask containing 100 ml of double distilled water. 50ml of pillaring solution was gradually added with vigorous stirring for 16 hours. The residue was washed several times with double distilled water till the complete removal of chloride ions was confirmed by $AgNO_3$ test. The residue thus obtained was dried in an oven at 100°C and is referred to as Pillared Acid Activated Bentonite (PAA-Ben).

Phosphotungstic intercalated Bentonite (PTA –Ben). In a round bottom flask (250 ml), bentonite (1g) was suspended in double distilled water (50 ml).To this, aqueous solution of 15 mmol % of phosphomolybdic acid (PTA) was added drop wise and then stirred for 16 hrs. After this, the mixture was filtered and washed with double distilled water to remove the excess of Phosphomolybdic acid. Dried the product at 100 ^{0}C.

General procedure for the synthesis of coumarin derivatives

To elucidate the catalytic efficiency of PTA-Ben as catalyst, a controlled reaction was carried out using PTA, bentonite, Al-Ben and PTA-Ben as catalyst with Benzene-1,4-diol as reactant. The best results were obtained with PTA-Ben in microwave. (Table 1).

Under microwave condition: phenols derivatives (10mmol) and ethyl acetoacetate (10 mmol) were mixed with the PTA-Ben (50 mg) (Table 3). The mixture was irradiated in the microwave. After irradiation of the mixture for a specified period, the content was cooled to room temperature. The completion of the reaction was checked by TLC. After the completion of the reaction the catalyst was recovered by filtration and washed with absolute ethanol to remove all the organic impurities. The PTA-Ben was reused for evaluating the performance in the next reaction. The extract was evaporated by rota-vapour under reduced pressure and the product was purified from column chromatography with $CHCl_3$: MeOH with increasing polarity.

Optimization of the Catalysts amount

Reactions have been performed using different amount of various catalysts under uniform conditions. Results of the investigation are presented in the Table 1.

Optimization of Time

The reaction time has been optimized by performing reactions at regular intervals of time. After a certain time period there is not much increase in the yield. That time has been selected as optimum time. Results of the investigation are presented in the Table 2.

Table 2. Optimization of reaction time

S.No.	Time, s	Yield, %
01	15	65
02	30	80
03	45	90
04	60	99
05	75	99
06	90	99

Results and discussion

Catalyst characterization

X-Ray Diffraction techniques. The XRD pattern of Ben,[33] Na-Ben and H^+-Ben show a sharp peak at 2θ = 5.93, 6.83 and 9.67 respectively corresponding to a d-value of 14.9 Å, 12.9 Å and 9.1 Å. A decrease in the *d*-value of 2 Å and 5.8 Å is observed when interlayer cations (Ca^{2+}) are replaced by the smaller ions, Na^+ and H^+ respectively. PAA-Ben, shows a further shift in the peak position, 2θ =5.30 and a *d*-value of 16.6 Å corresponding to an increase in the interlayer region by 7.5 Å w.r.t H^+-Ben confirms the intercalation of Al Keggin ion into the interlayer region of H^+-Ben.

 DOI: 10.17628/ECB.2014.3.63-69

Table 3. Efficiency of the catalyst (PTA-Ben) for different reactants

S. No.	Reactant	Product	Time, Sec.	Yield, %	Remarks
01	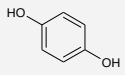	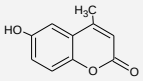	60	99	Single product
02		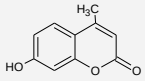	90	98	Single product
03	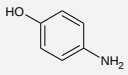	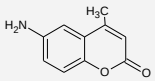	120	95	Single product
04		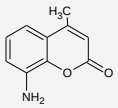	120	92	Single product
05	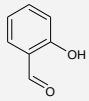	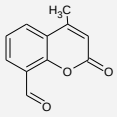	300	83	Single product
06	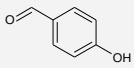	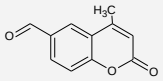	300	87	Single product
07	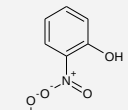	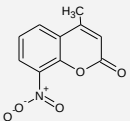	360	76	Single product
08	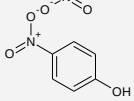	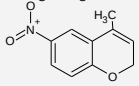	360	80	Single product
09		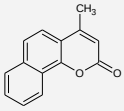	420	72	Single product
10	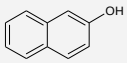	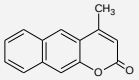	420	75	Single product

The Al-Ben shows a peak at 2θ = 5.20 and a *d*-value of 16.9 Å corresponding to an increase in the d-value of 4 Å w.r.t Na-Ben thus confirming the intercalation of Al Keggin ion in the interlayer region of Na-Ben. PTA-Ben show a peak at 2θ = 5.42 corresponding to a d-value of 16.3 Å respectively. This increase in the *d*-value 3.4 Å w.r.t Na-Ben confirms the intercalation of PTA in the interlayer region of Na-Ben.

Total Surface Area Measurement. Total surface area studies have been performed by EGME method. Surface area values of Ben, Na-Ben, H^+-Ben, Al-Ben, PAAC- Ben and PTA-Ben are represented in the (Table 4). Total surface area of Ben has been found to be 215 m^2 g^{-1}. After conversion to Na-Ben total surface area has been found to be 121 m^2/g which may be due to the decrease in d-spacing as indicated by XRD data. Total surface area of H^+- Ben has been found to be 327 m^2 g^{-1} which is due to replacement of Na ions by H^+ ions. Acid activation also causes the formation of small pores, consequently increasing the surface area.[34,35] Total surface area of Al-Ben has been found to be 295 m^2/g. Due to the intercalation of Al-Keggin ion the inner surface also becomes assessable. PAAC-Ben has been found to have a total surface area of 350 m^2/g which is again due to intercalation of Al-Keggin ion in H^+-Ben. Total surface area of PTA-Ben has been found to be 301 m^2/ g respectively which confirms intercalation of PTA

FT-IR Studies. Vibrational spectra of Ben, Na-Ben, H^+-Ben, Al-Ben and PAA-Ben clays (Figure 1 and 2) indicate two strong absorption bands ~3626 cm^{-1} and ~3436 cm^{-1} corresponding to the stretching vibrations of the O-H group originating from the surface adsorbed and interlayer water. The ~1642 cm^{-1} band in these samples has been assigned to the H–O–H bending vibrations of water.

 DOI: 10.17628/ECB.2014.3.63-69

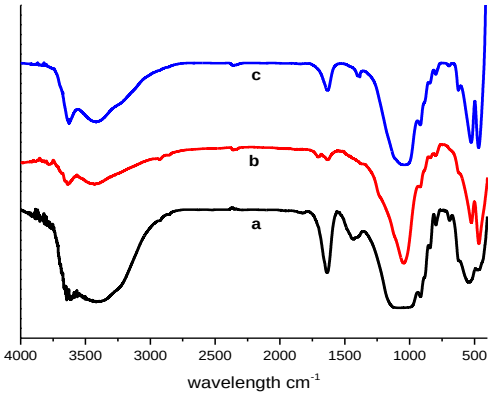

Figure 1. FTIR spectra of (a) Ben, (b) Na-Ben, (c) H^+-Ben

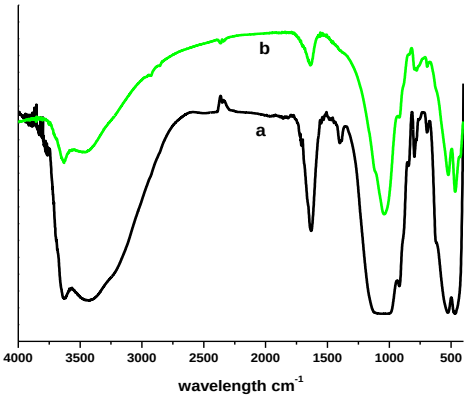

Figure 2. FTIR spectra of (a) Al-Ben, (b) PAA-Ben

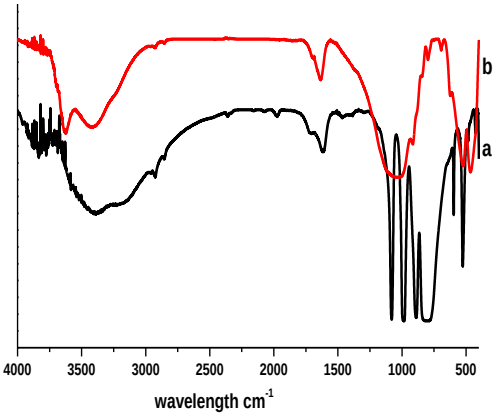

Figure 3. FTIR spectra of (a) PTA, (b) PTA-Ben

The ~1043 cm^{-1} and ~796 cm^{-1} bands are attributed to the stretching vibration of the Si-O bond. The ~522 cm^{-1} and ~466 cm^{-1} bands have been assigned to the Si–O–Al and Si–O–Si deformation vibrations respectively[36,37].The FT-IR spectra of PTA (Figure 3) shows an absorption band at ~3154 cm^{-1} and have been assigned to the stretching vibrations originating from the O-H groups present in the Keggin structure of PTA. The absorption band at ~1699 cm^{-1} have been assigned to the bending vibrations of the O-H group of PTA.

Thermal Method of Analysis. The thermogram (TGA) of Ben, Na-Ben, H^+-Ben (Figure 4) shows four step weight loss pattern. The first step, up to 180^0C, corresponds to dehydration of surface adsorbed water. The second step, 180 °C to 550 °C, is attributed to dehydration of interlayer water. The third step 550 °C to 675 °C, is attributed to the gradual dehydroxylation of clay layers. Beyond 675 °C the clay loses its structure and practically shows no weight loss.[36]

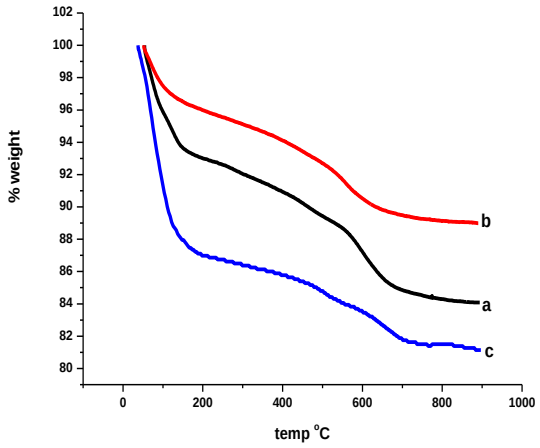

Figure 4. TGA studies of (a) Ben, (b) Na-Ben, (c) H^+-Ben

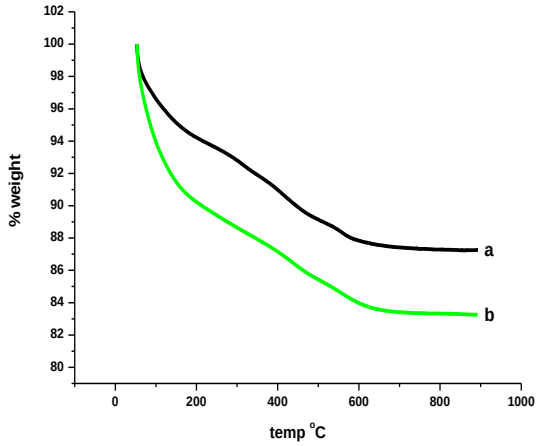

Figure 5. TGA studies of (a) Al-Ben, (b) PAA-Ben

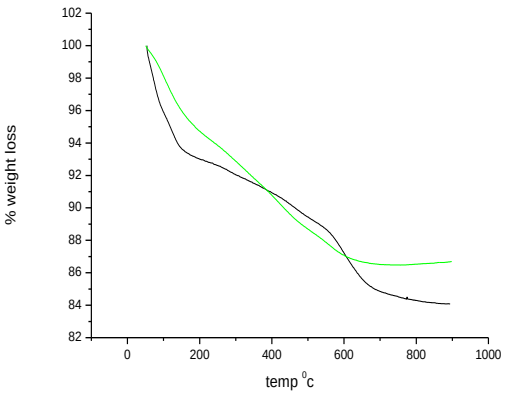

Figure 6. TG-MS curves of (a) PTA, (b) PTA-Ben

 DOI: 10.17628/ECB.2014.3.63-69

The thermogram (TGA) of PAA-Ben, Al-Ben (Figure 5) shows a similar four step weight loss pattern. The first step, up to 200^{0}C, corresponds to dehydration of surface adsorbed water. The second step, 200^{0}C to 350^{0}C, is attributed to dehydration of interlayer water. The third step, 350^{0}C to 600^{0}C, is attributed to the gradual dehydroxylation of clay layers. Beyond 600^{0}C the clay loses its structure and practically shows no weight loss.[36]

The TGA of pure PTA (Figure 6) shows two step weight loss. The first step, up to 200^{0}C corresponds to the loss of water of crystallization. The second step, ~200^{0}C to 600^{0}C corresponding to the decomposition of keggin unit of PTA.

The TGA of PTA-Ben (Figure 6) shows four step weight loss pattern, the first step, up to 150^{0}C, corresponds to dehydration of surface water. The second step, 150^{0}C to 500^{0}C, is attributed to dehydration of interlayer water. The third step, 500^{0}C to 700^{0}C, is attributed to the dehydroxylation of clay layers and the loss of keggin ion structure. The heteropoly acids are stable up to 600^{0}C but after intercalation the catalyst becomes stable up to 800^{0}C.

SEM Studies with EDX analysis. The SEM pictures (magnification of 832X) of Ben, PTA-Ben are represented in Figure 7 a and b respectively. The SEM pictures of Ben and PTA-Ben show no distinct change in the surface morphology and appears to have the layered structure. Therefore, it appears that PTA is not adsorbed on the surface of the clay but is intercalated in the layers of the clay. This fact is also supported by the XRD and IR studies.

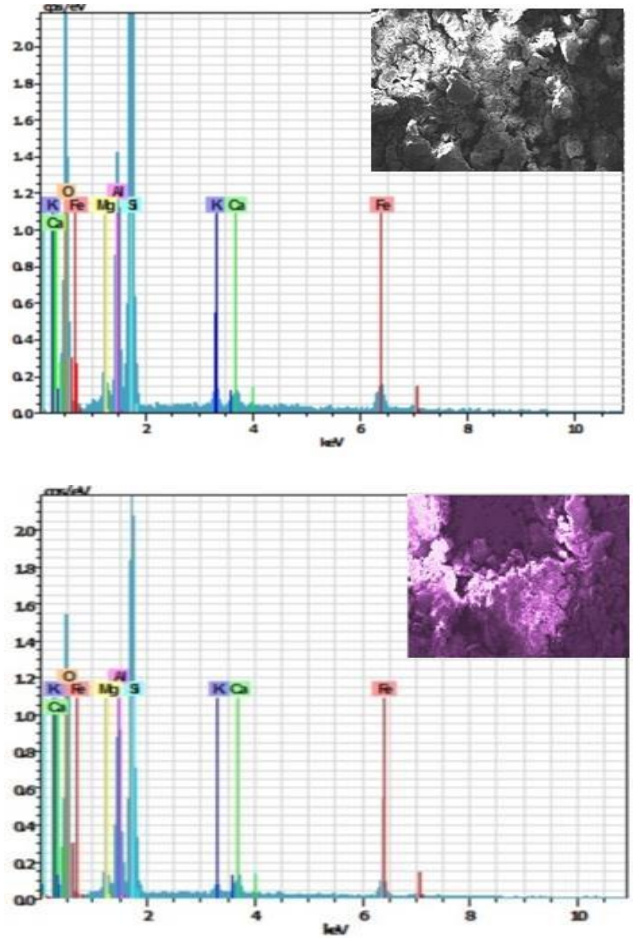

Figure 7. SEM-EDX of (a) Ben, (b) PTA-Ben

The SEM results are also supported by the EDX analysis (Figure 7a and 7b). In all the cases surface composition consist of Al, Si, O, Mg, Fe, Ca & K. No signal corresponding to P and W was supported by the EDX data which further confirms intercalation of PTA in to the layers of Bentonite.

Reusability of PTA-Ben for the Synthesis of 6-OH-4-Me-coumarin

The reusability of PTA-Ben has been investigated up to six repeated cycles using synthesis of 6-OH-4-Me-Coumarin. The catalyst, PTA-Ben, was washed with MeOH after every cycle and was characterized using FT-IR, TGA, DSC, XRD, SEM and EDX etc. techniques. No noticeable changes were observed even after six cycles, which not only indicates the stability of the catalyst but also indicates that none of the reactants/products remain with the catalyst. The product/s, after separation and isolation, was characterized by the earlier described methods and the yield in each case was calculated (Figure 8). The variation in the yield was found to be in the range of ~ 99% to 75%.

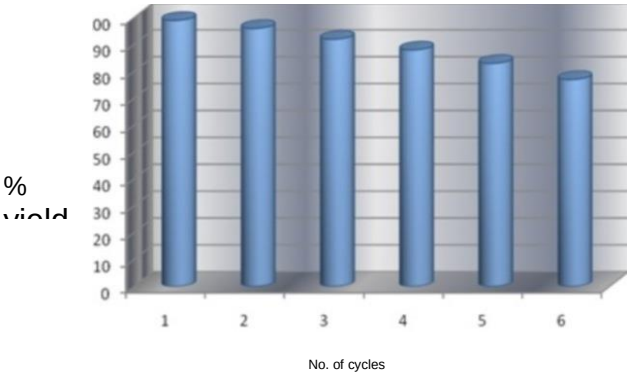

Figure 8. Reusability of PTA-Ben up to 6 repeated cycles

The catalyst characterization was performed on the catalyst after the 6th cycle of reaction was performed on the catalyst and following observations was made. The SEM picture (Figure 9) does not show any change in the surface morphology, the layered structure is maintained. The EDX data indicates the same elemental composition as earlier, i.e. Al, Si, O, Mg, Fe, Ca, K and Na.

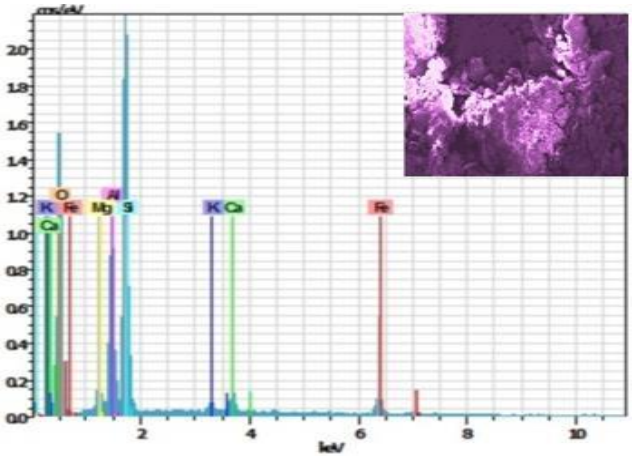

Figure 9. SEM and EDX of PTA-Ben after 6th cycle

 DOI: 10.17628/ECB.2014.3.63-69

The thermal stability of the catalyst was found to be unaffected after reuse except a slight change in the weight loss (from 11.7 % to 14%) which may be due to the presence of small quantity of adsorbed organic matter after the 6th cycle (Figure 10).

XRD and FTIR data (Figure 11) of PTA-Ben has been found to have no significant change.

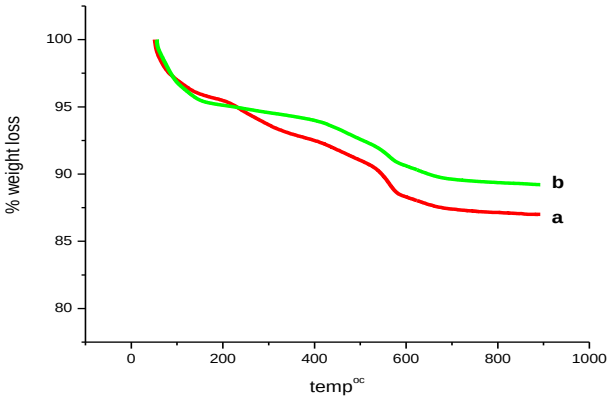

Figure 10. TGA studies of (a) PTA-Ben after 1st cycle, (c) PTA-Ben after 6th cycle

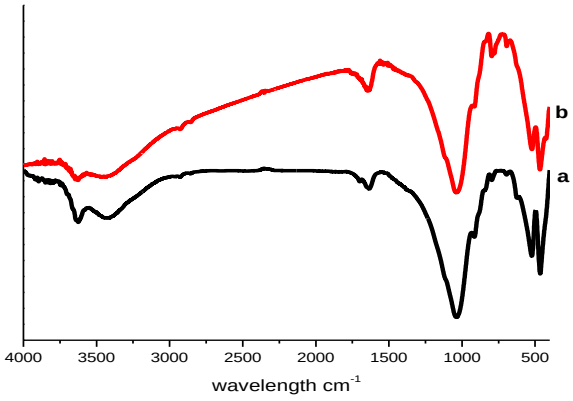

Figure 11. FTIR spectra of (a) PTA-Ben after 1st cycle, (c) PTA-Ben after 6th cycle

Characterization of coumarine derivatives

Structural assignments of the various coumarin derivatives are based on their ^{1}H NMR and IR analysis. The analysis of complete spectral and compositional data revealed the formation of coumarin derivatives.

6-Hydroxy-4-methylcoumarin. IR (υ in cm^{-1}) 3258 (OH strech), 1516, 1473 (aromatic ring), 1689 (C=O), 1209, 1096 (C-O); ^{1}H NMR δ 9.4 (s, 1H, OH), 7.5 (d, 1H, H $_{8\ Aromatic}$), 6.8 (d, 1H, H $_{7\ Aromatic}$), 6.2 (s, 1H, H $_{5\ Aromatic}$), 3.0 (s, 1H, H $_{3\ Aromatic}$), 2.2 (s, 3H, CH_3).

7-Hydroxy-4-methylcoumarin. IR (υ in cm^{-1}) 3502 (OH strech), 1504, 1455 (aromatic ring), 1671 (C=O), 1277, 1074 (C-O); ^{1}H NMR δ 10.5 (s, 1H, OH), 7.5 (s, 1H, H $_{8\ Aromatic}$), 6.8 (d, 1H, H $_{6\ Aromatic}$), 6.6 (d, 1H, H $_{5\ Aromatic}$), 3.4 (s, 1H, H $_{3\ Aromatic}$), 2.3 (s, 3H, CH_3).

6-Amino-4-methylcoumarin. IR (υ in cm^{-1}) 3376, 3234 (NH strech), 1610, 1512, 1493 (aromatic ring), 1636 (C=O), 1286, 1170 (C-O); ^{1}H NMR δ 10.1 (s, 2H, NH), 8.3 (d, 1H, H $_{8\ Aromatic}$), 8.1 (d, 1H, H $_{7\ Aromatic}$), 7.2 (s, 1H, H $_{5\ Aromatic}$), 3.4 (s, 1H, H $_{3\ Aromatic}$), 2.3 (s, 3H, CH_3).

8-Amino-4-methylcoumarin. IR (υ in cm^{-1}) 3467, 3248 (NH strech), 1519, 1578, 1457 (aromatic ring), 1644 (C=O), 1248, 1155 (C-O); ^{1}H NMR δ 10.1 (s, 2H, NH), 7.5 (s, 1H, H $_{8\ Aromatic}$), 6.8 (d, 1H, H $_{6\ Aromatic}$), 6.6 (d, 1H, H $_{5\ Aromatic}$), 3.4 (s, 1H, H $_{3\ Aromatic}$), 2.3 (s, 3H, CH_3).

6-Formyl-4-methyl coumarin. IR (υ in cm^{-1}) 1598, 1574, 1411 (aromatic ring), 1773,1607 (C=O), 1281, 1263 (C-O); ^{1}H NMR δ 10.1 (s, 1H, CHO), 8.3 (d, 1H, H $_{8\ Aromatic}$), 6.9 (d, 1H, H $_{7\ Aromatic}$), 6.7 (s, 1H, H $_{5\ Aromatic}$), 4.5 (s, 1H, H $_{3\ Aromatic}$), 1.9 (s, 3H, CH_3).

8-Formyl-4-methylcoumarin. IR (υ in cm^{-1}) 1606, 1558, 1474 (aromatic ring), 1716, 1610 (C=O), 1211, 1091 (C-O); ^{1}H NMR δ 10.0 (s, 1H, CHO), 7.8 (d, 1H, H $_{7\ Aromatic}$), 6.9 (d of d, 1H, H $_{6\ Aromatic}$), 6.7 (d, 1H, H $_{5\ Aromatic}$), 6.1 (s, 1H, H $_{3\ Aromatic}$), 2.8 (s, 3H, CH_3).

6-Nitro-4-methylcoumarin. IR (υ in cm^{-1}) 1500 1496 (aromatic ring), 1613 (C=O), 1592,1335 (NO_2), 1294,1199 (C-O); ^{1}H NMR δ 8.1 (d, 1H, H $_{7\ Aromatic}$), 7.2 (s, 1H, H $_{5\ Aromatic}$), 6.9 (d, 1H, H $_{8\ Aromatic}$), 6.4 (s, 1H, H $_{3\ Aromatic}$), 1.9 (s, 3H, CH_3).

8-Nitro-4-methylcoumarin. IR (υ in cm^{-1}) 1510, 1450 (aromatic ring), 1600 (C=O), 1591,1335 (NO_2), 1295, 1195 (C-O); ^{1}H NMR δ 7.8 (d, 1H, H $_{7\ Aromatic}$), 7.1 (d of d, 1H, H $_{6\ Aromatic}$), 6.9 (d, 1H, H $_{5\ Aromatic}$), 3.3 (s, 1H, H $_{3\ Aromatic}$), 2.5 (s, 3H, CH_3).

7,8-Benzo-4-methylcoumarin. IR (υ in cm^{-1}) 1593, 1576, 1474 (aromatic ring), 1632 (C=O), 1278, 1084 (C-O); ^{1}H NMR δ 8.5 (d, 1H, H $_{Aromatic}$), 7.8 (d, 1H, H $_{Aromatic}$), 7.5-7.6 (m, 2H, H $_{Aromatic}$), 7.4 (d, 1H, H $_{aromatic}$), 6.9 (d, 1H, H $_{aromatic}$), 6.4 (s, 1H, H $_{3\ Aromatic}$), 2.5 (s, 3H, CH_3).

6,7-Benzo-4-methylcoumarin. IR (υ in cm^{-1}) 1601,1512, 1466 (aromatic ring), 1631 (C=O), 1277, 1216 (C-O); ^{1}H NMR δ 7.7 (s, 2H, H $_{Aromatic}$), 7.6 (d, 1H, H $_{Aromatic}$), 7.2-7.4 (m, 2H, H $_{Aromatic}$), 7.1 (d, 1H, H $_{aromatic}$), 5.2 (s, 1H, H $_{3aromatic}$), 1.7 (s, 3H, CH_3).

References

[1]Jiao, C.X., Niu,C.G., Chen, L.X., She, G.L., Yu, R.Q., *Anal Bioanal Chem*, **2003**, *376*, 392-398.

[2] Singer, L.A., Kong, N.P., *J. Am. Chem. Soc*., **1996**, *88*, 5213.

[3]Zahradnik, M., *The Production and Application of Fluorescent Brightening Agents*, Wiley &Sons, **1992**.

[4]Mitra, A., Misra, S.K., Patra, A., *Synth. Commun*., **1980**, *10*, 915. doi: 10.1080/00397918008061851

[5]Johnson, J. R., *Org. React*, **1942**, *1*, 210.

[6]Hepworth, J.D., Gabbut, C.D., Heron, B.M., *in Comprehensive Heterocyclic Chemistry*, Pergamon Press, Oxford, 2nd edn, **1996**.

[7]Donnelly, B.J., Donnelly, D.M.X., Sullivan, A.M.O., *Tetrahedron*, **1968**, *24*, 2617. doi.org/10.1016/S0040-4020(01)82536-9

[8]Hua, D. H., Saha, S., Roche, D., Maeng, J. C., Iguchi, S., Baldwin, C., *J. Org. Chem*., **1992**, *57*, 399–403. doi: 10.1021/jo00027a075

[9]Al-Bayati, R.I., Al-Amiery A.A.H., Al-Majedy, Y.K., *African J. Pure Appl. Chem.*, **2010**, *6*, 74-86.

[10]Bulut, M., Erk, C., *Dyes Pigments*, **1996**, *30*, 99. doi.org/10.1016/0143-7208(95)00060-7.

[11]Robertson, A., Sandrock, W.F., Henery, C.B., *J. Chem. Soc*., 1931, 2426-2432. doi: 10.1039/JR9310002426

[12]Soares, V.C.D., Alves, M.B., Souza, E.R., Pinto, I.O., Rubim, J.C., Andrade, C.K.Z., Suarez, P.A.Z., *Int. J. Mol. Sci.*, **2007**, *8*, 392-398. doi:10.3390/i8050392.

[13]John, E., Israelstam, S., *J. Org. Chem*., **1961**, *26*, 240. doi: 10.1021/jo01060a602

[14]Reddy, B.M., Reddy, V.R., Giridhar, D., *synthetic comm.*, **2001**, *31*, 3603-3607.doi:10.1081/SCC-100107007

[15]Rajitha, B., Kumar, V.N., Someshwar, P., Madhav, J.V., Reddy, P.N., Reddy, Y.T., *Arkivok*, **2006**, *Xii*, 23-27.

[16]Li, T.S., Zhang, Z.H., Yang, F., Fu, C.G., *J. Chem. Research (S)*, **1998**, 38–39. doi: 10.1039/A703694I.

[17]Pope, M. T., Muller, A., *Angew. Chem., Int. Ed. Engl*. **1991**, *30*, 34.

[18] Pope, M. T., Muller, A., *Polyoxometalates: from Platonic Solids to Anti-retroviral Activity*, Kluwer Academic Publishers: Dordrecht, The Netherlands, **1994**.

[19]Kozhevnikov, I.V., Matveev, K.I., A*ppl. Catal.*, **1983**, *5*, 135-150. doi.org/10.1016/01669834(83)80128-6.

[20] Pope, M. T. *Heteropoly and Isopoly Oxometalates*; Springer-Verlag: New York, **1983**.

[21] Okuhara, T., Mizuno, N., Misono, M., *Adv. Catal.*, **1996**, *41*, 113. doi.org/10.1016/S0360-0564(08)60041-3.

[22]Kozhevnikov, I.V., *Chem. Rev*., **1998**, *98*, 171. doi: 10.1021/cr960400y.

[23]Kozhevnikov, I.V., *Catalysts for fine chemicals, in: Catalysis by Polyoxometalates*, vol. 2, Wiley, Chichester, **2002**.

[24]Adams, J.M., *Appl. Clay Sci*., **1987**, *2*, 309. doi.org/10.1016/0169-1317(87)90039-1.

[25]Lasrlo, P., *Acc. Chem. Res.*, **1986**, *19*, 121. doi: 10.1021/ar00124a004.

[26] Smith, K., *Solids Supports and Catalysis in Organic Synthesis*, Ellis Horwood. Chichester, **1992**, 100-122.

[27] Fowden, L., Barrer, R.M., Tinker, P.B., *Clay Minerals: Their Structure, Behaviour and Use*, The Royal Society, London, **1984**.

[28]González, E., Moronta, A., *Applied Catalysis A: General*, **2004**, *258*, 99–105. doi.org/10.1016/j.apcata.2003.08.004.

[29]Kurian, M., Sugunan, S., *Microporous and Mesoporous Materials*, **2005**, *83*, 25–34. doi.org/10.1016/j.micromeso.2005.03.001.

[30]Chae, H.J., Nam, I.S., Ham, S.W., Hong, S.B., *Catalysis Today*, **2001**, *68*, 31–40. doi.org/10.1016/S0920-5861(01)00320-0.

[31]Salerno, P., Asenjo, M.B., Mendioroz, S., *Thermochimica acta*, **2001**, *379*, 101. doi.org/10.1016/S0040-6031(01)00608-6.

[32] Tyagi, B., Chudasama, C.D., Jasra, R.V., *Appl Clay Science*, **2006**, *31*, 16. doi.org/10.1016/j.clay.2005.07.001.

[33]Abd El-Wahab, M.M.M., Said, A.A., *Journal of Molecular Catalysis A*, **2005**, *240*, 109. doi.org/10.1016/j.molcata.2005.06.038.

[34]Yildiz, N., Aktas, Z., Calimli, A., *Particulate Science and Technology*, **2004**, *22*, 21. doi:10.1080/02726350490422392.

[35]Temuujin, J., Jadambaa, T., Burmaa, G., Erdenechimeg, Sh., Amarsanaa, J., *Ceramics International*, **2004**, *30*, 251. doi.org/10.1016/S0272-8842(03)00096-8.

[36]Araujo, E.M., Melo, T.J.A., Santana, L.N.L., Neves, G.A., Ferreira, H.C., Lira, H.L., Carvalho, L.H., Avila, J.M.M., Ponte, M.K.G., Araujo, I.S., *Materials Sci Eng B*, **2004**, *112*, 175. doi.org/10.1016/j.mseb.2004.05.027.

[37]Valverde, J.L., Canizares, P., Kou, M.R.S., Molina, C.B., *Clays and Clay Minerals*, **2000**, *48*, 424.

Received: 17. 09. 2013.
Accepted: 19. 11. 2013.

DISTRIBUTION OF POLYCYCLIC AROMATIC HYDROCARBONS IN SURFACE SEDIMENTS OF KOH SICHANG ANCHORAGE AREA IN THAILAND

Gullaya Wattayakorn[a]* and Chatt Boonperm[b]

Keywords: polycyclic aromatic hydrocarbons (PAHs); source apportionment; diagnostic isomer ratios; Thailand

The levels and distribution of polycyclic aromatic hydrocarbons (PAHs) were investigated in surface sediments of Koh Sichang anchorage area of Thailand using gas chromatography with flame-ionization detection (GC/FID). The total concentrations of 16 PAHs US EPA priority pollutants varied from 65.2 to 18,970 ng g^{-1} dw, with a median concentration of 282±3,660 ng g^{-1} dw. The sediment samples were classified as moderately contaminated compared to those observed in other regions. PAH compositional signatures of surface sediments of the study area were dominated by higher molecular weight PAHs (4-6 rings) comprising about 87 per cent of total PAHs concentrations. Dibenzo[a,h]anthracene, benzo[b]fluoranthene, benzo[g,h,i]perylene, benzo[a]pyrene, fluoranthene, indeno[1,2,3-cd]pyrene, and pyrene represented the highest fractions in most surface sediment samples. Source apportionment using diagnostic PAH ratios indicated that composition of PAHs in most sediment samples originated mainly from incomplete combustion of organic matter (pyrolytic origin), with a mixture of pyrolytic and petrogenic PAHs were observed in some of the study sites. The presence of almost all human carcinogenic PAHs in the study area indicated that these sediments can be considered contaminated sites, suggesting that future monitoring programs together with an effective coastal management program must be implemented to ensure health and safety for all.

* Corresponding Authors
Fax: +6622550780
E-Mail: gullaya.w@chula.ac.th; gullaya@gmail.com
[a] Department of Marine Science, Faculty of Science, Chulalongkorn University, Pathumwan, Bangkok, 10330, Thailand
[b] Inter-Department of Environmental Science, Graduate School, Chulalongkorn University, Pathumwan, Bangkok, 10330, Thailand

Introduction

Polycyclic aromatic hydrocarbons (PAHs) are a class of diverse organic compounds containing two or more fused aromatic rings of carbon and hydrogen atoms. They are widespread contaminants in marine, river and lake sediments and are always found as a mixture of individual compounds. PAHs enter the environment by a variety of pathways. They are present in unburned petroleum (petrogenic PAHs) and can be released directly to the environment both by human activities (oil spill) and natural processes (oil seepage). Diagenetic processes are also suspected to generate certain PAHs (e.g. perylene) from biogenic precursors. In general, biosynthesis is considered a localized source, with little impact on global concentrations. The most prominent and ubiquitous source of PAHs to the environment is the incomplete combustion of modern (wood) and fossil (petroleum and coal) biomass.[1,2] High-molecular-weight PAHs from anthropogenic sources can reach toxic concentrations that are detrimental to the environment and human health. Several PAHs are known to be carcinogens and/or mutagens or precursors to carcinogenic sister compounds.[3,4] Accordingly, they had been included in the USEPA and the EU priority monitoring pollutants list. PAH compounds persist in the environment and, due to their hydrophobic nature, become associated with particulate matter, and preferentially concentrate on sediment or soil particles. Owing to their aromatic structure, PAHs are inherently stable in the environment, particularly under reducing conditions, such as encountered in sediments.[5] Even under favourable conditions, the sorbed PAHs will be released to the water as an extended source to threaten the aquatic ecosystem through bioaccumulation in food chains.[6] Thus, understanding the contributions of the various sources is essential and important for appropriately managing PAH levels in the environment. However, our knowledge of PAH contamination in Thailand has been limited.

The presence of PAHs in the marine environment has attracted the attention of the scientific community as these compounds are frequently detected in sediments at increasing levels and many of these compounds are potential or proven carcinogens, hence finding the sources of PAH contamination are commonly of environmental concerns. The major sources of PAHs may be either natural or anthropogenic. There are two anthropogenic PAH sources: pyrolytic hydrocarbons from combustion sources and petrogenic hydrocarbons from petroleum sources. Pyrolytic PAHs, characterized by a predominance of parent compounds with four or more aromatic rings, can be emitted from the incomplete combustion of fossil fuel, urban and industrial activities, natural fire and biomass burning that produce high molecular weight and less or non-alkylated PAHs.[1,2,7] Combustion sources of PAHs in the industrialized countries include power plants, refineries, and automobiles.[8] Petrogenic PAHs, compounds with two to three aromatic rings, are mainly derived from the release of crude oil and petroleum products such as lubricating oil, diesel fuel, gasoline, asphalt and kerosene.[9,10] In this respect, the molecular indices based on the ratio of selected PAH concentrations in sediments can be used to elucidate the possible sources. The ratios between low and high molecular weight PAHs[9] and those of specific compounds, such as Flt/(Flt+Pyr), BaA/(BaA+Chr), Flt/Pyr and BaA/Chr have been proposed as valuable source indicators.[10] In addition,

diagnostic ratios of BaA/Chr, BbF/BkF, BaP/BeP and InP/BgP have been applied to identify specific types of combustion, such as vehicle exhaust, coal/coke combustion, forest fires, and smelters.[11-13]

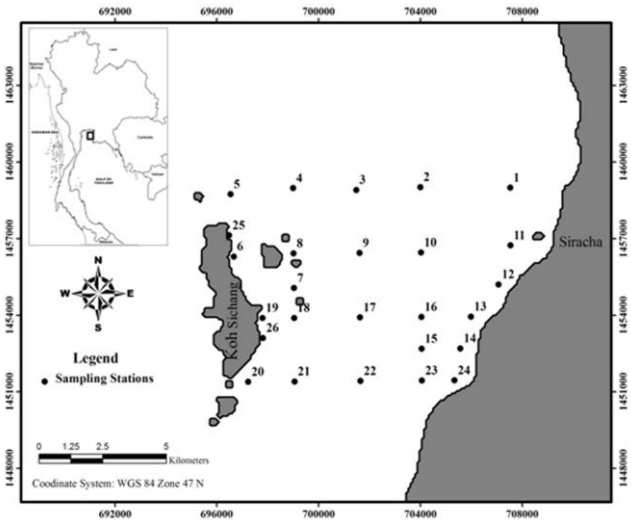

Figure 1. Map of Koh Sichang and Siracha anchorage area in the inner Gulf of Thailand showing the sample collection sites.

Koh Sichang (Sichang Island) is a small island located along the eastern coast of the inner Gulf of Thailand (latitude 13º7.4′ - 13°11.5′N, longitude 100º49.1′ - 100°54.9′E), twelve kilometres offshore from the town of Siracha, Chonburi Province (Fig. 1). Due to its proximity to shipping lane, the marine area between Koh Sichang and Siracha has made a convenient anchorage spot for dozens of barges which tranship their cargoes to lighter boats for the trip up the Chaophraya River to the Bangkok Port. The transhipment activities of coal in the area has resulted in an increase of fine coal dust and particles which will eventually settle down and act as a likely source of PAHs into the ambient environment. The area also experienced more than twenty oil spill events during the last two decades.[14] In addition, human activity along Siracha and Koh Sichang coasts has resulted in a number of possible point sources of contamination; including a variety of industry activities, an oil refinery, ports, ferry terminals and fishing piers, being discharged into the receiving environment. Accordingly, this ecosystem during the years has accumulated in sediments both elevated levels of organic matter and petroleum hydrocarbons;[14] Hence it is necessary to investigate the pollution sources and their environmental impacts on this coastal marine environment.

The objective of the present work was to quantify and determine the distribution of the 16 US EPA priority pollutant PAHs in sediments from the Koh Sichang anchorage area. In addition, the possible sources of PAH contamination were studied using PAH diagnostic ratios. The study will provide valuable information to be referenced by engineers, planners and officials for future management strategies on PAH contamination in this area.

Experimental

Sample collection

Surface sediment samples (0–3 cm depth) were collected by using modified Van Veen grab sampler in February 2012; from 26 sites distributed along four transect lines in the coastal area of about 100 square kilometres between Koh Sichang and Siracha (Fig. 1). Two replicate grabs from each site were mixed thoroughly in a bowl to provide a single composite sample for each site. Immediately after collection, the samples were scooped into aluminium boxes, which have been pre-washed with n-hexane and kept in an icebox, and then transported to the laboratory, where they were divided for physico-chemical analysis and for further PAH assessment. The considered physico-chemical parameters included the analysis of percentage water content, percentage organic carbon, and sediment characterization while sediments for PAH analysis were kept frozen until further processing. Prior to extraction sediments were thawed at room temperature, mixed thoroughly, freeze dried and sieved through a 250 µm sieve to remove coarse substances.

Analytical methods

Samples were analysed for PAHs using the procedure of IAEA/IOC/UNEP,[15] with slight modification. About 50 g of the dried sediment sample was carefully transferred into the extraction thimble and placed in the extraction chamber of the Soxhlet extraction unit. An internal standard (9,10-dihydroanthracene) was added, and the sample was Soxhlet extracted with methylenechloride for 12 h. The extract was reduced in volume, cleaned up and fractionated on a silica gel-alumina column,[16] reduced in volume again with a gentle stream of ultra-pure nitrogen until 0.5 mL, and finally the extract was analysed by using capillary gas chromatography.

PAHs were analysed with Agilent 6890 gas chromatography coupled with flame ionization detector (FID) system equipped with a fused silica capillary column coated with HP-5 5 % phenylmethylsiloxane (30 m length and 0.32 mm ID 0.25µm film thickness). A 1.0 µL aliquot of the extract was injected while the injector port was held at 250 °C and operated in splitless mode. The oven temperature program started at 70°C covered a range from 70 °C to 290 °C at 6 °C min^{-1} with 15 min hold. Helium was used as carrier gas with flow rate at 1.0 mL min^{-1} constant flow and detector temperature was 300 ºC. Hydrogen and air ratios were optimized and their values were chosen as 30 mL min^{-1} and 300 mL min^{-1} respectively.

The following 16 PAHs were quantified: naphthalene (Nap), acenaphthylene (Acy), acenaphthene (Acn), fluorene (Flu), phenanthrene (Phe), anthracene (Ant), fluoranthene (Flt), pyrene (Pyr), benzo[a]anthracene (BaA), chrysene (Chr), benzo[b]fluoranthene (BbF), benzo[k]fluoranthene (BkF), benzo[a]pyrene (BaP), indeno[1,2,3-cd]pyrene (InP), dibenzo[a,h]anthracene (DBA), and benzo[g,h,i]perylene (BgP). Total PAHs (∑PAHs) was the sum of the 16 PAHs.

Table 1. Mean(±sd) and range of the measured physico-chemical parameters of sediments of Koh Sichang anchorage area.

	% Sand	% Silt	% Clay	Texture	% Water	%OC	pH	E_h (mV)
Mean±s.d.	26.9±19.7	47.7±17.1	25.4±5.7	silty clay	48.4±13.2	1.5±0.6	7.5±0.2	-79±55
Range	4.3-80.8	1.9-65.5	15.5-39.2		21.7-65.3	0.4-2.5	7.2-8.0	55-(-187)

Compound concentrations below detection limits were assumed to be zero for the summation of ∑PAHs in each sample. The identification of PAHs was based on comparison of the retention times of the peaks with those obtained from standard mixture of PAHs (Supelco Ltd.) and from spiked samples analysed under the same conditions. Quantification was based on external calibrations curves prepared from the standard solution of each of the PAHs. The coefficients of determination (r^2) for the PAH standard calibration plots were Nap (0.994), Acy (0.997), Acn (0.993), Flu (0.994), Phe (0.996), Ant (0.996), Flt (0.992), Pyr (0.998), BaA (0.992),Chr (0.995), BbF (0.991), BkF (0.990), BaP (0.990), InP (0.991), DBA (0.994), and BgP (0.991). All the analysis was carried out in three times. The relative standard deviations ranged from 0.07 to 0.45 %.

Analysis of procedural blanks and spiked samples with each set of analysed samples was used to assess quality control measurements. Four deuterated PAH surrogates (d_8-napthalene, d_{10}-fluorene, d_{10}-fluoranthene, d_{12}-perylene) were added to the samples and matrix blank prior to extraction. Recoveries of surrogates generally ranged from 80 % to 105 % of the spike concentration, with the overall mean of recovery 85±8.2 %. Concentrations of PAH compounds were not corrected for surrogate recoveries, and are expressed on a dry-weight (dw) basis.

Results and Discussions

Sediments characteristics

The results of sediment characteristics are presented in Table 1. The grain size was utilized to analyse the types of sediments. Sieve analysis and fine grain analysis show the majority of the sediments consisted of a silt mixture. The average mean grain size of surface sediments for most of the studied sites was silty clay. The organic carbon (OC) content ranged from 0.4 % to 2.5 %, with the average value of 1.5±0.6 %. Sites 7, 8, 25 and 26 had the highest OC contents, which is expected since these sites are either close to the coal transhipment area (7 and 8) or located near the ferry terminals (25 and 26). Sites 1 and 6, had the lowest OC contents due to more sand-sized material (>65 %) in the sediments.

Distribution and composition of PAHs

The ∑PAHs concentrations in surface sediments of the Koh Sichang-Siracha anchorage area ranged from 65.2 ng g^{-1} to 18,970 ng g^{-1}, with a median concentration of 282±3,660 ng g^{-1} dw. The highest ∑PAHs concentration was found at site 26, which is the nearest site to a ferry terminal and ship repairing facilities. The second highest concentration was found at site 7 (1.795 ng g^{-1}), which is the coal transhipment area. The ∑PAHs concentration detected in sediment sample of site 26 is around 290 times higher than the lowest level detected at site 16. Based on the PAHs levels suggested by Baumard et al.,[17] most sediment samples in the study area can be classified as moderately contaminated (∑PAHs = 100-1,000 ng g^{-1} dw). The Pearson correlation coefficients for ∑PAHs concentration and sediment characteristics in the study area were carried out. Results show that the sediment ∑PAHs concentrations were not significantly correlated to either OC or particle size ($p > 0.05$). The observation suggests that OC and particle size are not major factors to control the ∑PAHs distribution.

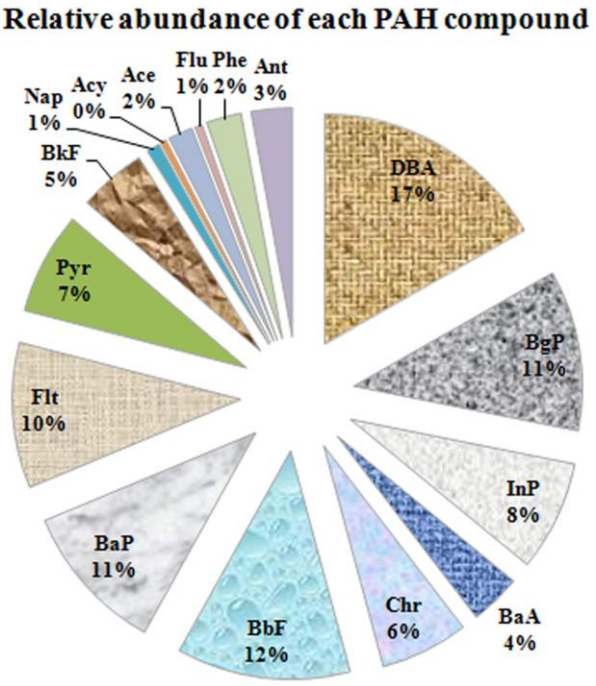

Figure 2. The percentage of mean concentration of each PAH compound in the study area.

The percentage of mean concentration of each PAH compound in the study area is shown in Fig. 2. Many of the PAH compounds were present at low concentration range. The individual PAH median concentrations (ng g^{-1} dw) found in the study area were in the order: DBA (45.5) > BbF (33.3) > BgP (30.9) > BaP (28.8) > Flt (28.0) > InP (21.2) > Pyr (19.6) > Chr (16.9) > BkF (13.0) > BaA (9.9) > Ant (7.8) > Phe (6.7) > Acn (4.7) > Nap (2.5) > Flu (1.4) > Acy (1.1). The difference in PAHs abundance in surface

sediments may be attributed to molecular weight and microbial degradation. A wide varieties of microorganisms including bacterial, fungal, and algal strains are known to degrade PAHs. Lower molecular weight PAHs such as Nap and Phe are degraded rapidly in sediments, but higher molecular weight PAHs such as Pyr, Flt, BaA and BaP are more resistant.[18] Hence, the distribution of PAHs found in sediments gives information about the precursor sources.

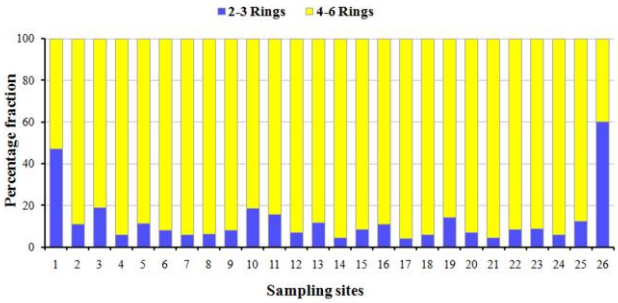

Figure 3. Relative distribution of %Σ(2-3)-rings and %Σ(4-6)-rings PAHs in Koh Sichang - Siracha surface sediments. 2-3-rings: Nap, Acy, Acn, Flu, Phe, Ant; 4-6-rings: Flt, Pyr, BaA, Chr, BbF, BkF, BaP, InP, DBA, BgP.

PAHs composition in the sediments of the Koh Sichang-Siracha anchorage area were generally similar in such a way that the relative contribution of low molecular weight (LMW) components with 2-3 rings (LPAHs) was lower (ranging from 4 % to 19%), while components with high molecular weight (HMW) with 4-6 rings (HPAHs) were dominant, ranging from 81 % to 96 %, except the sediments from sites 1 and 26, where the 2- & 3-ring PAHs were predominant at 47-60 %, respectively (Fig. 3). The result suggests that the PAHs contamination in these two sites comes from a different source than those for the PAHs found in other locations. The spatial distribution patterns of ∑PAHs, ∑LPAHs and ∑HPAHs in the study area shown in Fig. 4 reveal the predominance of high molecular weight PAHs in the sediments which reflects the presence of significant combustion products from pyrolytic processes and/or pyrolytic sources.[1,2,7]

PAH diagnostic ratios

Several PAH isomeric ratios have been used to identify different sources of PAHs to environmental samples. These ratios are useful indicators of PAH sources, and have been widely used to infer the source of PAHs found in sediments.[10-13,19] For example, ratios of Phe/Ant and Flt/Pyr have been widely used to distinguish petrogenic and pyrogenic (pyrolytic) sources of PAHs.[10-13,19-22] It is generally accepted that PAHs with Flt/Pyr values >1 are related to pyrolytic origins and values <1 are attributed to petrogenic origin. PAHs of petrogenic origin are also characterized by Phe/Ant > 10, while combustion process often result in Phe/Ant < 10. Other common ratios that have been used include Ant/(Ant+Phe) and Flt/(Flt+Pyr).[23-28] Ratios of Ant/(Ant+Phe) < 0.1 and Flt/(Flt+Pyr)<0.4 usually imply a petrogenic source, whereas ratios of Ant/(Ant+Phe) > 0.1 and Flt/(Flt+Pyr) > 0.5 suggest a pyrogenic source and combustion source of biomass (grass, wood, or coal combustion), respectively.

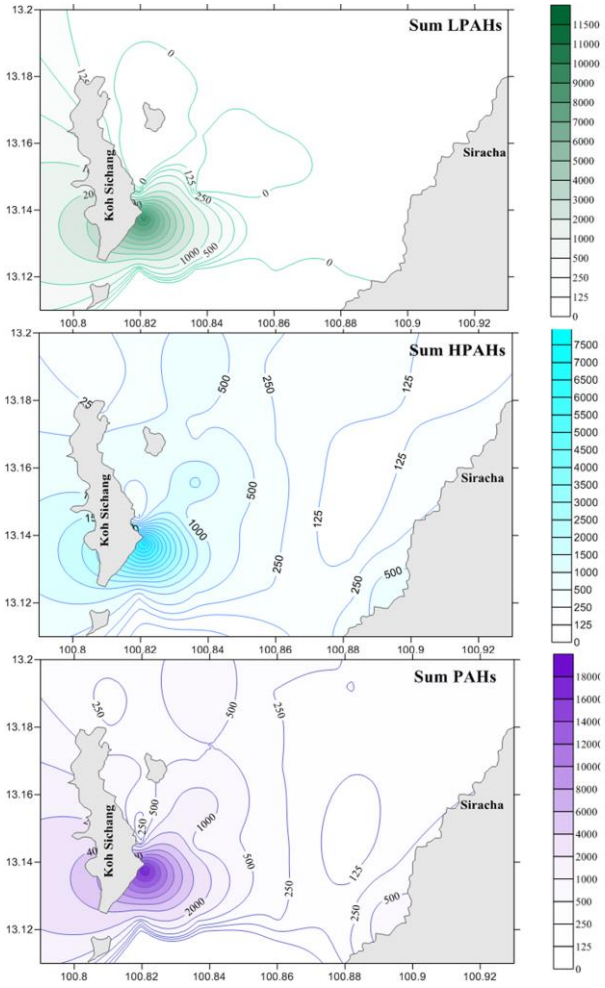

Figure 4. The spatial distribution of ΣLPAHs, ΣHPAHs and ΣPAHs concentrations (ng g^{-1} dw) in the study area.

Flt/(Flt+Pyr), BaA/Chr, BaA/(BaA+Chr), InP/(InP+BgP), Phe/Ant and Flt/Pyr were calculated for the sediment samples in the study area in order to determine probable PAH sources (Table 2). Ratio of different isomer pairs were plotted for use to identify PAH sources as shown in Fig. 5. At most of the sites investigated in this study, the Ant/(Ant+Phe) ratios were generally > 0.1, ratios of Flt/(Flt+Pyr) were >0.4, ratios of InP/(InP+BgP) > 0.2, ratios of Phe/Ant > 10, ratios of Flt/Pyr > 1.0. These indicate that pyrolytic sources were the primary sources of sedimentary PAHs in the study area. However, the BaA/Chr and BaA/(BaA+Chr) ratios indicated the mixed petrogenic and pyrolytic sources of the sedimentary PAHs.

Fig. 5 shows the cross plots for the ratios of Flt/(Flt+Pyr) vs. Ant/(Ant+Phe) and InP/(InP+BgP) vs. BaA/(BaA+Chr) in sediments, which indicated that most sediment samples have mixed combustion sources. Several of the Koh Sichang-Siracha sediment samples, however, have InP/(InP+BgP) ratios indicated that the main sources of PAHs were combustion of petroleum, while several sediment samples have InP/(InP+BgP) ratios indicated that of grass or wood combustion source.

Table 2. The diagnostic PAH source ratio guidelines* and those obtained for surface sediments in the study area.

Diagnostic ratios	Petrogenic source	Pyrolytic source	This study	
			Mean ± sd	Range
Ant/(Ant+Phe)	<0.1	>0.1	0.51±0.19	0.03 – 0.82
Phe/Ant	>15	<10	2.27±5.47	0.22 – 28.52
Flt/Pyr	<1.0	>1.0	1.91±1.61	0.28 – 8.86
Flt/(Flt+Pyr)	<0.4	>0.4	0.6±0.15	0.22 – 0.90
BaA/Chr	<0.4	>0.9	0.60±0.31	0.04 – 1.55
BaA/(BaA+Chr)	<0.2(0.2-0.35)	>0.35	0.35±0.12	0.04 – 0.61
InP/(InP+BgP)	<0.2	>0.2	0.43±0.15	0.17 – 0.77

*Modified from Yunker *et al.*[12, 28]

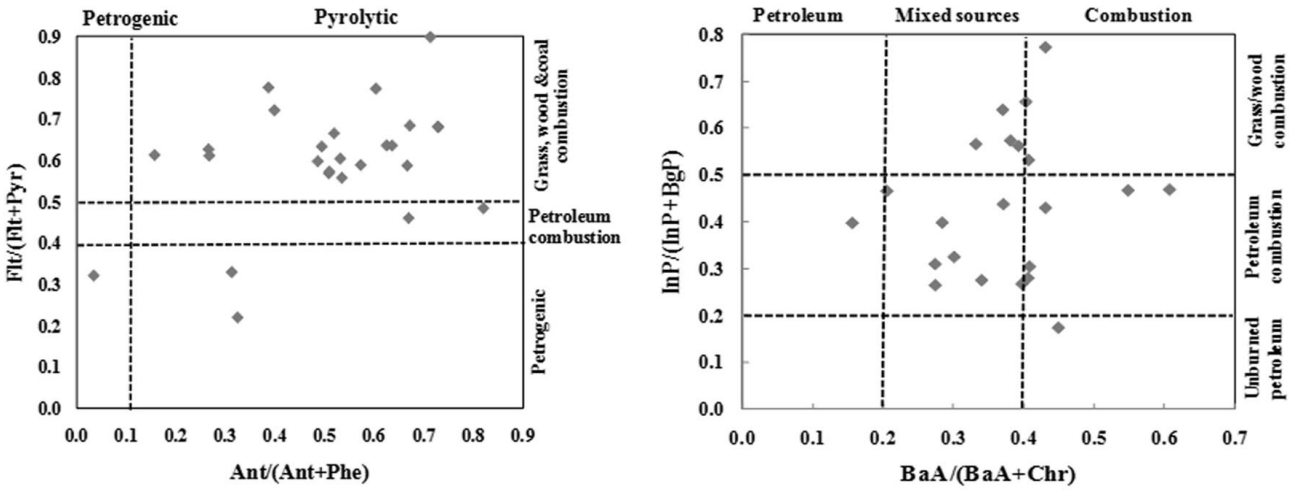

Figure 5. PAH cross plots for the ratios of Flt/(Flt+Pyr) vs. Ant/(Ant+Phe) and InP/(InP+BgP) vs. BaA/(BaA+Chr) in sediments of Koh Sichang-Siracha marine area.

Conclusion

This study provides important data set on PAH levels in surface sediments of Koh Sichang-Siracha marine area in Thailand. The PAH concentration levels of 16 PAH priority pollutants ranged from 65.2 to 18,970 ng g^{-1} dw with a median concentration was 282±3,660 ng g^{-1} dw. The overall levels of PAHs were moderate compared to coastal areas in other regions. The PAH distribution profile indicated potential source dependence, as the levels were generally higher in the vicinity of known inputs such as coal transshipment area, ferry terminals and ports. PAH diagnostic ratios indicated that PAHs in surface sediments mainly from pyrolytic sources (i.e. derived from combustion of petroleum and other organic materials) and very similar to PAH signatures of many coastal marine sediments elsewhere. The pyrolytic part of the pattern could arise from atmospheric transported coal derived particles from coal transshipment area, ship/boat emissions and other combustion processes. At most of the sites investigated in this study, the sedimentary PAH concentrations were dominated by DBA, BbF, BgP, BaP, and InP, which are IARC probable and possible human carcinogens.[3] Hence, high contaminated sediment samples in the study area are expected to have a high toxic potential. At present, no criteria or standards have been set for PAHs by any regulatory agency for the protection of sensitive species of aquatic organisms in Thailand. It is recommended that detailed assessment of ecological and human health risks associated with these compounds should be carried out as a matter of priority.

Acknowledgements

This study was financially supported by the National Research Council of Thailand, under the project Knowledge Management for Marine Pollution Abatement and Biodiversity Conservation around Sichang and Siracha, Chonburi Province (2nd Year) and the 90th Anniversary of Chulalongkorn University Fund (Ratchadaphiseksomphot Endowment Fund). The authors wish to thank the personnel of the Aquatic Resources Research Institute, Chulalongkorn University for their help in the field. The authors also gratefully acknowledge the anonymous reviewers for their useful comments which have helped to improve the quality of the manuscript.

References

[1]LaFamme, R.E. and Hites, R.A., *Geochim. Cosmochim. Acta*., **1978**, *42*, 289.

[2]Boehm, P.D., "Polycyclic Aromatic Hydrocarbons (PAHs)". In:Morrison, R. and Murphy, B. (eds.) *Environmental Forensics, Contaminant Specific Guide*, Academic Press, **2006**, *15*, 313,

[3]International Agency for Research on Cancer, *Some Non-heterocyclic Polycyclic Aromatic Hydrocarbons and Some Related Exposures*, **2010**, *92*, 773. [Online]: http://monographs.iarc.fr/ENG/Monographs/vol92/index.php [March 11, 2013].

[4]Schoeny, R. and Poirier, K., *Provisional Guidance for Quantitative Risk Assessment of Polycyclic Aromatic Hydrocarbons*, U.S. Environmental Protection Agency, Office of Research and Development, Office of Health and Environmental Assessment, Washington, DC, **1993**, *EPA/600/R-93/089 (NTIS PB94116571).*

[5]Volkering, F. and Breure, A.M., In: Douben, P. (ed.). "*PAHs: An Ecotoxicological Perspective",* Wiley, Chichester, **2003**.

[6]Zhang, C. and Zheng, G., "Characterization and desorption kinetics of PAHs from contaminated sediment in Houston Ship Channel", *Environmental Institute of Houston 2003 Annual Report*, **2003**, 39.

[7]Venkataraman, C. and Friedlandar, S.K., *Env. Sci. Technol*., **1994,** *28*, 563.

[8]Yang, H.H., Hsieh, L.T., Liu, H.C. and Mi, H.H., *Atm. Environ.*, **2005**, *39*, 17.

[9]Zakaria, M.P., Takada, H., Tsutsumi, S., Ohno, K., Yamada, J., Kouno, E. and Kumata, H., *Env. Sci. Technol.*, **2002,** *36*,1907.

[10]Stout, S.A., Uhler, A.D. and Emsbo-Mattingly, S.D., *Env. Sci. Technol.*, **2004**, *38*, 2987.

[11]Xiang, L., Li, Y.X., Yang, Z.F. and Shi, N.H., *J. Environ. Sci. Health*, **2010**, Part A *45(3)*, 339.

[12]Yunker, M.B., Macdonald, R.W., Vingarzan, R. and Mitchell, R.H., *Org. Geochem.*, **2002**, *33(4)*, 489.

[13]Soclo, H.H., Garrigues, P. and Ewald, M., *Mar. Pollut. Bull.*, **2000**, *40*, 387.

[14]Wattayakorn, G. and Rungsupa, S., *Coast. Mar. Sci.*, **2012**, *35(1):*122.

[15]IAEA/IOC/UNEP, *Determination of Petroleum Hydrocarbons in sediments. Reference Methods for Marine Pollution Studies*, **1992**, *No. 20*, 75.

[16]Ravanbakhsh, S., Abolfasl, F., Farzad, K. and Parvin, B., *Iran. J. Chem. Eng*., **2007**, 26(2): 27.

[17]Baumard, P., Budzinski, H. and Garrigues, P., *Environ. Toxicol. Chem*., 1998, 17, 765.

[18]Yuan, S.Y., Shiung, L.C., Chang, B.V., Bull. *Environ. Contam. Toxico*., **2002**, *69*, 66.

[19]Budzinski, H., Jones, I., Bellocq, J., Pie´rard, C. and Garrigues, P., *Mar. Chem.*, **1997**, *58*, 85.

[20]Magi, E., Bianco, R., Ianni, C. and Di Carro, M., *Environ. Pollut*., **2002**, *119*, 9.

[21]Wattayakorn, G. and Chaipuriwong, J., *J. Sci. Res. Chula. Univ., Special Issue II (NRC-EHWM)*, **2006**, *31*, 76.

[22]Boonyatumanond, R., Wattayakorn, G., Togo, A. and Takada, H., *Mar. Pollut. Bull*., **2006**, *52*, 942.

[23]Olajire, A.A., Altenburger, R., Kuster, E. and Brack, W., *Sci. Total. Environ.*, **2005**, *340(1-3)*, 123.

[24]Fang, M.D., Hsieh, P.C., Ko, F.C., Baker, J.E. and Lee, C.L., *Mar. Pollut. Bull.*, **2007**, *54*, 1179.

[25]Morillo, E., Romero, A.S., Madrid, L., Villaverde, J. and Maqueda, C., *Water Air Soil Pollut.*, **2008**, *187(1-4)*, 41.

[26]Jiang, J.J., Lee, C.L., Fang, M.D. and Liu, J.T., *Mar. Pollut. Bull.*, **2009**, *58*, 752.

[27]Inengite, A.K., Oforka, N.C. and Osuji, L.C., *Int. J. Appl. Environ. Sci.*, **2010**, *5(1)*, 127.

[28]Yunker, M.B., Perreault, A. and Lowe, C.J., *Org. Geochem.*, **2012**, *46*, 12.

Received: 31.10.2013.
Accepted: 21.11.2013.

A XYLIDINE PONCEAU DYE BASED PHOTOGALVANIC CELL: ENERGY CONVERSION FOR SUSTAINABLE DEVELOPMENT

K. R. Genwa[a]* and C. P. Sagar[a]

Keywords: xylidine ponceau, conversion efficiency, storage performance, Tween 60, fill factor, photogalvanic cell, ascorbic acid

The photogalvanic behavior of Xylidine ponceau dye was studied in Xylidine ponceau – Tween 60 – ascorbic acid system. The experimental studies were performed at different pH conditions and dye concentrations. The effects of electrode area, light intensity and diffusion length on cell electrical parameter are studied in various experimental conditions. Cell generates maximum power of 68.77 μW in ideal conditions. conversion efficiency was calculated by observed photopotential and photocurrent values at power point.

Corresponding Authors
Fax: +91- 291- 2720840;
E-Mail: krg2004@rediffmail.com
[a] Department of Chemistry, Jai Narain Vyas University, Jodhpur – 342005 (INDIA)

INTRODUCTION

The source for the renewable energies is the sun and is linked either directly or indirectly to the power of the earth's internal and external changes. The sun's heat and the earth's surface temperatures cause heating and cooling of air masses that become powerful winds. Electricity generation from renewables is assuming increasing importance in the context of large negative environmental externalities caused by electricity generation.[1] The utility of solar energy is one from many renewable sources of energy especially in photogalvanic cells, so the photogalvanic cells are worthwhile source of energy and have future applications and uses. The photogalvanic effect was first reported by Rideal and Williams[2], but Rabinowitch[3-4] made the first photogalvanic cell using thionine-iron system. Later on Kaneko and Yamada[5] were reported the photopotential and photocurrent induced by tolusafranine- ethylenediamine-tetraacetic acid system and Kaneko and Wohrle[6] used cation radical formed electrochemically in the presence of oxygen. Murthy et al.[7-9] studied photogalvanic effect in system containing methylene blue, riboflavin ethylenediaminetetraacetic acid and toluidine blue and shown the importance of the determination of electrochemical properties of dyes and flat band potentials of a few thin film semiconductor electrodes. Rohatgi Mukherjee et al.[10-11] were studied photo voltage generation of the phenosafranine-EDTA system in photogalvanic cell on temperature effect**.** Folcher and Paris[12], Alfredo et al.[13] reported the electron transfer via organic dye for solar energy conversion. Pan et al.[14], Jana and Bhowmik[15-16] were calculated solar energy efficiency (SEE) and other cell characteristics of mixed dye-solar cell is larger in comparison to the cell with single dye. whereas Bayer et al.[17], Matsumoto et al.[18-19], Shiroishi et al.[20] have studied some interesting photogalvanic systems with reasonable power. Bisquert et al.[21], Bisquert and Belmonte[22] and Bisquert et al.[23] have reviewed the importance's analysis of galvanostatically synthesized polypyrole films, correlation of ionic difference and capacitance parameters with the electrode morphology, whereas Mayer[24] has presented the molecular approaches to solar energy conversion.

Gangotri and Bhimwal[25] studied the performance of photogalvanic cell for solar energy conversion and storage in methyl orange –D xylose NaLS systems whereas Gangotri and Bhati[26] was studied photogalvanic cells having different surfactants, reductants and photosensitizers and tried to get the better electrical output and storage capacity. Sharma et al.[27-28] used Brilliant cresyl blue – Fructose and rodamine B – fructose systems for enhancement of solar energy conversion and storage capacity of photogalvanic solar cells. Recently, attention has been paid to use of some new dyes as photosensitizer in photogalvanic systems and surfactants as stabilizing agents[29-30]. In the present work, electrical output of Tween 60 – Xylidine ponceau – Ascorbic acid system examined experimentally to increase storage performance of cell and to development cost effective photogalvanic cell system for sustainable development.

Experimental

Xylidine ponceau (scheme I) is a solid red power with a absorption of 480 nm, its molecular formula is $C_{18}H_{14}N_2Na_2O_7S_2$, molecular weight is 480.42 and it is soluble in water.

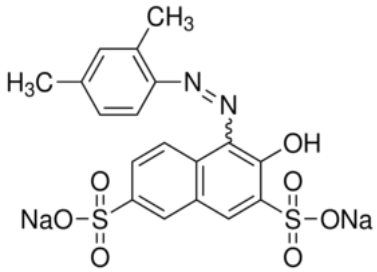

Scheme I

Tween 60 (Polyoxyethylene sorbitan monostearate) (Scheme II) is a pale yellow semisolid liquid, molecular formula is $C_{24}H_{46}O_6(C_2H_4O)_n$, molecular weight is 1312 and it is soluble in water.

 DOI: 10.17628/ecb.2014.3.76-80

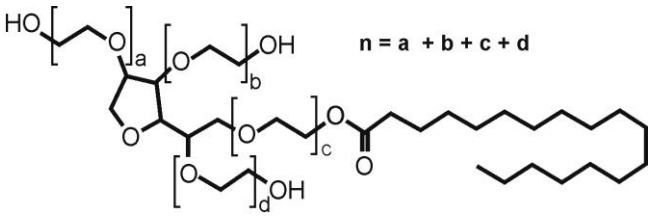

Scheme II

Ascorbic acid (scheme III) is white to slightly yellowish crystalline powder its molecular formula is $C_6H_8O_6$, molecular weight is 176.13 and it is soluble in water.

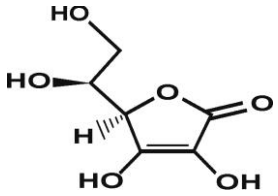

Scheme III

Photogalvanic effect of dye was studied using H- shaped glass tube which consist known amount of the solution of Xylidine ponceau ($5.6x10^{-5}$ M), Tween 60 ($1.08x10^{-3}$ M), Ascorbic acid ($2.08x10^{-3}$ M) and NaOH (1.0 N). A Platinum electrode (1.0x1.0 cm^2) was dipped in one limb and a saturated calomel electrode (SCE) is immersed in another limb of the H- tube. The terminals of the electrodes were then connected to a digital pH meter and the whole cell is placed in dark. The photopotential was measured in dark when the cell attains a stable potential. The limb containing platinum electrode was focused to the light source (projector Tungsten lamp). The light intensity was varied by employing tungsten lamp of 200 W and solarimeter. A water filter placed between the illuminated chamber and the light source to cut off thermal radiations. Photopotential and photocurrent were measured by digital pH meter (Systronics model 335) and digital ammeter (Osaw). Absorption spectra were recorded using Spectrophotometer (Systronics 106) with the matched pair of silica cuvetts (path length 1cm). All spectral measurements were duplicated in a constant temperature water bath maintained with in ±1 ^{0}C and mean values were processed for data analysis.

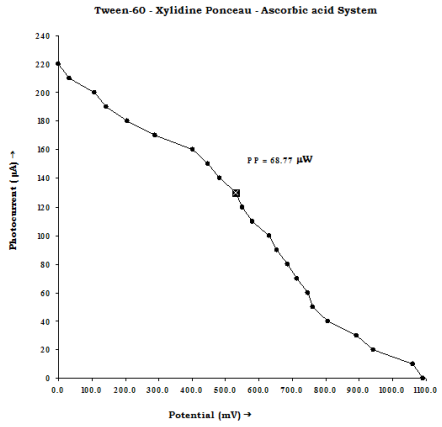

Figure 1. Absorption spectrum of dye and dye + surfactant

The dye shows absorption peak (λ_{max}) in visible region with maximum at 480 nm. Maximum absorption is recorded at Xylidine ponceau - Tween 60 combination of concentration $5.6x10^{-5}$ M + $1.08x10^{-3}$ M. The changes in the spectra are shown in Figure 1.

Results and discussion

Effect of variation of dye, surfactant, and reductant concentration

Effect of dye, surfactant and reductant concentration on photopotential and photocurrent are summarized in Table 1. In Tween 60 – Xylidine ponceau – Ascorbic acid system for the better performance of the photogalvanic cell proper concentration of dye needed. It was observed that photopotential and photocurrent increased with increase in concentration of the xylidine ponceau. A maxima was obtained at certain dye concentration ($5.6x10^{-5}$ M). On further increasing in dye concentration, a decrease in the electrical output was observed. On the lower concentration range of dye, there are limited number of dye molecules to absorb the major portion of the light in the path and therefore, minimum electrical output observed, where as high concentration of dye intensity of light reaching the molecule near the electrode decreased due to absorption of the major portion of the light by the dye molecules present in the path. Therefore corresponding fall in the power of the cell was observed.

Table 1. Effect of variation of Xylidine ponceau, Tween 60 and Ascorbic acid concentration.

Concentration	Photopotential, mV	Photocurrent, µA
[Xylidine ponceau] x 10^{-5} M		
4.8	712	154
5.2	769	179
5.6	880	197
6.0	760	181
6.4	725	160
[Tween 60] x 10^{-3} M		
0.28	620	97
0.68	778	143
1.08	880	197
1.48	730	170
1.88	590	128
[ascorbic acid] x 10^{-3} M		
1.28	663	142
1.68	790	176
2.08	880	197
2.48	810	180
2.88	720	168

[a]Light Intensity = 10.4 mW cm^{-2}, [b]Temp. = 303 K, [c]pH = 10.80

 DOI: 10.17628/ecb.2014.3.76-80

Tween 60 is used as a surfactant in the photogalvanic cell system. The photopotential and photocurrent of the cell was increased on increasing the concentration of Tween 60. A maxima was obtained at a certain value ($1.08x10^{-3}$ M) and decrease on further increase in surfactant concentration. The miceller systems have the ability to solubilize a variety of molecules and substantial catalytic effect on chemical reaction. Photopotential and photocurrent was found to increase with increase in reductant (ascorbic acid) concentration to maximum value of photopotential of 880.0 mV and photocurrent of 197.0 µA and then decrease in electrical output because fever reductant molecule were available for electron donation to photosensitizer (dye) molecule. Higher concentration of reductant again resulted in a decrease in electrical output, due to the large number of reductant molecules hinder the dye molecule from reaching electrode in the desired time limit.

Effect of variation of pH

Photogalvanic cell containing Tween 60 - Xylidine ponceau – ascorbic acid system was found to be quite sensitive to pH of the solution. The photopotential and photocurrent is increased with increase pH value (in alkaline range) of the cell. At pH 10.80, maximum photopotential and photocurrent of 880.0 mV, 197.0 µA recorded, further increase in pH, photopotential and photocurrent decreased. The results showing the effect of pH are summarized in Table 2.

Table 2. Effect of pH on photogalvanic parameters

pH	Photopotential, mV	Photocurrent, µA
10.72	690	92
10.76	760	135
10.80	880	197
10.84	762	170
10.88	670	108

[a][Tween 60] = 1.08 x 10^{-3} M, [b][Xylidine ponceau] = 5.6 x 10^{-5} M, [c][ascorbic Acid] = 2.08 x 10^{-3} M, [d]Light Intensity = 10.4 mW cm^{-2}, [e]Temp. = 303 K

Table 3. Effect of diffusion length

Diffusion length D_L, mm	Maximum photocurrent, i_{max}, µA	Rate of initial generation of current, µA min^{-1}
50	191	9.55
55	202	10.15
60	215	10.75
65	228	11.40
70	242	12.10

[a][Tween 60] = 1.08 x 10^{-3} M, [b][Xylidine ponceau] = 5.6 x 10^{-5} M, [c][ascorbic Acid] = 2.08 x 10^{-3} M, [d]Light Intensity = 10.4 mW cm^{-2}, [e]Temp. = 303 K

Effect of diffusion length

Effect of variation of diffusion length (distance between two electrodes) on the current parameters (i_{max}, i_{eq}) and initial rate of generation of photocurrent are studied using H-Shaped cell of different diameters. Results are reported in Table 3. It is observed that in the first few minutes of illumination there is sharp increase in the photocurrent (i_{max}). The conductivity of electroactive species depends on its population between electrodes. As diffusion length increased, the volume of dye solution and intern population of dye molecule(Xylidine ponceau) increased leading higher i_{max} the electroactive nature of dye/dye^- is provide by the fact that i_{max} increase with diffusion length. There for it may be concluded that the main electro active species are the leuco or semi form of dye- and the dye in the illumination and the dark chamber respectively.

Effect of variation of electrode area and light intensity

The effect of variation of electrode area on the current parameters of the cell also studied using thin platinum electrodes of different diameters. Experimentally, it was observed that with increase electrode area the value of maximum photocurrent (i_{max}) was found to increase and (i_{eq}) is all most independent to change in electrode cell. The results are summarized in Table 4.

Table 4. Effect of electrode area on photocurrents

Electrode area, cm^2	Maximum photocurrent, i_{max}, µA	Equilibrium photocurrent, I_{eq}, µA
0.25	188	171
0.64	198	183
1.00	215	197
1.21	231	207
1.96	246	228

[a][Tween 60] = 1.08 x 10^{-3} M, [b][Xylidine ponceau] = 5.6 x 10^{-5} M, [c][ascorbic Acid] = 2.08 x 10^{-3} M, [d]Light intensity = 10.4 mW cm^{-2}, [e]Temp. = 303 K

The intensity of light is also affects the electrical output of the cell. This effect was observed by varying intensity using solar intensity meter. Effect of light intensity graphically represented in Figure 2. It was observed that photocurrent showed a linear increasing behavior with the increase in light intensity whereas photopotential increase in logarithmic manner.

Current – voltage (i-V) characteristics of the cell

The open circuit voltage (V_{oc} 1091.0 mV) and short circuit current (i_{sc} 197.0 µA) of the photogalvanic cell were measured under the continuous illumination of light, with the help of digital pH meter (keeping the circuit open) and a micro ammeter (keeping the circuit closed), respectively. The external parameters (photopotential and photocurrent) of the photogalvanic cell in between this two extreme values (V_{pp} and i_{pp}) were recorded with the help of a carbon pot (log 407 K) connected in the circuit of micro ammeter, through which an external load applied on it (Figure 3). A point in the i-V curve, called power point (pp), was determined where the product of current and potential was maximum and the Fill-factor (*ff*) was calculated as 0.33 and conversion efficiency (η) of the cell was determined as 0.6613% using the following relationship

 DOI: 10.17628/ecb.2014.3.76-80

$$ff = \frac{V_{pp} i_{pp}}{V_{oc} i_{sc}} \quad (1)$$

$$\eta = \frac{V_{pp} i_{pp}}{10.4 \cdot A} 100 \quad (2)$$

where V_{pp}, i_{pp} and A are photopotential at power point, photocurrent at power point and electrode area, respectively.

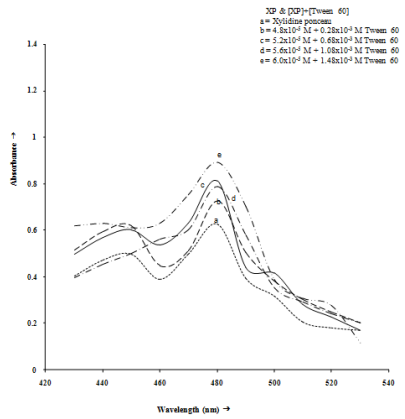

Figure 2. Variation of photocurrent and log V with light intensity

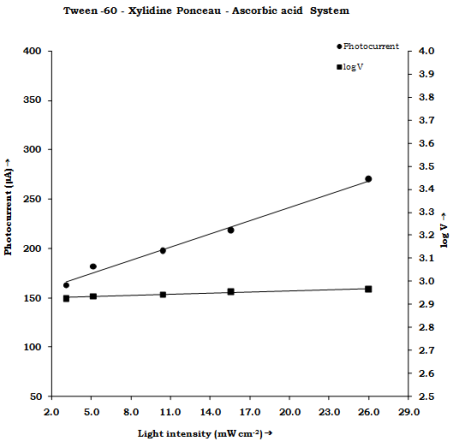

Figure 3. Current - potential (i-V) curve of the cell

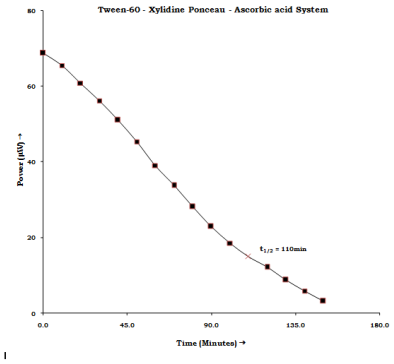

Figure 4. Time - power curve of the cell

Storage capacity (performance) of the cell

The performance of the photogalvanic cells containing the Tween 60 – Xylidine ponceau - ascorbic acid system was studied by applying the desired external load necessary to have the potential and the current corresponding to power point, after removing the source of illumination till the output (power) its half value at the power point in the dark. The performance of the cell was determined in terms of $t_{1/2}$ i.e. time required in fall of the output (power) to its half value at power point in dark. It was observed that cell can be used in the dark for 110.0 minutes (Figure 4).

Mechanism

The mechanism is photocurrent given in the photogalvanic cell may be proposed as follow:

In illuminated chamber

On irradiation, dye molecule get excited

$$\text{Dye} \xrightarrow{h\nu} \text{Dye}^* \quad (3)$$

The excited dye molecule accept an electron from reductant and convert into semi or luco form of dye, and the reductant into its excited state state form

$$\text{Dye}^* + \text{R} \rightarrow \text{Dye}^- + \text{R}^+ \quad (4)$$

At platinum electrode

The semi or luco form of dye loses an electron and converted into original dye molecule

$$\text{Dye}^- \rightarrow \text{Dye} + e^- \quad (5)$$

Dark chamber

At counter electrode (SCE)

$$\text{Dye} + e^- \rightarrow \text{Dye}^- \quad (6)$$

Finally luco/semi form of dye and oxidized form of reductant combine to give original dye and reductant molecule

$$\text{Dye}^- + R^+ \rightarrow \text{Dye} + R \quad (7)$$

where Dye, Dye*, Dye$^-$, R and R$^+$ represents the dye, excited form of dye, reduced form of dye, reductant and oxidized form of reductant, respectively.

 DOI: 10.17628/ecb.2014.3.76-80

Acknowledgements

The authors are thankful to UGC, New Delhi for providing financial assistance under UGC Major Research Project (No. 40-55/2011 (SR) dated 5 July 2011).

References

[1]Rubbia, C., Opening remarks at the 18th IAEA Fusion Energy Conference Sorrento, Italy, 4th October **2000.**

[2]Rideal, E. K., Williams, E. G., *J. Chem. Soc. Trans*., **1925**, *127*, 258.

[3]Rabinowitch, E., *J. Chem. Phys.*, **1940**, *8*, 551.

[4]Rabinowitch, E., *J. Chem. Phys.*, **1940**, *8*, 560.

[5]Kaneko, M., Yamada, A., *J. Phys. Chem.*, **1977**, *81*, 1213.

[6]Kaneko, M., Wohrle, D., *J. Electroanal. Chem*., **1991**, *307*, 209.

[7]Murthy, A. S. N., Reddy, K. S., *Int. J. Energy Res.*, **1979**, *3*, 205.

[8]Murthy, A. S. N., Dak, A. C., Reddy, K. S., *Int. J. Energy Res.*, **1980**, *4*, 339.

[9]Murthy, A. S. N., Reddy, K. S., *Solar Energy*, **1983**, *30*, 39.

[10]Rohatgi-Mukherji, K. K., Roy, M., Bhowmik, B. B., *Solar Energy*, **1983,** *31*, 417.

[11]Rohatgi-Mukherjee, K. K., M. Bagchi, M., Bhowmik, B. B., *Electrochim. Acta*, **1983**, *28*, 293.

[12]Folcher, G., Paris, J., J. USA Patent, **1983,**US 4,391,881

[13]Alfredo, O., Georgina, P., Sebasteian, P. J., *Solar Energy Material Solar Cells*, **1990**, *59***,** 137.

[14]Pan, R. L., Bhardwaj, R., Gross, E. L., *J. Chem. Tech. Biotech. Chemtech*., **1983**, *33*, 39.

[15]Jana, A. K., Bhowmik, B. B., *J. Photochem. Photobiol. A: Chem*., **1997**, *110***,** 41.

[16]Jana, A. K., *J. Photochem. and Photobiol. A: Chem.*, **2000**, *132*, 1.

[17]Bayer, L.S., Erogle, I., Turker, L., *Int. J. Energy Res*., **2001**, *25*, 207.

[18]Erabi, T., Matsumoto, K., Fujimura, K., Nomura, K., Wada, M., *Electrochemistry*, **1997**, *65*, 673.

[19]Matsumoto, K., Fujioka, S., Mii, Y., Wada, M., Erabi, T., *Electrochemistry*, **2001**, *69*, 340.

[20]Shiroishi, H., Kaburagi, Y., Seo, M., Hoshi, T., Nomura, T., Tokita, S., Kaneko, M., *J. Chemical Software*, **2002**, *8*, 47.

[21]Bisquert, J., Belmonte, G. G., Santiago, F. F., Bueno, P. R., *Electrochem. Commun*., **1999,** *1*, 429.

[22]Bisquert, J., Belmonte, G. G., *Electrochim. Acta*, **2002**, *47*, 4263.

[23]Bisquert, J., Belmonte G. G., Pitarch, A., *ChemPhysChem*., **2003**, *4*, 287.

[24]Meyer, G. J., *Inorg. Chem*., **2005**, *44***,** 6852.

[25]Gangotri, K. M., Bhimwal, M. K., *Energy Sources Part-A*, **2011,** *23*, 2058.

[26]Gangotri, K. M., Bhati, K. K., *Int. J. Electrical Power Energy Systems*, **2011,** *33*, 155.

[27]Sharma, U., Koli, P., Gangotri, K. M., *Fuel*, **2011**, *90*, 3336

[28]Sharma, U., Koli, P., Gangotri, K. M., *Renewable Energy*, **2012**, *37*, 250.

[29]Genwa, K. R., Kumar, A., *Energy Sources Part A*, **2012**, *34*, 1261.

[30]Genwa, K. R., Singh, K., *Smart Grid and Renewable Energy*, **2013**, *4*, 306.

Received: 08.10.2013.
Accepted: 21.11.2013.

CHARACTERIZATION OF WATER/n-PROPANOL/NONIONIC SURFACTANT/PHENYLACETYLENE MICROEMULSIONS

Monzer Fanun[a]*, Ahmad Shakarnah[a], Michael Schwarze[b], Reinhard Schomäcker[b], Zackaria Nairoukh[c], Jochanan Blum[c]

Keywords: nonionic surfactants, phase behaviour, hydrodynamic diameter, emulsification of substrate, hydration of alkynes

Water/*n*-propanol/nonionic surfactant /phenylacetylene micellar systems were formulated and used for the hydration of phenylacetylene. The ratio (w/w) of *n*-propanol/surfactant equals 2/1. The surfactants were sucrose laurate (L1695) and Marlipal 24/70 (M2470). The extent of the micellar region as function of temperature was determined. The particle hydrodynamic diameters of the oil-in-water micellar systems measured using dynamic light scattering and were found to decrease with temperature for sucrose laureate and to increase for Marlipal 24/70 based systems. In the diluted region microemulsion systems were observed. Highly efficient hydration of phenylacetylene was performed in these microemulsions. The reaction results indicate that hydration of phenylacetylene is more efficient when sucrose laurate was used for the formulation of the microemulsions.

Corresponding Authors
Tel: + 972522406061;
Fax: + 972 22 79 69 60
E-Mail: Fanunm@gmail.com; mfanun@science.alquds.edu
[a] Colloids and Surfaces Research Center, Al-Quds University, East Jerusalem 51000, Palestine
[b] Institut für Chemie, Technische Universität Berlin, Strasse des 17. Juni 124, D-10623 Berlin, Germany
[c] Institute of Chemistry, The Hebrew University of Jerusalem, Jerusalem 91904, Israel

Introduction

In our previous studies, we have demonstrated that applying a three phase emulsion (or microemulsion)-solid state-transport method (EST) system can be applied successfully for catalytic hydrogenation, hydroformylation and carbon-carbon coupling of hydrophobic substrates in aqueous microemulsions.[1-5] Hydration of alkynes usually still involve either toxic mercury derivatives or some other environmentally disfavoured late metal compounds.[6] Ultra-low palladium catalysts was used for phenylacetylene semi hydrogenation.[7] Hydration of phenylacetylene using Brönsted acidic ionic liquids in the absence of Nobel metal catalyst/sulphuric acid was reported.[8] A possible mechanism of hydration of phenylacetylene in near-critical water was also proposed.[9] A new method for the hydration of alkynes that is expected to reduce the hazards associated with industrially important processes and to convert the conventional methods into environmentally favoured syntheses was reported.[10] Internal and aliphatic acetylenes were hydrated by treatment of their microemulsions with 0.33 M mineral acid between 80 and 140 °C. The products are easily isolated from the reaction mixtures by phase separation.[10] In this study we continue our efforts to formulate new microemulsions composed of water/*n*-propanol/nonionic surfactant /phenylacetylene to be used as a reaction media for the hydration of phenylacetylene. The nonionic surfactants used were sucrose laurate (L1695) with a hydroxylated head group and Marlipal 24/70 (M2470) with an ethoxylated head group. The objective is to study the effect of the surfactants head group on the phenylacetylene hydration in oil-in-water microemulsions.

Experimental

Phenylacetylene (PAC), Sucrose laurate (L1695) was obtained from Mitsubishi-Kasei Food Corp. (Mie, Japan). Marlipal 24/70 (M2470) was obtained from Sasol Company (Hamburg, Germany). All the components were used as supplied without further purification. Triply distilled water was used for all experiments.

Sample preparation for pseudo ternary phase diagram at constant temperature

The phase behaviour of a four-component system is described in pseudo ternary phase diagrams in which the weight ratio of surfactant/cosurfactant is fixed. The determination of the phase behaviour was performed in a thermo stated bath ($T \pm 0.1$ K). Ten weighted samples composed of mixtures of (surfactant + cosurfactant) and oil were prepared in culture tubes sealed with Viton-lined screw caps at predetermined weight ratios of oil/surfactant/cosurfactant. The mixtures were titrated with water and were equilibrated during a time interval of up to 24 h. The different phases were determined visually and optically using crossed polarizer's method. Appearance of turbidity was considered as an indication

for phase separation. The phase behaviour was determined only after sharp interfaces had become visible. Every sample that remained transparent and homogeneous after vigorous vortexing was considered as belonging to the one phase region in the phase diagram.[11,12]

Dynamic light scattering

Particle size measurements were performed using Zetasizer Nano S (ZEN 1600) for the measurements of size and molecular weight of dispersed particles and molecules in solution by Malvern Instruments Ltd. (Worcestershire, United Kingdom). The equipment includes a 4 mW, 633 nm He-Ne laser. Size measurement range between 0.6 nm to 6 μm, size measurement angle equals 173º, concentration range for size measurement was between 0.1 ppm (0.00001 vol %) – 40 wt %, molecular weight range between 10^3 to 10^7 Da and temperature measurement range between 275 K to 363 K. 1.5 ml micellar sample was introduced in a disposable polystyrene cuvettes and measured at temperatures range between 273 and 323 K by steps of 5 K. The particle hydrodynamic diameter is calculated from the translational diffusion coefficient (D) using the Stokes-Einstein relationship:

$$d_H = k_B T/6\pi\eta D \qquad (1)$$

where d_H is the hydrodynamic diameter, k_B is Boltzmann's constant, T is the absolute temperature and η is the solvent viscosity. The results are averages of 3 experiments.

Emulsification of the substrates

Typically, a mixture of triply distilled water (TDW, 89.3 wt. %), and a suitable surfactant (3.3 wt. %) was stirred at room temperature. Then, the substrate (0.8 wt.%) was added drop wise under vigorous stirring. The emulsion, so formed, was titrated with *n*-propanol until a clear transparent mixture was obtained (usually 6.6 wt.%). A calculated amount of the desired acid was added to the microemulsion in order to obtain a 0.33 M microemulsion.

General procedure for the hydration of alkynes

The above microemulsion of the substrate was placed in either an autoclave or in a pressure vessel and heated with stirring to the desired temperature for the required length of time. The reaction vessel was cooled to room temperature and the microemulsion was treated with NaCl (2 g) which caused phase separation. The aqueous phase was extracted with Et_2O (2×15 mL) and the combined organic phases were neutralized with aqueous $NaHCO_3$, dried ($MgSO_4$), concentrated and chromatographed on silica gel. The products were then analyzed by ^1H NMR, MS, and GC in the usual manner and compared with authentic samples.

Results and Discussion

Phase behavior

Figures 1 and 2 present the phase behaviours of water/ sucrose laurate /*n*-propanol/ phenylacetylene and water/ Marlipal 24/70 /*n*-propanol/ phenylacetylene systems at 298 K. The ratio (w/w) of *n*-propanol/ surfactant equals 2/1. As shown in the Figure, the phase behaviour indicates the appearance of transparent micellar region after the first addition of water. Similar findings on the behaviour of sucrose ester surfactants in the presence of other cyclic oils were reported.[12-14] The area of the one phase region A_T (%), varies slightly with temperature for Marlipal 24/70. The phase behaviour of the system based on sucrose laurate shows temperature independency. Similar behaviours of the dependence of the phase behaviour on temperature of nonionic surfactants were reported elsewhere.[14-17]

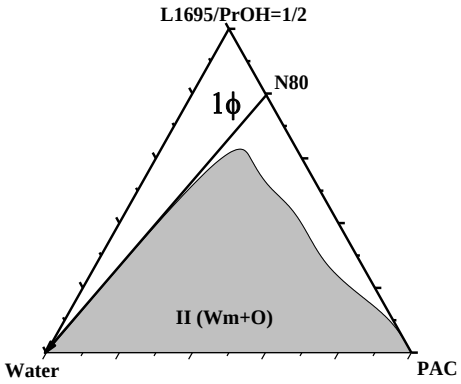

Figure 1. Pseudoternary phase diagram of the water/*n*-propanol/ sucrose laurate/phenylacetylene system at 298 K. The mixing ratio (w/w) of *n*-propanol/ sucrose laurate equals 2/1. The one phase region is designated by 1Φ, and the multiple phase regions are designated by (MΦ). N80 is the dilution line where the weight ratio of (sucrose laurate + propanol)/ phenylacetylene equals 4/1.

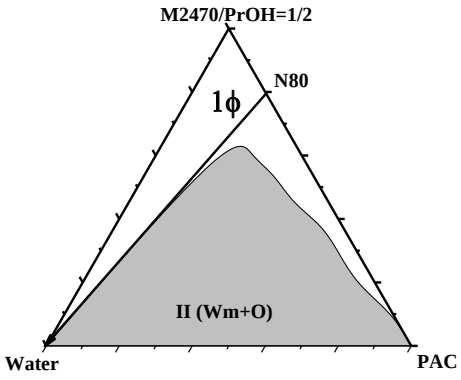

Figure 2. Pseudoternary phase diagram of the water/*n*-propanol/ Marlipal 24/70 /phenylacetylene system at 298 K. The mixing ratio (w/w) of *n*-propanol/ Marlipal 24/70 equals 2/1. The one phase region is designated by 1Φ, and the multiple phase regions are designated by (MΦ). N80 is the dilution line where the weight ratio of (Marlipal 24/70 + propanol)/ phenylacetylene equals 4/1.

 DOI: 10.17628/ecb.2014.3.81-84

Diffusion properties

The hydrodynamic diameter (d_H) of the oil-in-water micellar systems were measured for water volume fractions equal 0.90 and 0.95. The variation in the values of the (d_H) for the sucrose laurate based system decreased as function of temperature (from 298 to 323 K) as shown in Figure 3. Similar behaviour of the hydrodynamic radius of sucrose laurate based systems was reported elsewhere.[14,18,19]

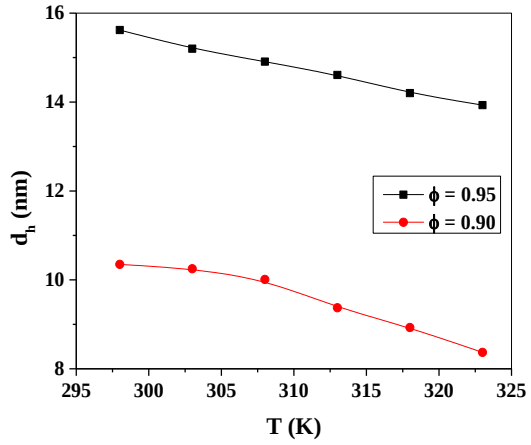

Figure 3. Variation of the particle hydrodynamic diameter as function of temperature for water/*n*-propanol/ sucrose laurate/phenylacetylene oil-in-water nanoemulsions along N80 dilution line.

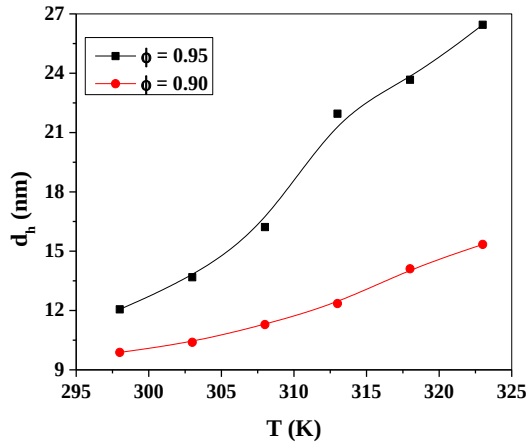

Figure 4. Variation of the particle hydrodynamic diameter as function of temperature for water/*n*-propanol/ Marlipal 24/70 / phenylacetylene oil-in-water nanoemulsions along N80 dilution line.

Figure 4 presents the variation of the hydrodynamic diameter of the oil-in-water micellar system as function of temperature for the ethoxylated Marlipal based system at 0.9 and 0.95 water volume fractions. The hydrodynamic diameters increase with increasing temperature. The values of the hydrodynamic diameter indicates that the micellar systems formed are microemulsions. These systems will be used as alternative reaction media for the hydration of phenylacetylene.

Hydration of phenylacetylene

Highly efficient hydration of alkynes have been performed in water upon addition of a suitable surfactant that solubilises the substrate. From previous studies, it had been showed that hydration of alkynes depends on the ionic nature of the surfactants.[10] In this report we introduced two different types of surfactants, both are non-ionic but they are different in structures. Some representative results summarized in Table 1 indicate that hydration of phenylacetylene is more efficient upon the addition of sucrose laurate.

Table 1. Dependence of the hydration of phenylacetylene on the nature of the surfactants. [a]

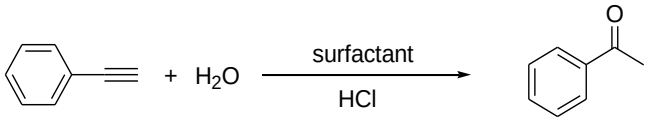

Entry	Surfactant	Isolated PhCOMe [%][b]
1	Marlipal	83
2	Sucrose laurate	97

[a] Reaction conditions as described in section 2 except that all experiments were performed for only 3 h at 140 °C.

[b] Average of at least two experiments that did not differ by more than ± 3 %.

Conclusion

New microemulsions were developed for performing hydration reactions of phenylacetylene that will lead to a significant reduction in the vast amount of organic solvents and toxic agents used currently in organic syntheses, and consequently increase the safety and diminish the cost of chemical processes. Determination of the particle size diameters of the diluted oil-in-water micellar systems enables the distinction of the diluted micellar systems as microemulsions. Since the particle size of the micellar system is an important parameter in determining the yield of hydration reaction of phenylacetylene, the results presented in this study recommend performing these reactions at water volume fractions above 0.90 or at surfactant contents slightly above the critical micelle concentration and at high temperatures.

Acknowledgment

We gratefully acknowledge the financial support of this trilateral study by the Deutsche Forschungsgemeinschaft (DFG) through grant SCHO 687/8-2.

References

[1]Abu Reziq, R., Avnir, D., Blum, J. , *Angew. Chem. Int. Ed*. **2002** , *41* , 4132-4134.

[2]Abu-Reziq, R., Blum, J., Avnir, D. , *Chem. Eur. J.* **2004** , *10* , 958-962.

[3]Abu-Reziq, R., Avnir, D., Blum, J., *Eur. J. Org. Chem*. **2005** , 3640-3642.

[4]Tsvelikhovsky, D., Blum, J. *Eur J. Org. Chem.* 2008 , 2117-2422.;

[5]Nairoukh, Z., Blum, J., *J. Mol. Catal. A*. **2012**, *358*, 129-133.;

[6]Hintermann, L., Labonne, A., *Synthesis* **2007**, 1121-1150.

[7]Karakhanov, E. A., Aksenov, I. A., Kardashev, S. V., Maksimov, A. L., Putilin, F. N., Shatokhin, A. N., Savilov, S. V., *Appl. Catalysis A:* **2013**, *464*, 253-260

[8]Kore, R., Kumar, T. J. D., Srivastava, R., *J. Mol. Catal. A*. **2013**, *360*, 61-70

[9]Li, S., Chang, Y. J., Wang, Y., Dai, L. Y. , *Chinese Chem Lett.* **2011**, *22*, 393-396

[10]Nairoukh, Z., Avnir, D., Blum, J. , *ChemSusChem* **2013**, *6*, 430-432

[11]Fanun, M., *J. Coll. Interf. Sci.* **2010**, *343*, 496-503.

[12]Fanun, M., Shakarnah, A., Meltzer, D., Schwarze, M., Schomaecker, R., Blum, J., *Tenside Surfact.. Deterg.*, **2011**, *48*, 400-407.

[13]Fanun, M., Ayad, Z., Mudalal, S., Dahoah, S., Meltzer, D., Schwarze, M., Schomaecker, R., Blum, J., *J. Surfact. Deterg*. **2012**, *15*, 505-512;

[14]Fanun M., *Colloids and Surf. A* **2010**, *369* , 246–252;

[15]Fanun M. , *J. Surfact. Deterg*. **2010**, *13* , 321-328;

[16]Fanun M., *Tenside Surfact.. Deterg* **2010**, *47* , 166-172;

[17]Fanun M. , *Open Colloid Sci. J.* **2010**, *3* , 9-14;

[18]Fanun M., Papadimitriou, V., Xenakis , A., *J. . Colloid Interf. Sci.* **2011**, *361*,115-121;

[19]Fanun M. , *J. Surface Sci. Technol.* **2010**, *26* ,137-158

Received: 08.11.2013.
Accepted: 25.11.2013.

A FACILE GREEN SYNTHESIS PROCESS OF 3-SUBSTITUTED-3-HYDROXYINDOLIN-2-ONES AND THEIR *IN VITRO* ANTIOXIDANT AND ANTIMICROBIAL POTENTIAL

Anshu Dandia[a]*, Deepti Saini[a], Dinesh Kumar Saini[b] and Manas Mathur[c]

Keywords: substituted indole-2,3-diones, substituted aryl ketones, aqueous medium, antioxidant, antibacterial and antifungal activity.

Potassium carbonate catalyzed synthesis of 3-substituted-3-hydroxyindolin-2-ones (**A**-**E**) by treating substituted indole-2,3-diones with substituted aryl ketones in aqueous medium under sonication with an object to develop potent antioxidant, antibacterial and antifungal agents of synthetic origin. It is revealed from the antioxidant screening results that the **Compound A** (3-hydroxy-3-[2-oxo-2-(4-chloro-phenyl)ethyl]indolin-2-one) and **Compound E** (5-Methyl-3-hydroxy-3-[2-oxo-2-(4-fluoro-phenyl)ethyl]indolin-2-one) manifested profound DPPH$^{\bullet}$, ABTS$^{\bullet+}$ and NO radical scavenging activity. **Compound C** elicited the potent inhibitory action against all the bacterial pathogens. **Compound A** (3-hydroxy-3-[2-oxo-2-(4-chloro-phenyl)ethyl]indolin-2-one) and **Compound C** (5-Methyl-3-hydroxy-3-[2-oxo-2-(4-chloro-phenyl)ethyl]indolin-2-one) have showed equivalent activity comparable to standard drug Ampicillin against *Pseudomonas aurigonosa*. The advantages of this green method utilizing potassium carbonate as an inexpensive, safe, and efficient basic catalyst are high efficiency, mild reaction conditions, convenient operation and environmentally benign conditions.

*Corresponding Authors
Tel: +91-9414073436
Tel: +91-141-2520301
Fax: 0091-141-2523637
Email: dranshudandia@yahoo.co.in
[a] Center of Advanced Studies, Department of Chemistry, University of Rajasthan, Jaipur-302004, India
[b] Radiation & Cancer Biology Lab, Department of Zoology, University of Rajasthan, Jaipur-302004, India
[c] Department of Botany, University of Rajasthan, Jaipur-302004, India

INTRODUCTION

After the discovery of the involvement of free radicals in oxidative tissue injury and diseases, the rapid development began in the area of free radical biology and medicine. Free radicals are produced as a result of normal biochemical reactions in the body. The human body uses an inherent antioxidant system to neutralize the excessive level of free radicals. In general, the cell is able to maintain an appropriate balance between oxidants and antioxidants under normal conditions. The imbalance between production of free radicals and the available antioxidant defence leads to a widely accepted phenomenon called oxidative stress, which is responsible for cellular and metabolic injury and accelerating aging, cancer, myocardial infarction, arthritis, cardiovascular diseases, neurodegenerative diseases and inflammation.[1] Around the world, life annoying contagious diseases caused by multi-drug-resistant pathogenic bacteria (Gram-positive/Gram-negative) increased at an alarming level. The presence and growth of pathogenic microorganisms (bacteria, mould, viruses, fungi) in food may cause its spoilage and results in a reduction in its quality and quantity.[2] This microbial contamination still poses important public health and economic concerns for human society.

Owing to various disorders caused by free radicals and increased microbial resistance, new classes of antioxidant and antimicrobial agents with novel mechanisms are today's need to fight against various disorders caused by free radicals and multi drug-resistant infections.

The indole nucleus, a common and important structural functionality of a variety of both natural and unnatural products, is probably the most well-known heterocycles. Isatins are versatile substrates because they can be used for the synthesis of a large variety of heterocyclic compounds as raw materials for drug synthesis. Oxindole derivatives are known to possess a variety of biological activities.[3] In particular, the 3-substituted-3-hydroxyindolin-2-ones, a class of compounds bearing the indole skeletal structure, are found in several biologically active alkaloids and pharmacological agents (Figure 1; Table 1).[4]

In context of this program, we have previously reported the synthesis of hydroxy derivatives and conversion of these into biodynamic heterocycles,[5] numerous methodologies have been developed and continue to be explored for the construction of this structure.[6] However, some of these methods suffer from certain drawbacks such as hazardous organic solvents, high cost, long reaction time, less selectivity and excess amount of base, unsatisfactory yields, cumbersome product isolation procedures, and environmental pollution. Therefore, there is still need for versatile, simple, and environmentally friendly processes for the synthesis of 3-substituted-3-hydroxyindolin-2-ones derivatives. Use of potassium carbonate as catalyst has inherent advantages including operational simplicity, low cost, and suitability in industrial applications.[7] An increasing number of examples are available in the literature where potassium carbonate alone has been used as a catalyst during organic transformations.[8]

Table 1. List of Compound Names, Bioactivity, Mode of Action

Entry	Natural Product	Target and mode of action	IC^{50}
1	Maremycin A-D[4a]	Cytotoxicity Mouse fibroblasts L-929 Human Leukemia K562	50 μg mL^{-1}
2	Paratunamide A-D[4b]	Cytotoxicity human epidermoid carcinoma KB cells	6 μg mL^{-1}
3	Spiroepoxyindoles[4c]	Anti-fungal, anti-tubercular anti-cancer	-
4	TMC-95 A-D[4d]	Reversible (non-covalent) inhibitors of 20S proteasome	5.4 nM
5	Convolutamydine A-E[4e]	Inhibit differentiation of promyelocytic leukemia cells HL-60	12.5-25 μg mL^{-1}
6	Spirotetrahydrofuryloxindole[4f]	Anti-cancer	16-32 μM
7	Spiroisoxazolidynyloxindole[4g]	anti-cancer, anti-tubercular	2-4 μM, 15-30 %

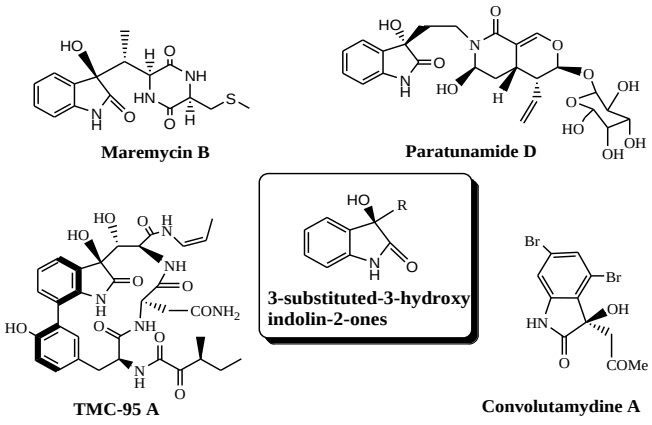

Figure 1. Examples of biologically active 3-substituted-3-hydroxyindolin-2-ones

An important technique that is widely used today in organic synthesis and has a profound impact on the way chemist approach organic and parallel synthesis, is "Ultrasonication", based on cavitation effects leading to mass transfer improvement. The benefits of this technology are reduction in reaction times, improved yields and suppression of side products, relative to traditional thermal heating.[9] Numerous examples under this condition for constructing the heterocycles with interesting properties have been reported in the literature.[10]

Considering the above points and in view of our quest for developing green protocols for heterocyclic frameworks,[11] herein, we report a greener, simple and efficient method for the synthesis of 3-substituted-3-hydroxyindolin-2-ones derivatives in water under ultrasonic irradiation by K_2CO_3 and their evaluation for antioxidant and antimicrobial potential.

However, to the best of our knowledge there is no report available in the literature describing the antioxidant potential of 3-substituted-3-hydroxyindolin-2-ones compounds, but compound A have been reported for its synthetic origin[6a] and also for anticonvulsant activity[6e] while compound B,[6a] and compound E[5c] have been reported for their synthetic origin.

RESULTS AND DISCUSSION

In order to study the present reaction in water with contemporary technique as ultrasound irradiation, we carried out the reaction of isatin **1** and 4-chloro acetophenone **2** as a model substrate in various catalysts and results are shown in Table 2.

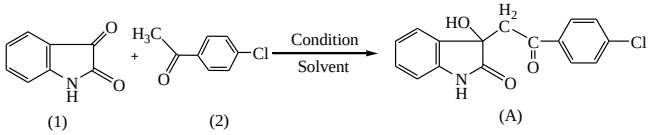

Model reaction: Synthesis of 3-hydroxy-3-[2-oxo-2-(4-chloro-phenyl)ethyl]indolin-2-one (**A**)

It was found that when the reaction was carried out without use of any catalyst, no product formation was detected confirming the necessity of a catalyst for the said conversion (Table 2, entry 1). Further, some bases such as sodium acetate, potassium acetate, and ammonium acetate can catalyze this reaction with low yields in longer time duration (Table 2, entry 2-4). Afterwards, evaluation of alkali metal carbonates such as sodium carbonate, potassium carbonate and cesium carbonate as catalyst was tried out as these catalysts find extensive use in synthetic organic chemistry.[12] Therefore, the synthesis of 3-hydroxy-3-[2-oxo-2-(4-Chloro-phenyl) ethyl]indolin-2-one (**A**) was carried out in aqueous medium under ultrasonic irradiation using these catalysts (Table 2, entry 5, 7 and 9). It was noticeable that a mixture of isatin **1** and 4-chloro acetophenone **2** in the presence of catalytic amount of potassium carbonate afforded (**A**) in satisfactory yields (69%) while with sodium carbonate and cesium carbonate, the product was formed in 60% and 55% yields respectively.

Further, optimization of the catalyst loading was done by using different concentration of potassium carbonate in the model reaction. It was found that increasing the amount of potassium carbonate from 10 to 20 and 25 mol%, the yields increased from 69% to 78% and 80%, respectively (Table 2, entries 9-11). Further increase in amount of catalyst does not seem to affect the overall yields of the product. Using 20 mol% of potassium carbonate in water under sonication is sufficient to push this reaction forward. More amount of the additive did not substantially improve the yield (entry 10 was considered to be better as almost same yield was obtained in case of entry 11 with longer reaction time).

In order to verify the effect of ultrasound irradiation on this reaction, the model reaction was also carried out in the absence of ultrasound under conventional manners both in stirring and refluxing conditions using water as a solvent (Table 2, entry 12, 13). As shown in Table 2, under refluxing conditions with high speed stirring, no reaction was observed at same time but a mixture of products was obtained after a prolonged reaction time. Thus, ultrasonic irradiation was found to have beneficial effect on the synthesis of 3-hydroxy-3-substituted indolin-2-one (**A-E**) derivatives which was superior to the traditional method with respect to yield, reaction time, particularly while considering the basic green chemistry concept.

Under the optimized reaction condition, we have synthesized 3-substituted-3-hydroxyindolin-2-ones by reaction of various aryl ketones and substituted isatins **(**Table 3**)** in good yields for screening them for antioxidant and antimicrobial potential. Compounds **A-E** are stable solids whose structures were established by IR, ^{1}H, ^{13}C NMR and mass spectroscopy and elemental analysis.

Table 2 Optimization of reaction condition for model reaction generating **A**

No.	Catalyst	Condition	Time	Yield,%
1	no catalyst	ultrasound	8 h	Traces
2	AcONa	ultrasound	5 h	30
3	AcOK	ultrasound	4 h	45
4	$AcONH_4$	ultrasound	6 h	40
5	Na_2CO_3	ultrasound	2 h	55
6	Na_2CO_3	rt, stirring	4 h	35
7	Cs_2CO_3	ultrasound	1 h	60
8	Cs_2CO_3	rt, stirring	3 h	42
9	K_2CO_3 10 mol %	ultrasound	38 min	69
10	K_2CO_3 20 mol %	ultrasound	35 min	78
11	K_2CO_3 25 mol %	ultrasound	40 min	80
12	K_2CO_3 20 mol %	rt, stirring	1 h	mixture of products
13	K_2CO_3 (20 mol %)	refluxing	1 h	mixture of products

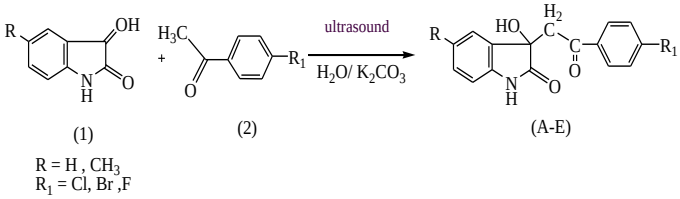

Scheme 1 Pathway for the synthesis of 3-substituted 3-hydroxyoxindole derivatives (**A-E**)

Table 3 Synthesis of 3-substituted 3-hydroxyoxindole (**A-E**) catalyzed by K_2CO_3

Entry	R	R^1	Time, min	M.p.,˚C	Yield, %
A	H	Cl	35	194	78 %
B	H	Br	37	192	79 %
C	Me	Cl	39	195	74 %
D	Me	Br	40	191	76 %
E	Me	F	36	177	70 %

Antioxidant Activity

The antioxidant activities of oxindoles were determined as an index of pharmacological usefulness. Three model systems were used namely $DPPH^{\bullet}$, $ABTS^{\bullet+}$ and NO scavenging activity. In the assessment of antioxidant activity, only synthetic relevant free radicals were used. The synthetic nitrogen-centered $DPPH^{\bullet}$, $ABTS^{\bullet+}$ and NO radicals were used as indicator compounds in testing hydrogen transfer capacity that are related to the antioxidant activity. The antioxidant properties were expressed as EC_{50} values. EC_{50} is defined as the concentration of substrate that scavenges 50 percent free radicals. A lower value of EC_{50} indicates the greater antioxidant activity of a test substance. In results, we have found correlation between substitution in indole ring at 5th position and substitution of phenacyl ring at 4th position. Overall, all compounds have good $DPPH^{\bullet}$ and NO scavenging activity whereas, all compounds have showed least $ABTS^{\bullet+}$ scavenging activity.

DPPH radical scavenging activity

Although the DPPH radical scavenging abilities of all the spiroindoline derivatives were significantly lower than those of ascorbic acid (409.75±0.288) µg ml-1, but the Compound **A** (3-hydroxy-3-[2-oxo-2-(4-chlorophenyl)ethyl]indolin-2-one) and Compound **E** (5-methyl-3-hydroxy-3-[2-oxo-2-(4-fluorophenyl)ethyl]indolin-2-one) have highest DPPH radical scavenging activity as compared to other compounds. All compounds have –OH and –NH group in their structure, the difference in their structure is the -H, $-CH_3$ (electron donating group) in indole ring at 5th position and Cl, Br and F (electron withdrawing group) in phenacyl ring at 4th position. The exact reason of activity of synthesized compounds is yet not clear, but it was anticipated that compound **A** possessing H at 5th position of indole ring and Cl substitution at 4th position of phenacyl ring showed good activity compared to all compounds. Compound **E** and Compound **B** incorporating $-CH_3$ and H at 5th position of indole ring respectively with F and Br substitution at 4th position of phenacyl ring showed moderate activity, while compound **C** and compound **D** showed least activity, both compound have $-CH_3$ group, an electron donating group and moderate electron withdrawing group Cl, Br substitution at 4th position of phenacyl ring showed least activity compared to all compounds. (The results are shown in Table 4 and Figure 2).

ABTS radical scavenging activity

Among the tested compounds in ABTS assay all compounds showed least activity, but when compared the activity results of all compounds, Compound **A** possessing H at 5th position of indole ring and Cl substitution at 4th position of phenacyl ring showed good activity compared to all other compounds. Compound **E** has H at 5th position of indole ring and Cl substitution at 4th position of phenacyl ring showed good activity. Compounds **B**, **C**. **D** with -H, and $-CH_3$, electron donating groups, in indole ring and p-Cl, p-Br, moderate electron withdrawing groups, in phenacyl ring showed least activity. (The results are shown in Table 4 and Figure 3).

Nitric Oxide scavenging activity

Among the tested compounds, in NO assay, compound E (5-methyl-3-hydroxy-3-[2-oxo-2-(4-fluorophenyl)ethyl]indolin-2-one) showed good activity. Combination of without any substitution in indole ring with p-Cl and p-Br substitution in phenacyl ring i.e. compound A and compound B showed moderate activity. The incorporation of CH_3 group at 5th position in indole ring with p-Cl and p-Br substitution in phenacyl ring gives least activity. (The results are shown in Table 4 and Figure 4).

Table 4 EC_{50} values of synthesized compounds.

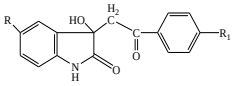

Compound	R	R_1	EC_{50} (µg ml^{-1})		
			DPPH	**ABTS**	**NO**
A	H	Cl	640.06±2.158	4117.08±3.856	732.30±1.237
B	H	Br	651.31±0.961	12463.75±1.462	734.30±1.641
C	CH_3	Cl	675.45±1.593	8294.16±2.427	760.22±0.982
D	CH_3	Br	665.86±1.688	12478.75±1.694	777.92±1.158
E	CH_3	F	649.48±2.146	4492.72±1.245	726.61±1.238
Ascorbic acid	-	-	409.75±1.384	550.00±1.136	544.21±0.832

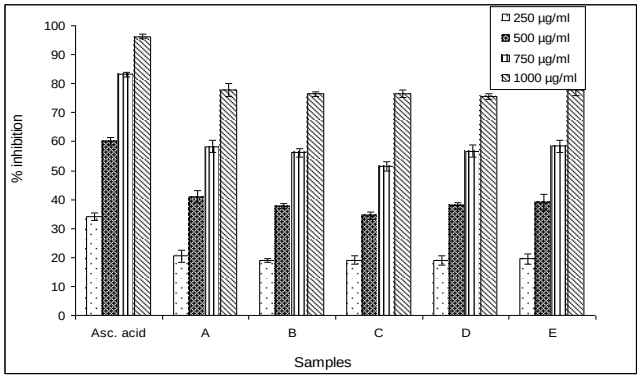

Figure 2. DPPH• scavenging activity (% inhibition) of synthesized compounds

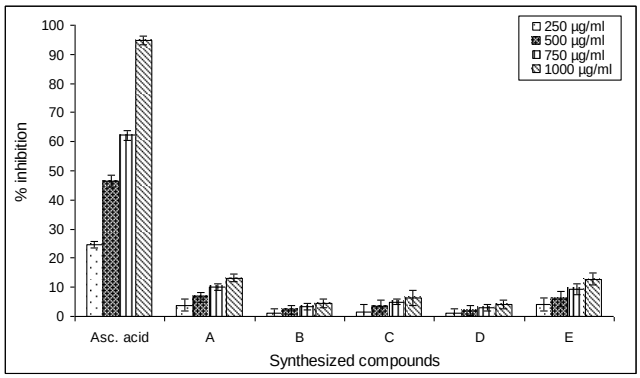

Figure 3. $ABTS^{\bullet+}$ scavenging activity (% inhibition) of synthesized compounds

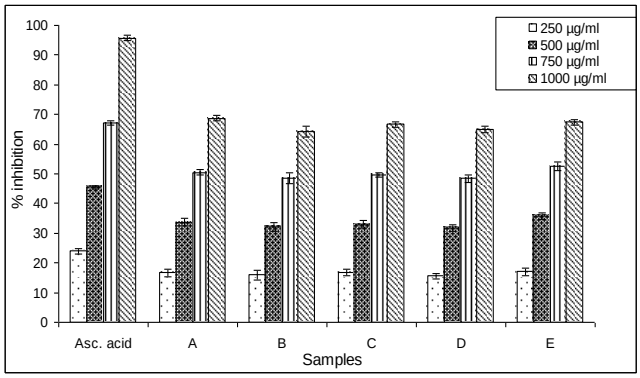

Figure 4 NO scavenging activity (% inhibition) of synthesized compounds

Antimicrobial activity

The synthesized compounds A-E were evaluated for their *in vitro* antibacterial activity against four bacterial strains *Klebsiella pneumoniae*, *Staphylococcus aureus*, *Pseudomonas aeruginosa*, *Escherichia coli* and *in vitro* antifungal activity against four fungal strains *Aspergillus niger*, *Alternaria flavus*, *Rhizopuss stonifer* and *Alternaria alternaria* by agar well diffusion method, using Ampicillin and Clotrimazole as standard for antibacterial and antifungal activities, respectively.

Antibacterial activity for 3-substituted-3-hydroxyindolin-2-ones derivatives

Antibacterial activity of the synthesized five compounds against human bacterial pathogens as determined by agar well diffusion method with Ampicillin as reference control was investigated. Antimicrobial results revealed that the maximum antibacterial activity was observed for compound C against *Staphylococcus aureus* and *Pseudomonas aeruginosa*. Compound **A** showed good antibacterial activity against *Escherichia coli*, *Staphylococcus aureus*, and *Pseudomonas aeruginosa*. Compound **B** and Compound **D** exhibited moderate activity against all tested antibacterial pathogens. Compound **E** did not show any activity against *Escherichia coli*. Compounds **C**, **D**, and **E** have not any antibacterial activity against *Klebsiella pneumonia*. The structure activity relationship demonstrates that 3-substituted-3-hydroxyindolin-2-ones derivatives **A** (R=H, R_1=Cl) and **C** (R=CH_3, R_1=Cl) showed good to moderate activity. From overall antibacterial activity results (Table 5), it was observed that compound **C** was the effective inhibitors against all the bacterial pathogens accept *Klebsiella pneumonia* and has shown equivalent activity comparable to standard drug Ampicillin against *Pseudomonas aurigonosa* but the activity of compound A was at par in case of *Pseudomonas aurigonosa*.

Antifungal activity for 3-substituted-3-hydroxyindolin-2-ones derivatives

The results of antifungal activity of synthesized compounds **A-E** revealed that only compound **B** showed moderate activity against *Alternaria flavus* and *Alternaria alternaria*. When the antifungal activity observed for all the compounds against *Aspergillus niger* Compound **B** does not show any resistance against this strain and compounds **A**, **C**,

Table 5. Effect of 3-hydroxy-3-phenacyl oxindoles derivatives (A-E) on the growth of some bacterial strains and fungicides

Compound	Antibacterial activity (zone of inhibition in mm)				Antifungal activity (zone of inhibition in mm)			
	E. coli	***P.aurigonosa***	***S. aureus***	***K.pneumonia***	***A. niger***	***A. flavus***	***R. stonifer***	***A.alternaria***
A	19.33±1.69	19.00±1.00	19.83±1.11	10.23±0.31	10±0.99	NA	NA	10.44±0.07
(AI)	**(0.698)**	**(0.926)**	**(0.743)**	**(0.406)**	**(0.357)**			**(0.413)**
B	19.91±0.87	13.21±1.69	16.28±0.73	18.45±0.33	NA	18.00±0.98	NA	18.23±0.22
(AI)	**(0.719)**	**(0.644)**	**(0.610)**	**(0.33)**		**(0.666)**		**(0.722)**
C	12.00±0.77	20±0.33	21.08±0.67	NA	11.66±0.51	14.78±0.67	NA	11.22±31
(AI)	**(0.433)**	**(0.975)**	**(0.790)**		**(0.416)**	**(0.547)**		**(0.444)**
D	18.66±0.87	17.55±0.91	14.22±0.35	NA	13.31±0.71	12.21±0.55	10.08±1.09	12.45±0.64
(AI)	**(0.674)**	**(0.856)**	**(0.533)**		**(0.698)**	**(0.452)**	**(0.555)**	**(0.493)**
E	NA	12±0.45	15.00±1.00	NA	8.88±0.32	11.21±0.31	NA	7.77±0.29
(AI)		**(0.585)**	**(0.562)**		**(0.317)**	**(0.415)**		**(0.307)**
Ampicillin	27.66±0.38	20.50±0.70	26.66±0.94	25.16±0.23	-	-	-	-
Clotrimazole	-	-	-	-	28.66±0.00	27.00±0.43	18.16±0.70	25.23±0.83

Mean± SE, NA= No activity, AI= activity index,

D, and **E** showed least activity against this strain when compared to reference strain i.e. Clotrimazole. When all the synthesized compounds were tested against *A. flavus*, compound **A** did not show any resistance against this fungal pathogen and compound **B** showed moderate activity while compounds **C**, **D**, and **E** showed least activity, while only compound **D** showed least resistance against *Rhizopuss stonifer* while other compounds **A**, **B**, **C**, **E** did not show any resistance. With *Alternaria alternaria*, only compound **B** showed moderate activity while compounds **A**, **C**, **D**, **E** showed least resistance. The results of antifungal activity are shown in Table 5.

From the results of antimicrobial activities, it is revealed that the majority of the synthesized compounds having $-CH_3$, an electron donating group in the indole ring and p-Cl, an withdrawing group substitution exhibited the maximum growth inhibitory activity. However, none of the compounds exhibited zone of inhibition more than that of the standards.

EXPERIMENTAL SECTION

The melting points of synthesized compounds were determined in open capillary tubes using Toshniwal apparatus. The purity of compounds was checked on thin layers of silica gelG–coatedglass plates with benzene ethylacetate (7:3) as eluent using iodine vapors as visualizing agents. ^1H and ^{13}C NMR spectra were recorded in $CDCl_3$ + DMSO-d_6 using tetramethylsilane (TMS) as an internal standard on a Bruker spectrophotometer at 400 and 100 MHz respectively. Mass spectrum of representative compound was recorded on a Jeol SX-102 spectrometer at 70eV. Infrared (IR) spectra were recorded on a Shimadzu Fourier transform (FT)–IR 8400S spectrophotometer using KBr pellets.

Sonication was carried out with the help of a standard ultrasonic irradiation instrument SonaprosPR-1000 MP (Oscar Ultrasonics Pvt. Ltd.) operating at 750W and generating 23-KHz output frequency. It has the following characteristics: Standard Titanium horn with a diameter of 6 mm/12mm, replaceable flat stain less steel tip, and digital thermometer to determine temperature. The glass reactor was designed and made from borosil glass.

General procedure for the synthesis of 3-hydroxy-3-substituted phenacyl indolin-2-one derivatives (A-E)

An equimolar mixture of isatin (2mmol, .294gm), p-Cl acetophenone (2mmol, .309gm) and K_2CO_3 (20mol%, .055 gm) in 5ml water was introduced in a 20-mL, heavy-walled, pear shaped, two necked flask with non standard taper outer joint. The flask was attached to a 12mm tip diameter probe, and the reaction mixture was sonicated at ambient temperature for the specified period at 50% power of the processor and 230W output in a 4-s pulse mode. At the end of the reaction period, thin-layer chromatography (TLC) was checked, and the flask was detached from the probe. The contents were transferred to a beaker. The formed solid was filtered off, washed thoroughly with warm water (2×20ml), and then dried to obtain crude products which were purified by crystallization from ethanol to give 3-hydroxy-3-substituted phenacyl indolin-2-one derivatives, giving satisfactory spectral and elemental analysis.

Synthesis of A[6a]. Yellow crystalline solid; Yield: 78%; IR (KBr, ν cm^{-1}): 1640 (CONH), 1760 ($COCH_2$), 3200 (NH), 3350 (OH). ^1H NMR ($CDCl_3$+DMSO-d_6) δ: 3.56 (d, J = 17.4 Hz, 1H), 4.06 (d, J = 17.4 Hz, 1H), 6.10 (brs, 1H), 6.79–7.91 (m, 8H, ArH), 10.30 (brs, 1H, NH); ^{13}C NMR($CDCl_3$+DMSO-d_6) δ: 44.2 ($CO\underline{C}H_2$), 71.6 (Spiro $\underline{C}$), 119.7, 121.9, 127.1, 128.0, 129.8, 133.2, 137.2, 141.2 (Aromatic $\underline{C}$), 176.9 ($\underline{C}ONH$), 193.6 ($\underline{C}OCH_2$). Anal. Calcd for $C_{16}H_{12}ClNO_3$: C, 63.69; H, 4.01; N, 4.64. Found: C, 63.67; H, 4.07; N, 4.68; Mass (m/z): 301 (M^+).

Synthesis of B[6a]. Yellow crystalline solid; Yield: 79%; IR (KBr, ν cm^{-1}) 1620 (CONH), 1720 ($COCH_2$), 3200 (NH), 3380 (OH). ^1H NMR ($CDCl_3$+DMSO-d_6) δ: 3.55 (d, J = 17.4, 1H), 4.05 (d, J = 17.4 Hz, 1H), 6.09 (brs, 1H), 6.63–7.60 (m, 8H, ArH), 10.61 (brs, 1H, NH); ^{13}C NMR ($CDCl_3$+DMSO-d_6) δ/ppm: 45.1 ($CO\underline{C}H_2$), 73.0(Spiro $\underline{C}$), 109.4, 121.2, 123.7, 127.6, 128.9, 129.9, 131.6, 131.8, 135.2, 142.9 (Aromatic $\underline{C}$), 178.2 ($\underline{C}ONH$), 195.8 ($\underline{C}OCH_2$).

Anal. Calcd for $C_{16}H_{12}BrNO_3$: C, 55.51; H, 3.49; N, 4.05. Found: C, 55.57; H, 3.52; N, 4.08; MS (m/z): 345 (M^+).

Synthesis of C. Yellow crystalline solid; Yield: 74%; IR (KBr, ν cm^{-1}): 1650 (CONH), 1720 ($COCH_2$), 3200 (NH), 3340 (OH); ^{1}H NMR ($CDCl_3$+DMSO- d_6) δ: 2.12 (s, 3H,-CH_3), 3.54 (d, *J* = 17.4 Hz, 1H), 3.99 (d, *J* = 17.4 Hz, 1H), 6.05 (s, 1H,-OH), 6.67-7.82 (m, 7H,-Ar-H), 10.23 (s, 1H,-NH); ^{13}C NMR ($CDCl_3$+DMSO- d_6) δ: 21.9 ($\underline{C}H_3$), 46.2 ($CO\underline{C}H_2$), 72.6 (Spiro $\underline{C}$), 120.7, 121.9, 127.1, 128.3, 129.0, 129.8, 133.2, 137.2, 141.2 (Aromatic $\underline{C}$), 176.7 ($\underline{C}ONH$), 193.8 ($\underline{C}OCH_2$). Anal. Calcd for $C_{17}H_{14}ClNO_3$: C, 64.70; H, 4.50; N, 4.48. Found: C, 64.67; H, 4.47; N, 4.44; Mass (m/z): 315 (M^+).

Synthesis of D. Yellow crystalline solid**;** Yield: 76%; IR (KBr, ν cm^{-1}): 1640 (CONH) , 1700 ($COCH_2$),3200 (NH), 3340 (OH); ^{1}H NMR ($CDCl_3$+DMSO-d_6) δ: 2.14 (s, 3H,-CH_3), 3.58 (d, *J* = 17.4 Hz, 1H), 4.09 (d, *J* = 17.4 Hz, 1H), 6.08 (s, 1H,-OH), 6.77-7.78 (m, 7H,-Ar-H), 10.23 (s, 1H,-NH); ^{13}C NMR ($CDCl_3$+DMSO- d_6) δ: 21.6 ($\underline{C}H_3$), 47.5 ($CO\underline{C}H_2$), 72.7 (Spiro $\underline{C}$), 120.8, 121.4, 127.8, 128.5, 129.5, 130.2, 133.8, 139.1 (Aromatic $\underline{C}$), 176.4 ($\underline{C}ONH$), 192.9 ($\underline{C}OCH_2$). Anal. Calcd for $C_{17}H_{14}BrNO_3$: C, 56.70; H, 3.92; N, 3..89. Found: C, 56.67; H, 3.90; N, 3.84; Mass (m/z): 359 (M^+).

Synthesis of E[5c]. Yellow crystalline solid; **(**Yield: 70%); IR (KBr, ν cm^{-1}): 1650 (CONH), 1780 ($COCH_2$), 3210 (NH), 3360 (OH); ^{1}H NMR ($CDCl_3$+DMSO- d_6) δ: ($CDCl_3$+DMSO-d_6) δ: 2.24 (s, 3H,-CH_3), 3.51 (d, *J* = 17.4 Hz, 1H), 3.96 (d, *J* = 17.4 Hz, 1H), 5.80 (s, 1H,-OH), 6.67-7.82 (m, 7H,-Ar-H), 10.27 (s, 1H,-NH); ^{13}C NMR ($CDCl_3$+DMSO- d_6) δ: 21.2 ($\underline{C}H_3$), 47.9 ($CO\underline{C}H_2$), 72.9 (Spiro $\underline{C}$), 115.8, 120.8, 127.7, 128.3, 130.0, 133.2, 133.8, 139.1, 166.5 (Aromatic $\underline{C}$), 176.1 ($\underline{C}ONH$), 190.9 ($\underline{C}OCH_2$). Anal. Calcd for $C_{16}H_{12}FNO_3$: C, 68.22; H, 4.71; N, 4.68. Found: C, 68.26; H, 4.72; N, 4.71;Mass (m/z): 299 (M^+).

Antioxidant activity

Antioxidant activities of test compounds were measured by estimating DPPH• and $ABTS^{+\bullet}$ scavenging activity *in vitro* using ascorbic acid as reference compound. All experiments were made in triplicate and results of the present study were expressed as mean ± SE.

DPPH• scavenging activity

Ability of test compound to scavenge the stable free radical DPPH• was measured by the method of Mensor *et al.*[13] Absorbance was recorded at 517 nm in a UV-Vis double beam spectrophotometer. The percent inhibition (φ, in %) was calculated by using the following formula.

$$\varphi = \frac{AC - AA}{AC} * 100$$

where

AC = absorption of control, and

AA = absorption of test.

ABTS radical scavenging activity

$ABTS^{+\bullet}$ scavenging activity of synthesized compounds were measured by the method of Re *et al.*[14]

Nitric oxide scavenging activity

The interaction of test compounds with nitric oxide (NO) was assessed by the nitrite detection method. Sodium nitropruside (5 mM) in phosphate buffer spontaneously generates NO in an aqueous solution.[15] NO interacts with oxygen and produces nitrite ions, which can be estimated by use of Greiss reagent.

Antimicrobial activity

Antibacterial and Antifungal activity of synthesized compounds were studied.

Microorganisms Used

Clinical laboratory bacterial isolates of Klebsiella pneumoniae, Staphylococcus aureus, Pseudomonas aeruginosa, Escherichia coli and fungal isolates viz. Aspergillus niger, A. flavus, Rhizopuss stonifer and Alternaria alternaria were collected from the stock cultures of Microbiology Laboratory, SMS Medical College, Jaipur India.

Culture and Maintenance of Bacteria

Pure cultures of *E. coli*, *P. aerugonosia. S. aureus* and *K. pnemonae* obtained from S.M.S. Medical College, Jaipur, India were used as indicator organisms. These bacteria were grown in Nutrient agar medium (prepared by autoclaving 8% Nutrient agar of Difeco-Laboratories, Detroit, USA, in distilled water at 15 lbs psi for 25-30 min) and incubated at 37°C for 48 hrs. Each bacterial culture was further maintained on the same medium after every 48 h of transferring.

A fresh suspension of test organism in saline solution was prepared from a freshly grown agar slant before every antimicrobial assay.

Determination of Antibacterial Assay

In vitro antibacterial activity of the synthesized compounds were studied against gram positive and gram negative bacterial strains by the agar well diffusion method.[16] Mueller Hinton agar no. 2 (Hi Media, India) was used as the bacteriological medium. The compounds' were diluted in 100% dimethylsulphoxide (DMSO) at the concentrations of 5 mg/mL. The Mueller Hinton agar was melted and cooled to 48-50ºC and a standardized inoculum (1.5×108 CFU/mL, 0.5 McFarland) was then added aseptically to the molten agar and poured into sterile petri dishes to give a solid plate. Wells were prepared in the seeded agar plates. The test compound (100 µL) was introduced in the well (the wells were made through cork borer vertically to Petri plate up to 10 mm). The plates were incubated overnight at 37ºC. The antimicrobial spectrum of

the extract was determined for the bacterial species in terms of zone sizes around each well. The diameters of zone of inhibition produced by the agent were compared with those produced by the commercial control antibiotics, streptomycin. For each bacterial strain controls were maintained where pure solvents were used instead of the synthetic compound. The control zones were subtracted from the test zones and the resulting zone diameter was measured with antibiotic zone reader in mm (the diameter is taken through the centre point of zone of inhibition and a zone of inhibition was calculated after adding the sample which can be visualized on the surface of the plate inoculated with bacteria and fungi). The experiment was performed three times to minimize the error and the mean values were presented.

Determination of Antifungal assay

Antifungal activity of the synthesized compounds were investigated by agar well diffusion method.[17] Fungus colonies were subcultured onto Sabouraud's dextrose agar, SDA (Merck, Germany) and respectively incubated at 37°C for 24 h and 25°C for 2-5 days. Suspensions of fungal spores were prepared in sterile PBS and adjusted to a concentration of 106 cells/mL. Dipping a sterile swab into the fungal suspension and rolled on the surface of the agar medium. The plates were dried at room temperature for 15 min. Wells of 10 mm in diameter and about 7 mm apart were punctured in the culture media using sterile glass tube. 0.1 mL of several dilutions of fresh extracts was administered to fullness for each well. Plates were incubated at 37°C. After incubation of 24 h bioactivities were determined by measuring the diameter of inhibition zone in mm. All experiments were made in triplicate and means were calculated.

CONCLUSION

We describe herein potassium carbonate catalysed highly efficient, green protocol for the synthesis of 3-substituted-3-hydroxyindolin-2-ones derivatives by the reaction of substituted indole-2, 3-diones and substituted aryl ketones in aqueous medium under ultrasound irradiation in excellent yields. The present methodology offered several advantages, such as simple procedure, lowcost, easywork-up, short reaction times, and milder conditions.We have also developed a novel and potent antioxidant and antimicrobial agents of synthetic origin. All desired products, showed good activities. **Compound A** (3-hydroxy-3-[2-oxo-2-(4-chloro-phenyl)ethyl]indolin-2-one) and **Compound E** (5-methyl-3-hydroxy-3-[2-oxo-2-(4-fluorophenyl)ethyl]indolin-2-one) have highest DPPH$^{\bullet}$, ABTS$^{\bullet+}$ and NO radical scavenging activity as compared to other compounds. **Compound C** (5-methyl-3-hydroxy-3-[2-oxo-2-(4-chloro-phenyl)ethyl]indolin-2-one) was the effective inhibitors against all the bacterial pathogens. **Compound A** (3-hydroxy-3-[2-oxo-2-(4-Chloro-phenyl)ethyl]indolin-2-one) and **Compound C** (5-methyl-3-hydroxy-3-[2-oxo-2-(4-chloro-phenyl)ethyl]indolin-2-one) showed equivalent activity comparable to standard drug Ampicillin against *Pseudomonas aurigonosa*.

ACKNOWLEDGEMENTS

Financial assistance from the C.S.I.R. (02(0143)/13/EMR-II), New Delhi is gratefully acknowledged. We are also thankful to the Central Drug Research Institute (CDRI), Lucknow for the spectral analyses and elemental analyses and Department of Zoology and Botany, University of Rajasthan, Jaipur for the biological evaluation.

REFERENCES

[1]Bast, A., Haenen, G., and Doelman, C., *Am. J. Med.* **1991,** *91*, (Suppl. 3C) 2S-13S.

[2]Bulkely, G. B., *Surgery*. **1993**, *113*, 479-483.

[3]Gazit, A., Osherov, N., Posner, I., Yaish, P., Poradosu, E., Gilon, C., and Levitzki, A., *J. Med. Chem.* **1991**, *34*, 1896-1907.

[4](a) Tang, Y. -Q., Sattler, I., Thiericke, R., Grabley, S., and Feng, X.-Z., *Eur. J. Org. Chem.* **2001,** 261-267; (b) Kagata, T., Saito, S., Shigemori, H., Ohsaki, A., Ishiyama, H., Kubota, T., and Kobayashi, J., *J. Nat. Prod.* **2006**, *69*, 1517-1521; (c) Schulz, V., Davoust, M., Lemarie´, M., Lohier, J. –F., de Oliveira Santos, J. S., Metzner, P., and Brière, J. –F., *Org. Lett.* **2007**, *9*, 1745-1748; (d) Koguchi, Y., Kohno, J., Nishio, M., Takahashi, K., Okuda, T., Ohnuki, T., and Komatsubara, S., *J. Antibiot.* **2000**, *53*, 105-109; (e) Kamano, Y., Zhang, H., -P., Ichihara, Y., Kizu, H., Komiyama, K., and Pettit, G. R., *Tetrahedron Lett.* **1995**, *36*, 2783-2784; (f) Franz, A. K., Dreyfuss, P. D., and Schreiber, S. L., *J. Am. Chem. Soc.* **2007**, *129*, 1020-1021; (g) Yong, S. R., Ung, A. T., Pyne, S. G., Skeltonb, B. W., and White, A. H., *Tetrahedron* **2007**, *63*, 5579-5586.

[5](a)Joshi, K. C., Dandia, A., and Bhagat, S., *J. Indian Chem. Soc.* **1990**, *67*, 753-756; (b) Joshi, K. C., Dandia, A., and Bhagat, S., *Indian J. Chem. Sec B.* **1992**, *31*, 98-104; (c) Dandia, A., and Gupta, A., *J. Indian Chem. Soc.* **1995**, *72*, 833-835; (d) Dandia, A., Kumar, A., Sehgal, V., and Rani, B., *Indian J. Chem. Sec B.* **1996**, *35*, 1314-1316; (e) Dandia, A., Singh, R., Kumar, G., Arya, K., and Sachdeva, H., *Heterocyclic comun.* **2001**, *7*, 571-576; (f) Dandia, A., Sati, M., Arya, K., Sharma, R., and Loupy, A., *Chem. Pharma. Bull.* **2003**, *51*, 1137-1141; (g) Dandia, A., Arya, K., Khaturia, S., and Yadav, P., *ARKIVOC* **2005**, *Xiii*, 80-88; (h) Dandia, A., Singh, R., and Bhaskaran, S., *Ultrason. Sonochem.* **2011**, *18*, 1113-1117.

[6](a) Chen, W.–B., Liao, Y.–H., Du, X.–L., Zhanga, X.–M., and Yuan, W.–C., *Green Chem.* **2009**, *11*, 1465-1476; (b) Srihari, G., and Murthy, M. M., *Synth. Commun.* **2011**, *41*, 2684-2692; (c) Allu, S., Molleti, N., Panem, R., and Singh, V. K., *Tetrahedron Lett.* **2011**, *52*, 4080-4083; (d) Kumar, V. P., Reddy, V. P., Sridhar, R., Srinivas, B., Narender, M., and Rao, K. R., *J. Org. Chem.* **2008**, *73*, 1646-1648; (e) Popp, F. D., and Donigan, B. E., *J. Pharma. Sci.* **1979**, *65*, 519-520; (f) Hanhan, N. V., Sahin, A. H., Chang, T. W., Fettinger, J. C., and Franz, A. K., *Angew. Chem. Int. Ed.* **2010**, *49*, 744-747; (g) Shanti, G., Lakshmi, N. V., and Perumal, P. T., *Arkivoc* **2009**, *X*, 121-130.

[7]Mondal, R., Gupta, A. D., and Mallik, A. K., *Tetrahedron Lett.* **2011**, *52*, 5020–5024.

[8]Imanzadeh, G., Kazemi, F., Zamanloo, M., and Mansoori, Y., *Ultrasonics Sono.* **2013**, *20*, 722-728.

[9]Cravotto, G., and Cintas, P., *Chem. Soc. Rev.* **2006**, *35*, 180-196.

[10]Cella, R., and Stefani, H. A., *Tetrahedron* **2009**, *65*, 2619-2641.

[11](a) Dandia, A., Singh, R., Joshi J. and Maheshwari, S., *Eur. Chem. Bull.*, **2013**, *2(10)*, 825-829; (b) Dandia, A., Singh, R., Joshi, J. and Kumari, S:, *Eur. Chem. Bull*., **2013**, *2(9)*, 683-686; (c) Dandia, A., Gupta, S. L. and Bhaskaran, S., *Eur. Chem. Bull*., **2013**, *2(11)*, 836-841; (d) Dandia, A., Parewa, V., Gupta, S. L. and Rathore K. S., *J. Mol. Catal. A- Chem.* **2013**, *373*, 61-71; (e) Dandia, A., Gupta, S. L., Sudheer and Quraishi M. A., *J. Mater. Environ. Sci.*, **2012**, *3*, 993-1000;

(f) Dandia, A., Jain, A. K., and Bhati, D. S., *Tetrahedron lett.* **2011**, *52*, 5333-5337; (g) Dandia, A., Singh, R., and Bhaskaran, S., *Ultrason. Sonochem.* **2010**, *17*, 399-401; (h) Dandia, A., Sati, M., Arya, K. and Loupy, A., *Green Chem.*, **2002**, *4*, 599-602; (i) Dandia, A., Singh, R., and Khaturia, S., *Bioorg. Med. Chem.*, **2006**, *14*, 1303-1308; (j) Dandia, A., and Arya, K., *Bioorg. Med. Chem. Lett.* **2008**, *18*, 114-119.

[12](a) Escudero, M. A., Kremenchuzky, L. D., Perillo, I. A., Cereletto, H. and Blanco, M. M., *Synthesis* **2011**, 571-576; (b) Chee, F. C., Buckle, M. J. C. and Rahman, N. A., *Tetrahedron Lett*. **2011**, *52*, 3120-3123; (c) Matsugi, M., Takeda, N., Takashi, A., Tazaki, T., Tamura, H. and Shioiri, T., *Chem. Pharm. Bull.* **2010**, *58*, 1107-1110; (d) Samanta, S., Jana, R. and Ray, J. K., *Tetrahedron Lett.* **2009**, *50*, 6751-6754; (e) Ballini, R., osica, G., Palmirri, A. and Bakhtiari, K., *Synlett* **2009**, 268-270.

[13]Mensor, L. L., Menezes, F. S., Leitao, G. G., Reis, A. S., Dos Santos, T. C., Coube, C. S. and Leitao, S. G. *Phytother Res.* **2001**, *15*,127-130.

[14]Re, R. E., Pellegrini, N., Proteggente, A., Pannal, A., Yang, M. and Rice-Evans, C., *Free Radical Biol. Med.* **1999**, *26*, 1231-1237.

[15] Sreejayan and Rao, M. N. A., *J. Pharma. Pharmacol.* **1997**, *49*, 105-107.

[16]Perez, C., Paul, M. and Bazerque, P., *Acta. Biol. Med. Exp.* **1990**, *15*, 113-115.

[17]Bonjar, S., Aghighi, S and Karimi , N. A., *J. Biol. Sci.* **2004**, *4*, 405-412.

Received: 10.06.2013.
Accepted: 26.11.2013.

ACTIVATION ENERGY FOR THE PYROLYSIS OF POLYMER WASTES

J. A. Al-Furhood,[a] F. D. Alsewailem,[b]* and L. A. Almutabaqani[a]

Keywords: pyrolysis, polystyrene (PS), high density polyethylene (HDPE), polyethyleneterephthalate (PET), activation energy, degradation

Pyrolysis of virgin and discarded polystyrene, polyethylene, and polyethyleneterephthalate was done by the means of thermo-gravimetric technique. Activation energy was measured by fitting the experimental data to the n^{th} order model. Results have shown that discarded polymers had less activation energy values than those of the virgin polymers. Consequently, energy required for the pyrolysis of discarded polymers must be much less than what is required for virgin polymers. The n^{th} order model has been modified by introducing a new factor which is called degradation index, d_i. The degradation index, d_i, accounts for the degradation history of the material. d_i ranges from 0 to 1 and when it approaches 0 it implies that degradation is anticipated to be severe. When d_i approaches 1 it implies that polymeric material is virgin. The approach given by current research, i.e. accounting for actual activation energy for discarded polymers, may be crucial for saving energy when recycling plastics materials by pyrolysis.

*Corresponding Author
Tel: +966-1-4813522
Fax: +966-1-4813670
E-Mail: fsewailm@kacst.edu.sa
[a] **C**hemistry Department, College of Science, Princes Norah Bint Abdulrahman University, P.O.Box 84428 Riyadh 11671, Saudi Arabia
[b] Petrochemicals Research Institute, King Abdulaziz City for Science and Technology (Kacst), P.O.Box 6086 Riyadh 11442, Saudi Arabia

Introduction

In quest to resolve polymeric waste problem, researchers have been attempting to find efficient, scientific, and technological sound solutions to reduce amounts of polymeric waste that end up in landfills. Pyrolysis is one of the methods of recycling polymeric waste into value added products such as lubricants, liquid fuels, and combustible gases. Pyrolysis is an endothermic process where polymers , mainly in form of plastics, are subject to enormous heat in the absence of oxygen. During the course of pyrolysis reaction, polymeric materials can undergo chemical decomposition which leads to the formation of small molecules. Temperature, pressure, and heating time are the most important parameters that control the pyrolysis reaction. Catalysts and solvents may be used to increase the rate of reaction and decrease the operating temperature of the pyrolysis process. At relatively high temperature, e.g. greater than 600 ºC, gases with low molecular weight such as methane can evolve while at lower temperature range, e.g. less than 400 ºC, and when the pressure inside the pyrolysis reactor increases, materials may decompose to viscous fluids and carbon black. Various polymers may be recycled by the means of pyrolysis; high density polyethylene (HDPE), polystyrene (PS), and polyethyleneterephthalate (PET), polypropylene (PP), and polyvinyl chloride (PVC) to name some. However some of these polymers such as HDPE wastes require very high temperature in order to efficiently recycle them by pyrolysis, and in spite of this fact some unwanted by products such as the low quality wax may be produced.[1,2] Dynamic thermo gravimetric analysis (TGA) is a suitable technique to study the thermal degradation of polymers and determine the kinetic parameters such as activation energy, reaction order, and frequency factor.

Several models are available in the literature for studying the kinetics of pyrolysis for polymers.[3-9] The origin of these mathematical models was based on a multiplication of two fundamental relations; Arrhenius equation and mass loss function; i.e.:

$$\frac{d\alpha}{dt} = k(T)F(\alpha) \qquad (1)$$

where α is the fraction of mass loss. $K(T)$, and $F(\alpha)$ are given by the following relations respectively:

$$k(T) = A_0 e^{-\frac{E}{RT}} \qquad (2)$$

$$F(\alpha) = (1-\alpha)^n \qquad (3)$$

where A_0 (min^{-1}) is Arrhenius equation constant or the frequency factor, E is the activation energy (kJ mol^{-1}), and n is the order of reaction.

Several researches have been conducted in the past to calculate the activation energy of the pyrolysis for most of commodity polymers such as HDPE, PS, and PET using thermal techniques.[10-16] Despite the relatively adequate available publications that dealt with calculating activation energy for polymers, most of the studies used virgin polymers and less attention has been made to quantitatively determine activation energy for discarded polymers. Most

importantly and to the best knowledge of the authors of this research, no single study has done a comparative investigation of the activation energy of virgin and discarded polymers. Discarded polymers are susceptible to different kinds of degradations. One form of degradation that may occur in recycled polymers is the thermo-oxidative degradation where polymeric materials are exposed to harsh weather including high temperature and humidity.[17]

Hypothesis and model development

Because pyrolysis process consumes high energy for converting plastic wastes, the aim of this work was to calculate the activation energies (using n^{th} order kinetic model) of the discarded polymers and compare them with those of the virgin polymers in order to provide adequate energy needed for the pyrolysis of recycling process. It is fairly logic to postulate that discarded plastics which were subject to some kinds of degradation may not require as high energy as that needed to pyrolysis virgin plastics. Therefore it might be necessary that n^{th} order model be modified by introducing a factor that accounts for degradation effect.

Combining equations 1 to 3 and taking the linear form would lead to the following relation

$$\ln\frac{d\alpha}{dt} = \ln A_0 - \frac{E}{RT} + n\ln(1-\alpha) \qquad (4)$$

Rearranging Equation 4 after introducing heating rate, $\beta = dT/dt$, gives us the following relation

$$\left[\ln\frac{\beta d\alpha}{dT} - n\ln(1-\alpha)\right] = \ln A_0 - \frac{E}{RT} \qquad (5)$$

However, activation energy, E in Equation 5 needs to be modified in order to be utilized for discarded plastics. Equation 5 may then be rewritten as

$$\left[\ln\frac{\beta d\alpha}{dT} - n\ln(1-\alpha)\right] = \ln A_0 - \frac{E_{act}}{RT} \qquad (6)$$

where E_{act} is the actual activation energy and equals $d_i \times E$, where d_i , degradation index, is a correction factor which indicates the degradation history of the plastic material. This factor, d_i, may be quantitatively correlated to some forms of detection of degradation in polymeric materials such as reduction in molecular weight or carbonyl group index in Fourier transform infrared (FT-IR). d_i may range from 0 to 1, and when d_i=1, $E_{act} = E$ which is the activation energy for virgin material.

Materials and methods

Materials used

Polymers tested in this study were categorized into the following groups:

Group I was the virgin polymers; high density polyethylene (HDPE), general purpose polystyrene (PS), and polyethyleneterephthalate (PET). All these polymers were supplied in pellet form by Saudi basic industries corporation (SABIC) in Saudi Arabia. Throughout the text of this research, materials of this group will be referred as HDPE-V, PS-V, and PET-V.

Group II was the virgin polymers that used in group I after subjected to sunlight during summer period for three months in open air where the average temperature was about 46.5° C and average humidity was 35.13%. Throughout the text of this research, materials of this group will be referred as HDPE-D1, PS-D1, and PET-D1.

Group III was some discarded polymer articles of the same kind of those used in group I with unknown degradation history. Samples; in form of bottles, dishes and cutlery, were collected from remote areas near Riyadh, Saudi Arabia where the environment is extremely harsh. Throughout the text of this research, materials of this group will be referred as HDPE-D2, PS-D2, and PET-D2.

Sample preparation and testing

All materials used in this study, i.e. groups I to III, were ground into small particles ~ less than 0.5 mm in size using a plastic granulator type IKA MF 10 equipped with a sieve of size 0.5 mm. Degradation assessment was done by using a Bruker Alpha FTIR. Pyrolysis of all samples was carried out by a Perkin-Elmer thermo-gravimetric analyzer (TGA) type TGA-7. Samples ranging from 10-15 μg were heated inside the TGA furnace from 25º C to 700º C under a continuous purging of helium.

Results and discussions

FTIR degradation analysis

It is important to clarify in the beginning of this section that the aim of current study was not to discuss in extensive details the FTIR analyses of the virgin and discarded polymeric materials used by this study. This has already been investigated thoroughly in the past. The objective of presenting FTIR results here was rather to prove the occurrence of degradation for the polymers of interest. Figures 1-3 show the FTIR spectra for all materials used in this study. One can see that there is a clear contrast in the absorption capacities of the main bands for the virgin polymers in comparison with those of the discarded polymers. The contrast is more pronounced when comparing virgin polymers, i.e. group I, with discarded polymers in group III where the polymeric materials were believed to be subjected to harsh degradation environment.

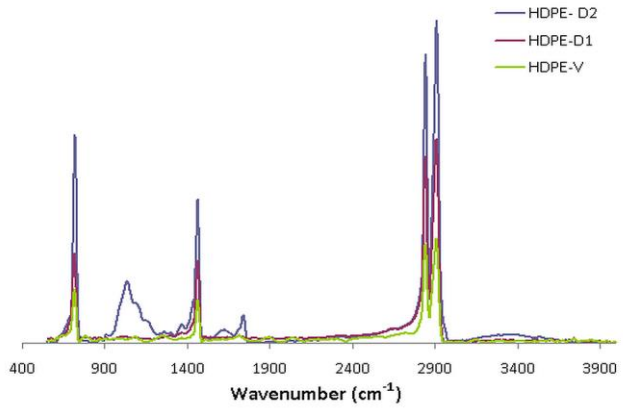

Figure 1. FTIR spectra showing the absorption by virgin and discarded HDPE samples

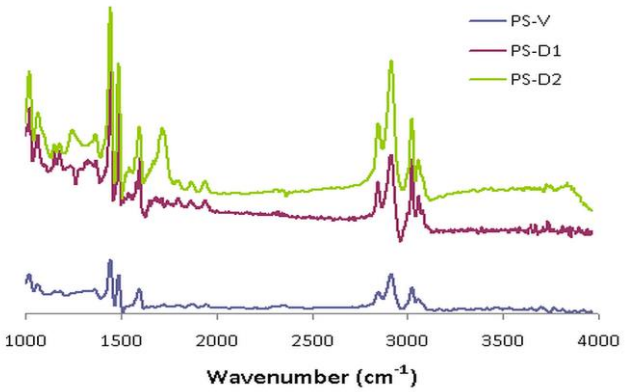

Figure 2. FTIR spectra showing the absorption by virgin and discarded PS samples.

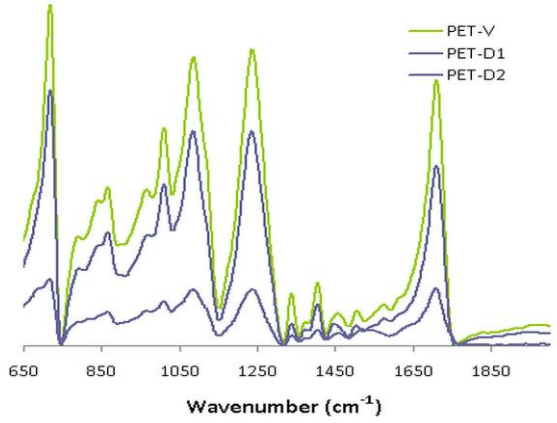

Figure 3. FTIR spectra showing the absorption by virgin and discarded PET samples**.**

It is also clear to notice that in the polyolefin's polymers, i.e. HDPE and PS, where the polymerization is done by addition or chain growth mechanism the absorption of infra red light is greater for discarded materials, i.e. HDPE-D1, HDPE-D2, PS-D1, and PS-D2. The prolonged exposure to sever temperature and sunlight may develop new chemical bonds within polymer chain in the presence of oxygen where some chemical groups such as the carbonyl may be present. This interpretation is consistent with that of other studies reported in the literature.[18,19] In contrast, the condensation or step growth polymer, i.e. PET, shows opposite FTIR behaviour in comparison with that of HDPE and PS. Here as seen in Figure 3, absorption capacities of main bands in PET tend to decrease upon increasing degradation history. Here one can conclude that the increase or decrease in capacities of FTIR absorption for the main bands of polymers used by this study with the virgin ones as references indicated the occurrence of degradation.

Pyrolysis analysis

The data of weight loss versus pyrolysis temperature as done by TGA were manipulated to get corresponding data needed to plot $1/T$ versus $\ln(\beta d\alpha/dT) - n\ln(1-\alpha)$ as given in Equation 5. Heating rate β = 10º C/min and n=1 were used for all calculations related to such data. Figure 4 shows the relationship between $\ln[(\beta d\alpha/dT)/(1-\alpha)]$ and the reciprocal temperature for the experimental data of pyrolysis of virgin and discarded polystyrene.

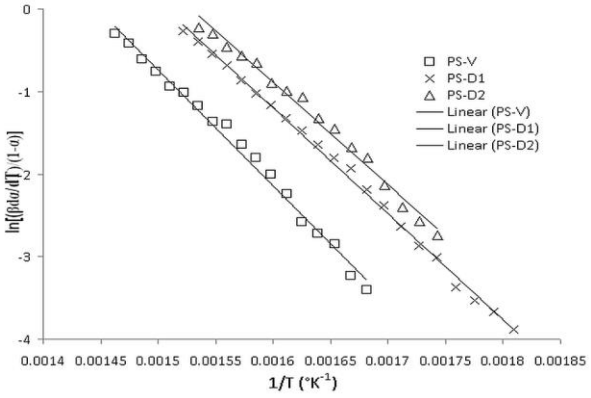

Figure 4. $1/T$ vs. $\ln[(\beta d\alpha/dT)/(1-\alpha)]$ for virgin and discarded PS. Solid lines show the fitting of experimental data to linear models.

Solid lines represent fitting of the experimental data to suitable linear models where activation energies, E, and frequency factors, A_0, may be easily calculated. These values, E and A_0 are tabulated in Table 1.

Table 1. Values of activation energies and frequency factors for virgin and discarded PS.

Material	Activation energy, E, kJ mol^{-1}	Frequency factor lnA_0, min^{-1}	R^2
PS-V	116.86	20.353	0.9909
PS-D1	106.93	19.383	0.9972
PS-D2	103.14	18.957	0.9889

Similarly Figures 5-6 and Tables 2-3 show the relationship between $\ln[(\beta d\alpha/dT)/(1-\alpha)]$ and $1/T$ and values of E and A_0 for HDPE and PET respectively.

Table 2. Values of activation energies and frequency factors for virgin and discarded HDPE.

Material	Activation energy, E, kJ mol^{-1}	Frequency factor lnA_0, min^{-1}	R^2
HDPE-V	176.010	21.947	0.9253
HDPE-D1	133.498	20.801	0.9877
HDPE-D2	117.419	19.233	0.9774

 DOI: 10.17628/ecb.2014.3.93-97

Table 3. Values of activation energies and frequency factors for virgin and discarded PET.

Material	Activation energy, E, kJ mol^{-1}	Frequency factor, lnA_0, min^{-1}	R^2
PET-V	235.62	37.366	0.9784
PET-D1	207.51	34.97	0.9624
PET-D2	113.96	20.42	0.9821

Tables 1-3 clearly show that the values of activation energy tend to decrease when the material has a degradation history. This is clearly seen in the group III materials were it is anticipated that degradation history was extremely severe.

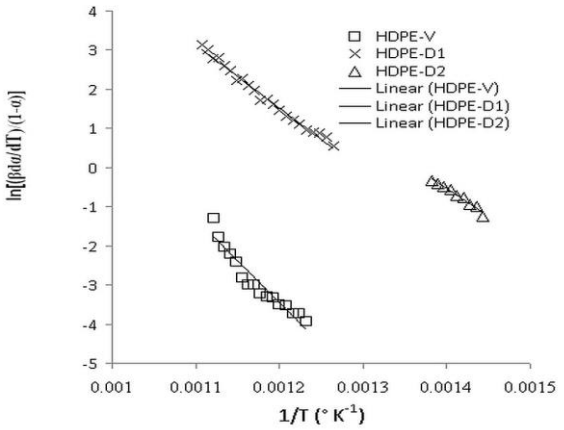

Figure 5. 1/*T* vs. ln[(βdα/d*T*)/(1-α)] for virgin and discarded HDPE. Solid lines show the fitting of experimental data to linear models.

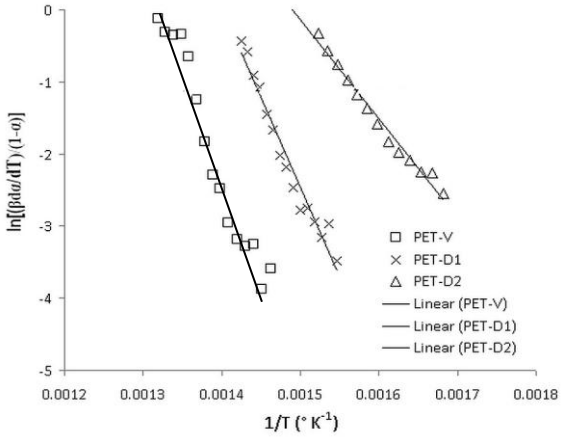

Figure 6. 1/*T* vs. ln[(βdα/d*T*)/(1-α)] for virgin and discarded PET. Solid lines show the fitting of experimental data to linear models.

With the exception of PET-D2 in Table 3, A_0 has an average value of 19 min^{-1} for PS, 20 min^{-1} for HDPE, and 36 min^{-1} for PET. This suggests that when discarded polymers are to be processed by pyrolysis, the activation energy must be less than that of the virgin polymers of same kinds. This may imply that energy can be saved when processing discarded polymers by pyrolysis. This is also supported by the TGA scans (not shown here) of virgin and degraded polymers of same type were degraded polymers tended to decompose at lower temperature values. Activation energy E is an important parameter in the n^{th} order relation that is routinely used to fit TGA data. The reduction in activation energy for the discarded polymers in comparison with that of the virgin ones is proportionally related to the degradation history of the material. Here, as given in Equation 6, the degradation index d_i , suggested by current study represents the degradation history of the material. The calculation of d_i for all materials used in this study is given in Table 4.

Table 4. Degradation index calculations

Material	Activation energy E, kJ mol^{-1}	Degradation index, d_i
PS-V	116.86	1
PS-D1	106.93	0.92
PS-D2	103.14	0.88
HDPE-V	176.01	1
HDPE-D1	133.498	0.76
HDPE-D2	117.419	0.67
PET-V	235.62	1
PET-D1	207.51	0.88
PET-D2	113.96	0.48

This degradation index may be correlated to some quantitative measurements that asses the degradation in polymeric materials such as the reduction in molecular weight or area under the curves of FTIR spectra. By knowing di, one may be able to estimate, using equation 6, the actual activation energy needed to pyrolysis discarded polymers. The modified correlation, equation 6, which is suggested by authors of current study, allows calculating actual activation energy which is required to pyrolysis discarded polymers by introducing a new factor, i.e. d_i ranging from 0 to 1 that accounts for degradation history. This strategy is crucial in saving energy by providing only actual activation energy for the pyrolysis of discarded polymers. The reader now should realize that pyrolysis of discarded polymers would require less activation energy than that of the virgin polymers, therefore one needs to calculate actual activation energy for such materials and hence overall energy may be saved.

Conclusions

Since the pyrolysis of discarded polymers would require less activation energy than that of the virgin polymers, one needs to calculate actual activation energy for such materials and hence overall energy may be saved. A new factor, di, which is called degradation index, has been suggested by authors of current study as a correction factor in the n^{th} order relation. This new correction factor accounts for degradation history of polymeric materials. The new term, actual activation energy (E_{act}), introduced by this study was used to modify n^{th} order model as given in equation 6. $E_{act} = d_i \times E$ where d_i may vary from 0 to 1 depending on the degradation history of the material. When $d_i = 1$, $E_{act} = E$ which is the activation energy for virgin material.

Acknowledgments

The experimental work of this study has been performed in the laboratories of king Abdulaziz city for science and technology (KACST). The authors highly appreciate Kacst's help.

References

[1]Scheirs, J., Kaminsky, W., *Feedstock Recycling and Pyrolysis of Waste Plastics: Converting Waste Plastics into Diesel and Other Fuels*, John Wiley, UK, **2006**.

[2]Vasile, C., Pakdel, H., Mihai, B., Onu, P., Darie, H., Ciocalteu, S., *J. Anal. Appl. Pyrol.*, **2001**, *57*, 287-303.

[3]Kissinger, H. E., *Anal. Chem.*, **1957**, *29*, 1702-1706.

[4]Flynn, J. H., Wall, L. A., *J. Polym. Sci. Part B: Polym. Lett*., **1966**, *4*, 323 -328.

[5]Friedman, H. L., *J. Polym. Sci. Part C*, **1965**, *6*, 183-195.

[6]Van Krevelen, D. W., Heerden, C. V., Huntjens, F. J., *Fuel*, **1951**, *30*, 253.

[7]Coats, A. W., Redfern, J. P., *J. Polym. Sci. Part B: Polym. Lett.*, **1965**, *3*, 917-920.

[8]Reich, L., *J. Polym. Sci. Part B: Polym. Lett*., **1964**, *2*, 621-623.

[9]Reich, L., *J. Polym. Sci. Part B: Polym. Lett*., **1965**, *3*, 231-234.

[10]Urzendowski, S. R., Guenther, A. H., *J. Therm. Anal. Calorim.*, **1971**, *4*, 179-395.

[11]Jenekhe, S. A. , Lin, J. W., Sun, B., *Thermochim. Acta*., **1983**, *61*, 287-299.

[12]Ravanetti, G. P., Zini, M., *Thermochim. Acta.*, **1992**, *207*, 53-64.

[13]Park, J. W., Oh, S. C., Lee, H. P., Kim, H. T., Yoo, K. O., *Polym. Degrad. Stab*., **2000**, *67*, 535-540.

[14]Lee, S. Y., Yoon, J. H., Kim, J. R., Park, D. W., *Polym. Degrad. Stab*., **2001**, *74*, 297-305.

[15]Saha, B., Ghoshal, A. K., *Chem. Eng. J.*, **2005**, *111*, 39-43.

[16]Yuan, X., Li, C., Guan, G., Xiao, Y., Zhang, D., *Polym. Degrad. Stab*., **2008**, *93*, 466-475.

[17]Alsewailem, F. D., *Int. J. Polym. Mat.*, **2009**, *58*, 77-86.

[18]Parres, F., Sanchez, L., Balart, R., Lopez, J., *J. Anal. Appl. Pyrol.*, **2007**, *78*, 250-256.

[19]Han, S. O., Lee, D. W., Han, O. H., *Polym. Degrad. Stab.*, **1999**, *63*, 237-243.

Received: 06.11.2013.

Accepted: 27.11.2013.

MINERAL ELEMENT CONTENT AND ANTIOXIDANT CAPACITY OF SOME LATVIAN BERRIES

Andrejs Skesters[a], Dénes Kleiner[b], Anna Blázovics[b], Zoltán May[c], Dóra Kurucz[b], Alise Silova[a], Klára Szentmihályi[c]

Keywords: mineral elements, free radical scavenging capacity, hydrogen-donating ability, berries

Berries are widely used nowadays in prevention and in adjuvant therapy of different diseases because of their valuable bioactive agents, antioxidant, anti-tumor and anti-inflammatory properties. It has been observed that berries are used very frequently but without medical control. The main aim of our study was to determine the element content and antioxidant activities in some Latvian varieties of berries (e.g. blueberry, *Vaccinium corymbossum* L., bilberry, *Vaccinium myrtillus* L. and red berry, *Vaccinium vitis-idaea* L.). Element content was measured by ICP-OES. Total antioxidant activity was determined by chemiluminometry and hydrogen-donating ability was measured by spectrophotometry. The berries under examination contain elements in relatively low concentrations and the consumption of these kind of berries is also poor, although they might be good sources for some essential elements; such as blueberry for Mo, bilberry for Li, Mn, Mo and red berry for Cr, Li, Mn, Mo. On the other hand, they have good antioxidant properties, especially bilberry. Beneficial antioxidant capacities and moderate metal ion concentrations support that berries can complete a diverse diet, and they may be a good supplement in some metal-accumulating disorders.

* Corresponding Authors
Fax: -
E-Mail: Andrejs.Skesters@rsu.lv
[a] Riga Stradiņš University, RSU Dzirciema Str. 16, Riga, LV-1007, Latvia
[b] Department of Pharmacognosy, Semmelweis University, H-1085 Budapest, Üllői str. 26. Hungary
[c] Institute of Materials and Environmental Chemistry Research Centre for Natural Sciences of the HAS, H-1025 Budapest, POBox 17, Hungary

Introduction

Berries contain valuable bioactive agents as unsaturated fatty acids, vitamin C, phenolic compounds such as polyphenols and anthocyanins. [1,2] Berries are frequently used in prevention and in adjuvant therapy of different diseases in our time since they are known to have several favorable effects because of their antioxidant, antitumor and anti-inflammatory properties. [3,4,5]

Berry fruits as foods products are widely available in the market in various forms (fresh fruits, dried or frozen fruits, jam, syrup, different food supplements, etc.) and as products (extracts, supplements) in drugstores and pharmacies, therefore people can consume a relatively large amount without any control from medical authorities. Since berries can be consumed almost every day, therefore a study on their quantity of essential and toxic metal ions is essential other than the bioactive agents (flavonoids, organic acids, polyphenols), as well as antioxidant effects in vitro and the investigation of absorption (availability).

In the present article our aim was to evaluate the element content and antioxidant activities in some Latvian variety of berries.

Experimental

Materials

Blueberry (*Vaccinium corymbossum L.*), bilberry (*Vaccinium myrtillus* L.) and red berry (*Vaccinium vitis-idaea L. var. vitis-idaea*) were collected in the forests near Riga or bought in from the local markets in Riga, Latvia.

Infuses were made by steeping of 5g berries in 50 mL water for a day at room temperature. After filtration the aqueous extracts were used for the antioxidant properties measurements.

Luminol, microperoxidase, 30% hydrogen peroxide and 2,2-diphenyl-1-picrylhydrazyl were obtained from Sigma-Aldrich (St. Luis, USA). Methanol and Na_2CO_3 were obtained from Reanal-KER (Budapest, Hungary). Nitric acid originated from Carlo Elba by Reanal (Budapest, Hungary) and multielement ICP standard solution were bought from Molar Chemical (Budapest, Hungary).

Measurement of elements

Element concentrations (Al, As, B, Ba, Ca, Cd, Co, Cr, Cu, Fe, K, Mg, Mn, Ni, P, Pb, S, Si, Sn, Sr, Ti, V, Zn) in the berries were determined by inductively coupled plasma optical emission spectrometry (ICP-OES). Type of instrument: Spectro Genesis ICP-OES (Kleve, Germany). After digestion of the samples (0.5 g from drug) with a mixture of nitric acid and hydrogen peroxide (10 mL + 4 mL) and dilution with de-ionized water to 25 mL, concentrations of elements were determined.[6]

Total scavenging capacity

A chemiluminescence assay adopted to a Berthold Lumat 9501 (Bad Wildbad, Germany) instrument applied for the determination of total scavenger capacity of the berries by the method of Blázovics et al. [7] The reaction mixture for standard background consisted of hydrogen peroxide (0.30 mL, 10^4 dilution), microperoxidase (0.30 mL, 1 mmol L^{-1}) as a catalyst and luminol (0.050 ml, $7x10^{-5}$ mol L^{-1} in pH 9.8 Na_2CO_3 solution). The volumes of berry infuses were 0.05 ml. The berry samples were added to luminol solution and mixed with vortex for 10 seconds before measuring. Scavenger capacities of the samples were expressed in the relative light unit (RLU%). The RLU% was calculated from the relative light intensity and the standard background.

Hydrogen-donating ability

Hydrogen donating ability was measured by Hatano et al.[8] Every 0.05 mL sample was diluted with 0.95 mL bidistilled water and 1.00 ml methanol. The samples were mixed with 0.50 mL 2,2-diphenyl-1-picrylhydrazyl free radical's methanolic solution (9 mg/100 mL). After 30 minutes, samples were measured with a Hitachi U-2000 spectrophotometer (Tokyo, Japan) at 517 nm against their blinds. The inhibition % of the samples was expressed in the percentage of the control.

Statistical analysis

Means and standard deviations (SD) were calculated from the results obtained. One way analysis of variance (ANOVA) was used for comparing the means of the groups by Graph PAD software version 1.14 (1990). Significance was determined as $P<0.05$.

Results

The element concentrations observed in berries are shown in Table 1. The concentrations of As, Co, Pb and V were under the detection limits therefore these elements were not shown in the table. The berries generally contain low amounts of elements similarly to the results of other berries obtained by several authors and various berries of Rubus family.[9,10,11,12] We noticed that almost all element concentrations were significantly different and red berry contains elements in the highest concentrations.

The antioxidant properties of the berries are shown in Figure 1. and 2. The luminol/H_2O_2/OH•-system emits light in alkaline solution, meaning scavengers can attenuate the emission. RLU% of red berry and bilberry is lower than that of blueberry in most of the concentration range, so their scavenging capacity is better than that of blueberry (Fig. 1.). This kind of lower antioxidant activity can be observed in the hydrogen-donating ability as well (Fig. 2.), and the difference between red berry and bilberry is higher than their chemiluminescent data. Finally after observations it was concluded that these three types of berries have good antioxidant activity. [1,2,13,14] Bilberry shows the highest and blueberry the weakest properties.

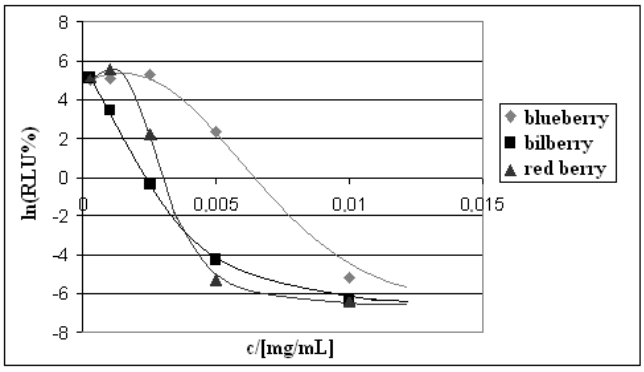

Figure 1. Free radical scavenging capacity in different berries originated from Latvia

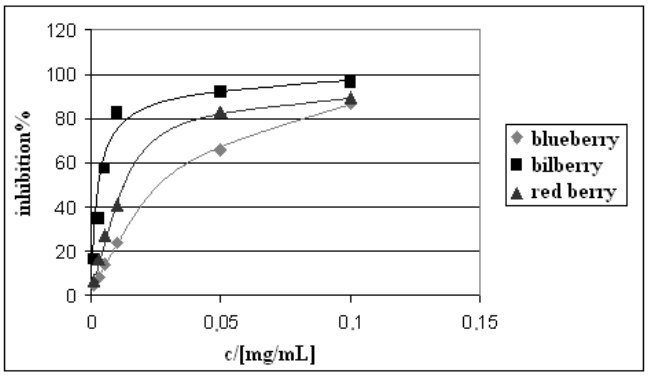

Figure 2. Hydrogen-donating ability in Latvian blueberry, bilberry and red berry

Discussion

The berries under investigations contain elements in relatively low concentration. The consumption of these kinds of fruits is also unsatisfactory. Even after consuming 100 g berry per day, the quantities of metal ions in berries do not cover the daily need. Nevertheless they may be good sources for some elements, since they contain some essential elements in higher quantity, which means 15% or higher rate of the Recommended Dietary Allowances (RDA) or Dietary Reference Intake (DRI). [15,16]

According to RDA parameters and taking into consideration consumption of 100 g sample of berries, the following berries are found to be good sources of: blueberry for molybdenum (37.4% of the daily need, RDA value: 50 µg day^{-1}/adult of 70 kg); bilberry for manganese (94.1 % of the daily need, RDA value: 2 mg day^{-1}/adult of 70 kg), molybdenum (27.6 % of the daily need, RDA value: 50 µg day^{-1}/adult of 70 kg) and red berry for chromium (15 % of the daily need, RDA value: 40 µg day^{-1}/adult of 70 kg), manganese (101 % of the daily need, RDA value: 2 mg day^{-1}/adult of 70 kg), molybdenum (60 % of the daily need, RDA value: 50 µg day^{-1}/adult of 70 kg). It should be also mentioned, that the Upper Level (UL) for manganese was 11 mg day^{-1}/adult earlier, nevertheless according to the EFSA,[17] there is not enough data available for the correct determination of this value and there is no UL value at present which would establish red berry as a safe fruit.

Table 1. Element concentrations (mg kg^{-1} wet weight ± standard deviation, n=3) in different berries originated from Latvia

	Blueberry	**Bilberry**	**Red berry**	**ANOVA (P<0.05)**
Al	1.63 ± 0.28	3.06± 0.17	5.91± 1.08	Sign.
B	1.53 ± 0.09	1.26± 0.11	2.55 ± 0.28	Sign
Ba	0.228 ± 0.011	1.25 ± 0.07	1.46 ± 0.04	Sign.
Ca	56.98 ± 2.35	160.4 ± 9.5	240.7 ± 16.8	Sign.
Cd	<0.01	0.013±0.017	<0.01	
Cr	0.038 ± 0.011	0.021 ± 0.003	0.060 ± 0.006	Sign.
Cu	0.728 ± 0.111	0.309 ± 0.021	0.907 ± 0.120	Sign.
Fe	2.36 ± 0.65	1.69 ± 0.06	3.25 ± 0.14	Sign.
K	387.7 ± 70.1	482.4 ± 15.5	1005 ± 48	Sign.
Li	0.00138 ± 0.00020	0.00196 ± 0.00032	0.00388 ± 0.00225	Non sign
Mg	43.72± 9.42	53.12 ± 4.28	103.2 ± 6.12	Sign.
Mn	0.684 ± 0.133	18.82 ± 0.49	20.29 ± 0.231	Sign.
Mo	0.187 ± 0.071	0.138 ± 0.029	0.309 ± 0.022	Sign
Na	6.17 ± 0.65	6.61 ± 1.02	9.76 ± 1.00	Sign.
Ni	0.0235 ± 0.0051	0.0217 ± 0.0067	0.0387 ± 0.0059	Sign.
P	72.51 ±-9.37	95.23± 4.09	166.4 ± 6.5	Sign.
S	43.44 ± 8.07	51.03 ± 3.60	94.33 ± 4.97	Sign.
Si	8.31 ± 0.69	5.11 ± 0.45	9.57 ± 2.32	Sign.
Sn	0.482 ± 0.207	0.051 ± 0.027	0.279 ± 0.187	Sign.
Sr	0.0623 ± 0.0066	0.0631 ± 0.0041	0.159 ± 0.0095	Sign
Ti	0.0508 ± 0.0103	0.0471 ± 0.0085	0.0691 ± 0.0096	Sign
Zn	0.637 ± 0.059	1.16 ± 0.17	2.19 ± 0.12	Sign.

It has to be mentioned here as well that they may contain other toxic bioactive agents, like arbutin and derivates, therefore the precaution is needed.[17]

The intake of non-essential elements is relatively low, instead of aluminum in the case of bilberry, which is 14.4-19.0% (DRI value between: 3.1-4.1 mg day^{-1}/adult of 70 kg), of boron in the case of blueberry and red berry which are 15.9 and 26.6% (DRI value: 0.96 mg day^{-1}/adult of 70 kg) and of lithium in the case of bilberry and red berry with intake of 19.6% and 38.8% (DRI value: 1 µg day^{-1}/adult of 70 kg).

All of these three varieties of berries have good scavenging capacity and hydrogen-donating activity. The best properties are in bilberry sample, but to evaluate their difference, a wider study is needed.

These fruits have good antioxidant properties that may be associated to their valuable compounds, like flavonoids, unsaturated fatty acids and vitamins which are very important in cellular signal transduction routes to rebuild the redox homeostasis in different diseases such as in various tumors, liver and bowel diseases as well as in simple flu. [1,2,4,17,18,19, 20,21,22] The relatively low metal content and the high antioxidant activity suggest, that these fruits could be good supplements in metal accumulating disorders as well, like Wilson-disease, *porphyria cutanea tarda*, hemochromatosis and some metal-accumulating tumors. [23]

References

[1]Bakowska-Barczak, A.M., Marianchuk, M., Kolodziejczyk, P., Canadioan, J., *Physiol. Pharmacol.*, **2007**, *85*, 1139-1152.

[2]Pimpao, R.C., Dew, T., Oliveira, P.B-, Williamson, G., Ferreira, R.B., Santos, C.N., *J Agr. Food Chem.*, **2013**, *61*, 4053-4062.

[3]Brown, E.M., Gill, C.I.R., McDougall, G.J., Stewart, D., *Curr. Pharm. Biotech.*, **2012,** *13*, 200-209.

[4]Johnson, S.A., Arjmandi, B.H., *Anti-Cancer Med. Chem.*, **2013**, *8*, 1142-1148.

[5]Seeream, N.P., Momin, R.A., Nair, M.G., Bourquin, L.D., *Phytomed*., **2001**, *8*, 362-369.

[6]Szentmihályi, K., Then, M., *Acta Aliment*., **2000**, *29*, 43-49.

[7]Blázovics, A., Kovács Á., Lugasi A., Hagymási K., Bíró L., Fehér J., *Clin. Chem.*, **1999,** *45*, 895-896

[8]Hatano, T, Kagawa H, Yasuhara T, Okuda T., *Chem. Pharm. Bull.*, **1988;** *36*, 2090-2097.

[9]Plessi, M., Bertelli, D., Albasini, A., *Food Chem*., **2007**, *100*, 419-427.

[10]Moilanen, M., Fritze, H., Nieminen, M., Piirainen, S., Issakainen, J., Piispanen, J., *Forest Ecol. Manag.*, **2006**, *226*, 153-160.

[11]Ochiman, I,. Grajkowski, J., Skupien, K., *Agric. Food Chem*., **2010**, *19*, 69-80.

[12]Pöjkiö, R., Maenpaa, A., Peramaki, M., Niemala, M., Valimaki, I., *Arch Environ. Contam. Toxicol*., **2005**, *48*, 338-343.

[13]Ieri F., Martini S., Innocenti M., Mulinacci N., *Phytochem. Anal.*, **2013,** 24, 467-475.

[14]Yang H., Jiang Y., *Wei Sheng Yan Jiu.*, **2010,** *39*, 525-528.

[15]*Recommended Dietary Allowances* (RDA) 10th ed. National academy Press, Washington D.C., **1989**.

[16]*Dietary Reference Intakes for vitamin A, vitamin K, arsenic, boron, chromium, copper, iodine, iron, manganese, molybdenum, nickel, silicon, vanadium, and zinc.* Food and Nutritional Board, Institute of Medicine. National Academic Press, Boston, **2002**, 772-773.

[17]*Tolerable upper intake levels for vitamins and minerals. European Food Safety Authority, Scientific Committee on Food,Scientific Panel on Dietetic Products, Nutrition and Allergies*, Parma, **2006**, 59-64.

[18]Tóth L., *Gyógynövények, drogok, fitoterápia [Herbs, drugs, phytotherapia]*. Debrecen University Press, Debrecen, **2009**, 454-515. [Hungarian]

[19]Chu, W., Cheung, S.C.M., Lau, R.A.W., Benzie., I..F.F., *Herbal Medicine: Biomolecular and Clinical Aspects. 2nd edition*. CRC Press, Boca Ration, **2011,** 55-72, http://www.ncbi.nlm.nih.gov/books/NBK92770/

[20]Boivin, D., Blanchette, M., Barrette, S,, Moghrabi, A., Béliveau, R., *Anticancer Res.* **2007**, 27, 937-948.

[21]Costa, S.S., Couceiro, J.N., Silva, I.C., Malvar, Ddo, C., Coutinho, M.A., Camargo, L.M., Muzitano, M.F., Vanderlinde, F.A., *Expert Opin Ther. Pat.* **2012,** 22. 1111-1121.

[22]Calder, P.C., Albers, R., Antoine, J.M., Blum, S., Bourdet-Sicard, R., Ferns, G.A., Folkerts, G., Friedmann, P.S., Frost, G.S., Guarner, F., Løvik, M., Macfarlane, S., Meyer, P.D., M'Rabet, L., Serafini, M., van Eden, W., van Loo, J., Vas Dias, W., Vidry, S., Winklhofer-Roob, B.M., Zhao, J., *Br J Nutr.*, **2009**, 101 1:S1-S45.

[23]Ionescu, J.G., Novotny, M.D., Stejskal, V., Lätsch, A., Blaurock-Busch, E., Eisenmann-Klein, M., *Maedica,* **2007,** *2,* 5-9.

Received: 15.11.2013.
Accepted: 30.11.2013.

APPLICATIONS OF GEORGIAN ZEOLITES FOR THE EXTRACTION OF USEFUL COMPONENTS FROM NATURAL AND WASTE WATERS

Marsagishvili T.,[a] Ananiashvili N.,[a] Metreveli J.,[a] Kikabidze-Gachechiladze M.,[a] Machavariani M.,[a] Tatishvili G.,[a] Tskhakaya E.,[a] and Khositashvili R.[a]

Keywords: adsorption; zeolites; natural waters; wastewaters; Ni-clinoptilolyte; hydrogen sulphide; ammonium ion; potassium ion

Present investigation reveals that Ni-modified Khekordzula clinoptilolyte is characterized by high adsorption capacity against hydrogen sulfide, and HNaX- modified Khekordzula clinoptilolyte has high adsorption capacity against potassium and ammonium ions. Therefore, present zeolites may be used for selective adsorption of hydrogen sulfide, potassium and ammonium ions.

* Corresponding Authors
E-Mail: tamaz.marsagishvili@gmail.com
[a] Iv.Javakhishvili Tbilisi State University, R.Agladze Institute of Inorganic Chemistry and Electrochemistry; 11, Mindeli str., Tbilisi, 0186, Georgia

Introduction

Useful energy resources and fossil fuels are limited and declining day by day at a very fast rate. Therefore, in previous years this problem attracted the attention of researchers to solve this huge problem.

Currently, the problem of searching of alternative energy sources is very important. One of the possible methods of obtaining of hydrogen (ecologically acceptable fuel) may be the use of the natural hydrogen sulfide from the hydrosulphurous water of the Black Sea. This water is rich in potassium ions and water of the rivers which flow into the Black Sea is rich in ammonium ions.

One of the extraction methods of these valuable components from natural waters is sorption concentration. Ion-exchanging materials are facing the challenges to obtain these objectives. Georgia is rich in sedimentary natural zeolites, which belong to calcium- sodium- potassium clinoptilolytes, according to available data.[1]

Some results of the trial experiments, conducted at the beginning of the investigations, with the aim of finding out adsorption possibilities of the above mentioned components on the native natural zeolites from different deposits of Georgia and also their modified forms, are the subject matter of the present investigation.

The results of the chemical analysis of Georgian natural clinoptilolytes[2] are shown in Table 1. A number of works[3-6] have been dedicated to the study of the adsorption properties of the natural and modified clinoptilolytes. Further, a step-by-step extraction of useful components from the complex solutions has not been conducted so far. Purposefully adsorption of hydrogen sulfide, potassium and ammonium ions on Dzegvi and Khekordzula clinoptilolytes in natural water and synthesized solutions has been studied in present work. A comparative study has been done with Cation exchanger KY-2-8.

Experimental

The experiment was carried out in static conditions at the room temperature. Determination of the under test components in solutions was carried out by iodometric, spectrophotometric and atomic absorption methods. Sorption curves for natural waters and synthetic solutions were received.

Results and Discussions

Volume capacity of the given zeolites concerning tested ions has been established. The results of the experiment are given in the Tables 2-4 and Figs. 1-3.

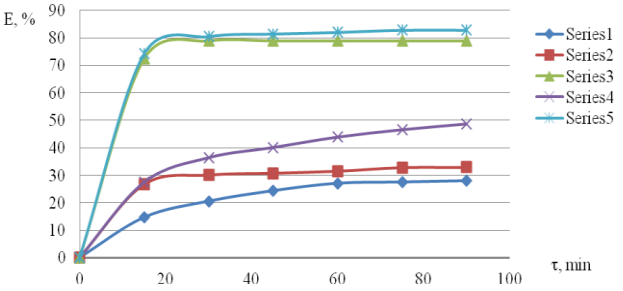

Figure 1. Kinetics of adsorption of hydrogen sulfide on the clinoptilolyte from natural sulfur-containing water. 1-Dzegvi untreated; 2-HNaX-modified Khekordzula; 3-Ni-modified Khekordzula; 4- 2 M HCl-modified Khekordzula; 5-KY-2-8.

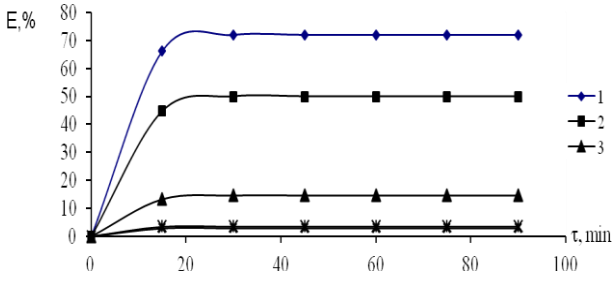

Fig. 2. Kinetic of adsorption of potassium ions on the clinoptilolyte from synthesized solutions. 1-Dzegvi untreated; 2-HNaX-modified Khekordzula; 3-Ni-modified Khekordzula; 4- 2 M HCl-modified Khekordzula; 5-KY-2-8.

Table 1. Chemical composition of dehydrated clinoptilolytes of Georgia.

Deposit	Oxid components, weight %							Molar ratio SiO_2/Al_2O_3
	SiO_2	Al_2O_3	Fe_2O_3	CaO	MgO	K_2O	Na_2O	
Khekordzula	68.69	13.70	3.46	5.63	1.57	2.29	4.20	8.54
Dzegvi	68.04	14.40	3.99	6.99	2.00	1.30	2.00	8.09

Table 2. Volume capacity, equilibrium concentration and extraction efficiency of hydrogen sulfide recovery by zeolites from the natural sulfur-containing water (C_0=22.1 mg L^{-1}) after 48 hours of delay.

Clinoptilolite	C_p, mg L^{-1}	*a*, mg g^{-1}	*E*, %
Dzegvi untreated	10.2	1.19	92.4
HNaX- modified Khekordzula	0.7	2.14	96.9
Ni-modified Khekordzula	0.0	2.21	100.0
2N HCl - modified Khekordzula	0.02	2.19	99.2
Ky-2-8	0.00	2.21	100.0

It is revealed from the experimental results, Ni-modified Khekordzula clinoptilolyte and cationite Ky-2-8 are characterized by high adsorption capacity. Adsorption capacity of the Dzegvi untreated clinoptilolyte is relatively less as compared to the treated one. Although, all tested zeolites almost completely adsorb hydrogen sulfide after 48 hours of delay.

Table 3. Volume capacity, equilibrium concentration and extraction efficiency of the potassium ion removal by zeolites from synthesized solutions (C_0=400.0 mg L^{-1}) after 48 hours of delay.

Clinoptilolyte	C_p, mg L^{-1}	*a*, mg L^{-1}	*E*, %
Dzegvi untreated	342.0	5.8	14.5
HNaX- modified Khekordzula	112.0	28.8	72.2
Ni-modified Khekordzula	388.4	1.16	2.9
2 M HCl - modified Khekordzula	387.0	1.3	3.4
Ky-2-8	200.0	20.0	50

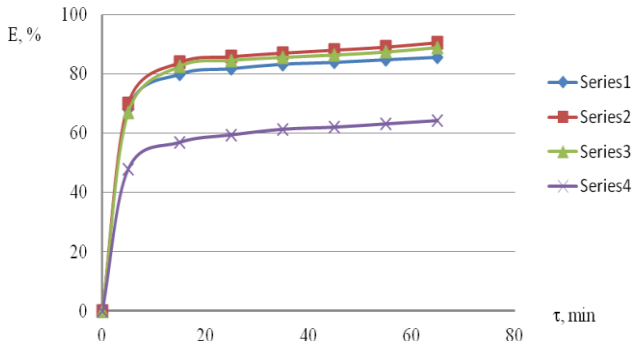

Figure 3. Kinetic of adsorption of the ammonium ions on the clinoptilolyte from synthesized solutions: 1-Dzegvi untreated; 2-HNaX-modified Khekordzula; 3-Ni-modified Khekordzula; 4- 2 M HCl-modified Khekordzula;

Table 4. Volume capacity, equilibrium concentration and extraction efficiency of ammonium ion removal by zeolites from synthesized solutions (C_0=34.0 mg L^{-1}) after 48 hours of delay

Clinoptilolyte	C_p, mg L^{-1}	*a*, mg g^{-1}	*E*, %
Dzegvi untreated	4.47	2.95	87.0
HNaX- modified Khekordzula	3.06	3.1	91.1
Ni-modified Khekordzula	3.4	3.06	90.0
2 M HCl-modified Khekordzula	11.9	2.21	65.0

Under sorption of ammonium ions from solutions with initial concentration 34.0 mg L^{-1}, the highest adsorption capacity has Khekordzula clinoptilolytes, modified by HNaX and Ni, and also untreated clinoptilolyte from Dzegvi.

Conclusion

It is evident from the results of the investigators, Ni-modified Khekordzula clinoptilolyte is characterized by high adsorption capacity against hydrogen sulfide, and HNaX-modified Khekordzula clinoptilolyte has high adsorption capacity against potassium and ammonium ions. Thus, above mentioned zeolites may be used for selective adsorption of hydrogen sulfide, potassium and ammonium ions.

Acknowledgement

We express gratitude to the fund for financing the work, which is conducted in frames of the program BBBS-ERA.NET.

References

[1]Tsitsishvili, G. V., *Zh. Fiz. Khim*., **1972**, *46*(12), 3016.

[2]Nikolina, V. Ya. Knysh, L. I., Krupennikova, A. Yu., *CLINOPTILOLITE. Proc. Symp. Probl. Clinoptilolite Stud. Appl.*, Tbilisi, 2-4 Nov. **1974**, 188-194.

[3]Karimova, A. M., Balyeva, I. V., Groysman, E. B., Avdeeva, E. I. *Use of the clinoptilolyte of the Uzbek deposit Kermene for elimination of ammonium nitrogen from natural and waste waters*, Tashkent NII VODGEO. Uzbekistan.

[4]Kyzmina, R. I., Kondrashova, A. V., *Dynamics and kinetics of the adsorption process of the ammonium ions on the flask*, Saratov State Institute.

[5]Mironova, L. I., Nikashina, V. A., *Proc. Conf. Geol. Phys.-Chem. Prop. Util. Natural Zeolites*, Tbilisi, 1-5 Nov. **1981**, 231-234.

[6]Diyarov, I. N., Mikhailov, A. S., Romanova, G. Ya., Shitovkin, N. T., Kozin, V. G., Galeeva, R. G., Seifiullin, T. R., *Natural Zeolites. Proc. Soviet-Bulgarian Symp. Stud. Phys-chem. Prop. Natural Zeolites*. Tbilisi, Oct. 29-31, **1976**, 269-273.

[7]Marchenko Z., *Photometric definition of elements*. "Mir", Moscow, **1971.**

Received: 01.11.2013.
Accepted: 03.12.2013.

NMR ANALYSIS AND HYDROLYSIS STUDIES OF GLYCYRRHIZIC ACID, A MAJOR CONSTITUENT OF *GLYCYRRHIA GLABRA*

Venkata Sai Prakash Chaturvedula[a]*, Oliver Yu[b] and Guohong Mao[a]

Keywords: *Glycyrrhiza glabra*, *Fabaceae*, triterpene glycoside, 1D and 2D NMR spectral data, structure characterization, hydrolysis, sugar conformation

From the commercial extract of the roots of *Glycyrrhia glabra*, a triterpene glycoside was isolated which was characterized as 18β-glycyrrhetinic acid-3-*O*-β-*D*-glucuronopyranosyl-(1→2)-β-*D*-glucuronide; also known as Glycyrrhizic acid or Glycyrrhizin. The complete ^{1}H and ^{13}C NMR assignments of Glycyrrhizin were achieved by the extensive 1D (^{1}H and ^{13}C), and 2D NMR (COSY, HMQC, and HMBC) as well as mass spectral data. Further, hydrolysis studies were performed on Glycyrrhizin to identify aglycone and sugar residues in its structure. Further, configuration of sugar moieties in the triterpene glycoside obtained during the course of acid hydrolysis studies were confirmed by preparing their corresponding thiocarbamoyl-thiazolidine carboxylate derivatives with L-cysteine methyl ester and *O*-tolyl isothiocyanate and in comparison of their retention times with standard sugars.

Corresponding Authors
Email: saipc@bluecal-ingredients.com
[a] Natural Ingredient Development, Blue California, 30111 Tomas, Rancho Santa Margarita, CA 92688, USA
[b] Wuxi NewWay Biotechnology, 401 North Xingyuan Road, Wuxi 210043, P.R. China.

Introduction

Glycyrrhiza glabra (*Fabaceae*) also known as Licorice is a well-known medicinal herb that grows in various parts of the world.[1] It is one of the oldest and widely used herbs known since several thousand years ago both in western and eastern countries. From the ancient medical history of Ayurveda, Licorice has been used both as a medicine and also as a flavoring agent to disguise the unpleasant flavor of other medications. In the traditional system of medicine, the roots and rhizomes of *G. glabra* have various pharmaceuticals activities like antispasmodic, demulcent, pectoral, anti-inflammatory, antiulcer, expectorant, antimicrobial and anxiolytic activities.[2-3] Varies species of *Glycyrrhiza* family has been shown to have great antioxidant, free radical scavenging and anticonvulsant activities. In some countries Licorice root is used in food and tobacco products.[4] *G. glabra* root extract have been used for more than 60 years in Japan to treat chronic hepatitis, and also have therapeutic benefit against other viruses, expectorant, antitussive, mild laxative and anti-aging activities.[4-5] The main chemical constituents of G. *glabra* is composed of triterpene saponin, flavonoids, polysaccharides, pectin, simple sugars, amino acids, mineral salts and various other components. Its major bio-active constituent of root is a triterpenoid saponin, 18β-glycyrrhetinic acid-3-*O*-β-*D*-glucuronopyranosyl-(1→2)-β-*D*-glucuronide (**1**); also known as glycyrrhizic acid or glycyrrhizin. Glycyrrhizic acid (GA) is the most studied active constituent of licorice which is a sweet-tasting material and is about 50 times sweeter than sugar, making it a widely used as a sweetening additive in the food industry.[6-7]

As a part of our continuing research to discover natural products, we have isolated several diterpene glycosides from the commercial extracts of the leaves of *S. rebaudiana*[8-11] and flavonoids from *Hovenia dulcis*.[12] The structures of the isolated compounds were characterized on the basis of extensive 1D (^{1}H and ^{13}C) and 2D (COSY, HSQC and HMBC) NMR as well as high resolution mass spectroscopic data and chemical modifications. In this paper, we are describing the structural characterization of a triterpenoid saponin, glycyrrhizic acid (**1**) isolated from the commercial extract of the roots of *G. glabra*, which were achieved on the basis of 1D (^{1}H and ^{13}C) and 2D (COSY, HMQC and HMBC) NMR and high resolution mass spectroscopic (MS) data, as well as by comparison of the physical and spectral data of reported in literature. Further, configuration of sugar moieties in the triterpene glycoside **1** was confirmed by preparing their corresponding thiocarbamoyl-thiazolidine carboxylate derivative with L-cysteine methyl ester and *O*-tolyl isothiocyanate in comparison of their retention times with standard sugars.

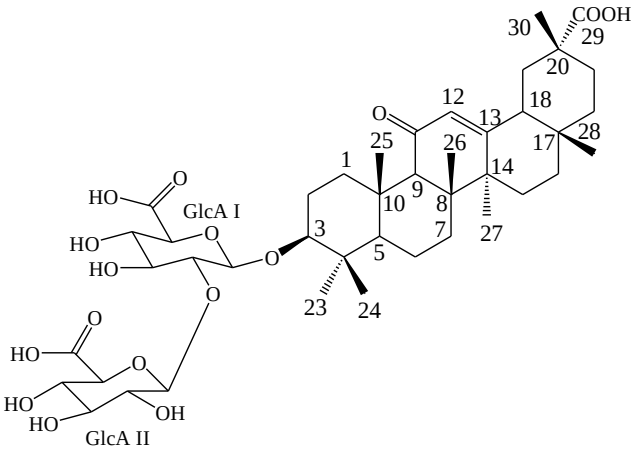

Figure 1. Structure of Glycyrrhizic acid (1)

 DOI: 10.17628/ecb.2014.3.104-107

EXPERIMENTAL

General Instrumentation Procedures

IR spectral data was acquired using a Perkin Elmer 400 Fourier Transform Infrared (FT-IR) Spectrometer with Universal attenuated total reflectance (UATR) polarization accessory. HPLC analysis was performed using a Dionex UPLC ultimate 3000 system (Sunnyvale, CA), including a quaternary pump, a temperature controlled column compartment, an auto sampler and a UV absorbance detector. Phenomenex Luna C18 reversed-phase with guard column, 150x4.6 mm, 3µm (100A) were used for the characterization of glycyrrhizin (1). NMR spectra were acquired on Bruker Advance DRX 500 MHz or Varian INOVA 600 MHz instrument instruments using standard pulse sequences. The NMR spectra were performed in C_5D_5N; chemical shifts are given in δ (ppm), and coupling constants are reported in Hz. MS and MS/MS data were generated with a Thermo LTQ-FTMS mass spectrometer (100,000 resolutions) equipped with a nanospray ionization source. Samples were diluted with methanol and introduced via infusion using the onboard syringe.

Isolation and Characterization

Compound **1** was purified from the commercial aqueous alcoholic extract of *G. glabra* root by using the HPLC method as summarized below:

A binary solvent system comprising distilled water with 1% acetic acid (A) and 100 % acetonitrile (B) was used as mobile phase at a flow rate of 0.9 ml min^{-1} separations were performed using a linear gradient of increasing acetonitrile. Buffer B was increased from 15 % to 100 % in 25 min. The compounds were confirmed by the retention time and UV absorption at 254 nm.

Using the above mentioned HPLC method, collected the peak eluting at t_R 12.023 min over several rounds of injection of crude extract; dried the corresponding solution under nitrogen yielded a pure compound, which was characterized as **1**.

18β-glycyrrhetinic acid-3-*O*-β-*D*-glucuronopyranosyl-(1→2)-β-*D*-glucuronide (Glycyrrhizic acid, 1)

White powder; IR ν_{max}: 3312, 2965, 1722, 1055, 910 cm^{-1}; ^{1}H-NMR (600 MHz, C_5D_5N, δ ppm) and ^{13}C-NMR (150 MHz, C_5D_5N, δ ppm) spectroscopic data see Table 1; HRMS $(M+H)^+$ *m/z* 823.4138 (calcd. for $C_{42}H_{63}O_{16}$: 823.4116); $(M+Na)^+$ *m/z* 845.3954 (calcd. for $C_{42}H_{62}O_{16}Na$: 845.3936).

Acid hydrolysis of 1

To a solution of compound **1** (5 mg) in MeOH (3 ml) was added 25 ml of 10 % H_2SO_4 and the mixture was refluxed for 72 hours. The reaction mixture was then extracted with ethyl acetate (EtOAc) (2 x 25 ml) to give an aqueous fraction containing sugars and an EtOAc fraction containing the aglycone part, which has been identified as glycyrrhetinic acid on the basis of comparison with the spectral data of the standard and co-TLC.[6-7] The aqueous phase was concentrated and compared with standard sugars using the TLC systems EtOAc/*n*-butanol/water (2:7:1) and CH_2Cl_2/MeOH/water (10:6:1);[13-15] the sugar was identified as glucose.

Determination of sugar configuration in 1

Compound **1** (3 mg) was hydrolyzed with 1 M HCl (10 mL) for 1.5 h. After cooling, the mixture was passed through an Amberlite IRA400 column and the eluate was lyophilized. The residue was dissolved in pyridine (5 mL) and heated with L-cysteine methyl ester HCl (15 mg) at 60 ºC for 1.5 h, and then *O*-tolyl isothiocyanate (100 µL) was added to the mixture and heated at 60 ºC for an additional 1.5 h. The reaction mixture was analyzed by HPLC: column Phenomenex Luna C18, 150 x 4.6 mm (5 u); 25 % acetonitrile-0.2 % TFA water, 1 mL min^{-1}; UV detection at 250 nm. The sugar was identified as D-glucuronic acid (t_R, 18.34 min) [authentic samples, D-glucuronic acid (t_R, 18.17) and L-glucuronic acid (t_R, 17.64 min)].[16]

Results and Discussion

Compound **1** was isolated as a colorless powder and its positive mode of ESI Time of Flight (TOF) mass spectrum indicated an $[M+H]^+$ ion at *m/z* 823.4138 together with $[M+Na]^+$ adduct ion at *m/z* 849.3954, respectively; which were in good agreement with the molecular formula $C_{42}H_{62}O_{16}$. The chemical composition of **1** was further supported by the ^{13}C NMR spectral data.

The ^{1}H NMR spectra of compound **1** showed the presence of seven methyl sinlgets at δ 0.79, 1.05, 1.21, 1.27, 1.37, 1.42 and 1.44. Liebermann-Burchard reaction indicated compound **1** is having a terpenoid skeleton.[17-18] The signal corresponding to the H-3 of the oxymethine proton in the terpene moiety of **1** was appeared as a doublet of doublets at δ 3.37. Compound **1** also showed a proton at δ 5.98 as a singlet suggesting the presence of a trisubstituted olefinic bond. Further, the down field shift value of the trisubstituted olefinic proton indicated the presence of a carbonyl group at C-11 position, which was supported by the carbonyl group resonating at δ 200.1. The above spectral data supported the presence of oleanane triterpene skeleton having a hydroxyl group at C-3 position with a double bond at C-12/C-13 with seven methyl groups.

The presence of two sugar units in its structure was supported by the ^{1}H NMR spectrum of **1** which showed the anomeric protons at δ 5.08, and 5.47 as doublets. Acid hydrolysis of **1** with 10 % H_2SO_4 afforded glycyrrhetinic acid[6-7] and glucuronic acid[13-15] which were identified by direct comparison with authentic samples by co-TLC. The stereochemistry of the sugar was identified as D- glucuronic acid by preparing its corresponding thiocarbamoyl-thiazolidine carboxylate derivatives with L-cysteine methyl ester and *O*-tolyl isothiocyanate, and in comparison of their retention times with the standard sugars as described in the literature.[16] The large coupling constants observed for the

 DOI: 10.17628/ecb.2014.3.104-107

two anomeric protons of the glucose moieties at δ 5.08 (d, *J*=8.1 Hz), and 5.47 (d, *J*=8.4 Hz), suggested their β-orientation as reported earlier.[19-21] The ^{1}H and ^{13}C NMR values for all the protons and carbons were assigned on the basis of COSY, HMQC and HMBC correlations and were given in Table 1.

Table 1. ^{1}H and ^{13}C NMR chemical shift values for Glycyrrhizic acid (**1**) recorded in C_5D_5N.[a-c]

Position	^{1}H NMR	^{13}C NMR
1	0.95 m, 3.05 dd (*J* = 8.1, 9.6)	39.9
2	1.75 m, 2.04 m	27.1
3	3.37 dd (*J* = 5.4, 11.6)	89.6
4	-	40.5
5	0.74 m	55.9
6	1.46 m, 1.68 m	18.1
7	1.48 m, 1.72 m	33.4
8	-	43.9
9	2.46 s	62.6
10	-	37.7
11	-	200.1
12	5.98 s	129.2
13	-	172.9
14	-	46.1
15	1.24 m, 2.12 m	27.2
16	1.08 m, 2.15 m	27.3
17	-	32.7
18	2.14 m	49.2
19	1.55 m, 2.34 m	42.2
20	-	44.6
21	1.53 m, 2.08 m	32.1
22	1.30 m, 1.73 m	38.9
23	1.21 s	28.6
24	0.79 s	17.2
25	1.27 s	17.3
26	1.37 s	19.3
27	1.42 s	24.1
28	1.05 s	29.2
29		179.7
30	1.44 s	29.3
Glucuronic Acid I (GlcA I)		
1′	5.47 d (*J* = 8.4)	107.5
2′	4.68 dd (*J* = 8.2, 9.4)	85.1
3′	4.32 dd (*J* = 8.1, 9.6)	78.0
4′	4.45 t (*J* = 9.4)	78.9
5′	4.66 t (*J* = 9.6)	78.2
6′		73.8
Glucuronic Acid II (GlcA II)		
1″	5.08 d (*J* = 8.1)	105.6
2″	4.64 dd (*J* = 8.4, 9.6)	78.3
3″	4.30 dd (*J* = 8.2, 9.1)	78.1
4″	4.38 t (*J* = 9.6)	77.3
5″	4.64 t (*J* = 9.4)	73.5
6″		172.6

[a] assignments made on the basis of COSY, HSQC and HMBC correlations; [b] Chemical shift values are in δ (ppm); [c] Coupling constants are in Hz.

In the absence of eighth methyl group and the appearance of a carbonyl group resonating at δ 179.7 from the ^{13}C NMR spectral data of **1** suggested the presence of an acid functional group. The presence of the carboxylic acid group was identified at C-29 position by the key COSY and HMBC correlations as shown in Figure 2.

Based on the results from NMR spectral data and hydrolysis experiments, it was concluded that the structure of **1** has a oleanane triterpene aglycone moiety with an α,β-unsaturated carbonyl group, a carboxylic acid group, seven methyl singlets and two β-D-glucuronyl units. Thus, the structure of **1** was assigned as the known compound glycyrrhizic acid. The physical and spectral data are consistent to the reported literature values of glycyrrhizic acid.[6-7]

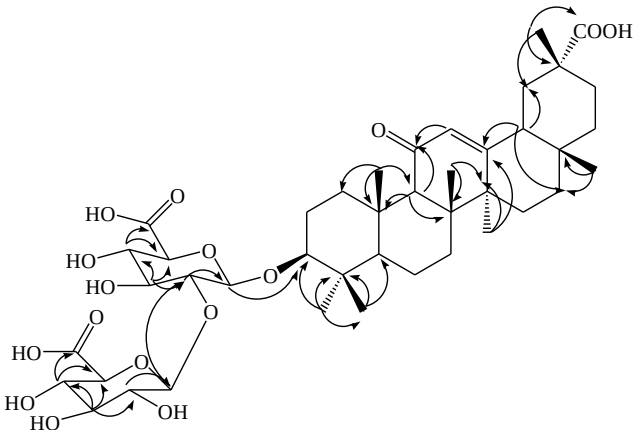

Figure 2. Key HMBC correlations of Glycyrrhizic acid (**1**)

Conclusions

We are herewith reporting the isolation and complete ^{1}H and ^{13}C NMR spectral assignments for 18β-glycyrrhetinic acid-3-*O*-β-*D*-glucuronopyranosyl-(1→2)-β-*D*-glucuronide (Glycyrrhizic acid, **1**) that were made on the basis of extensive 1D and 2D NMR spectral data as well as high resolution mass spectral data.

Further, acid hydrolysis of **1** furnished D-glucuronic acid suggesting the presence of only one sugar unit and its configuration was confirmed for the first time by preparing its corresponding thiocarbamoyl-thiazolidine carboxylate derivatives with L-cysteine methyl ester and *O*-tolyl isothiocyanate.

Acknowledgements

We wish to thank Dr Wu Shaoxiong, and Dr Bing Wang of Emory University, Atlanta, USA for obtaining some selected spectral data and other chemistry related help.

References

[1]Biondi, D.M., Rocco, C., Ruberto, G. *J. Nat. Prod.* **2005**, *68*, 1099–1102.

[2]Cinatl, J., Morgenstern, B., Bauer, G., Chandra, P., Rabenau, H. *Res. Lett.* **2003**, *361*, 2045-2046.

[3]Hennell, J.R., Lee, S., Khoo, C.S., Gray, M.J. *J. Pharm. Biomed. Anal.* **2008**, *47*, 494-500.

[4]Akao, T. *Biol. Pharm. Bull*. **2000**, *23*, 104-107.

[5]Bombardelli, E., Curd, S. B., Della Loggia, R., Del Negro, P., Tubaro, A. and Gariboldi, P. *Fitoterapia* **1989**, *60*, 29-37.

[6]El-Refai. A.M.H.. Sallam, A.R., El-Menoufy, H., Amin, H.A.S. *Malays. J. Microbiol*. **2012**, *8*, 75-82.

[7]Li, L., Yang, Z., He-shui, Y., Hong-zhi, H., Li-ping, K., Man, C., Jiang-ming, C., Li-yan, Y., Xin-boo, S., Bai-ping, M.A. *Chinese Herb. Med*. **2012**, *4*, 324-328.

[8]Chaturvedula, V.S.P., Chen, S., Yu, O., Mao, G. *Food Nutr. Sci*. **2013**, *4*, 1004-1008.

[9]Chaturvedula, V.S.P., Chen, S., Yu, O., Mao, G. *Biomolecules* **2013**, *3*, 733-740.

[10]Chaturvedula, V.S.P., Yu, O., Mao, G. (2013). *J. Chem. Pharm. Res*. **2013**, *5*, 606-611.

[11]Chaturvedula, V.S.P., Yu, O., Mao, G. (2013). Int. *J. Pharm. Sci. Inv*. **2013**, *2*, 36-40.

[12]Chaturvedula, V.S.P., Ruo, H. (2013). *J. Pharmacog and Phytochem*. **2013**, *2*, 113-115.

[13]Bedir, E., Toyang, N. J., Khan, I. A., Walker, L. A., Clark, A. M., *J. Nat. Prod.* **2001**, *64*, 95-97.

[14]Chaturvedula, V.S.P., Schilling, J. K., Miller, J. S., Andriantsiferana, R., Rasamison, V. E., Kingston, D. G. I. *Planta Med.* **2003**, *69*, 440-444.

[15]Huan, V. D., Yamamura, S., Ohtani, K., Kasai, R., Yamasaki, K., Nham, N. T. *Phytochemistry* **1998**, *47*, 451-457.

[16]Tanaka, T., Nakashima, T., Ueda, T., Tomii, K., Kouno, I. *Chem. Pharm. Bull*. **2007**, *55*, 899-901.

[17]Kandati, V., Govardhan, P., Reddy, C.S., Nath, A.R., Reddy, R.R. *Int. Curr. Pharm. J*. **2012**, *1*, 199-204.

[18]Raju, V.H., Ganapaty, S., Prasanna, S.S., Vijaya, G.J., Kishore, P.S., Asif, A.K., *Int. Curr. Pharm. J*. **2012**, *1*, 213-216.

[19]Chaturvedula, V. S. P., Prakash, I. *Eur. Chem. Bull.* **2013**, *2*, 298-302.

[20]Chaturvedula, V. S. P., Prakash, I. *Molecules* **2013**, *18*, 13510-13519.

[21]Prakash, I., Chaturvedula, V. S. P., Markosyan, A. *Nat. Prod. Commun*. **2013**, *8*, 1523-1526.

Received: 19.11.2013.
Accepted: 09.12.2013.

KINETICS OF DECOLORIZATION OF ALIZARIN RED S IN AQUEOUS MEDIA BY FENTON-LIKE MECHANISM

Z. M. Abou-Gamra[a]*

Keywords: Alizarin Red S; decolorization; kinetics; Fenton-like

The decolorization kinetics of Alizarin Red S (ARS) in aqueous solution was studied using Fenton like reaction in dark environment. The effects of dye, iron(III) ions and hydrogen peroxide concentrations were investigated. The reaction was first order in ARS, H_2O_2 and zero order in iron(III) chloride. Increasing the hydrogen peroxide concentration (2-8 x10^{-3} mol dm^{-3}) increases the rate constant from 1.05x10^{-3} to 3.2 x 10^{-3} s^{-1} and excess of hydrogen peroxide shows no effect on the rate constant. Iron(III) ions concentration shows soft retardation effect on the degradation rate of ARS. Increasing the initial ARS concentration from 1 to 4x 10^{-4} mol dm^{-3} decreases the decolorization from 85 % to 55 % within 15 minutes. Increasing temperature in the range of 298-313 K increases the rate of degradation and no optimal value detected. In addition, the influence of inorganic additives such, carbonate, nitrate and chloride on the efficiency of dye removal were examined.

*Corresponding Authors
E-Mail: zanibabougamra@yahoo.com
[a] Chemistry Department, Faculty of Science, Ain-Shams University, Abbassia, Cairo, Egypt

Introduction

Textile dyeing process is significant source of environmental pollution. One of the most problems of textile waste water in addition to toxic and carcinogenic nature is color effluent. It does not reflect atheistic problem because it is visible pollutant but also depletes sunlight penetration which reduces the photosynthetic activity in aquatic plants, thereby having undesirable impact on their growth. Many physical, chemical and biological methods are used to remove the dyes from waste water.[1-6]

This study is concerned with removal of Alizarin Red S from water. Alizarin Red S is widely used for dyeing textile materials.[7-9] Alizarin Red S is (1,2–dihydroxy-9,10-anthraquinonesulfonic acid sodium salt). It is synthesized by sulfonation of Alizarin which is extracted from root of madder plant. Alizarin Red S is used as stain microscopy, acid-base indicator and in determination of fluorine. The removal of anthraquinone dyes like Alizarin Red S is crucial process from both economical and environmental points of view.[10]

In recent years a great efforts has been done to remove Alizarin Red S using photocatalytic techniques.[2,7-8] In the same time less attention was given to advanced oxidation process such as Fenton and Fenton like process which could be good option to treat and remove Alizarin Red S. Fenton's reagent is an attractive reagent due to the fact that, iron is an abundant and non-toxic element, hydrogen peroxide is easy to handle and can be broken down to environmentally benign product and there is no need for special equipment.

The main object of this study is to examine the effect of the major system parameters on the decolorization kinetics of Alizarin Red S dye. Such parameters are the pH, concentration of iron (III) ions, H_2O_2, dye and temperature of ambient. Also the study gave attention to the effect some inorganic electrolytes.

Experimental

Reagents and materials

All chemicals were of pure grade and were used without further purification. Alizarin Red S purchased from LOBA Chemie PVT Mumbai: 400005 India (molecular formula, $C_{14}H_7O_7NaS$, Molecular weight = 342.26, λ_{max} = 430 nm). The chemical structure and UV-vis spectrum of ARS is given in (Figure1). $FeCl_3$, $NaNO_3$ and Na_2CO_3 were purchased from Merck. Hydrogen peroxide solution (35 %) was of analytical grade. All solutions were prepared using bidistilled water. Stock solutions of dye (1 mM), $FeCl_3$ (10 mM) were prepared in 0.01 M of HCl. All experiments were performed at pH below 3.

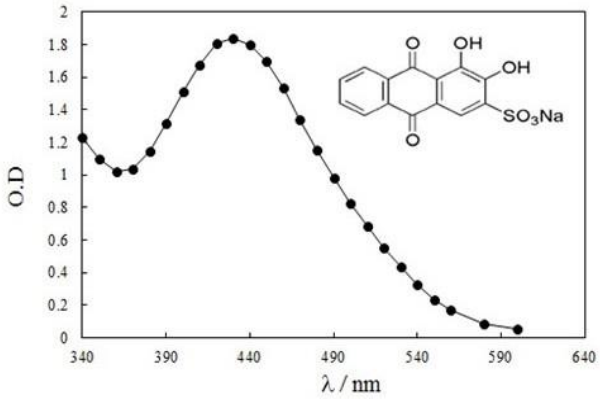

Figure 1. Chemical structure, UV-visible spectrum of ARS. [ARS] = 5 x 10^{-4} mol dm^{-3}

Kinetic experiments

Kinetic experiments were conducted by mixing the solutions of dye and hydrogen peroxide and adjusting [H^+] to the required value with NaOH/HCl using a Griffin pH-meter fitted with a glass calomel electrode. The reaction initiated by adding $FeCl_3$ to thermostated solution (dye + H_2O_2). The progress of the reaction was monitored at λ_{max} = 430 nm using a thermostated 292 Cecil spectrophotometer.

 DOI: 10.17628/ecb.2014.3.108-112

Results and Discussion

Effect of pH

Advanced oxidation processes are powerful alternative methods of wastewater treatment. This method based on the production of powerful oxidant, HO$^{\bullet}$ (E = 2.8 V versus NHE). These radical are capable to degrade recalcitrant organic compounds under mild experimental conditions.[11] The general mechanism of Fenton reaction[12] is

$$Fe^{2+} + H_2O_2 \rightarrow Fe^{3+} + HO^{\bullet} + HO^{-} \quad (1)$$

k = 76.5 mol^{-1} dm^3 s^{-1}

Then, Fe^{3+} ions can be reduced by excess H_2O_2 to form Fe^{2+} ions and more HO$^{\bullet}$ Radicals. Second reaction is called Fenton-like[13] allowing Fe^{2+} regeneration leading to catalytic mechanism (reactions, 2-4),

$$Fe^{3+} + H_2O_2 \leftrightarrow FeOOH^{2+} + H^{+} \quad (2)$$

K_{eq} = 3.1 x 10^{-3}

$$FeOOH^{2+} \rightarrow Fe^{2+} + HO_2^{\bullet} \quad (3)$$

k = 27x10^{-3} s^{-1}

$$Fe^{3+} + HO_2^{\bullet} \rightarrow Fe^{2+} + O_2 + H^{+} \quad (4)$$

$k <$ 2x10^3 mol^{-1} dm^3 s^{-1}

The perhydroxy radicals ($HO_2^{\bullet}$) are unstable and converted to hydroxyl free radicals (HO$^{\bullet}$) as in reaction 5

$$2HO_2^{\bullet} \rightarrow 2HO^{\bullet} + O_2 \quad (5)$$

$$dye + HO^{\bullet} \rightarrow product \quad (6)$$

As clear from equation (1) the amount of HO$^{\bullet}$ depends on the pH of solution. It was reported that the optimum pH value is 3.[4, 6, 14-17]

It was difficult to study the effect of pH on the rate of decolorization of ARS since it is chemical indicator and spectrum changes completely by changing the pH, (Figure 2). Consequently all experiments were performed at pH=2.87

Effect of H_2O_2 concentration

Decolorization reaction rate of ARS dye by Fenton-like process can be represented by equation 7

$$Rate = k[H_2O_2][ARS][Fe^{3+}]^0 \quad (7)$$

$$Rate = k_{obs}[ARS] \quad (8)$$

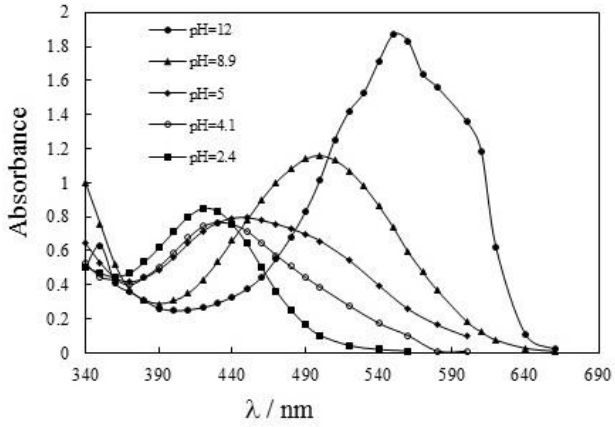

Figure 2. Effect of pH on the absorption spectrum of ARS in aqueous solution. [ARS]= 2x 10^{-4} mol dm^{-3}

k_{obs} is obtained from the slope of plot of ln A_t(absorbance of ARS at time interval, t) versus time. Figure 3 showed that the decrease in dye concentration as function of time was dependent of hydrogen peroxide concentration. The data were in good agreement with pseudo first order kinetics model.[18-19] Increasing the hydrogen peroxide concentration (2-8x10^{-3} mol dm^{-3}) increases the rate constant from 1.05x10^{-3} to 3.2x10^{-3} s^{-1}, Table 1. Excess of hydrogen peroxide shows no effect on the rate constant. This attributed to production of less reactive radical ($HO_2^{\bullet}$) or consumption of HO$^{\bullet}$ radicals by self-scavenging.[4,6,11,20] Plot of ln k_{obs} versus ln [H_2O_2] yields straight line with slope of unity indicates the reaction is first order in hydrogen peroxide.

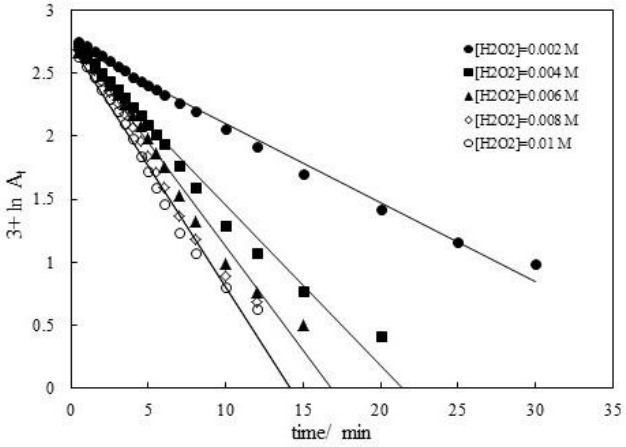

Figure 3. First order plots for the decolorization of ARS by Fenton-like reaction at various H_2O_2 concentrations. pH= 2.87, T = 30 ^{o}C, [ARS] = 2x10^{-4} mol dm^{-3}, [Fe^{3+}] = 2x10^{-4} mol dm^{-3}

Efficiency of decolorization was 90% within 15 minutes at 8x10^{-3} mol dm^{-3} of hydrogen peroxide.

Effect of iron(III) chloride concentration

Although no reaction was observed between ARS and hydrogen peroxide in absence of iron(III) ions, iron(III) ions concentration shows soft retardation effect on the degradation rate of ARS. Keeping temperature at 30 ^{o}C, [ARS]= 2x10^{-4} mol dm^{-3} and [H_2O_2] = 4 x 10^{-3} mol dm^{-3} using different concentrations of iron(III) chloride namely,

2-6 x10^{-4} mol dm^{-3}, the degradation rate dropped from 91% to 86% within 20 minutes by increasing the concentration from 2x10^{-4} to 6 x10^{-4} mol dm^{-3}. This could be attributed to the increasing in [Fe^{3+}] increases [Fe^{2+}] which scavenging the HO·.[4,6,17] Alireza et al[20] reported that increasing of iron(III) ions concentration increases the decolorization rate of brilliant blue and maximum rate was at [Fe^{3+}] =2x10^{-4} mol dm^{-3}.

Table 1. Observed first order rate constants of the decolorization of ARS by Fenton-like reagent at temperature = 30 °C, pH=2.87

Concentrations, mol dm^{-3}			k_{obs} x10^3 s^{-1}
[ARS]x10^4	H_2O_2x10^3	[Fe^{3+}]x10^4	
1	4	4	2.05
2	4	4	1.70
3	4	4	1.15
4	4	4	0.72
2	2	2	1.05
2	4	2	2.13
2	6	2	2.75
2	8	2	3.20
2	10	2	3.20
2	4	2	2.65
2	4	4	2.70
2	4	6	2.52

The values of first order rate constant, k_{obs}, are given in Table 1, no change with rise of iron(III) chloride concentrations indicates the reaction is zero order in iron(III) chloride. This could attribute to fast formation of very weak complex between iron(III) and ARS in step proceed the rate determining step. M. Tariq et al[21] observed weak complex between Cu^{2+} and ARS and Cu^{2+} retarded the photodegradation of ARS.

Effect of dye concentration

The effect of initial dye concentration of aqueous solution of ARS on Fenton-like process was investigated since pollutant concentration is important parameter in wastewater treatment. Increasing the initial ARS concentration from 1 to 4x 10^{-4} mol dm^{-3} decreases the decolorization from 85 % to 55 % within 15 minutes. Plotting ln A_t versus time, (Figure 4) showed that drop of the rate of decolorization by increasing the dye concentration. This attributed to relatively lower of HO· results from the increasing of ARS concentration while concentration of H_2O_2 and iron(III) chloride remains the same. The obtained results was in good agreement with earlier reported.[15-17]

Effect of Temperature

The variation of the temperature in range of 298-313 K increases the rate of decolorization of ARS, (Figure 5). No optimal temperature in this study was detected as opposed to the literature reports[22-23] in which 30 ºC is stated as optimal temperature for Fenton oxidation. Another optimal temperature, 50 ºC was reported on decolorization of some dyes by Fenton-like reaction.[4]

The activation energy was calculated from Arrhenius plot and Eyring equation and was found to be 47.04 kJ mol^{-1}.

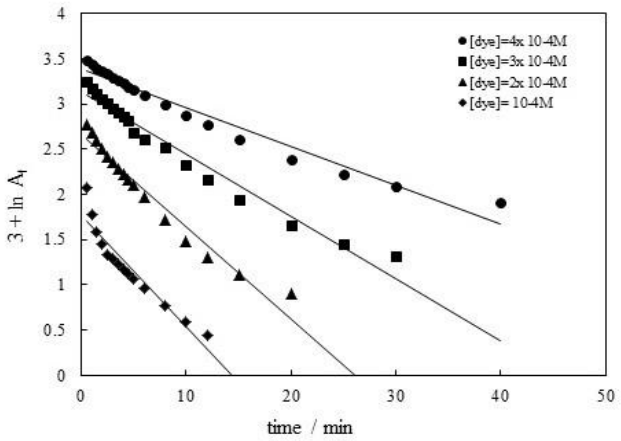

Figure 4. First order plots for the decolorization of ARS by Fenton-like reaction at various ARS concentrations. pH= 2.87, T = 30 °C, [H_2O_2] = 4x10^{-3} mol dm^{-3}, [Fe^{3+}] = 4x10^{-4} mol dm^{-3}

Effect of inorganic anions

Inorganic anions occur naturally in wastewater (e.g. NO_3^-) or may be added to facilitate the dyeing (e.g. Cl^- and CO_3^{2-}). The presence of inorganic anions in textile wastewaters plays an important role in the oxidation kinetics of different dyes. Inorganic anions may induce or reduce the rate of photooxidation. For example, formation of HO· radicals during the radiation of nitrate ion may induce the rate of photooxidation[24-25] while scavenging of hydroxyl radicals by chloride and carbonate ions[26-27] reduces the reaction rate.

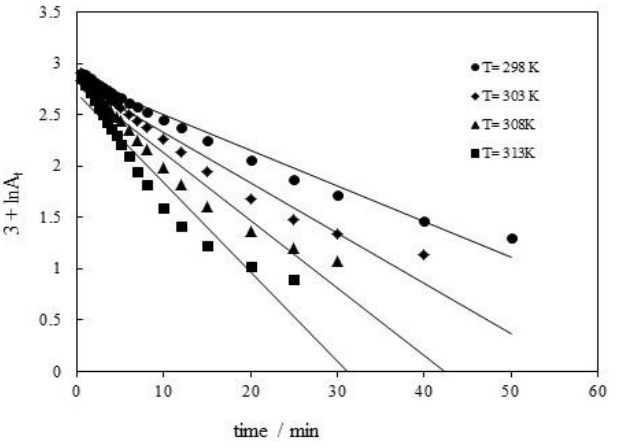

Figure 5. First order plots for the decolrization of ARS by Fenton-like reaction at various temperatures. [ARS] =2x10^{-4} mol dm^{-3}, [Fe^{3+}] =2x10^{-4} mol dm^{-3}, [H_2O_2] =2x10^{-3} mol dm^{-3}, pH=2.87

Effect of $NaNO_3$

Figure 6, shows pseudo first order decolorization of ARS at different concentrations of $NaNO_3$. Addition of 5 g L^{-1} $NaNO_3$, rate constant increased from 1.95x10^{-3} s^{-1} (in absence of nitrate) to 2.53 x 10^{-3} s^{-1}. Increasing the concentration of nitrate up to 20 g L^{-1} had no effect. According to that reported in literature[24-25] increasing the rate was attributed to generation of HO· radicals by rapid protonation of ^-O· as follow

$$NO_3^- + h\nu \rightarrow NO_3^{-}\cdot \rightarrow NO_2^- + O^-\cdot$$

$$O^-\cdot + H_2O \rightarrow HO^- + HO\cdot$$

 DOI: 10.17628/ecb.2014.3.108-112

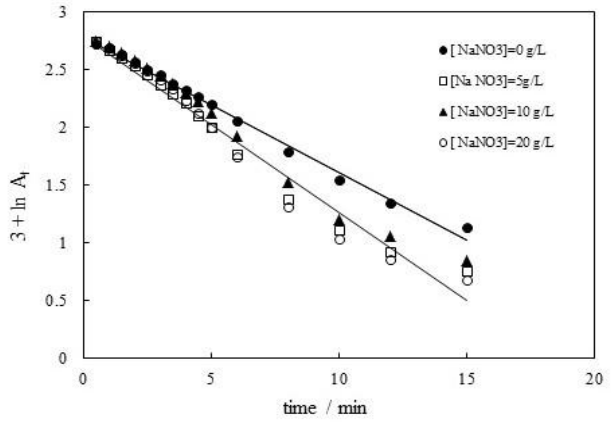

Figure 6. First order plots for decolorization of ARS by Fenton-like reaction at various $NaNO_3$ concentrations. [ARS]=$2x10^{-4}$ mol dm^{-3}, [H_2O_2] = $2x10^{-3}$ mol dm^{-3}, [Fe^{3+}] =$2x10^{-4}$ mol dm^{-3}, *T*= 35 °C, pH= 2.87

In this study the reason was not clear since the reaction occurred in absence of light.

Effect of Na_2CO_3

Different concentrations of Na_2CO_3 were used to study the effect of carbonate ions on the oxidation of Alizarin red S. Carbonate ions were present mainly as H_2CO_3, since the experiments were performed at pH ≤ 3. Presence of bicarbonate ions in the course of oxidation may decrease the decolorization rate due to scavenging of OH· by HCO_3^- (HCO_3^-+HO· → $CO_3^{-\cdot}$ + H_2O). Production of $CO_3^{-\cdot}$ which is less reactive than hydroxyl radical[27] lowered the levels of HO· during the course of the reaction hence decreasing the decolorization rate as shown in (Figure 7). It was observed that the decolorization rate constant (1.78 x 10^{-3} s^{-1}) in the absence of carbonate ions decreased to 1.12 x 10^{-3} s^{-1} due to the presence of 8×10^{-3} mol dm^{-3} Na_2CO_3.

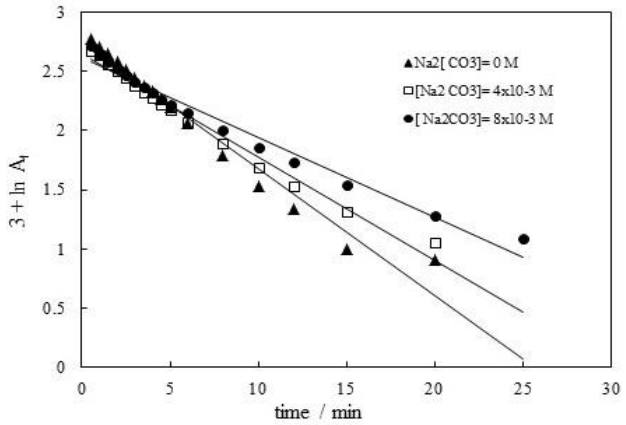

Figure 7. First order plots for the degradation of ARS by Fenton-like reaction at various Na_2CO_3 concentrations. [ARS] =$2x10^{-4}$ mol dm^{-3}, [H_2O_2] =$2x10^{-3}$ mol dm^{-3}, [Fe^{3+}] = $2x10^{-4}$ mol dm^{-3}, T=35 °C, pH=2.87

Effect of NaCl

In absence of chloride, the dye decolorization was 90% in 20 minutes. The addition of 5 g L^{-1} to the dye solution caused 15% increase in decolorization in first 5 minutes after that the decolorization rate decreased in comparison in absence of chloride. Figure 8 shows pseudo first order decolorization of ARS at different concentrations of NaCl. High chloride concentration had no effect on the rate of dye decolorization.

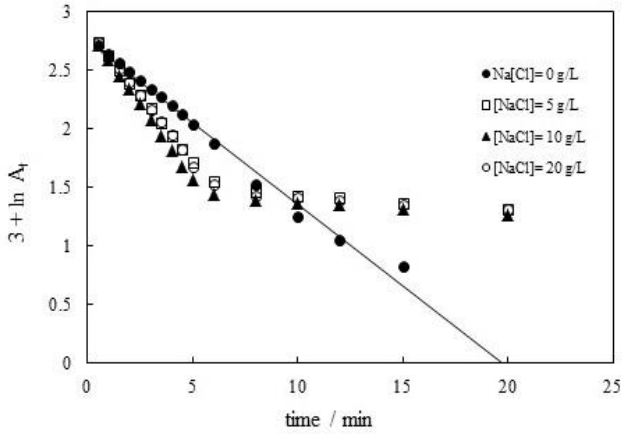

Figure 8. First order plots for degradation of ARS by Fenton-like reaction at various NaCl concentrations. [ARS] =$2x10^{-4}$ mol dm^{-3}, [H_2O_2] = $2x10^{-3}$ mol dm^{-3}, [Fe^{3+}] =$2x10^{-3}$ mol dm^{-3}, T= 35 °C, pH = 2.87

Conclusion

The decolorization kinetics of Alizarin Red S in aqueous solution was studied using Fenton like reaction in dark environment. The results showed that the Fenton like is powerful method for decolourization of ARS. The rate of decolorization is decreased by increasing the concentration of dye and addition of carbonate. The rate of decolorization is increased by increasing the concentration of hydrogen peroxide and addition of nitrate. The reaction was first order in ARS, H_2O_2 and zero order in ferric chloride.

References

[1]Abou-Gamra, Z. M., Medien, H. A., *Eur. Chem. Bull*., **2013**, *2(7)*, 417.

[2]Joshi, K. M., Shrivastava, V.S., *Int. J. Environ. Sci.*, **2011**, *2(1)*, 8.

[3]Rehman, R., Mahmud, T., Anwar, J., S F. alman, M., Shafique, U. Uz-Zaman, W. Ali, F., *J. Chem. Soc. Pak.*, **2011**, *33(2)*, 228.

[4]Medien, H. A., Khalil, S. M. E. *J. King Saud Univ. (Science)*, **22**, 147 (2010).

[5]Xiang-Rong Xu, Xiang-Zhong Li, *Sep. Purif. Technol.*, **2010**, *72(1)*, 105.

[6]Papic, S. M., Koprivanac, N., Peternel, I., Deanovic, M., *Chem. Biochem. Eng. Q.*, **2010**, *24 (1)*, 9.

[7]Parra, S., Sarria, V., Maloto, S., Periner, P., pulgarin, P., *J. Appl. Catal., B: Environ*, **2004**, *51*, 107.

[8]Kannan, N., Nagnathan, G.G., *Int. J. Environ.Prot.*, **2007**, *27*, 1103.

[9]Pirillo, S., Ferreira, M., Rueda, E.H., *J. Hazard. Mater.* **2009**, *168*, 168.

[10]Zucca, P., Vinci, C., Sollai, F., Rescigno, F., Sanjust, E., *J. Mol. Catal. A*, 2008, *288*, 97.

[11]Parsons, S., "Advanced Oxidation processes for Water and Wastewater treatment", IWA Publishing, London, (**2004**).

[12]Haber, F., Weiss, J., *Proc. Res. Soc. Ser. A*, **1934**, *147*, 332.

[13]Pignatello, J., J. *Environ. Sci. Technol*., **1992**, *26*, 944.

[14]Neamtua, M., Yediler, A., Siminiceanu, I., Kettrup, A., *J. Photochem. Photobiol. A: Chem.*, **2003**, *161*, 87.

[15]Chiing-Chang Chen, Ren-Jang Wu, Yi-You Tzeng, Chung-Shin Lu, *J. Chin. Chem. Soc.*, **2009**, *56*, 1147.

[16]Habib, Md., Ismail, I., Abu Jafar Mahmood Ullah, Md., *African J. Pure Appl. Chem.*, **2012**, *6(14*), 153.

[17]Hashemian, S., Tabatabbaee, M., Gafari, M., *J. Chem.*, Article ID 509097, **2013**, 1.

[18]Swaminathan, K., Sandhya, S., Sophia, A. C., Pachhade, K., Subrahmanyam, Y. V., *Chemosphere*, **2003**, *50*, 619.

[19]Wang, S., *Dyes and Pigm.*, **2008**, *76*, 714.

[20]Khataee, A., Vatanpour , V., Farajzadeh, M., *Turkish J. Eng. Env. Sci*., **2008**, *32*, 367.

[21]Tariq, M., Chuncheng, C., Lili, L., Dan, Z., Wanghong, M., Jun, L., Jincai1, Z., *J. Environ. Sci.*, **2009**, *21*, 263.

[22]Guedes Anabela, M. F. M., Madeira Luis, M. P. A., Boaventura Rui, R., Costa Carlos, A.V., *Water Res*., **2003**, *37*, 3061.

[23]Ramirez, J. H., Costa, C. A., Madeira, L. M., *Catal. Today*, **2005**, *107-108*, 68.

[24]Zepp, R.G., Hoigne, J., Bader, H., Environ. *Sci. Technol*., **1987**, *21*, 443.

[25]Elmorsi, T., Riyad, Y., Mohamed, Z., Abd El Bary, H., *J. Hazard. Mater.*, **2010**, *174*, 352.

[26]Dong, Y., Chen, J., Li, C. Zhu, H., *Dyes and Pigm.*, **2007**, *73*, 261.

[27]Buxton, G.V., Greenstock, C.L., Helman, W.P., Ross, A.B., *J. Phys. Chem. Ref. Data*, **1988**, *17*, 513.

Received: 21.10.2013.
Accepted: 10.12.2013.